

Anaerobic Digestion CHP Solutions for the Urban and Rural Environments

Nathan Curry

A Thesis

In the Department

of

Electrical and Computer Engineering

Presented in Partial Fulfillment of the Requirements

For the Degree of

Doctor of Philosophy (Electrical and Computer Engineering) at

Concordia University

Montreal, Quebec, Canada

March, 2015

© Nathan Curry, 2015

**CONCORDIA UNIVERSITY
SCHOOL OF GRADUATE STUDIES**

This is to certify that the thesis prepared

By: Nathan Curry

Entitled: Anaerobic Digestion CHP Solutions for the Urban and Rural Environments

and submitted in partial fulfillment of the requirements for the degree of

PhD in Electrical Engineering

complies with the regulations of the University and meets the accepted standards with respect to originality and quality.

Signed by the final examining committee:

<u>Dr. Christian Moreau</u>	Chair
<u>Dr. Serge Guiot</u>	External Examiner
<u>Dr. Anjali Awasthi</u>	External to Program
<u>Dr. Catherine Mulligan</u>	Examiner
<u>Dr. Luiz Lopes, Dr. Sheldon Williamson</u>	Examiner
<u>Dr. Pragasen Pillay</u>	Thesis Supervisor

Approved by

Chair of Department or Graduate Program Director

Dean of Faculty

ABSTRACT

Providing anaerobic digestion combined heat and power solutions for emergency and backup power in the urban and rural environments.

**Nathan Curry, Ph. D.
Concordia University, 2015**

Urban waste generation and disposal remains a major global issue. As the world's population grows past the 7 billion mark and more people move to urban areas, the amount of waste generated will grow accordingly. The most promising solutions to this problem are waste to energy technologies in the form of biological treatment of organics through anaerobic digestion and thermal decomposition via plasma arc gasification. These two technologies can be used in the urban environment separately or complementarily to reduce the volume of the waste being processed while also generating heat and power (CHP) and reducing transportation costs and greenhouse gas emissions. In this research, the feasibility of heating a small-scale anaerobic digester using an air source heat pump and solar heat gains from a greenhouse located on the roof of an urban building in Montreal, Canada, is investigated during the coldest month of the year. Small-scale implementation of anaerobic digestion systems for backup and emergency power is also investigated for both the urban and rural environments as a solution for increased grid blackouts caused by more frequent and more severe storms. Derating curves are determined for generators operating under extreme unbalanced load conditions in both the urban and rural environments. The benefits and disadvantages of induction and synchronous generator systems are presented for small to large-scale systems (20kW to 2000kW).

TABLE OF CONTENTS

TABLE OF CONTENTS	<i>iv</i>
LIST OF FIGURES	vii
LIST OF TABLES	xii
LIST OF SYMBOLS AND ABBREVIATIONS	xiii
Chapter 1.	1
Introduction	1
1.1 <i>Urbanization and the Growing Waste Problem</i>	<i>1</i>
1.2 <i>Climate Change, Extreme Weather Events, and Grid Vulnerability</i>	<i>7</i>
1.3 <i>The Food, Water, and Energy Nexus</i>	<i>12</i>
1.4 <i>Contributions of the Research</i>	<i>16</i>
1.5 <i>Conclusions</i>	<i>17</i>
Chapter 2.	18
Waste to Energy Technologies	18
2.1 <i>Introduction</i>	<i>18</i>
2.2 <i>Determining Energy Content of MSW</i>	<i>19</i>
2.3 <i>Mass Burn Incineration</i>	<i>20</i>
2.4 <i>Pyrolysis/Gasification</i>	<i>21</i>
2.5 <i>Plasma Arc Incineration</i>	<i>22</i>
2.6 <i>Summary of Thermal Waste to Energy Technologies</i>	<i>25</i>
2.7 <i>Anaerobic Digestion</i>	<i>26</i>
2.8 <i>Conclusions</i>	<i>29</i>
Chapter 3.	31
Integrating Solar Energy Into an Urban Small-Scale Anaerobic Digester for Improved Performance	31
3.1 <i>Introduction</i>	<i>31</i>
3.2 <i>Description of the Proposed System</i>	<i>32</i>

3.3 Digester Tank Heat Loss Modeling	35
3.4 System Model with no Heating Added	38
3.5 Solar Energy 3-D Model.....	43
3.6 Air Source Heat Pump Heat Transfer Model for Digester Tank.....	47
3.7 Available Solar Energy with Shadowing Effect.....	50
3.8 Heat Loss Model with Air Source Heat Pump.....	52
3.9 Experimental Verification of Temperature Fluctuation in Anaerobic Digestion of Food Waste.....	57
3.10 Conclusions.....	69
Chapter 4.	71
Waste to Energy Systems for Emergency Power in Urban Environments	71
4.1 Introduction.....	71
4.2 Energy Available from Small-Scale CHP Systems for Urban Emergency Power Systems	75
4.3 CHP Sizing for Small-Scale Anaerobic Digestion CHP Systems	77
4.4 Feasibility and Design of Biomass System To Meet Emergency Power Load Requirements	80
4.4.1 Biogas Production Required	80
4.4.2 Amount of Waste Required	80
4.4.3 Digester Tank Sizing.....	81
4.5 Electric Machines for Biomass CHP for Urban Emergency Power Generation	82
4.5.1 Self-Excited Induction Generators (SEIG)	84
4.5.2 Synchronous Generators (Wound Rotor).....	85
4.5.3 Permanent Magnet Synchronous Generator (PMG).....	86
4.6 Derating for Synchronous Machine with Rectifier/Inverter	88
4.6.1 Derating and Voltage Unbalance Overview	88
4.6.2 Overvoltage and Undervoltage Concerns for Emergency and Backup Power	92
4.6.2 Simulation of Derating of Synchronous Generator with Unbalanced Load	95
4.6 Conclusions.....	102
Chapter 5.	103
Waste to Energy Systems for Backup Power in the Rural Environment.....	103
5.1 Introduction.....	103

5.2 Waste to Energy CHP System as Backup power for a Dairy Farm.....	108
5.3 Case Study of Anaerobic Digestion System for Backup Power for 140 Cow Dairy Farm	114
5.4 Determining Derating Curve for a Synchronous Generator Operated Under Extreme Unbalanced Load Conditions	126
5.5 Experimental Determination of Derating Curve for Generator Operated under Extreme Unbalanced Load Conditions	131
5.6 Electric Machines for Rural Anaerobic Biogas Systems	133
5.7 Implementation Concerns for Biogas CHP Systems.....	135
5.9 Conclusions.....	136
Chapter 6	137
6.1 Conclusions.....	137
6.2 Future Work.....	139
REFERENCES.....	141
Appendix A – Code for Simulations.....	155
A.1 Air Source Heat Pump Heating of Digester (System Modeler).....	155
A.2 Synchronous Generator Derating Test (System Modeler)	178

LIST OF FIGURES

CHAPTER 1

Figure 1.1 Largest annual anthropogenic producers of methane in the US and Canada.	3
Figure 1.2 Annual MSW Composition in US 2012 (EPA).	5
Figure 1.3 Annual MSW Composition in N. America IPCC	5
Figure 1.4 Energy accumulation with distinct components of Earth's climate system from 1971 to 2010.	8
Figure 1.5 ADAPT Power framework for climate change related risk assessment for power utilities.	11
Figure 1.6 Power generation and cooling technologies and median water use.	13
Figure 1.7 Water usage from power production in India under different power production scenarios to 2040.	15

CHAPTER 2

Figure 2.1 Waste Management hierarchy.	18
Figure 2.2 Net energy production to grid per tonne of MSW at a theoretical 500 tpd facility.	25
Figure 2.3 Net annual revenue before taxes for a 500 tpd waste to energy facility.	26
Figure 2.4 Anaerobic digestion stages.	28

CHAPTER 3

Figure 3.1 Diagram of proposed system location with air source heat pump diagram.	34
Figure 3.2 Electrical equivalent thermal model of the proposed tank showing conductive, convective, and radiative loss paths.	35
Figure 3.3 Heat loss model for digestion tank including air source heat pump input.	36
Figure 3.4 Hourly temperature fluctuation ($^{\circ}\text{C}$) in T_{ambient} , T_{dew} , and T_{sky} for January 14-21, 2012, starting at 4pm on January 14.	40
Figure 3.5 Wind speed fluctuation in m/s during the proposed week in January, 2012.	41
Figure 3.6 Tank Heat losses in Watts for the week with an average value of 502 W shown in red.	41

Figure 3.7 Internal tank temperature drop from 35°C with a week of no heating beginning at sundown on Jan 14, 2012.	42
Figure 3.8 Theoretical effect of temperature decrease on biogas production of mesophilic OFMSW digester.	42
Figure 3.9 Dimensions of greenhouse being investigated.	44
Figure 3.10 3-D model of the proposed greenhouse location and surrounding buildings.	44
Figure 3.11 Annual path of sun around location being investigated.	46
Figure 3.12 Shadowing effect of surrounding buildings.	46
Figure 3.13 Average useful weekly temperature gains in greenhouse from solar radiation above baseline temperature for the month of January	
Figure 3.14 Proposed air source heat pump system for digester tank	48
Figure 3.15 Heat pump model	50
Figure 3.16 Total average hourly total solar radiation for the month of January.	51
Figure 3.17 Analysis of shading effect on total solar radiation for a single day, January 16 th	52
Figure 3.18 Ambient, Dewpoint, and Sky temperature values for the month of January, 2012.	53
Figure 3.19 Wind speed data input, corrected for height, for the month of January, 2012.	55
Figure 3.20 Tank temperature fluctuation for the month of January, 2012, with air source heat pump active during daylight hours.	
Figure 3.21 Coefficient of Performance of heat pump for daily heating in the month of January	56
Figure 3.22 Temperature fluctuation for the month of January with heat pump used every other day during daylight hours.	56
Figure 3.23 Temperature fluctuation for case where heat pump is only active for a third of the daylight hours of January.	57
Figure 3.24 W8 Anaerobic digestion system used for temperature fluctuation experiment.	59
Figure 3.25 Temperature ranges for Anaerobic Digestion process.	59
Figure 3.26 Total weight of food waste groups from UK food waste study (2008)	

with major groups highlighted that were chosen as major representatives.	63
Figure 3.27 Breakdown of food waste representatives used in the experiment.	63
Figure 3.28 Percent COD removed.	64
Figure 3.29 Volatile fatty acid levels in digestate in mg/l and pH.	65
Figure 3.30 pH of slurry in tank.	65
Figure 3.31 Biogas production level in ml/gVS.	67
Figure 3.32 Percent methane in biogas over time.	67
Figure 3.33 COD loading rate in gCOD/l/day.	68

CHAPTER 4

Figure 4.1 Methane potential of major US Sources in m ³ (NREL).	74
Figure 4.2 Range of electric machine size for 0.25 to 5 tonnes of daily food waste production.	78
Figure 4.3 Power and heat recovery ratings for 0.25-5 tpd anaerobic digestion systems with 367 m ³ /tonne _{dry} biogas production at 65% methane.	79
Figure 4.4 Power and heat recovery ratings for 0.25-5 tpd anaerobic digestion systems with 1000 m ³ /tonne _{dry} biogas production at 65% methane.	79
Figure 4.5 Self-Excited Induction Generator charging battery bank for emergency lighting system.	85
Figure 4.6 Synchronous Generator charging battery bank for emergency lighting system.	86
Figure 4.7 Permanent Magnet Synchronous Generator charging battery bank for emergency lighting system.	87
Figure 4.8 Percentage decrease in expected life of electric machine vs. temperature increase.	89
Figure 4.8 Overview of system being modeled including generator, rectifier, DC link, inverter, and load.	84
Figure 4.9 Percent temperature rise due to voltage unbalance.	90
Figure 4.10 Derating factor vs. percent voltage unbalance curve from NEMA MG-1.	91
Figure 4.11 Overview of system being modeled including generator, rectifier, DC link, inverter, and load.	95

Figure 4.12 Matlab/Simulink schematic of generator, rectifier, DC link, and inverter.	96
Figure 4.13 Output voltages of generator (460 RMS Value).	97
Figure 4.14 Output current of generator (phase A) (19.8 A RMS Value).	98
Figure 4.15 DC link output voltage (600 V).	98
Figure 4.16 Output phase voltages and currents from inverter (340 V _{peak} and 32.2 A _{peak}).	99
Figure 4.17 Derating factor of generator versus percent voltage unbalance.	100
Figure 4.18 Rating of Inverter versus percent unbalance in voltage.	101

CHAPTER 5

Figure 5.1 Biogas potential (m ³) by source in the United States.	104
Figure 5.2 Biogas potential in Canada by source.	106
Figure 5.3 Flow chart of energy production from biogas produced through anaerobic digestion.	107
Figure 5.4 Major Power US outages (at least 50,000 customers) from 1984 to 2012.	108
Figure 5.5 Typical energy use by equipment category on a dairy farm.	110
Figure 5.6 Survey of herd size and installed generator capacity of agricultural AD systems.	111
Figure 5.7 Agricultural biogas system cost range per number of cows (100 – 250).	113
Figure 5.8 Range of energy demand for a dairy farm with energy content of manure.	113
Figure 5.9 Annual heating and electricity load profile for dairy farm.	115
Figure 5.10 Price range of biogas gensets from 12 kW to 100 kW based on market data.	116
Figure 5.11 Agricultural biogas CHP system schematic.	118
Figure 5.12 US Milk Farm Price Received Chart (2010 to September 2014).	119
Figure 5.13 Losses for 100-200 cow dairy farm without backup diesel access for up to 1 week.	120
Figure 5.14 Total Revenue, Expenses, and Income for a survey of Ontario Dairy Farms from 2004 to 2013.	122
Figure 5.15 Case 1: Cash flow analysis for biogas system replacing biomass heating system including the effect of 7 days/year of blackouts and feed in tariff (\$0.26/kWh).	123
Figure 5.16 Case 2: Cash flow analysis for biogas system replacing natural gas heating	

system including the effect of 7 days/year of blackouts and feed in tariff (\$0.26/kWh).	124
Figure 5.17 Case 3: Cash flow analysis for biogas system replacing propane heating system including the effect of 7 days/year of blackouts and feed in tariff (\$0.26/kWh).	125
Figure 5.18 Schematic of generator and load in System Modeler.	128
Figure 5.19 Figure 5.19 Derating curve for different percent unbalance for 30 kW synchronous generator	130
Figure 5.20 Derating curve under different percent unbalance loads for 6.7 kW synchronous generator.	130
Figure 5.21 11 kW generator and series combination of 5 hp DC and induction motors.	131
Figure 5.22 Three-phase resistive load bank used in experiment.	132
Figure 5.23 Comparison of experimentally determined and simulated derating curves.	133

LIST OF TABLES

CHAPTER 1

Table 1.1 Comparison of WTE Technologies assuming all food waste is digested anaerobically and remaining waste is processed with a plasma arc gasification	6
--	---

CHAPTER 3

Table 3.1 Heat conduction characteristics of digestion tank and insulation.	38
Table 3.2 Greenhouse materials and properties selected in Ecotect modeling software.	43
Table 3.3 Food waste substrate characteristics.	61
Table 3.4 Food waste breakdown as determined for the experiment.	62
Table 3.5 Literature review of experimental biogas yields of food waste.	66

CHAPTER 4

Table 4.1 German food waste distribution by volume.	72
Table 4.2 Literature review of experimental biogas yields of food waste.	75
Table 4.3 Overview of affected public housing developments in NYC and daily waste production.	77
Table 4.4 Overvoltage conditions tested in report.	93
Table 4.5 Summary of overvoltage testing of residential equipment.	94
Table 4.6 Example of voltages, currents, and inverter rating for a specific derating case.	101

CHAPTER 5

Table 5.1 Electricity generation potential for agricultural biogas systems.	105
Table 5.2 Energy potential of different waste sources in Canada.	105
Table 5.3 Examples of substrates and theoretical biogas yield and electrical power production.	107
Table 5.4 Typical wattages of standard dairy farm equipment.	111
Table 5.5 Diesel generator sizing, fuel consumption and \$/day of operation at full load.	114
Table 5.6 Synchronous generator parameters from Wolfram's System Modeler.	126

LIST OF SYMBOLS AND ABBREVIATIONS

CHP: Combined heat and power

kW: Kilowatt

MSW: Municipal solid waste

OFMSW: Organic fraction of municipal solid waste

t: Metric tonne

Mt: Megatonnes

MWh: Megawatt hour

TWh: Terawatt hour

TPD: Tonnes Per Day

AD: Anaerobic digestion

ASHP: Air source heat pump

W/K: Watts per Kelvin

G_c : Thermal conductance

$v_w(h)$: Velocity of wind at height h in m/s

v_{10} : Velocity of wind at height of 10 meters in m/s.

a : Hellman exponent (*for stable air over inhabited areas, $a = 0.34$*)

T : Temperature in Kelvin

ϵ_s : Emissivity of sky

\dot{m}_c : Mass flow rate of the heat pump condenser in kg/s

\dot{m}_e : Mass flow rate of the heat pump evaporator in kg/s

T_c : Temperature of the condenser in degrees C

T_e : Temperature of the evaporator in degrees C

c_w : Heat capacity of water or 4200 J/kg/K

c_a : Heat capacity of air or 1000 J/kg/K

Q_c : Heat rejected by the heat pump condenser in watts

Q_e : Heat absorbed by the heat pump evaporator in watts

COP : Coefficient of performance of heat pump

C : Heat capacity of the tank in J/K

E_{input} : Electrical input of the heat pump in watts

TS: Total solids

VS: Volatile solids

COD: Chemical oxygen demand

VFA: Volatile fatty acid

cwt: Centum weight

DR: Derating factor

kW: Kilowatt

V: Volts

A: Amps

RMS: Root mean square in volts

SCL: Stator copper losses in watts

RCL: Rotor copper losses in watts

%UB: Percent unbalance

CHAPTER 1.

INTRODUCTION

1.1 Urbanization and the Growing Waste Problem

As of 2014, global population currently stands at 7.3 billion and has almost tripled since 1950 (2.5 billion) and by 2050 it will have quadrupled to around 10 billion [1]. Projections from the United Nations show that the rapid depletion of essential human resources will only speed up as the population continues to grow at exponential levels. In addition, environmental pressures from changing global climate systems will put unprecedented strains on food, water, and energy systems. New consumption and energy production paradigms are necessary.

Currently more than 50% of the global population lives in urban environments with this number predicted to grow to 75% by 2050 as the total population grows toward 10 billion [2]. The waste generated by this increased urbanization will have to be sorted and processed in some way. Globally, the total amount of municipal solid waste (MSW) produced each year has been estimated at approximately 1.5 Gt [3]. By 2025, it has been predicted that this amount will increase by 50% to 2.2 Gt [4]. Currently most of the waste produced by the cities of the world is sent to surrounding landfills but these landfills are quickly running out of space. The last landfill in the greater New York City area closed in 2001 and now garbage is currently transported outside the state by truck and train. London, UK, sends its annual waste to 18 different landfills that filling to capacity. The UK government is implementing Zero Waste policies to fall in line with the Waste Framework Directive which requires all European Member states to achieve 50% waste reuse or recycling by 2020 [5]. By 2020, the UK will be legally required to generate 15% of its energy requirements from renewable sources [6]. In Montreal, Canada, the closest landfill accepting waste is 40 km away with permits that were set to expire in 2009 but were extended

through 2017. In Montreal, organic waste comprises almost 50% of the 1 million tonnes of waste sent to landfill each year with only 8% of this organic waste reclaimed. By 2020, there is a municipal directive for landfills across Quebec to no longer accept organic waste [7]. In 2006, nearly a million tonnes of the waste generated in Toronto, Canada, was trucked to landfills across the U.S. border into Michigan because landfills surrounding the city were filled to capacity. As a solution, the City of Toronto has purchased a landfill site that is over 200 km away from the downtown area that opened in 2010 [8]. Mexico City produces 12,600 tonnes of trash per day and sends it to sprawling, polluted landfills that are running out of space. The largest landfill supporting Mexico City was closed in 2011 leaving a deficit of almost 5000 tonnes of trash daily without a place to go [9]. As of 2013, two thirds of China's cities are being overrun with garbage. Of the almost 200 million tonnes of waste generated annually in China, 80% ends up in landfills. Only 5% of landfill sites can be classified as sanitary landfills, 40% of landfills do not meet the sanitary landfill standards, and over 50% of landfill locations are open dumps [10].

In addition to the problem of not having enough space to process the increasing urbanization of humans, landfills also contribute a large amount of anthropological greenhouse gases. According to estimates by The Environmental Protection Agency of the United States, more than 50 percent of total global methane emissions are due to human-related activities and landfilling is third on the list; the remaining 50 percent of methane production comes from natural sources. Looking at similar methane emissions from Environment Canada, it can be seen that landfills are one of the top three contributors of methane to overall greenhouse gas emissions. The list of top methane producers in the US and Canada are summarized in *Figure 1.1* [10][11].

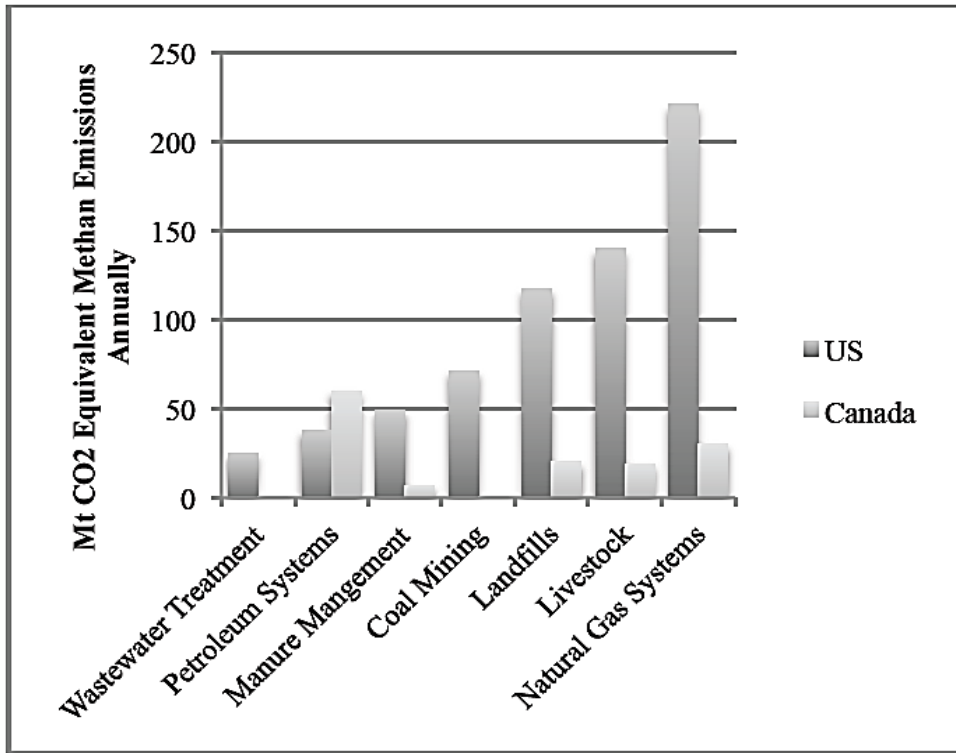


Figure 1.1 Largest annual anthropogenic producers of methane in the US and Canada

There are presently about six thousand landfills in operation in the United States releasing an estimated 13-18 billion cubic meters of methane each year which directly contributes to global warming as methane is more than 20 times more effective as a greenhouse gas than carbon dioxide by volume over a 100 year time span. The National Renewable Energy Laboratory has confirmed the obvious fact that the largest landfills producing the most methane are those that surround the largest cities in the country [12].

In 2012 (latest available data), the United States generated 251 million tonnes of municipal solid waste (MSW) comprised mainly of food scraps, yard waste, plastic packaging, furniture, tires, appliances, paper, and cardboard. This discarded MSW came from two main sources: Residential (55-65%) and Commercial / Institutional (35-45%) with construction and

hazardous wastes not considered in the grouping. Nearly half of this waste was recycled or reclaimed but 134 million tonnes (54%) was still sent to landfill [13].

In Canada, the total amount of waste sent to landfill in 2010 (latest available data) was 25 million tonnes, which roughly scales to the population difference (Canada 34 million, US 314 million, 1:10) [14]. Due to the lack of a comprehensive waste analysis report for the whole of Canada, it is assumed that the composition of MSW is similar for the US and Canada and the waste breakdown from the US Environmental Protection Agency is used (*Figure 1.2*). This assumption can be verified by checking the available waste reports of individual provinces in Canada (Ontario, British Columbia) to verify the waste percentages [15]. The US Environmental Protection Agency estimated that second largest contributor to total landfill waste in 2012 was food waste, representing 14.5% of the total MSW. This estimate does not consider commercial food waste which substantially increases the available tonnage. Using a comprehensive waste analysis overview from the Intergovernmental Panel on Climate Change (IPCC) for North American MSW, a breakdown of major components places total food waste as the most prominent component of total MSW at 35% and can be viewed in *Figure 1.3* [16]. Using this value, an estimated 10Mt of food waste is available for energy reclamation each year in Canada and 47 Mt in the US.

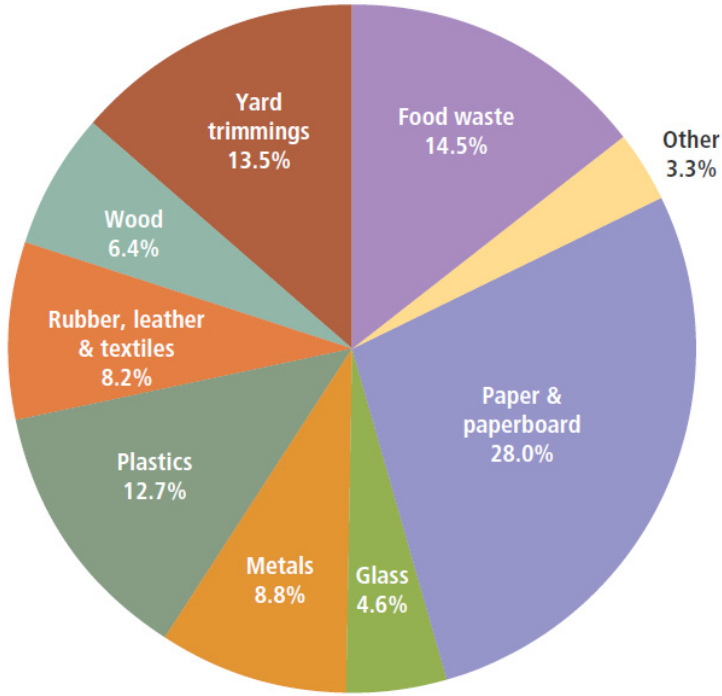


Figure 1.2 Annual MSW composition in US 2012 (EPA).

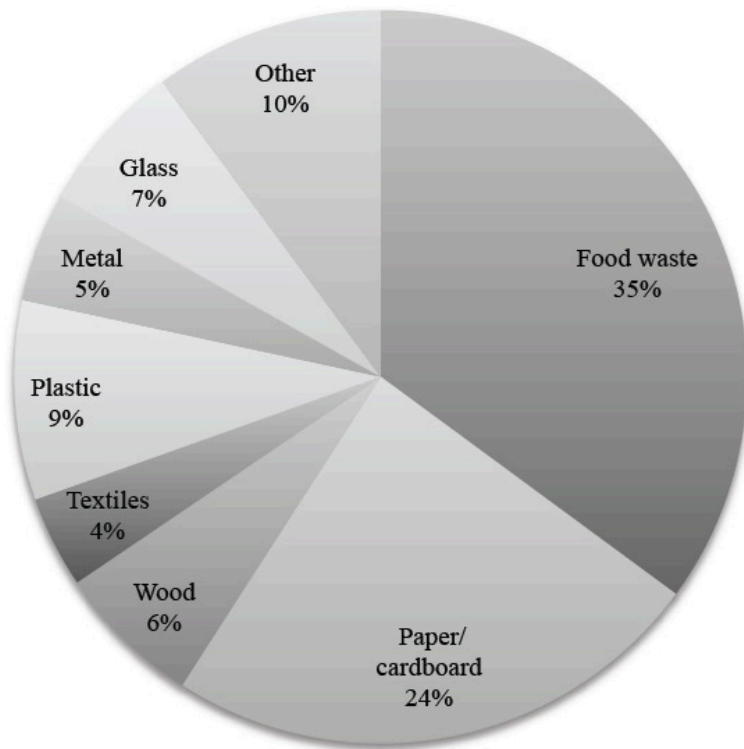


Figure 1.3 Annual MSW Composition in N. America according (IPCC).

A report on global food waste published in 2013 by the Food and Agriculture Organization (FAO) of the United Nations claims that 1.3 billion tonnes - or one third of all food produced for human consumption in the world - goes to waste [17]. The estimated cost of this amount of wasted food has been estimated at around \$750 billion USD and it also represents 3.3 billion tonnes of equivalent CO₂ emissions – roughly the same amount of total CO₂ emissions generated by the European Union [18]. In addition, this wasted food represents approximately 250 km³ of surface and groundwater resources as well as 30% of global agricultural land [19]. To put it in energy terms, if all of the food waste was to be used for energy reclamation via the anaerobic digestion process (2.3 MWh/tonne VS) described in this proposal, there would be 837 TWh of thermal energy or 360 TWh of electricity available from the produced biogas, equivalent to the output of 30 nuclear power plants (12.2 TWh average output) [20].

Looking again at North America, the 10 Mt of food waste available for energy reclamation each year in Canada and 47 Mt in the US represent 21TWh and 108 TWh respectively if treated with the anaerobic digestion process. If the remaining waste is treated with the plasma gasification process (1.4 MWh/t), 22 TWh is available in Canada and 122 TWh in the US. A summary of the potential annual energy production of these two technologies can be seen in *Table 1.1*.

Table 1.1 Comparison of WTE Technologies assuming all food waste is digested anaerobically and remaining waste is processed with a plasma arc gasification waste treatment system

	Food (Mt)	Other (Mt)	AD	Plasma
US	47	87	108 TWh	122 TWh
Canada	9	16	21 TWh	22 TWh

This is a substantial amount of available unclaimed energy that is currently going straight to the

landfill. There is an initiative to capture landfill gas in the US and Canada and it is presently only being captured in approximately 5% of the total landfills. It is obvious that there is no simple solution to the global waste crisis. It is clear that new waste management solutions are in order that could provide volume reduction of waste as well as substantial amounts of energy to the urban areas where the waste is generated.

1.2 Climate Change, Extreme Weather Events, and Grid Vulnerability

Over the last few decades, scientists have observed and reported a change in global climate systems with more frequent extreme weather events occurring due to increased amounts of carbon dioxide in the atmosphere. Carbon dioxide is a greenhouse gas and as more of it collects in the atmosphere, it leads to higher land and water temperatures, which then leads to larger and more frequent storms, floods, and droughts as long-standing weather patterns are disrupted by the increasing amount of energy stored in the Earth's climate system. *Figure 1.4* taken from Chapter 3 of the 2013 IPCC report, shows the increase of energy accumulation of distinct components of the Earth's climate system from 1971 to 2010 [21]. The increase of energy accumulating in the upper oceans and deep oceans of the world is the most obvious.

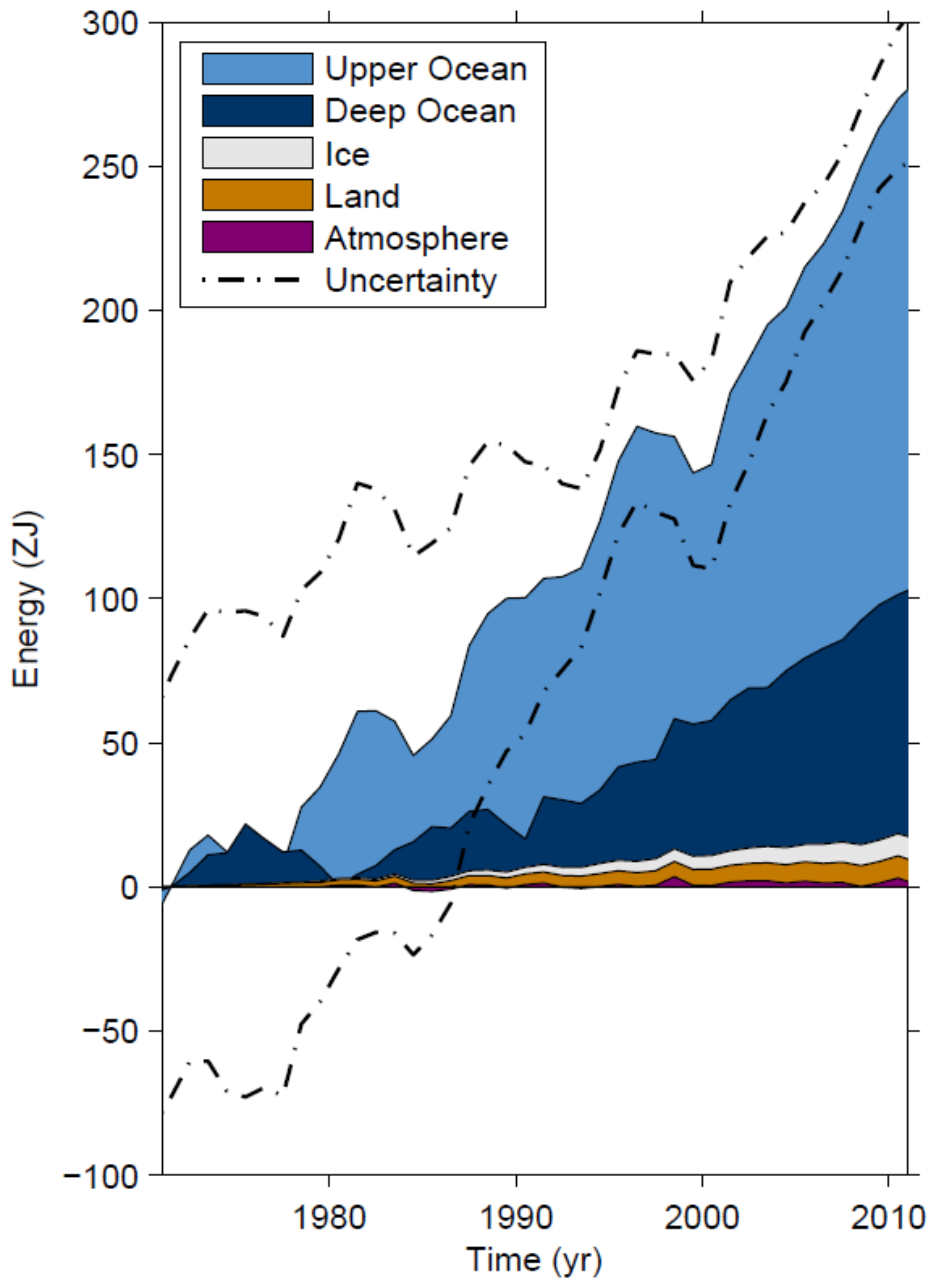


Figure 1.4 Energy accumulation with distinct components of Earth's climate system from 1971 to 2010. Found in Chapter 3 of 2013 IPCC report.

In order to implement proper public policy with regard to the recent changes in global climate systems and increase in extreme weather events, an accurate perception of the scientific consensus regarding the cause of these changes is necessary. A study published in 2013 examined 11,944 papers in the scientific literature regarding anthropogenic global warming

(AGW) ranging from 1991 to 2012. The literature survey excluded books, discussions, proceedings papers and other document types and focused only on published articles. The study found that 97.1% of investigated from scientific journals endorsed the consensus that the planet is warming and that human activities (the burning of fossil fuels) are the main cause. Only 0.7% of the literature rejected AGW outright and 0.3% of papers expressed uncertainty about the cause of warming [21]. Thirteen of the first 14 years of the 21st century have been the warmest on record. In 2013, the global average land surface temperature was 1°C above the 20th century average and the fourth highest average on record [22]. This pattern of increased average temperatures and extreme weather events shows no signs of slowing. In fact, some climate scientists claim that if carbon emissions are not immediately reduced, it is possible that the average global temperature could rise by 4°C by 2050 with potentially catastrophic results – large parts of southern Europe would be turned to desert, sea levels would rise by several meters and flood coastal cities, large areas of landmass on the planet would become uninhabitable due to heat waves, 85% of Amazon rainforest would die, coral reefs would not be able to survive in the oceans due to acidity (dissolved CO₂) and temperature increases. Incredible losses of biodiversity would occur as well as general human suffering [23][24]. Reducing greenhouse gas emissions from all sectors of society – transportation, construction, energy production, and agriculture - is a clear necessity. Anaerobic digestion of organic waste can simultaneously reduce methane emissions from landfill while also reducing greenhouse gas emissions from transportation of waste to landfills while providing combined heat and power.

As the climate changes, so does the likelihood of unprecedented and extreme weather events – both hot and cold - with regard to seasonal timing, intensity, frequency, duration, and land area affected. These changes can be influenced by a variety of different factors including

shifted means in normal weather patterns, increased variability in weather patterns, and a change in symmetry between hot and cold weather events. The extreme events that will become more likely over the coming years and decades are typhoons, hurricanes, and other tropical storms, winter storms, wildfires, heat waves, droughts, floods, precipitation, and sea level surges [22]. All of these extreme weather events can have a direct impact on the reliability of agricultural systems, water systems, transportation systems, and electricity generation and distribution systems.

A report published by the US Department of Energy (DOE) states that from 2008 to 2012, the average number of weather-related power outages more than doubled in frequency compared with the previous five years and have becoming increasingly more costly in the range of tens of billions of dollars [25][26]. Utilities presently understand the weak links in their transmission and distribution networks but don't currently analyze this alongside relevant climate change predictions. Recently, some companies are developing sophisticated climate models that incorporate power utility risk and damage parameters in order to provide accurate risk management information in the case of extreme weather events and other disasters. One specific application of this idea takes climate projections (temperature, precipitation, wind fields, soil moisture, sea level, etc.) and couples that with the probability of specific hazards (storms, flooding, surges, heat waves, winter storms, drought, wildfires, etc.) in order to determine the impact on electricity supply, delivery, and usage as well as provide estimates for power equipment damage, electricity revenue losses, and other economic losses [27]. This risk management framework is shown in *Figure 1.5*.

ADAPT-POWER: Extreme weather and climate change risk and adaptation framework for electricity infrastructure

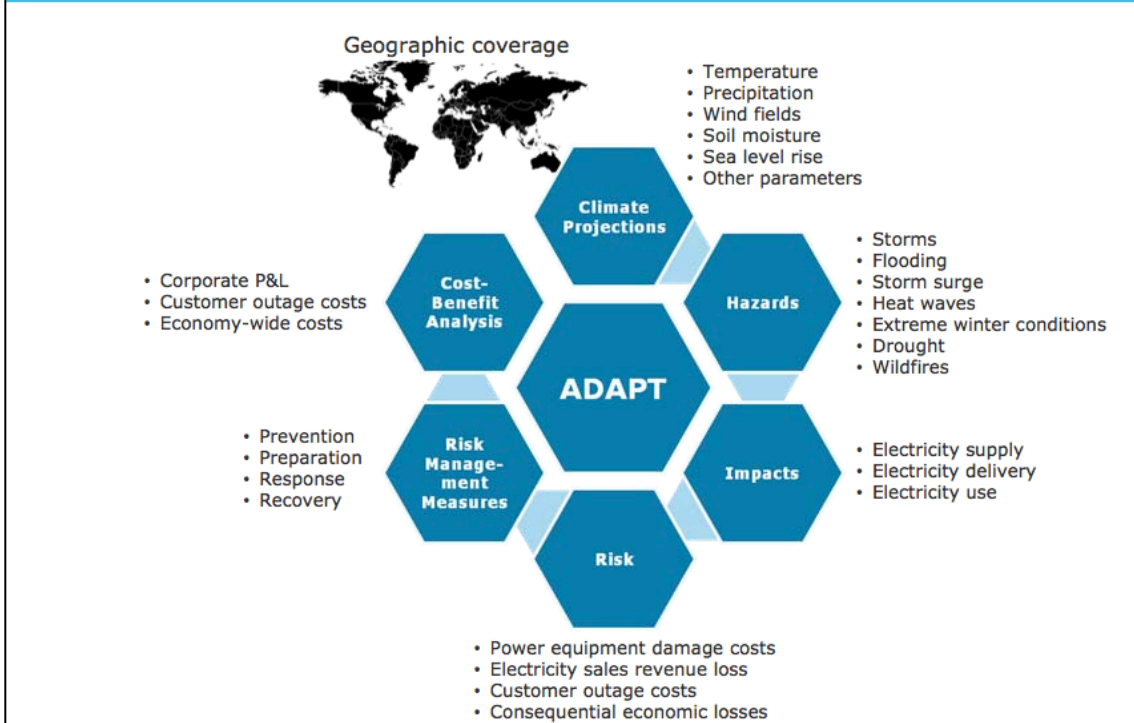


Figure 1.5 ADAPT Power framework for climate change related risk assessment for power utilities.

As cascading blackouts and localized power outages become more frequent due to an aging and increasingly complex grid infrastructure coupled with extreme weather events related to changing global climate systems, it is necessary to investigate decentralized renewable energy sources for backup power generation and emergency lighting capable of operating without a grid connection. Integration of black-start capable combined heat and power systems (CHP) supplied by a constant flow of energy-rich biogas from the anaerobic digestion of *in situ* organic waste could provide a reliable way for ensuring backup power in the case of more frequent and extended blackouts.

1.3 *The Food, Water, and Energy Nexus*

In recent years, the complex interactions and synergies of food, water, and energy systems have come into focus globally. These systems are inextricably linked but currently managed separately and looking towards the future, integrated management techniques of these systems will have to be enacted. To make the importance of integrated management techniques clear, currently 70% of global water demand is used for agriculture and food production, and the whole supply chain of food production represents 30% of global energy consumption [28]. At the same time, 80% of electricity produced globally comes from steam-powered turbines that rely on a constant water supply and this critical constraint is often overlooked by policy and planning reports. The steam used for power production is generated through combustion of coal, natural gas, or through nuclear fission and the inefficiencies in the energy conversion processes produce waste heat that requires large amounts of water for cooling [28]. In the U.S. in 2005, thermoelectric cooling accounted for the largest percentage of all freshwater usage (41%), beating out agricultural systems (37%) [29]. In *Figure 1.5* the total median water usage for various power generation technologies and cooling techniques is presented. As can be seen in the figure, coal plants with carbon capture and sequestration technology to reduce greenhouse gas emissions consume almost twice the water as conventional coal fired power plants. As total water and energy demand increase with population growth, and changing global climate systems place greater strains on dwindling water supplies, the competition for water resources between food, water, and energy systems will become a pressing global issue.

Fuel Type	Cooling Technology	Median Water Use (m ³ /MWh) ^a	
		Withdrawal	Consumption
Nuclear	Once-through	168	1.0
	Tower	4.2	2.5
Natural Gas ^b	Once-through	43	0.4
	Tower	1.0	0.7
Coal w/CCS ^c	Tower	4.3	3.2
Coal ^d	Once-through	86	0.4
	Tower	2.3	1.9
Solar Photovoltaic	n/a	0.1	0.1
Wind	n/a	0	0

Source:

- a. One cubic meter (m³) is equal to 264 gallons of water. MWh means megawatt-hour.
- b. Natural gas combined cycle (NGCC).
- c. CCS is carbon capture and sequestration.
- d. Supercritical/advanced coal.

Figure 1.6 Power generation and cooling technologies and median water use.

According to [30], the amount of water used by humans under an average economic growth scenario could increase 50% by 2030. Currently, approximately 4.5 trillion m³ of water are consumed each year, with agriculture accounting for 3.1 trillion m³ (70%) of this. By 2030, total demand could grow to 6.9 trillion m³ with agricultural water demand equalling total current global demand of 4.5 trillion m³. This total predicted demand under “business-as-usual” circumstances by 2030 is 40% greater than current reliable, accessible sources of water. Additionally, this study does not factor in the future effects of climate change on already stressed global water systems.

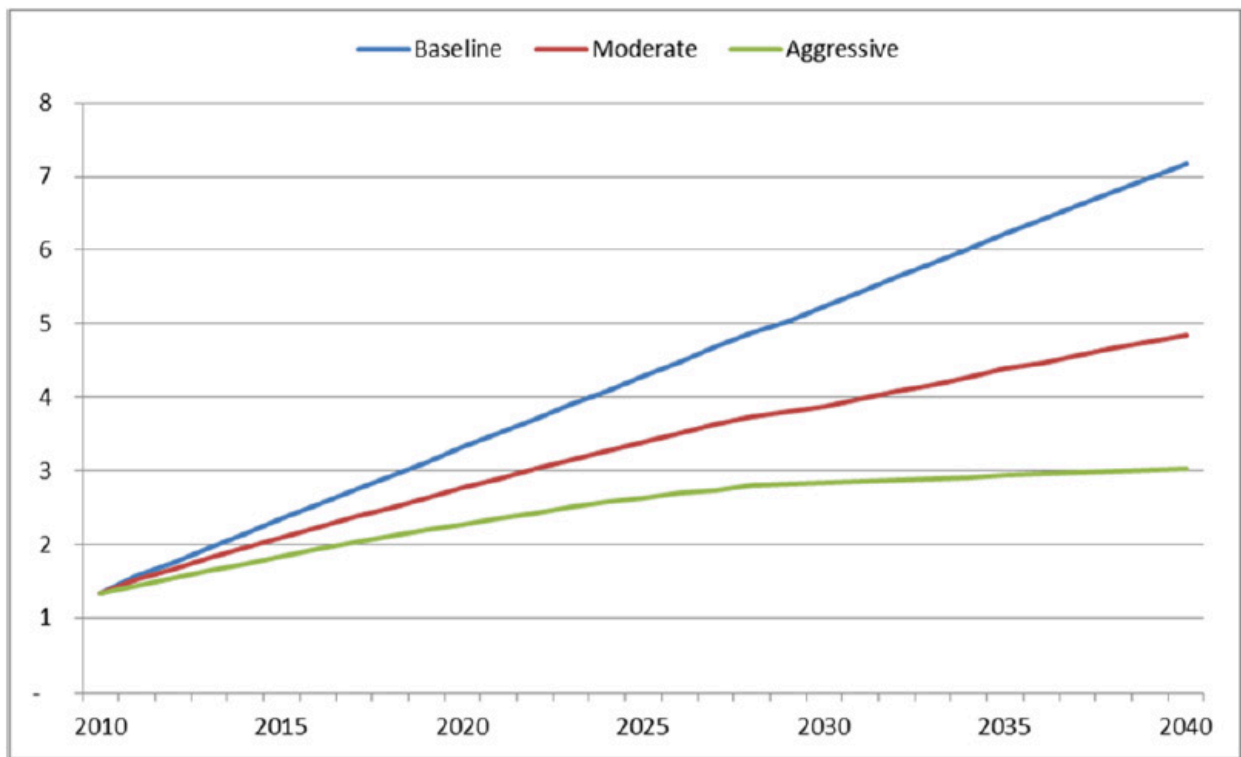
In a 2014 report by the UN’s Intergovernmental Panel on Climate Change (IPCC), the risks of the human interference with the climate system on all continents and across the oceans were assessed and management of adaption and mitigation of the worst effects were discussed [31]. In regard to food systems, the report claims with “high confidence” that the negative

impacts of climate change on crop yields are more common and likely than positive effects. As the global population increases over the coming decades, the amount of a food production will have to grow as well. By 2030, food demand has been predicted to increase by 50% and will increase further to 70% by 2050 with corresponding increases in water demand needed [32]. In addition, between 20,000 and 50,000 km² of potentially productive agricultural lands are lost each year around the world to soil erosion and degradation, further stressing an already stressed agricultural system [33]. In the 2007 IPCC summary report for policy makers, it is predicted that by 2020, between 75 and 250 million people in Africa will be subjected to reduced water access due to climate change and a possible 50% reduction in yields from agriculture in rain-fed areas. In Asia, freshwater access in Central, South, East, and South-East Asia in large river basins has been predicted to decrease by 2050 and heavy populated areas near mega-deltas face risk of extreme flooding from the seas. In addition, it has been predicted that heat and water stress could reduce agricultural yields by 25% by 2050 in both China and India [34].

Without access to water and energy, it will be hard to meet the basic human needs of a growing global population – especially in developing nations where currently 1.3 billion lack access to electricity and clean water [35]. Without a “systems” approach to water management, power production, and food production, the likelihood of widespread suffering, social dissent, and political upheaval will only increase.

The importance of integrated management of food, water, and energy systems can be illustrated by looking at India. Currently around 52% of the population lives in water stressed areas and 73% of electricity production occurs in these same areas. Currently about 25% of the population has no access to electricity, with the government increasing installed capacity to close this gap in electricity access. Increased electricity production can come with an increased water

cost though, and special care must be paid to the way in which electricity is generated. *Figure 1.4* shows potential water usage from power production in India under three scenarios up to 2040. The base case assumes 70% energy production via advanced coal fired power plants. The moderate case considers coal fired power production decreasing to 34% of total generation by 2040 and solar and wind power production increasing to 34% and 17% respectively. In the aggressive case, more end-use efficiency is assumed and more wind power generation is assumed. In the base case, 7 times more water is needed for power production than currently being used. In the best-case (aggressive) scenario, still 3 times more water is needed by 2040 for power production [36].



Units = bcm/year

Figure 1.7 Water usage from power production in India under different power production scenarios to 2040.

1.4 Contributions of the Research

One of the major contributions of this research involves the development of a new energy management paradigm for anaerobic digestion systems. Using the solar heat gains from a greenhouse and an air source heat pump to provide heating during daylight hours instead of using produced biogas for heating is a novel approach that can free up 15-30% of biogas for higher value energy applications. This approach also presents a holistic vision of waste management for the urban environment. Instead of traveling 40-200 km outside of a city center to be landfilled, food waste (comprising up to 40% of municipal solid waste stream) becomes an on-site energy source and a source of fertilizer via the digestate produced from the process to help grow more food inside the city in greenhouses instead of transporting it into cities from elsewhere. The modelling performed in this research to determine the feasibility of the proposed novel heating technique involves bringing together two complicated, disparate software programs and using them in a synergistic way. The ECOTECT solar modelling package allows accurate solar heat energy values to be obtained for the greenhouse under investigation by taking into consideration the shadowing effect of surrounding buildings. The use of Wolfram's recent System Modeler software package allows real weather data to be input into a heat loss model for an outdoor digester tank on an urban roof in order to obtain realistic heat loss results.

Another contribution of this research is the investigation of anaerobic digestion waste to energy systems as emergency or backup power generation systems. Integration of black-start capable combined heat and power systems (CHP) supplied by a constant flow of energy-rich biogas from the anaerobic digestion of *in situ* organic waste could provide a reliable way for ensuring backup power in the case of more frequent and extended blackouts due to changing climate systems and extreme weather events.

1.5 Conclusions

In conclusion, it has been shown that there is a problem with the growing amount of waste being produced around the world as well as increased risk of food and water shortages from the effects of increased population growth coupled with a changing global climate. The likelihood of increased severe weather events will lead to an increase of power outages and rolling blackouts as well as threaten agricultural yields and water supplies. Using anaerobic digestion as a waste-to-energy solution to not only reduce the amount of waste that goes to landfills by up to 40%, but also the amount of methane emissions produced by humans and the amount of fossil fuel consumption by replacing natural gas with the biogas produced from the AD process. In addition, small-scale anaerobic digestion systems can be used as emergency or backup power generators to in order to provide combined heat and power in the case of extended blackouts.

In this dissertation, Chapter 2 presents different waste-to-energy technologies and their net energy outputs to the grid, Chapter 3 presents simulations of a case study of a novel way to heat a small-scale anaerobic digestion system via solar heat gains in a greenhouse and an air source heat pump. Chapter 4 discusses the use of small-scale AD systems as backup and emergency power generators for extreme weather events in the urban environment, Chapter 5 deals with the use of AD systems for back up and emergency power systems on dairy farms in the rural environment, and Chapter 6 deals with conclusions and future work recommendations.

CHAPTER 2.

WASTE TO ENERGY TECHNOLOGIES

2.1 Introduction

Although landfilling is currently the most widely practiced waste management solution, there are waste management technologies available that can reduce transportation costs, greenhouse gas emissions, and waste volume, while also providing combined heat and power (CHP). They are divided into thermal and biological categories. This section will provide a summary of net energy production and overview of each technological process along with advantages and drawbacks of each. Future MSW processing and landfill reduction will need to incorporate a combination of biological treatment of the organic fraction of the waste and thermal treatment of the rest. The hierarchy of waste management from the most recent IPCC report (shown in *Figure 2.1*), and outlined by the European Commission, shows energy recovery as the most important waste management technique after the most important Reduce – Reuse – Recycle techniques [37].

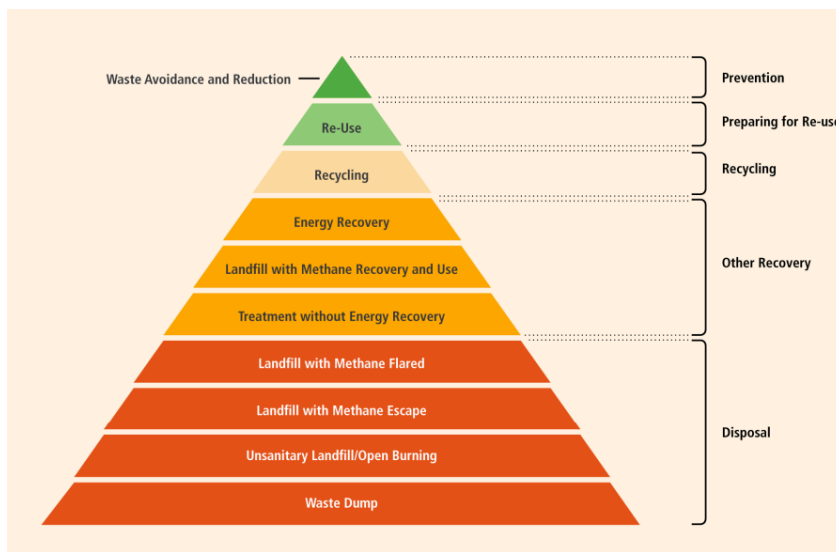


Figure 2.1 Waste Management hierarchy.

2.2 Determining Energy Content of MSW

MSW can vary in composition at different locations due to heterogeneity of materials and different recycling or reclaiming practices but several standard compositions have been determined for waste used for energy reclamation. The heating value for MSW can be based on an approximate hydrocarbon structure of $C_6H_{10}O_4$. The most important parameters to know about a given MSW substrate are ultimate analysis (carbon, hydrogen, oxygen, nitrogen content) and/or proximate analysis (volatile solids, moisture, carbon, and ash content). Proximate and ultimate analysis values for MSW are given in [38].

Ultimate analysis of MSW:

$$C = 0.37418$$

$$H = 0.05138$$

$$O = 0.29908$$

$$N = 0.01186$$

$$S = 0.00132$$

$$\text{Ash} = 0.2556$$

From this ultimate analysis, a Higher Heating Value (HHV) can be determined according to the following formula [38]:

$$\text{HHV (MJ/kg)} = (34.91 * C) + (117.83 * H) - (10.34 * O) - (1.51 * N) + (10.05 * S) - (2.11 * \text{Ash})$$

Using the above ultimate analysis gives a HHV of 15.48 MJ/dry kg MSW. Additionally, the Dulong formula for determining HHV can be used [38]:

$$\text{HHV (MJ/kg)} = (33.6 * C) + [(144.4 * (H - (O/8)))] + (9.428 * S)$$

Using the same MSW mass fraction yields a HHV of 17 MJ/dry kg of MSW.

In the case that the ultimate analysis of the MSW is not available, it's possible to calculate the HHV of the waste from the proximate analysis. It is claimed in [39] that the most accurate approximation of HHV from proximate analysis comes from the formula:

$$\text{HHV (MJ/kg)} = (0.3536 \cdot \text{FC}) + (0.1559 \cdot \text{VM}) - (0.0078 \cdot \text{ASH})$$

Where FC is fixed carbon, VM is volatile material and ASH is ash content. Using the above formula and proximate analysis values for MSW found in [38],

FC = 8%

VM = 55%

Ash = 16%

Moisture = 21%

A MSW HHV of 11.28 MJ/dry kg is determined. Once HHV has been determined then total net energy available can be predicted taking into consideration the amount of energy that each treatment process consumes depending on scale of operation and stages of the process.

2.3 Mass Burn Incineration

Mass burn incineration is a waste disposal method that involves combustion of waste material from 550-1200°C. Incinerators use an excess of oxygen to convert waste materials into heat, gas, steam, and ash while reducing the original volume of the MSW by up to 85%. The heat and high-pressure steam produced can be used to power a turbine to generate electricity and thereby qualifies incineration as a WTE technology.

The major drawback of incineration is that it costs more money to run the system than is available from the production of heat or electricity. In addition, major concerns remain about the

toxicity of the flue gases and fly ash produced during the process. The exhaust gases need to be scrubbed of particulates, acids, and dioxin and furan content as they pose serious environmental and health hazards. The fly ash produced from the process can contain significantly high concentrations of heavy metals such as lead, cadmium, copper, and zinc. This ash needs to be buried in a designated toxic area and many communities are not comfortable with toxic materials being located nearby. Incinerators remain a contentious environmental and social issue but are still employed around the world in places like Japan and Denmark that are short on space. Denmark and Sweden have been using this waste disposal technology for more than a century and often have district heating schemes that run exclusively off the heat produced by the process. In 2005, Denmark produced 14% of its domestic heating and almost 5% of its electricity through waste incineration [40]. The incineration process can produce 600 kWh/t MSW of net energy to the grid [38].

2.4 Pyrolysis/Gasification

Pyrolysis/Gasification is a waste to energy treatment that is related to incineration but it occurs at higher temperatures (750-1500°C) and produces different byproducts due to the fact that it is performed in an oxygen-starved environment. Pyrolysis is the first stage of the process and it involves the chemical decomposition of organic materials at temperatures above 430°C and it produces mainly a biochar ash which is rich in carbon and can be used as a fertilizer. Instead of the carbon in the organic materials bonding with oxygen and forming CO₂, as occurs in incineration and decomposition, the carbon is essentially “stored” in the biochar. As a result, Pyrolysis is considered a “carbon negative” process because it can break the natural occurring

carbon cycle by sequestering the carbon. Storing carbon in biochar has received interest recently as a technique to help reduce atmospheric CO₂ levels.

Gasification is the second stage of the process. In this phase, a controlled amount of oxygen is added to the heated carbonaceous materials to supply the exothermic combustion reactions that provide high enough temperatures for the organic compounds to break down into smaller molecules such as CO and H₂ which form the basis for synthetic gas or “syngas.” The syngas produced by the process can be used as a fuel and has about half the energy content of natural gas. As with mass burn incineration, a toxic ash and/or slag is produced that needs to be buried in a landfill, raising environmental concerns about the long-term sustainability of the process. Data on pyrolysis/gasification of MSW is scarce although it is a promising technology. Not much is known about emissions and cost analysis as there are currently no large-scale pyrolysis plants operating in North America. Pyrolysis/Gasification can provide a theoretical value of 755 kWh/t MSW of net energy to the grid while reducing the volume of the waste input by up to 90% [38].

2.5 Plasma Arc Incineration

Although technically falling under the label of “incineration,” plasma arc technology is a different entity than the other forms of incineration though it is often confused or lumped in with the rest. Plasma exists as a fourth state of matter in the physical world and occurs when a gas is heated to the point where it becomes ionized. Lightning is a natural example of plasma and the phenomenon has been turned into a technology with the plasma torch. When used in a lab or with an industrial purpose, plasma torch technologies can reach temperatures of around 7,000-

14,000 degrees Celsius which is hotter than the surface of the sun. It is interesting to note that plasma technologies were developed in the early 1960's along with the space program in the US and the former Soviet Union to simulate atmospheric re-entry conditions and test the durability of heat shields built for space vehicles.

Plasma torches convert electrical energy into thermal energy by forcing a flow of gas through an electrical arc that is formed between two electrodes. The gas becomes ionized and generates a large amount of heat in a "plume" or plasma arc column. The extreme heats produced with plasma torches can be used to cut metal in industrial applications but it can also be used to vaporize municipal solid waste. As a technology, it is often confused with incineration or pyrolysis, but it is actually a special case of both. Plasma arc incineration is a form of incineration that occurs at much higher temperatures than standard incineration and it occurs in an anaerobic environment like pyrolysis. In this high-heat, high-energy environment, the energy density becomes greater than the bonding energy between the elemental atoms that form molecules and any material that is fed through a plasma arc plume is broken apart into its elemental compositions. It is in this way a "return to the periodic table." This disassociation is permanent and total and works not just for organic wastes but also solid wastes, plastics, glass, metals, and hazardous wastes.

The main product of the process is a gas, known as synthesis gas (syngas), which can be used for the production of energy in reciprocating generators and can be further processed to produce various hydrocarbon fuels such as gasoline, diesel, ethanol, and methanol which are usually refined from fossil fuels. The other byproduct of the process is an inert vitreous glassy material known as slag, which is non-toxic and non-leaching and can be used as a rocky aggregate for building buildings and roads.

The process itself is straightforward: MSW is shredded and fed into a double air-locked tank where a plasma torch or torches vaporizes the waste and the syngas produced escapes through the top and the slag pools in the bottom where it hardens. Any heavy metals sink to the very bottom and can be removed separately. The gas is scrubbed and cleaned and fed to a turbine where it is combusted and produces electricity the gas is send through a reformation process where fuels such as ethanol are produced. The total energy consumed has been estimated at approximately 25% of what is produced netting 900 kWh/t MSW to the grid [41][42][43].

These attributes qualify plasma gasification as a renewable energy source and an attractive waste to energy technology. Unfortunately, at this time, there exist few environmental or engineering standards for the technology as a waste-to-energy solution although recent developments are promising.

Plasco Energy Group in Ottawa, Canada, have had a pilot plasma gasification facility capable of processing 100 tonnes of unsorted MSW per day since 2007 and have raised over 250 million dollars to further develop their technology. They claim 1.4 MWh of energy available produced per tonne of waste input. They are currently installing a 300 TPD plant in Red Deer, Canada, and have interest from Los Angeles, China, and several places in Europe. Another company, Plasma Energy Applied Technology (PEAT) has been making plasma gasification systems since 2002 and has recently opened facilities in California and Virginia to treat US Army waste as well as research systems in India and Taiwan. A Montreal based company named Pyrogenesis has supplied plasma gasification systems to the US Navy and Carnival cruise lines for use on their ships.

2.6 Summary of Thermal Waste to Energy Technologies

To summarize the thermal WTE technologies discussed in the previous sections, *Figures 2.2 and 2.3* provide an overview of net energy to grid per tonne of MSW as well as projected net annual revenue before taxes for a hypothetical 500 tonne per day waste to energy facility according to [38]. Plasma gasification stands out from the other thermal processes as the most benign as there are little to no toxins produced and the glass slag produced is completely neutral and doesn't need to be buried or disposed of in a landfill as in mass burn incineration and gasification processes and can be used repurposed for other applications.

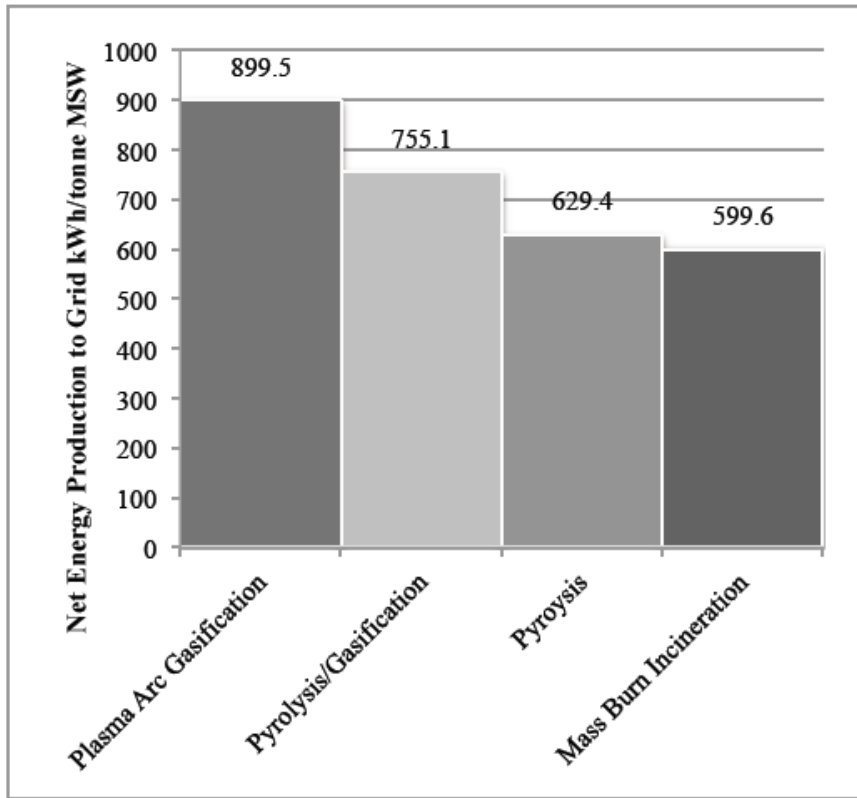


Figure 2.2 Net energy production to grid per tonne of MSW at a theoretical 500 tpd facility.

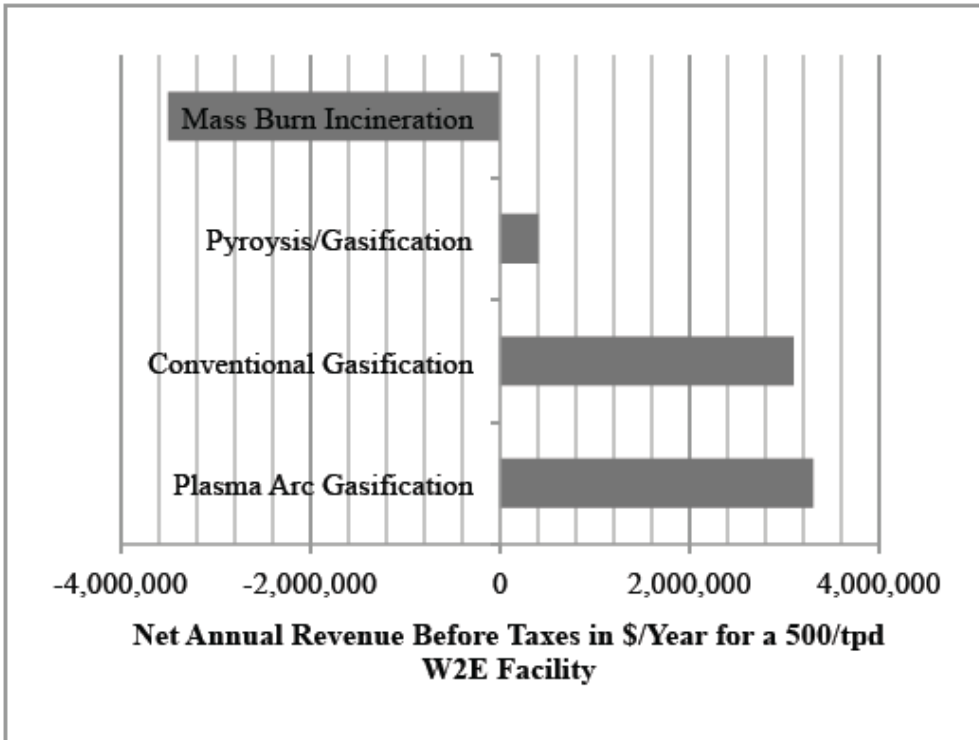


Figure 2.3 Net annual revenue before taxes for a 500 tpd waste to energy facility.

2.7 Anaerobic Digestion

Anaerobic Digestion is a naturally-occurring biological process in which microbes convert organic materials into biogas and neutral digestate sludge in the absence of oxygen. It is considered a renewable waste-to-energy technology because the methane-rich biogas produced (often 55-70% methane) can be burned as a fuel and offset the need for fossil fuels. Most of the methane is produced within one month of adding the organic material to the digestion process whereas in composting, several months are required for neutralization. Unlike incineration technologies, there are no toxic byproducts and the digestate that comes from this process can be spread directly as a fertilizer. This process can reduce the volume of the input material from 50% up to 80%.

The advantage of using anaerobic digestion in an urban environment to treat organic waste as opposed to composting it is that anaerobic digestion produces biogas with a high percentage of methane which can be used as fuel whereas composting produces mostly carbon dioxide which has no energy value. Importantly, AD also prefers cooked and oily food waste to be digested where composting does not. In fact, the AD process produces more biogas when used cooking oil and cooked meats are added. AD could be applied to the organic fraction of MSW either “en situ” or directly at the landfills if it is presorted by the producers. Anaerobic digestion has been a usable energy source for over 100 years and is currently being employed in countries around the world in rural settings to generate electricity and heat, but it has yet to make a large impact in the urban environment. Applied to the organic waste produced in cities, anaerobic digestion could provide a critical solution to growing garbage problems while simultaneously reducing external energy requirements.

Anaerobic digestion is considered a renewable energy source because the methane-rich biogas produced is suitable for energy production and can replace fossil fuels. As part of an integrated waste management system, AD reduces the amount of methane that would be released into the atmosphere if the waste was sent to the landfill and decomposed naturally. Additionally, the nutrient-rich solids and liquids left after digestion can be used as fertilizer.

The anaerobic process itself is a very complicated biochemical process. Based on temperature and input substrate, different strains of bacteria digest complex chains of carbohydrates, fats and proteins into their component parts. Anaerobic digestion occurs in four separate phases: Hydrolysis, Acidogenesis, Acetogenesis, and Methanogenesis (*Figure 2.4*). The

last stage of the process, Methanogenesis, is where the biogas is produced and it can contain 50-70% methane which can be used for heat and power applications.

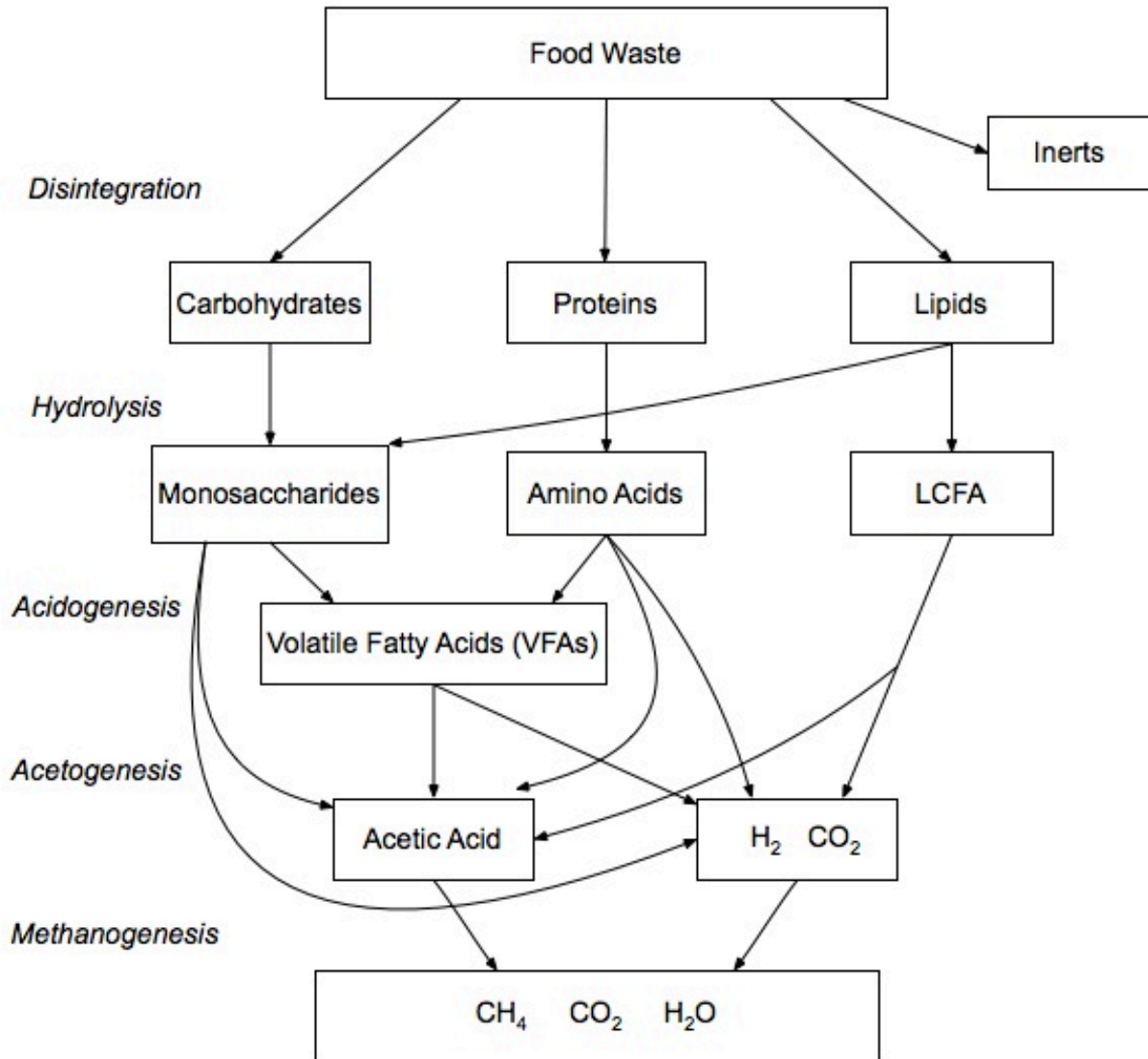


Figure 2.4 Anaerobic digestion stages.

In order to estimate the amount of energy in the biogas it is necessary to know the average biogas yield per tonne of food waste input. Each substrate is different and studies have been performed to determine appropriate values. For mixed food waste, a year-long study (released March 2008) performed by the Environmental Protection Agency in East Bay,

California, fed 100 tonnes of mixed food waste daily into a mesophilic digester and yielded an average of 367 m³ of biogas per tonne of food added to the digester [44]. Once the biogas output has been determined, there are many available references to determine the energy content of biogas, but an agreed heat of combustion value is 6.25 kWh/m³ [45]. This gives an energy yield of 2.3 MWh/tonne VS for the anaerobic digestion of food waste under mesophilic conditions. Anaerobic digestion systems have been demonstrated to work on a small scale and are fairly inexpensive to construct.

2.8 Conclusions

The waste generated by the increasing population and urbanization of humans will soon become unmanageable. Cities around the world are running out of places to send their waste and landfills are reaching limits and closing down. The organic fraction of municipal solid waste constitutes the main part of the methane produced from landfilling and is a powerful greenhouse gas directly contributing to anthropogenic global warming. The possibility of generating CHP from this waste stream should be a major focus of waste management in the future. Large-scale as well as small-scale anaerobic digestion could be used to generate heat and electricity from the organic waste in the urban environment and while reducing transportation costs and the amount of waste that is sent to the landfill. Accompanying this, or in place of it, plasma gasification could emerge as a very desirable candidate for disposal of MSW with the added benefit of energy reclamation. Interest in these technologies is currently growing and as landfills fill to capacity, a combination of anaerobic digestion of OFMSW and plasma gasification of the remainder will emerge as an attractive and responsible way of dealing with all of the world's

waste. Coupled with recycling, these technologies could provide manageable solutions for growing waste concerns for both municipal and private urban institutions.

CHAPTER 3.

INTEGRATING SOLAR ENERGY INTO AN URBAN SMALL-SCALE ANAEROBIC DIGESTER FOR IMPROVED PERFORMANCE

3.1 Introduction

In 2014, the US Department of Energy released a comprehensive climate change action plan to reduce methane emissions by targeting biogas production from organic waste with the overall goal of reducing greenhouse gas emissions by 25% by 2020 [46]. The study states that in the U.S. there are currently over 2,000 biogas facilities in operation with the potential for over 11,000 further systems to be implemented by 2030. As a waste-to-energy technology, anaerobic digestion represents an opportunity to greatly reduce greenhouse gas emissions while also providing a carbon-neutral source of heat and electricity.

The anaerobic digestion of OFMSW is feasible at smaller scales than currently being employed on farms and wastewater treatment facilities and can also be adapted to different urban environments. As fossil fuel prices continue to rise, implementation concerns with regards to the energy demand for maintenance of near constant temperatures (35°C for mesophilic and 55°C for thermophilic systems) need to be weighed against the energy content of the produced biogas [47][48][49]. At smaller scales and in colder climates, a larger percentage of the biogas produced is needed to heat the digester. If solar energy is used as the primary energy source for maintaining digestion process temperatures, the high methane content (60-70%) biogas produced from OFMSW could be made available for higher value energy applications (building heating, biofuels) [50].

In this chapter, the feasibility of using an air source heat pump (ASHP) to transfer the solar heat gains of a greenhouse to a 30m³ mesophilic digester located adjacent on the roof of an urban building in the downtown area of Montreal, Canada, is investigated during the coldest month of the year. A heat loss model for an insulated tank and a heat pump heat transfer model have been developed. Hourly ambient temperatures, dew point temperatures, and wind speed data from National Resources Canada were used for the month of January 2012. In order to calculate the solar energy available during this time to heat the digester, a 3-D model of the proposed building and the neighboring buildings has been constructed. The model is analyzed for hourly solar radiation with the shadowing effect of surrounding buildings considered to increase the accuracy of calculations.

3.2 Description of the Proposed System

The anaerobic digester tank is to be located outdoors, adjacent to an existing greenhouse with a volume of 1725 m³ and 627 m² of surface area on the roof of a 13-story building at a height of 43 meters oriented south by southwest. Instead of being vented to the atmosphere, the low-grade heat that builds up in the apex of the greenhouse during the day will be ducted to an air source heat pump, upgraded, and used as the main heating source for the digester. In order to ensure stable and optimum biogas production, the OFMSW slurry in the tank requires minimal daily temperature fluctuations as the bacteria are sensitive to temperature shock.

The tank proposed is a 30,000 liter polyethylene rainwater storage tank with a diameter of 4.3 m, a height of 2.6 m, and wall thickness of 0.025m. Polyurethane spray foam is considered for tank insulation as it will provide a uniform covering without seams and will therefore have lower heat losses than using Rockwool insulation plus aluminum or steel cladding. Insulation for

the tank bottom is selected to be 0.076 m foam glass insulation. The bottom of the tank is resting on 0.2 m of concrete with an indoor temperature of 20°C maintained below. A diagram of the proposed ASHP system and urban rooftop location can be seen in *Figure 1*.

For this system a mesophilic temperature range (35°C) with a 30 day retention time has been chosen as opposed to a thermophilic system (55°C) due to the fact that when dealing with a small-scale system in a cold climate, the heating requirements as well as insulation requirements will be considerably lower. It is plausible that any surplus yield in energy production from a slightly higher biogas output available from thermophilic digestion would be less than the increase in energy demand required to increase process temperature by 20°C or 35%. Although thermophilic digestion allows for smaller digester size (a possible benefit for urban implementation) there are other issues to consider as well. Thermophilic digestion allows for shorter retention times for similar methane production as mesophilic digestion, but it has been shown that the treatment of substrates with high biodegradability as well as variability, like food waste, can lead to increased acidity as the volatile fatty acids produced build up faster than the methanogens can convert them, leading to a generally more unstable system [51].

The system being investigated includes a smaller hydrolysis tank located indoors with a grinder attached to the top that the food waste (diluted with warm water) is loaded into on a daily basis. Fresh substrate is added to the main digester tank outdoors through a three way valve that leads to a circulation loop with heat-jacketed piping that provides heating and additional stirring of the tank slurry. There should be little if any heat shock to the system from loading fresh food waste.

The normal stable temperature range for mesophilic digestion occurs around 35°C +/- 3°C [52]. In the *Municipal Wastewater Treatment Manual of Practice* it states that the daily temperature variation for an anaerobic digestion system should not exceed 0.6-1.2°C [52]. These temperature ranges will be taken into consideration when determining the feasibility of simulated tank temperature fluctuation when heating with the air source heat pump.

The system is investigated during the month of January, the coldest month of the year, which has an average of 8 hours of usable solar radiation. Once the sun sets in the evening, the digester tank will receive no heating for approximately 16 hours until the next sunrise. A heat loss model of the system was developed in order to verify insulation requirements and ensure the feasibility of stable biogas production under these cold-climate operating conditions.

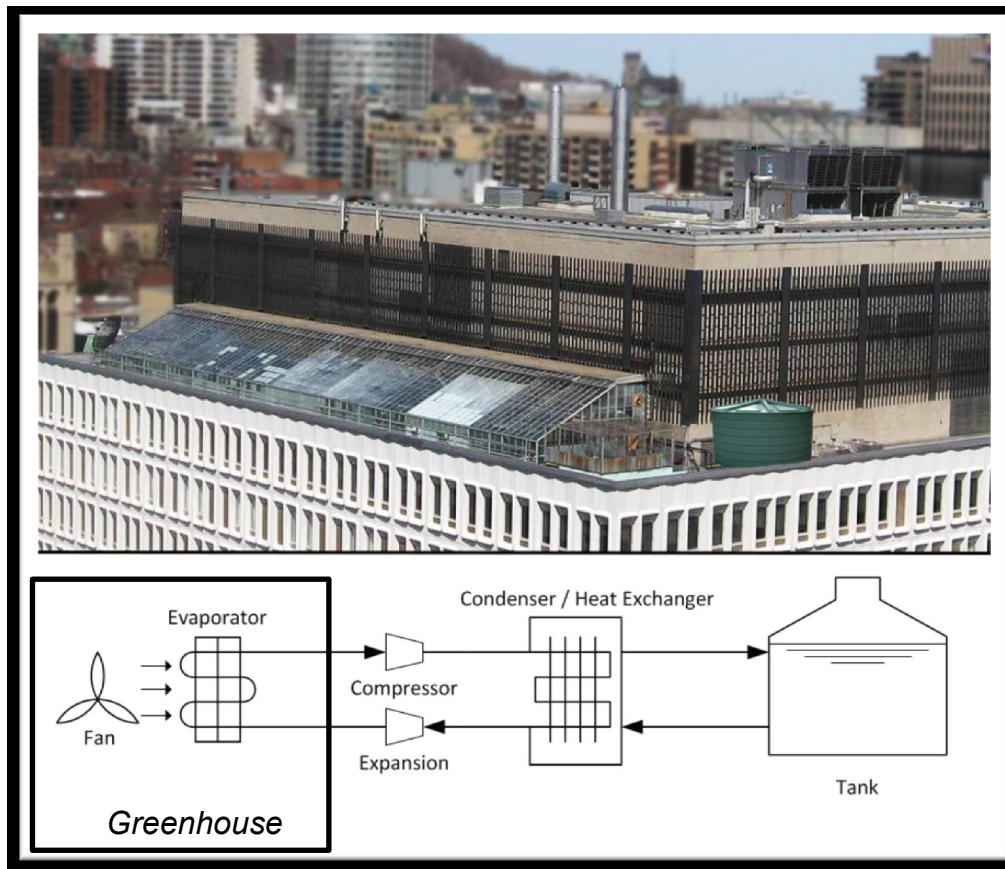


Figure 3.1 Diagram of proposed system location with air source heat pump diagram.

3.3 Digester Tank Heat Loss Modeling

A basic electrical equivalent model of the thermal model of the system is shown in *Figure 3.2*. Due to the fact that the tank will be stirred for fewer than 8 hours per day, it is assumed that the slurry is stationary and there is no internal convection between the slurry and the tank walls or the slurry and the gasses located above. It is also assumed that the gas is the same temperature as the slurry. In *Figure 3.2*, conductive heat losses propagate from the thermal capacitance (*Thermcap*) through the walls, roof, and floor of the tank and then continue through the insulation and are referenced as $R_{condtank}$ and $R_{condinsul}$ for each of the branches in the diagram. In the case of the floor, the heat losses continue through the insulation to the concrete below in an effort to equalize with the indoor temperature maintained at 20°C ($T_{indoors}$). From the outer shell of the wall and roof insulation, forced convection losses occur in parallel with radiation losses to the sky and are labeled as $R_{convinsulair}$ for the walls and roof branches. Due to the fact that the actual ambient temperatures, sky temperatures, and the wind speed values required for an accurate simulation are neither constant nor sinusoidal, a more flexible and dynamic model is required. A model of the system that includes input tables for measured hourly weather data (temperature, wind speed) was developed using Wolfram's *System Modeler*. An air source heat pump model was developed and connected to the thermal capacitance of the tank as a heat source. Additionally, the model could be expanded to allow for multiple types of heating inputs in parallel. The *System Modeler* schematic overview can be seen in *Figure 3.3* with nested models for the heat pump, T_{sky} calculation, and wind speed coefficients for the convection modules.

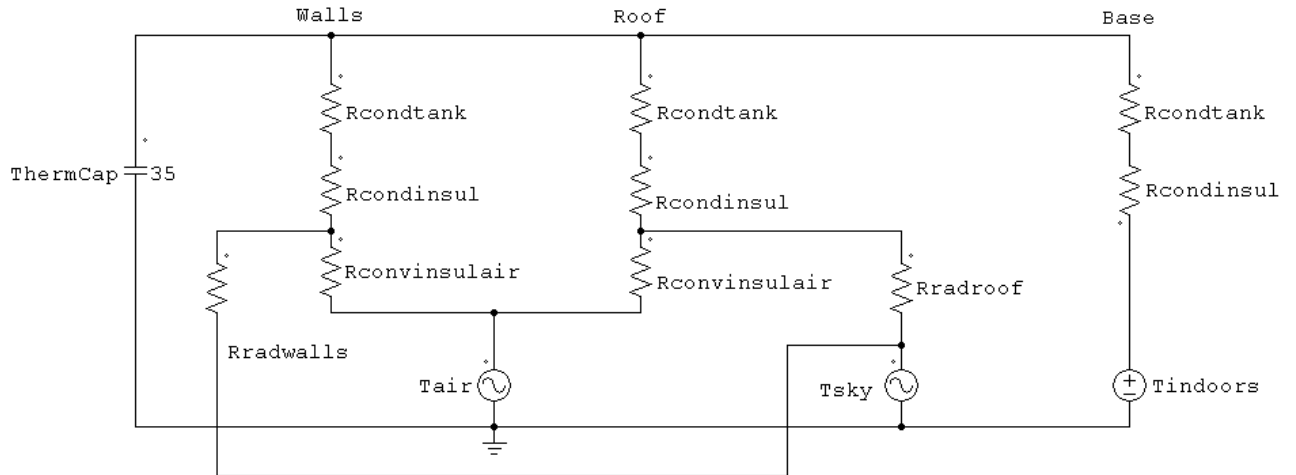


Figure 3.2 Electrical equivalent thermal model of the proposed tank showing conductive, convective, and radiative loss paths.

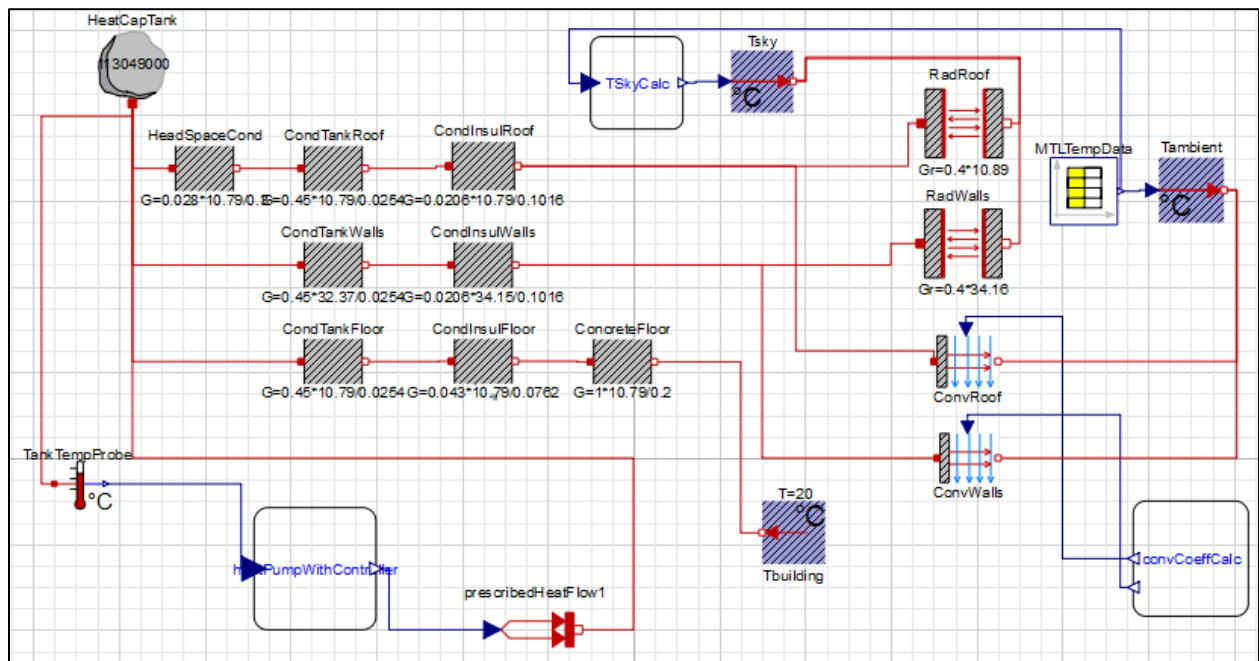


Figure 3.3 Heat loss model for digestion tank including air source heat pump input.

The components of *Figure 3.3* include a heat capacity module, three parallel branches of conduction modules for the headspace, polyethylene tank and insulation floor, walls, and roof, two forced convection modules for the walls and roof in series with the conduction modules with inputs for height-corrected wind speed data, two radiation modules for the tank walls and roof in

parallel with the convection modules that are connected to the sky temperature which is derived from hourly dew point and ambient temperature data. A constant internal building temperature was set at 20°C.

The thermal conduction properties and surface areas of the tank and insulation are shown in *Table 3.1*. The System Modeler heat transfer conduction modules require only the thermal conductance in (W/K) to be input for each conduction component. For the convection modules, the convective thermal conductance (G_c) is required and the following equation (defined in the module) for forced air convection is needed as an input parameter:

$$G_c = Area * 7.8 * (windspeed \text{ in } m/s)^{0.78} \text{ in } W/(m^2 * K) \quad (3.1)$$

The wind speed data was obtained by adapting NRCAN measurements taken at 10 meters and correcting for building height by using the power law described in *Equation 2* [53]:

$$v_w(h) = v_{10} * \left(\frac{h}{10}\right)^a \quad (3.2)$$

Where:

$v_w(h)$ = velocity of wind at height h (43m) in m/s

v_{10} = velocity of wind at height of 10 meters in m/s.

a = Hellman exponent (*for stable air over inhabited areas, $a = 0.34$*)

Sky temperatures needed for determining radiative losses were calculated using the ambient and dewpoint temperatures and the algorithm described by *Equations 3 and 4*.

$$T_{sky} = \epsilon_s^{\frac{1}{4}} * T_{ambient} , \quad (3.3)$$

where T is in K , and ϵ_s is the emissivity of the sky and can be described by:

$$\epsilon_s = 0.787 + 0.764 * \ln\left(\frac{T_{dew}}{273}\right) \text{ according to [54,55].} \quad (3.4)$$

The radiation heat transfer blocks are calculated by the radiation conductance equations:

$$Q_{flow} = Gr * \sigma (T_{portA}^4 - T_{portB}^4) \quad (3.5)$$

$$G_r = e * A \quad (3.6)$$

Where σ is the Stefan-Boltzmann constant ($\sigma = 5.670373 \times 10^{-8} \text{ W m}^{-2} \text{ K}^{-4}$), e is the emission value of object from 0 to 1, and A is the surface area of the object. The emissivity of the spray foam insulation was selected to be 0.4 from manufacturer specifications.

The heat capacity value for the tank was determined by considering the 30,000 liter tank to be 90% full with 27,000 kg of OFMSW slurry at < 15% total solids. Considering the mix to have the same specific heat capacity as water gives a value of approximately 113 MJ/K. The ASHP heat input module shown in *Figure 3.3* is described in detail in a later section.

Table 3.1 Heat conduction characteristics of digestion tank and insulation.

	Area (m ²)	Thermal Conductivity (W/m*K)	Thickness (m)	Thermal Conductance (W/K)
Poly Tank Walls	32.37	0.45	.0254	573.55
Spray Foam Walls	34.15	.0206	.1016	6.92
Poly Tank Roof	10.79	0.45	.0254	191.16
Spray Foam Roof	10.79	0.0206	.1016	2.20
Foam glass bottom	10.79	0.043	.0762	6.08
Cement base	10.79	1	.200	53.95

3.4 System Model with no Heating Added

In order to confirm the tank is properly insulated for the climate, the heat losses of the digester tank are simulated with no heat source applied in order to determine how much the

internal temperature of the tank will drop during a full week without heating. The hourly temperature fluctuations in T_{ambient} , T_{dewpoint} , and T_{sky} are shown in *Figure 3.4* for the week of January 14th to the 21st, 2012 (coldest week of the year). Similarly, the hourly wind speed fluctuation (in m/s) at 43 meters for the same time period can be seen in *Figure 3.5* [56]. In *Figure 3.6*, the heat losses are shown for the week as well as the average heat loss value of 392 W. The results of the simulation show a drop of 0.3°C per night totalling a drop of 2.1°C for the week in the temperature of the slurry in the tank (*Figure 3.7*). This simulation anticipates the case where there is a full week of severe cloud cover with little solar radiation and the ASHP is not in use or a case in which the heating system has been shut down for a week for maintenance or repair. A temperature drop down to 32.3°C still maintains the system above the lower limit of acceptable temperature fluctuation for mesophilic anaerobic digestion (32-38°C) but the average gas production will decrease.

Further experimental research is needed in order to know the effect that small daily temperature fluctuations will have on the amount and composition of produced biogas, but a preliminary estimate can be performed using a modified de van't Hoff-Arrhenius equation [57]. This equation provides a way of estimating how the reaction rate (k) changes in relationship to changes in temperature.

$$\frac{k_2}{k_1} = e^{\left[\frac{E_a(T_2-T_1)}{RT_1T_2}\right]} \quad (3.7)$$

In this equation, k_2 is the reaction rate at T_2 , and k_1 is the rate of reaction during standard operating conditions at T_1 (35°C). E_a is the energy of activation of the reaction. In this case, the energy of activation constant functions as a measure of the temperature response of the bacteria. This parameter can be determined experimentally or it can be selected from literature. For this

model, an E_a of 63,492 J/mol is chosen based on [58]. R is the ideal gas constant for biogas with 65% methane and 35% CO_2 and is calculated as 8.3144 J/mol*K.

The reaction rate (k) is proportional to the biogas production rate of the system and thus an estimation of theoretical biogas production can be made. For mixed food waste, a year-long study performed by the Environmental Protection Agency in East Bay, California, fed 100 tonnes of mixed food waste daily into a mesophilic digester and yielded an average of 367 m^3 of biogas per dry tonne added, with a 65% methane content [59]. The energy value of biogas with a 65% methane content is 6.25 kWh/m^3 . This means there is approximately 2.3 MWh of energy available from each dry tonne of food waste. *Figure 3.8* provides a theoretical comparison of biogas production versus temperature fluctuation of the anaerobic digestion system based on *Equation 3.7* and the experimentally determined biogas yield per dry tonne from literature.

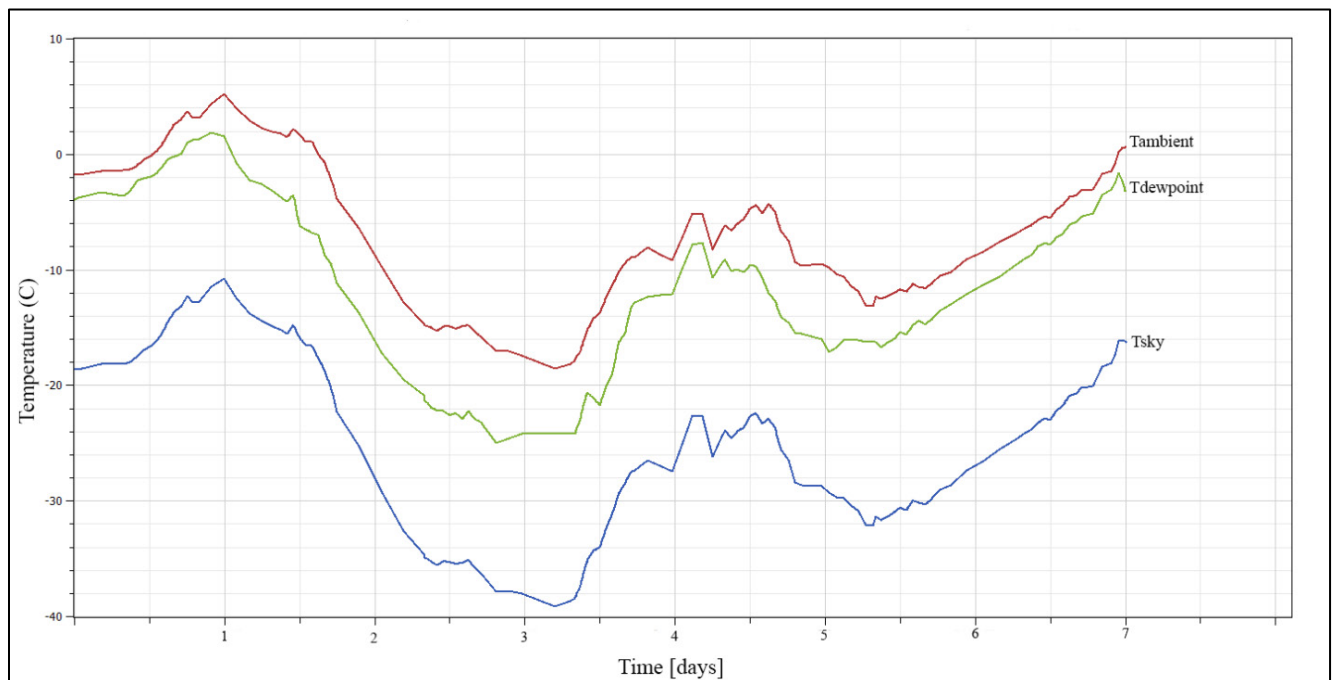


Figure 3.4 Hourly temperature fluctuation ($^{\circ}\text{C}$) in T_{ambient} , T_{dew} , and T_{sky} for January 14-21, 2012, starting at 4pm on January 14.

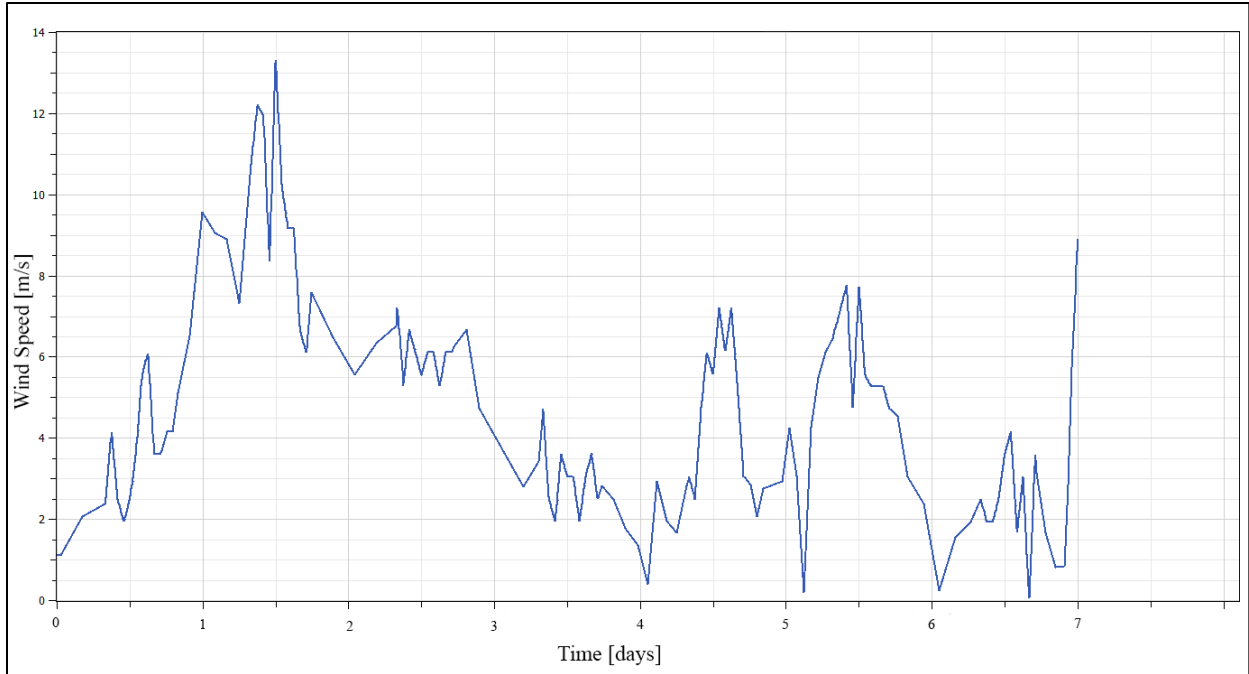


Figure 3.5 Wind speed fluctuation in m/s during the proposed week in January, 2012.

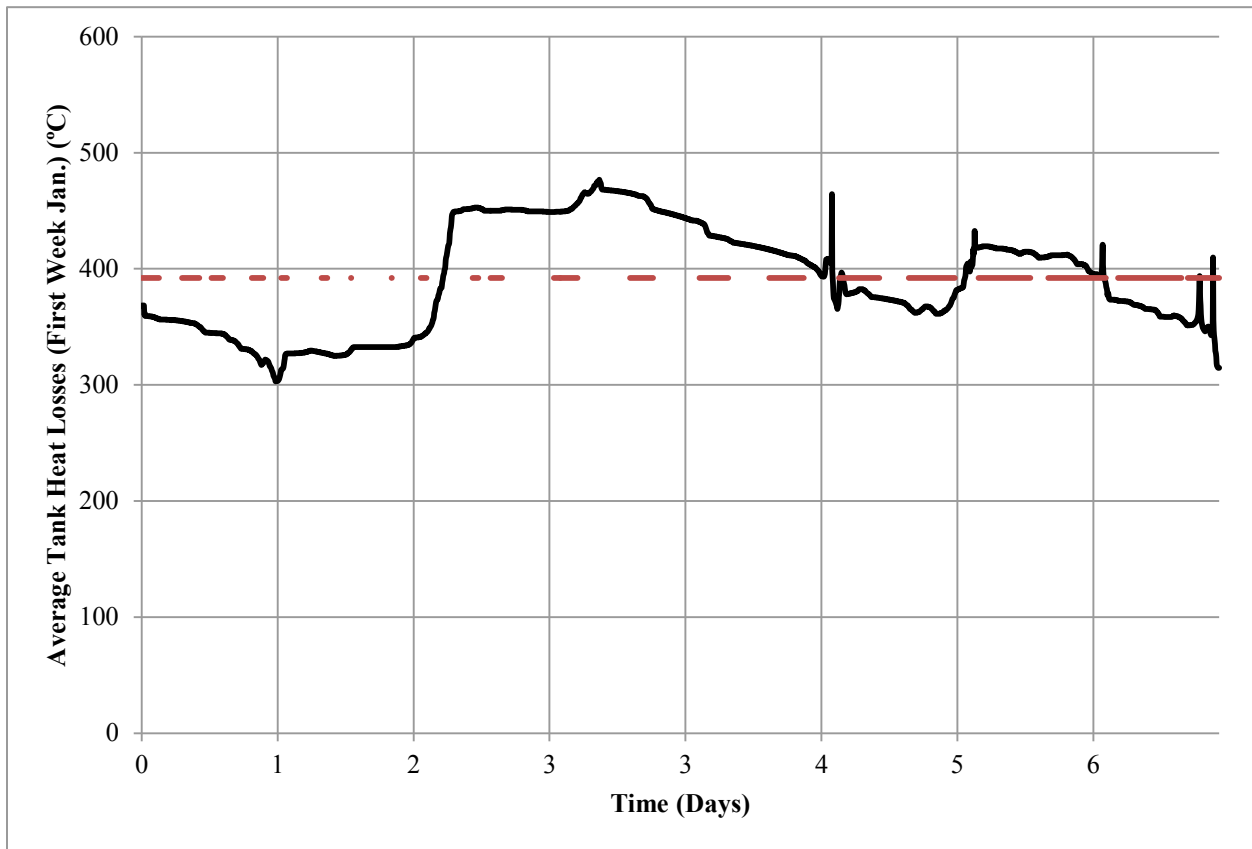


Figure 3.6 Tank Heat losses in Watts for the week with an average value of 392 W shown in red.

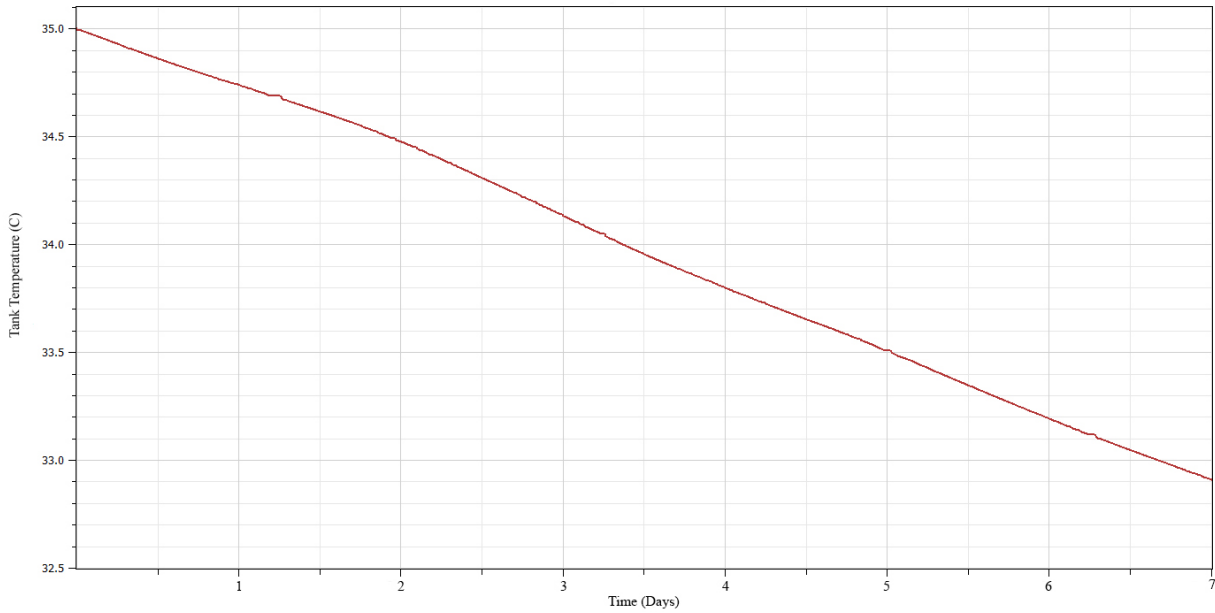


Figure 3.7 Internal tank temperature drop from 35°C with a week of no heating beginning at sundown on Jan 14, 2012.

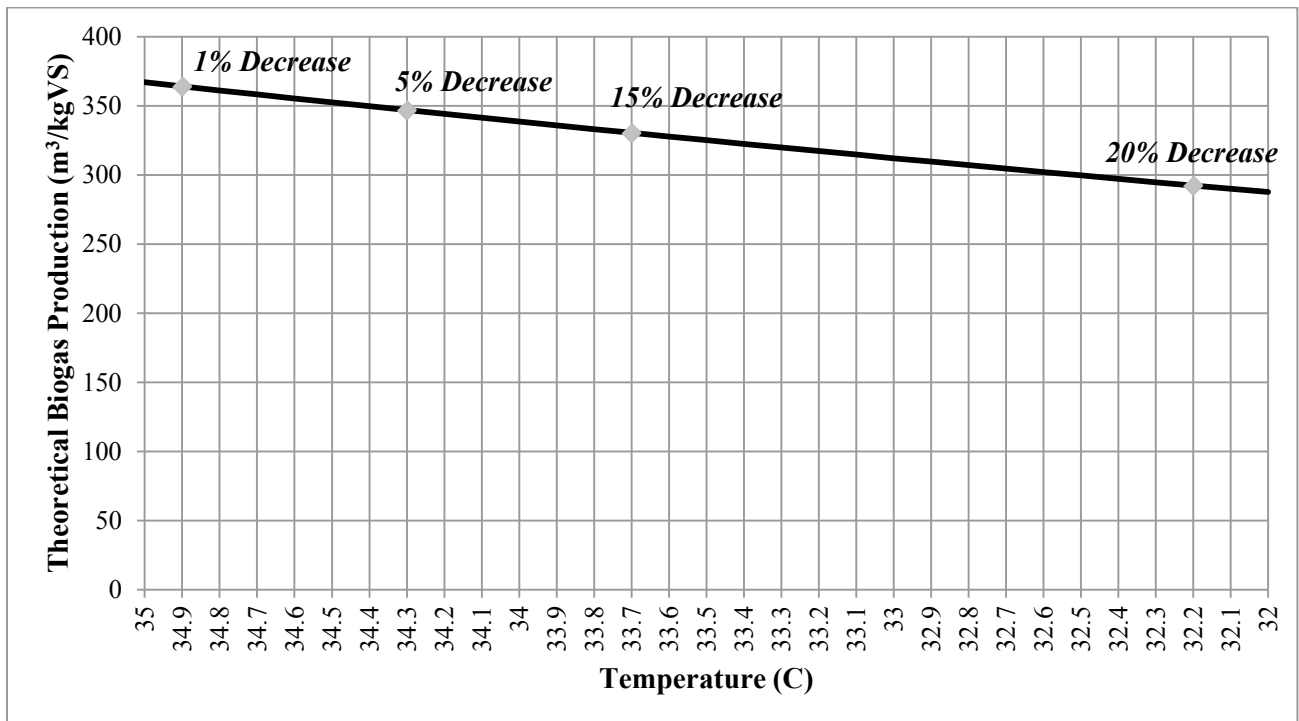


Figure 3.8 Theoretical effect of temperature decrease on biogas production of mesophilic OFMSW digester.

3.5 Solar Energy 3-D Model

Before the heat pump model can be implemented, it is necessary to investigate the total solar insolation and subsequent heat gains occurring in the greenhouse during the month of January. The greenhouse under investigation has a surface area of approximately 627 m² and an internal volume of 1,680 m³. The greenhouse is heated in the winter via the building's hot water radiator system with a set point of 20°C. A diagram of the greenhouse with dimensions can be seen in *Figure 3.9*. For the greenhouse model, the properties of materials selected for the glass, the frame, and the front wall and flooring are shown in *Table 3.2*.

Table 3.2 Greenhouse materials and properties selected in Ecotect modeling software.

	Double Glazed Low E Aluminum Frame Windows	Concrete front wall	Concrete Floor
Emissivity	0.1	-	-
U-value (W/m2.K)	6.5	1.8	0.88
Admittance (W/m2.K)	2.38	3.36	6
Solar Heat Gain Coeff.	1	0.7	0.65
Visible Transmittance (0-1)	0.91	0	0
Refractive Index of Glass	1.74	-	-
Thickness (mm)	5	130	200
Thermal Decrement (0-1)	-	0.78	0.3
Thermal Lag (hours)	-	5	4.6

According to NRCAN, there is an average hourly insolation of approximately 150-170 W/m² for the month of January and a total average insolation of 94-107 kW available for each of the 8 hours of daylight [56]. Considering the fact that the digester tank has a heat capacity of 31kWh/°C (113 MJ/K), it would require 10-15% of the solar energy added to the greenhouse to heat the tank by 1°C over the course of 4 daylight hours. This provides a reasonable first estimate of the amount of solar energy available but these insolation values are based on a southern-oriented, flat surface at ground level located outside of the urban center. A more detailed solar energy calculation is necessary in this case due to the effect that the shadows of surrounding buildings can have on net insolation. In order to do this, a geographically accurate 3-

D model was constructed of the building under investigation as well as the surrounding buildings using *Google Earth* data and municipal zoning maps. The 3-D model is shown in *Figure 3.10* with the greenhouse under investigation visible on the roof of the building atop the z-axis.

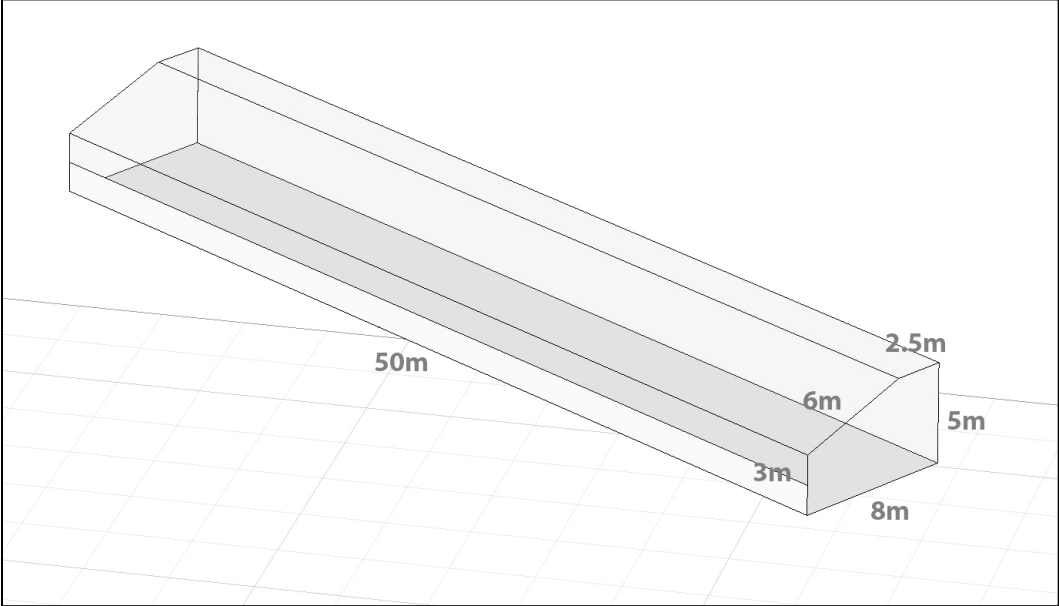


Figure 3.9 Dimensions of greenhouse being investigated.

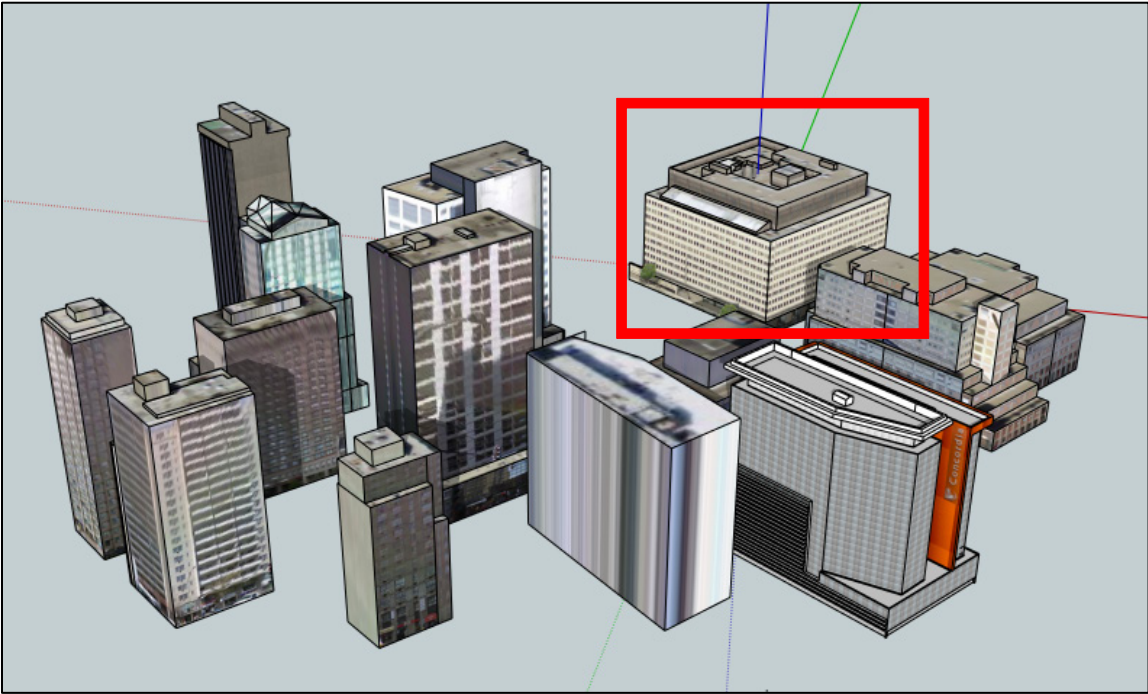


Figure 3.10 3-D model of the proposed greenhouse location and surrounding buildings.

Once constructed, the 3-D model was analyzed for direct and diffuse solar radiation using the Autodesk's *Ecotect* solar access analysis software. Solar analysis was performed on an hourly basis with and without the shadowing effect of surrounding buildings considered. *Figure 3.11* shows the annual path of the sun around the buildings being considered. In *Figure 3.12*, a graphic representation is provided of how the shadowing effect is implemented in the software with the greenhouse highlighted for visibility. Due to the fact that the digester tank is located in the shade for the majority of the time, the incident solar radiation is not considered in this model.

The temperature gains inside the greenhouse during the month of January were determined by comparing the total heat losses in the greenhouse with the total hourly heat gains absorbed by the greenhouse. From the *Ecotect* simulation, the total thermal admittance of the greenhouse is calculated to be 4,784 W/K. The hourly temperature rise was calculated by *Equation 7* which takes into consideration an estimated energy transfer from the greenhouse to the heat pump of 6 kW (verified in the next section).

$$\text{Total Heat Gain (W)} - 6 \text{ kW} = \text{Total Admittance over Surface Area of Greenhouse} * (\Delta T) \quad (7)$$

For the first hour of positive heat gains, the resulting temperature increase was added to the baseline temperature (21°C) and each hour of daylight with positive heat gains was calculated in the same way. The resulting daily temperature increases in the greenhouse were averaged for each week of January and the results are shown in *Figure 13*. These results were input to the heat pump model as hourly evaporator input temperatures.

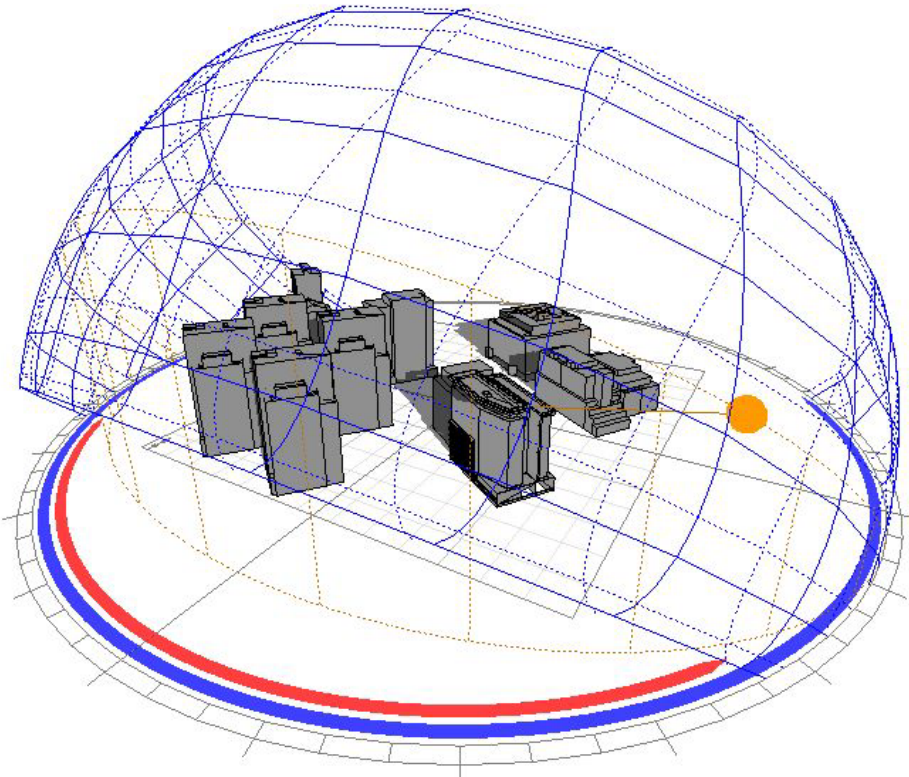


Figure 3.11 Annual path of sun around location being investigated.

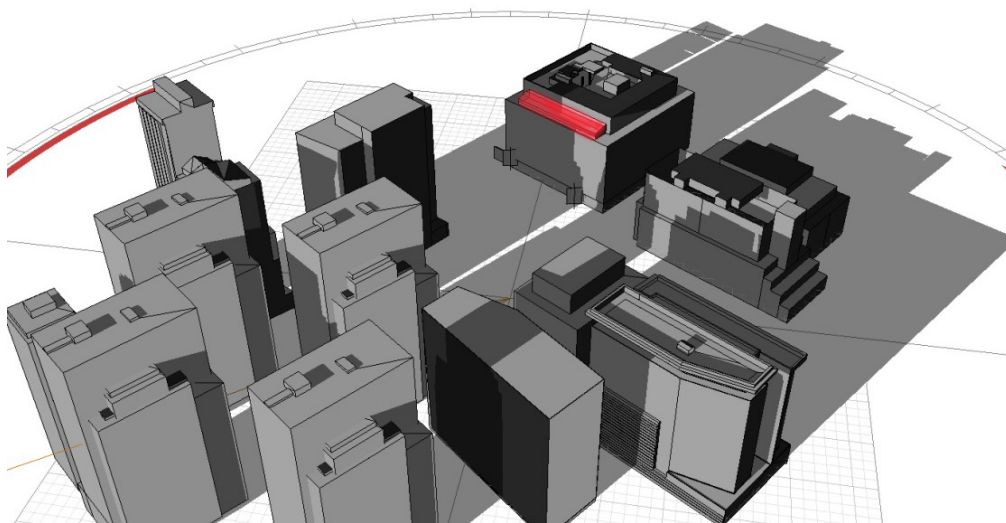


Figure 3.12 Shadowing effect of surrounding buildings.

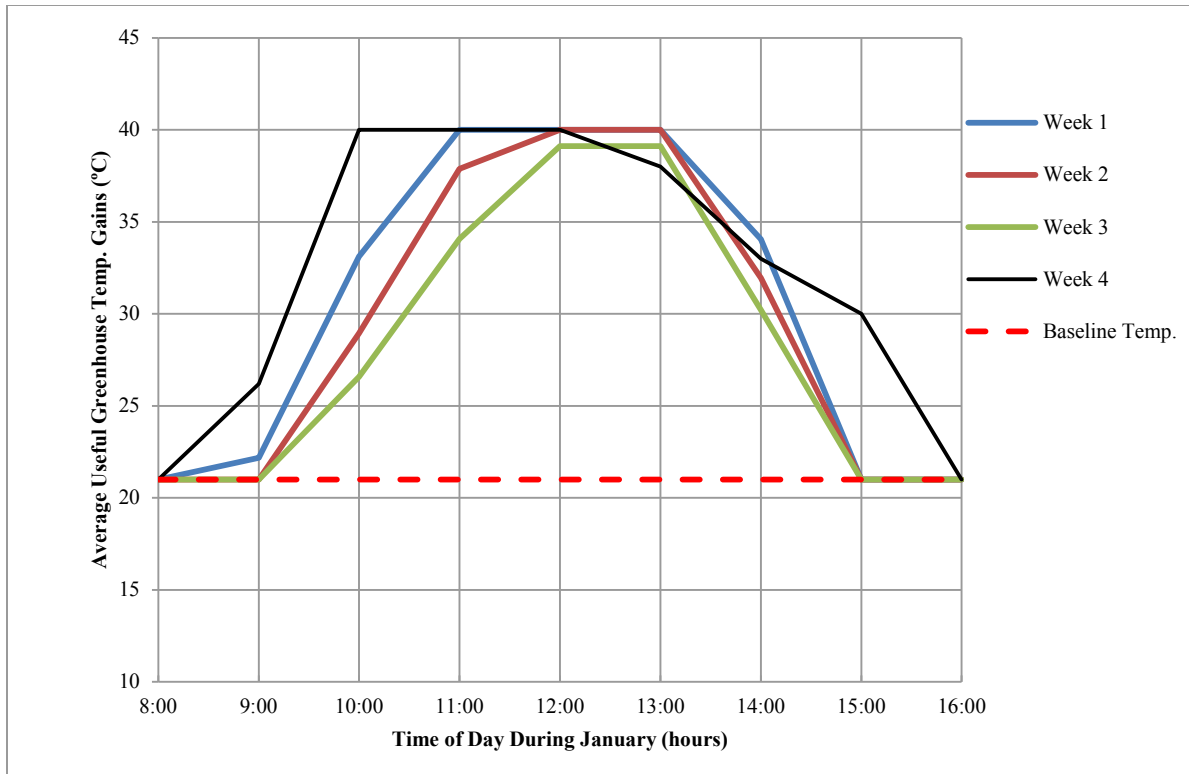


Figure 3.13. Average useful weekly temperature gains in greenhouse from solar radiation above baseline temperature for the month of January

3.6 Air Source Heat Pump Heat Transfer Model for Digester Tank

In order to provide an energy efficient heat source for this urban anaerobic digestion process, the feasibility of an air source heat pump (ASHP) has been investigated. The proposed heat pump diagram is shown in *Figure 3.14*. In this case, the ASHP uses a vapor compression refrigeration cycle to transfer the daily solar heat gains in the greenhouse via an air-to-water heat exchanger to the slurry circulation system of the digester tank. Often the excess heat that builds up in the greenhouse during the coldest months of the year is vented to the environment and wasted. Modern ASHP manufacturers claim to achieve a coefficient of performance (COP) of 4-5 with an outdoor temperature as low as 5 to 7°C and a leaving hot water temperature of 35°C [60]. Even greater COPs can theoretically be achieved when considering a greenhouse temperature that can routinely surpass 30°C at the apex in the middle of the day even when the

outdoor temperature is below freezing. To make the heating system independent of grid electricity, the compressor and the fan used in the heat pump system (2kW peak) could be powered by a 10-15 solar panel system, but this option is not explored in this research.

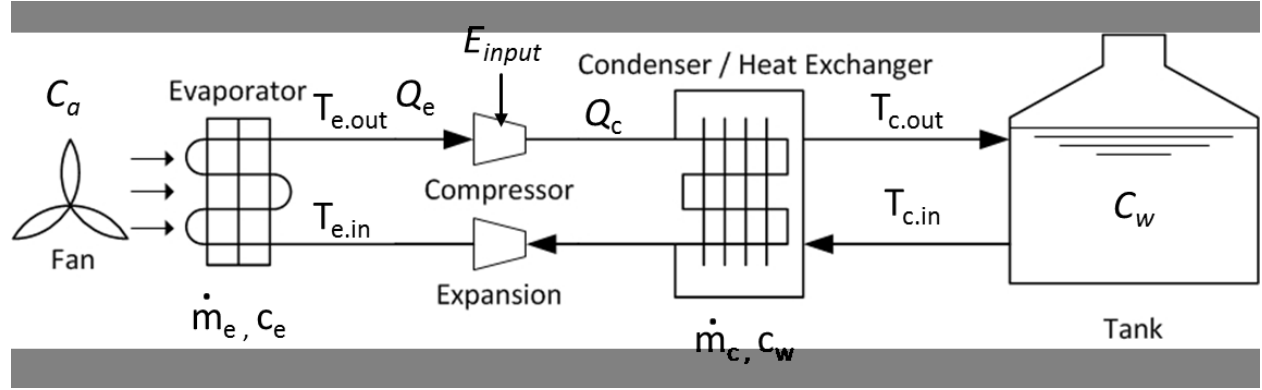


Figure 3.14 Proposed air source heat pump system for digester tank

The heat exchange for the heat pump system shown in *Figure 3.15* is modeled using the system of differential equations given in *Equations 8-14* [61,62,63]. In this model, the condenser and heat exchanger are lumped together and it is assumed that the condenser input temperature is the same as the temperature of the slurry in the tank and the temperature of the condenser output is the same as the water used to heat the slurry via high-efficiency heat-jacketed piping. The evaporator input temperature changes with the estimated greenhouse temperature profiles shown in *Figure 3.13*.

$$C_w \frac{dT_{c.out}}{dt} = \dot{m}_c c_w (T_{c.in} - T_{c.out}) + Q_c \quad (3.8)$$

$$C_w = c_w \cdot \rho_w \cdot V_w \quad (3.9)$$

$$C_a \frac{dT_{e.out}}{dt} = \dot{m}_e c_a (T_{e.in} - T_{e.out}) - Q_e \quad (3.10)$$

$$C_a = c_a \cdot \rho_a \cdot V_a \quad (3.11)$$

$$COP = \frac{(T_{c.out} + 273.15)}{(T_{c.out} - T_{e.out})} (0.4) \quad (3.12)$$

$$Q_c = COP * E_{input} \quad (3.13)$$

$$Q_e = (COP - 1) * E_{input} \quad (3.14)$$

Where \dot{m}_c is the mass flow rate of the condenser in kg/s , \dot{m}_e is the flow rate of the evaporator, T_c and T_e are the temperatures of the condenser and evaporator in degrees C, c_w is the heat capacity of water or $4200 J/kg/K$, c_a is the heat capacity of air or $1000 J/kg/K$, Q_c is the heat rejected by the condenser in W , Q_e is the heat absorbed by the evaporator in W , COP is the theoretical Carnot cycle coefficient of performance of the heat pump scaled by an efficiency estimate of 0.4 for transferring the heat energy in the air to water, C_w is the heat capacity of the tank in J/K , C_a is the heat capacity of the air in the greenhouse in J/K , ρ_a and ρ_w are the densities of air and water, V_w is the volume of the tank, V_a is the volume of the greenhouse, and E_{input} is the $2000W$ electrical input of the heat pump.

The values for the mass flow rates of the condenser ($0.38 kg/s$) and evaporator ($0.11 kg/s$) were extrapolated from the specifications provided by the manufacturer of an $8kW_{thermal}$ ASHP and the standard heat energy equation [62]. A simulation of heating the digester with the ASHP was performed with an input evaporator (greenhouse apex) temperature of $30^\circ C$ and a leaving condenser hot water temperature of $55^\circ C$ (specification of manufacturer). The temperature input to the condenser/heat exchanger changes dynamically with the daily heat losses of the tank and is regulated around $35^\circ C$ using an on/off controller available in *System Modeler*. The on/off controller is only activated during the 8 hours of daylight during the proposed week and is shut off accordingly. The heat pump heat transfer model (*Figure 3.14*) representing *Equations 3.8-3.14* is connected to the heat capacity module of the tank as “*prescribed heat flow*” as can be seen in the overview of the system model presented in *Figure 3.3*.

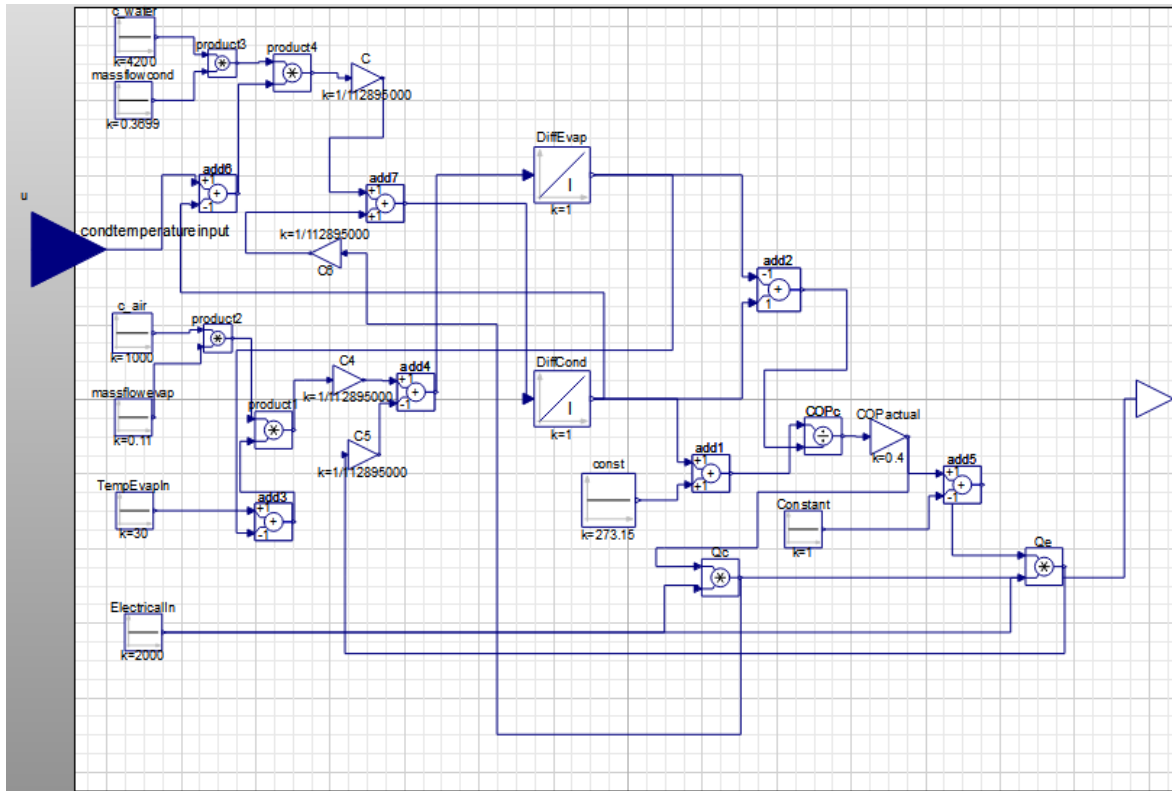


Figure 3.15 Heat transfer model implementation.

3.7 Available Solar Energy with Shadowing Effect

A simulation of the effect that the shadows of surrounding buildings have on the total monthly radiation for the greenhouse is presented in *Figure 3.16*. The results show that the shadowing effect leads to 25% lower solar radiation than the case where it has not been taken into consideration. The daily average radiation for the whole month was calculated to be 170 W/m² for the greenhouse without the shadowing effect and 126 W/m² with shadowing. The total radiation on the greenhouse surface (627 m²) was calculated to be 107 kW per hour for no shadowing and 80 kW per hour with shadowing.

Although the shadowing effect averaged over the month has a 25% effect on the total solar radiation, on specific days the effect can be as much as 80% which needs to be taken into consideration when designing an ASHP heating system. For example, the total radiation for

the 16th of January is shown in *Figure 3.17*. On this particular day there are regular daylight hours where the combination of cloud cover and the shadowing effect have effectively removed any direct or diffuse radiation. In this case, if the heat pump is running during those hours, it will be increasing the load on the building's existing heating system, defeating the purpose. As the optimum temperature range for a greenhouse is between 15-25°C, a temperature set point could activate the heat pump when the greenhouse temperature surpasses 25°C in the lower portion and/or the apex temperature surpasses 30°C. This would signify sufficient solar heat gains and prevent the need to open windows to decrease the greenhouse temperature.

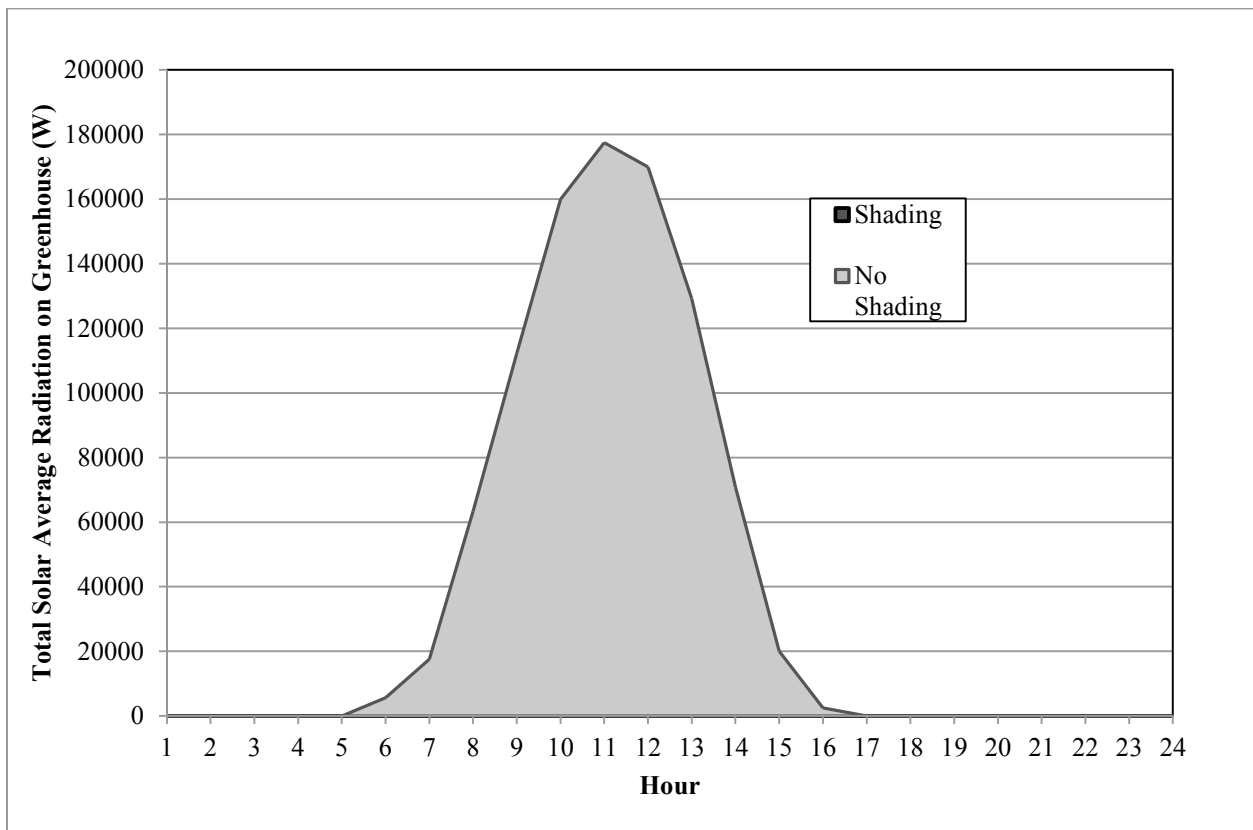


Figure 3.16 Total average hourly total solar radiation for the month of January.

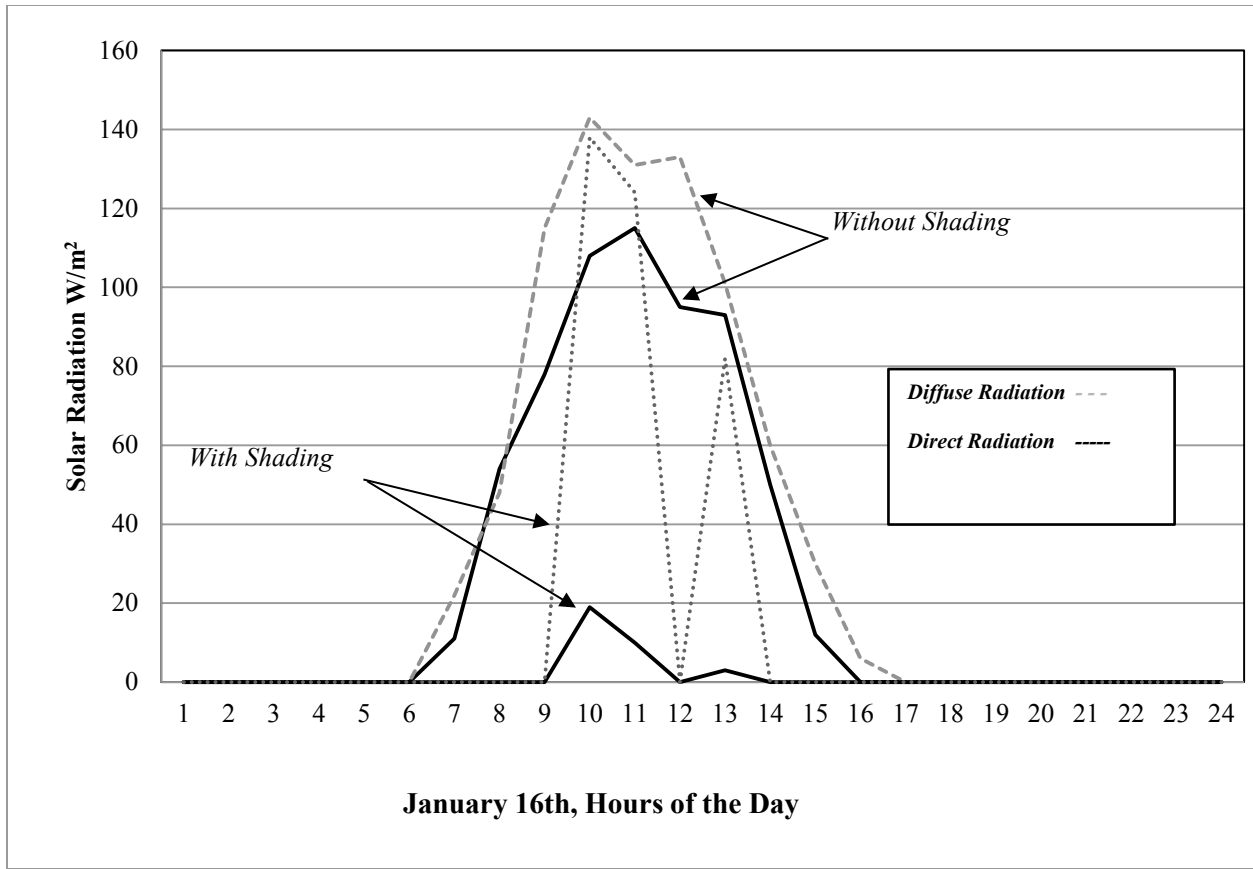


Figure 3.17 Analysis of shading effect on total solar radiation for a single day, January 16th.

3.8 Heat Loss Model with Air Source Heat Pump

Using temperature and wind speed data for the full month of January, 2012, shown in *Figures 3.18* and *3.19*, with weeks delineated by alternating shaded blocks, a dynamic simulation of the system was performed with the heat pump providing a daily heat input. The resulting tank temperature fluctuation is shown in *Figure 3.20*. The temperature drop during each night is between 0.2 - 0.25°C and the temperature of the slurry is returned to the requisite 35°C within two hours of the return of solar radiation. The tank requires a total of 8-10kWh of heating energy or 6-8kWh of solar heat gains from the greenhouse to correct the temperature drop. This represents 1-2% of the total daily solar radiation or 10% of the hourly solar radiation available

during the hours of operation. The daily energy input from the heat pump operating with a COP of ~4.1 (as predicted by the manufacturer) can be seen in *Figure 21*. Referring back to the gas production versus temperature graph shown in *Figure 3.8*, the expected gas production would only decrease 1-2%. This temperature fluctuation falls within the range of standard operating conditions.

Another simulation was performed for a case where the heat pump was used every other day during daylight hours. The temperature fluctuation ranges from 0.5-0.6°C in this case and can be seen in *Figure 3.22*. The heat pump model provides 8.25 kW of constant thermal energy and returns the tank temperature to 35°C in 2-3 hours. Referring again to *Figure 3.8*, the theoretical biogas production of the system could be reduced by up to 5%.

An extreme case was also simulated where the heat pump is active for only 10 days out of the month (or 33% of the daylight hours), including a full week with no heating. The resulting temperature fluctuation is shown in *Figure 3.23* and ranges from 0.25°C up to 2.1 °C. It can be seen in the figure that after a week of no heating, it only take the heat pump one daylight cycle to return the system back to the required 35°C. The resulting biogas production from a 2.5°C drop in process temperature could be affected by up to 17% for the week with no heating (see *Figure 3.8*).

It is useful to make a comparison between the proposed ASHP heated anaerobic digestion system and a base case where the digestion system is heated with produced biogas only. For the month of January, the heat demand of the tank to maintain a constant temperature is approximately 393 W. The tank is predicted to produce an average of 312 kWh per day of biogas energy. Assuming that a gas-fired hot water heater attached to the heat jacketed piping is sized at

2 kW – or the smallest possible gas-fired boiler on the market capable of providing the flow rate of hot water necessary to the piping - 48 kWh of biogas energy would be required per day to heat the tank representing 15% of the produced biogas. In the case of a solar-heated digester operating on daily basis, an additional 1.1 MWh of energy would be available for the month of January for higher-value heating applications in the associated building. For the worst case scenario in which the heat pump is only active for 10 days out of month, the available biogas energy would be similar to the biogas heated base case as the biogas production could drop by 15% as predicted in *Figure 3.8* due to the temperature fluctuation of the slurry.

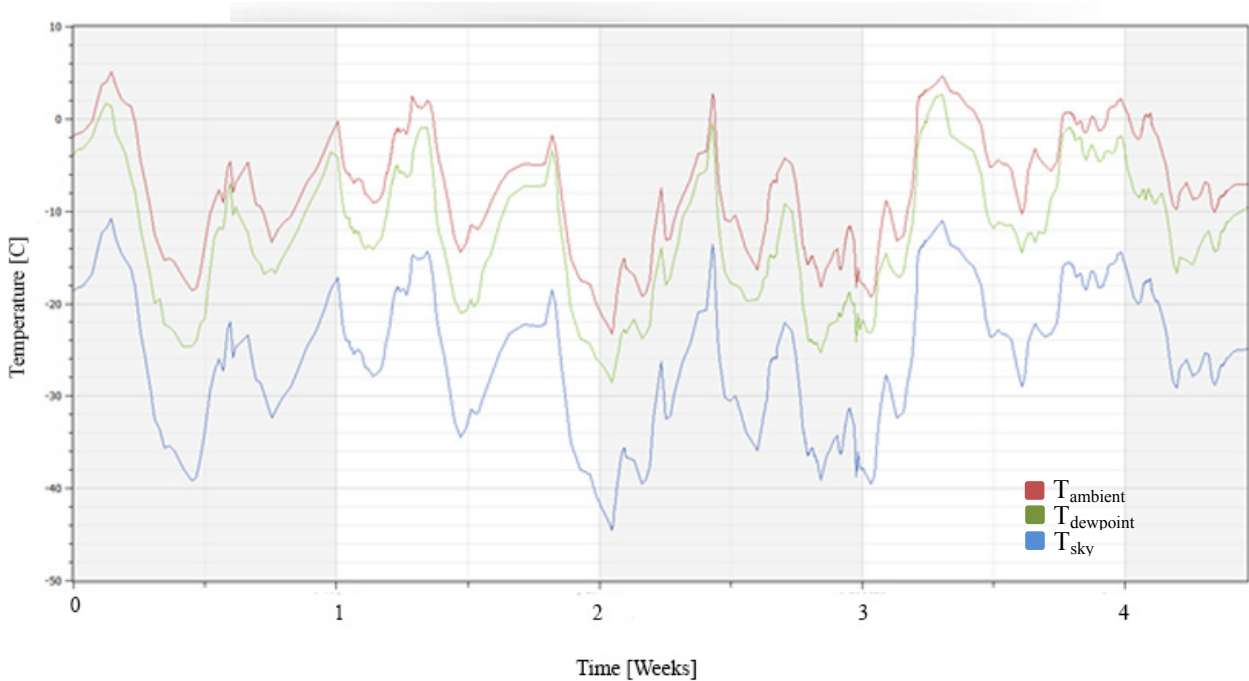


Figure 3.18 Ambient, Dewpoint, and Sky temperature values for the month of January, 2012.

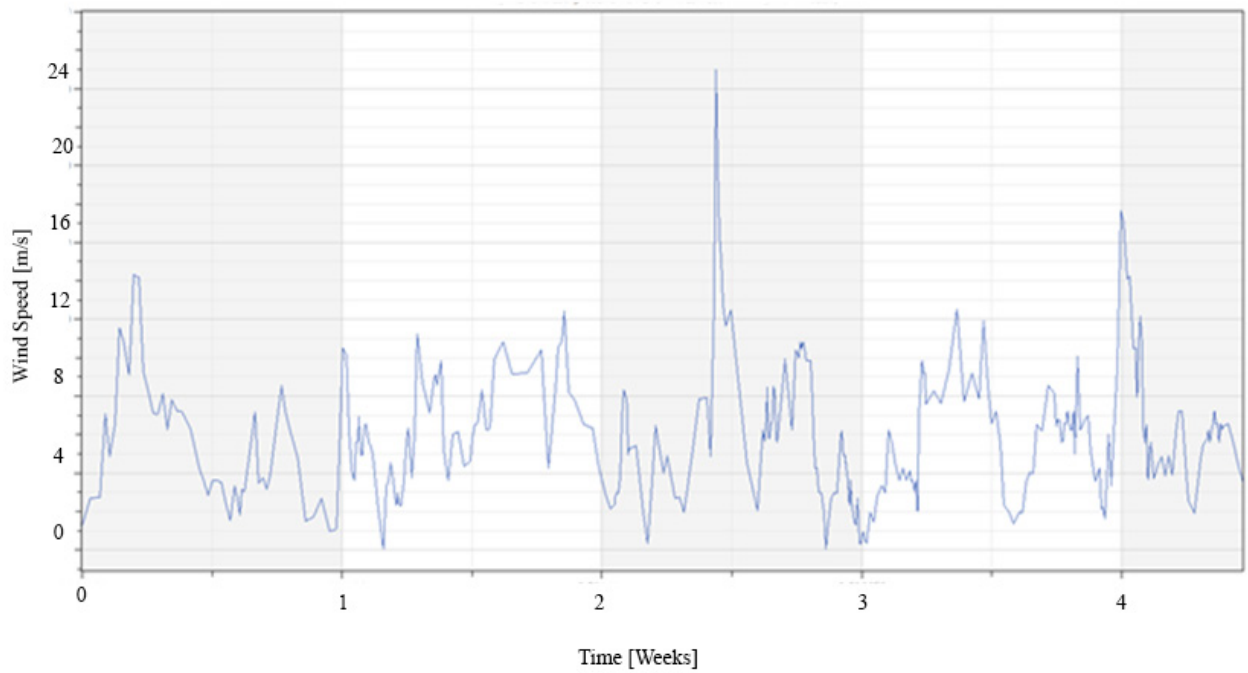


Figure 3.19 Wind speed data input, corrected for height, for the month of January, 2012.

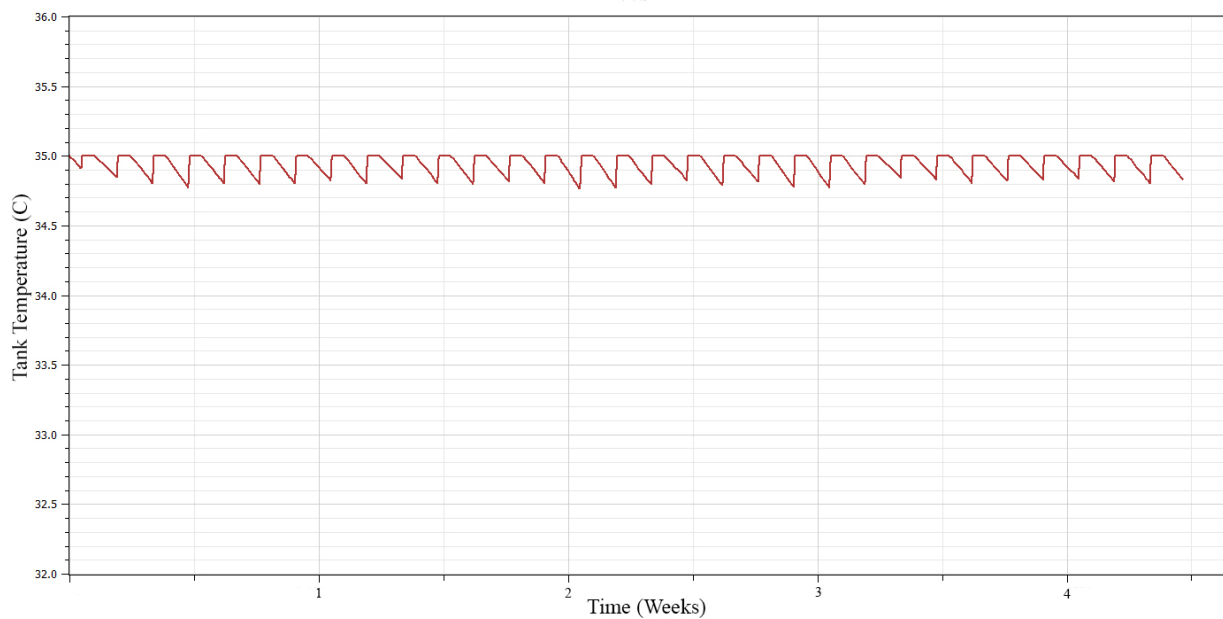


Figure 3.20 Tank temperature fluctuation for the month of January, 2012, with air source heat pump active during daylight hours.

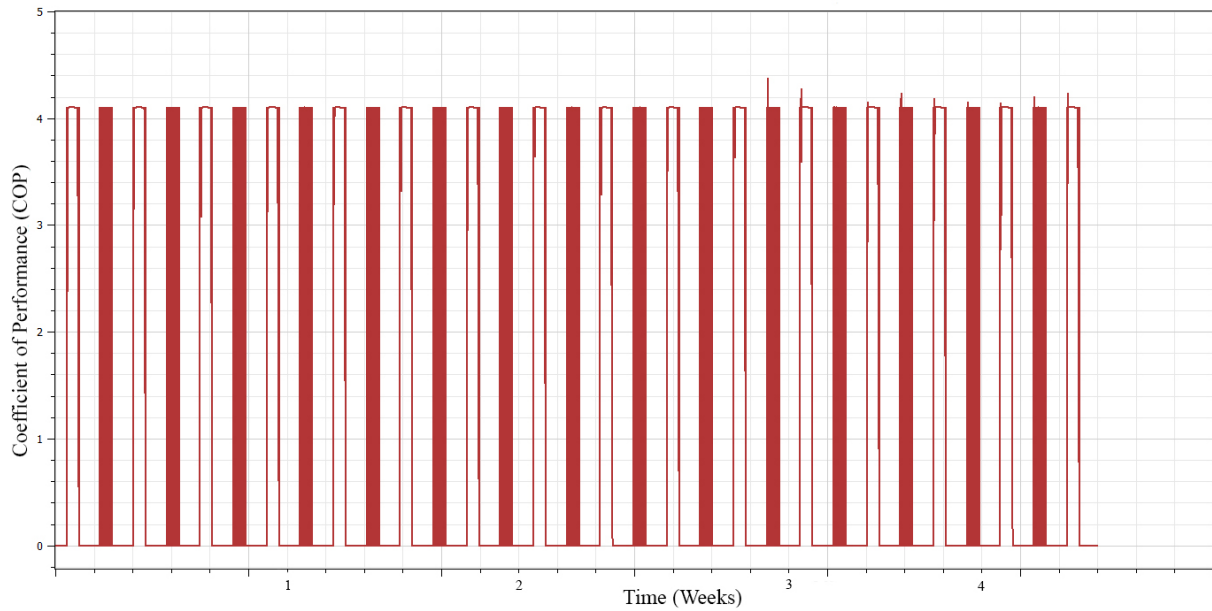


Figure 3.21 Coefficient of performance of heat pump for daily heating in the month of January.

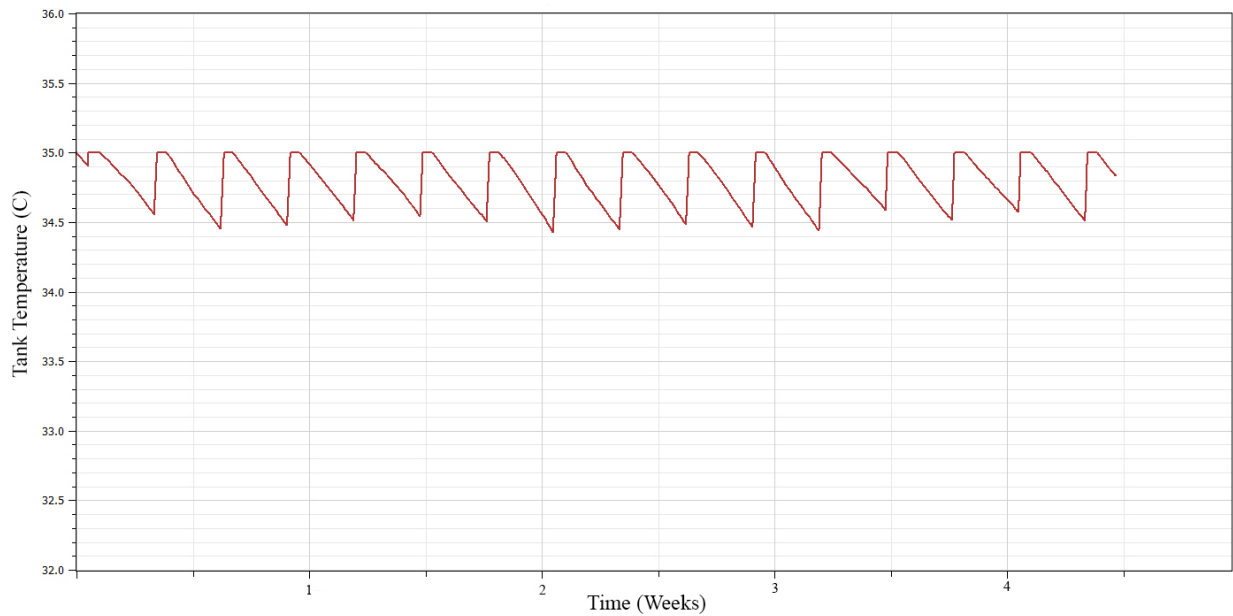


Figure 3.22 Temperature fluctuation for the month of January with heat pump used every other day during daylight hours. Days represented by vertical stripes.

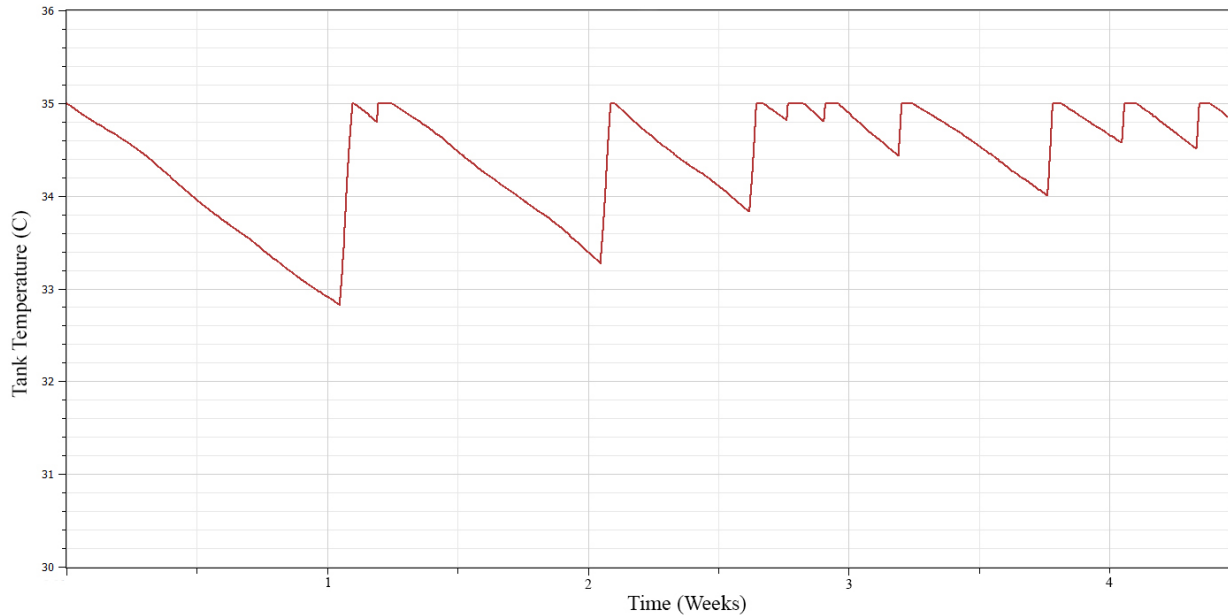


Figure 3.23 Temperature fluctuation for case where heat pump is only active for a third of the daylight hours of January. Weeks represented by vertical stripes.

3.9 Experimental Verification of Temperature Fluctuation in Anaerobic Digestion of Food Waste

In order to verify the effectiveness of solar heating of an anaerobic digestion system, it is first necessary to observe the effect that a small, daily fluctuation in process temperature will have on biogas production. Depending on the insulation of the tank and associated heating pipes, the temperature of the tank could drop anywhere from fractions of a degree up to 4 or 5 degrees Celsius each night during the coldest months of the year. In the case of the AD system modeled for a Concordia University rooftop in the previous sections, it took a full week of no heating applied for the internal temperature of the tank to drop by 2.5°C. An up-flow anaerobic sludge blanket (UASB) Armfield W8 bench-scale anaerobic digestion system will be used for this experimental verification and can be seen in *Figure 3.24*. The system has two temperature

controlled five-liter tanks for digesting various substrates in series or in parallel as well as two five-liter calibrated gas collection tanks.

Anaerobic digestion systems can be run in three different temperature ranges as seen in *Figure 3.25*. The mesophilic and thermophilic temperature ranges are the most commonly used. A recent study on the digestion of OFMSW in Europe shows that through 2014, the cumulative installed systems are approximately 67% mesophilic and 33% thermophilic [64]. Due to the lower temperature and energy demand needed for digestion, as well as being more biologically stable, mesophilic digesters have been preferred historically. With updates in technology, thermophilic systems built for digesting of OFMSW are becoming more prevalent due to the potential for 30-50% more biogas yields.

However, in colder climates, it is plausible that any surplus yield in energy production from a slightly higher biogas output available from thermophilic digestion would be less than the increase in energy demand required to increase process temperature by 20°C or 35%. Although thermophilic digestion allows for smaller digester size (a possible benefit for urban implementation) there are other issues to consider as well. Thermophilic digestion allows for shorter retention times for similar methane production as mesophilic digestion, but it has been shown that the treatment of substrates with high biodegradability as well as variability, like food waste, can lead to increased acidity as the volatile fatty acids produced build up faster than the methanogens can convert them to biogas, leading to a generally more unstable system [49][65][66]. In this research, a mesophilic temperature range will be investigated.



Figure 3.24 W8 Anaerobic digestion system used for temperature fluctuation experiment.

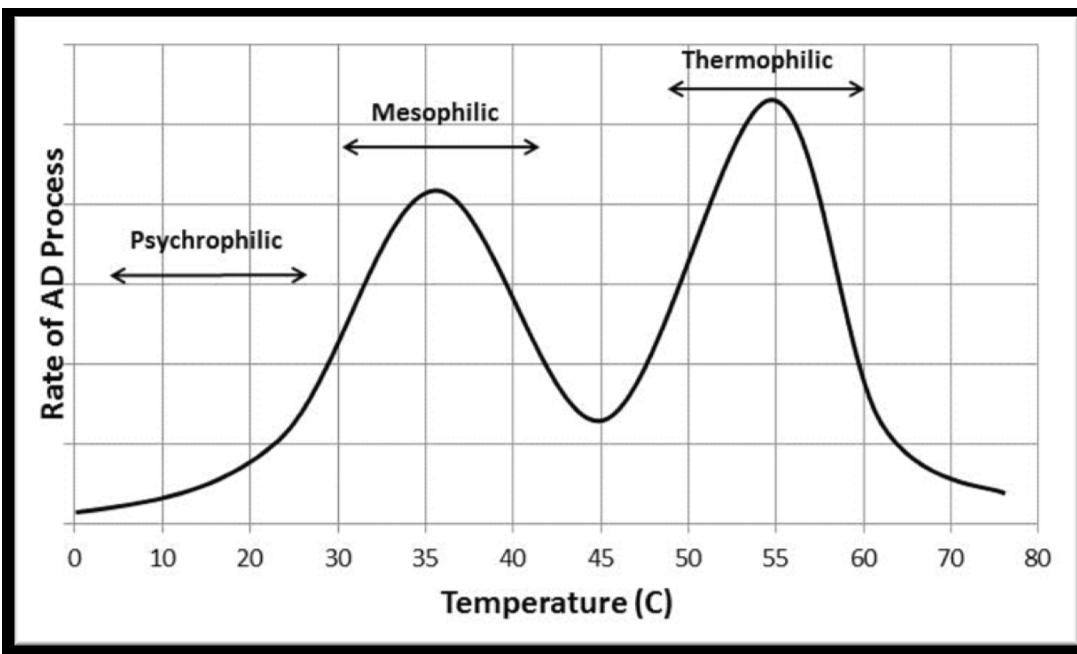


Figure 3.25 Temperature ranges for different rates of the anaerobic digestion process.

In order to verify the feasibility of a daily temperature drop in process temperature of a solar-heated urban mesophilic AD system, an experiment was performed. This experiment was run for approximately 3 months, seven days a week, in order to determine the effect that a small temperature fluctuation would have on volume and composition of biogas production. Samples of mixed food waste were prepared based on a complete breakdown of UK food waste [67].

The selected food waste mix was prepared on a weekly basis and blended with an immersion blender and diluted 40x from its prepared form. The system was inoculated with anaerobic granular sludge taken from a wastewater treatment facility. In order to activate the sludge, the system was filled with approximately 2 liters of sludge and 2.5 liters of diluted food waste, brought to temperature, and monitored until gas production began. This took approximately 14 days. Once the system was producing biogas, a continuous flow of food waste substrate was added slowly and ramped up to 1 gVS/liter/day over the first three retention times. For food waste, the organic loading rate can range from 1-10 grams of VS per liter per day [44][47][48][49][51][65][70]. The substrate was pumped into the 5-liter UASB reactor tank via calibrated peristaltic pump at a continuous rate in order to achieve the desired organic loading rate. Samples were taken from the digester tank (both input and output) every other day and analyzed for total solids (TS), volatile solids (VS), chemical oxygen demand (COD), pH, and volatile fatty acids (VFAs).

Total solids were determined by taking samples of the food waste blend and weighing them before and after heating them in an oven at 150°C for 24 hours. The average value of total solids after five different tests was 29% TS +/-1%. The amount of volatile solids was determined by taking the total solids results and placing them in a furnace at 550°C for 1.5 hours. The average result after the five tests was 96% VS +/- 1%. The average COD value of the input food

waste substrate was 7,881 mg/l +/-5%. The average hydraulic retention time (HRT) was 6.5 days. The carbon to nitrogen ratio (C:N) was estimated to be 23:1 on dry weight basis. The food waste substrate characteristics can be seen in Table 3.3.

Gas samples were taken from top of the 5 liter UASB tank via airtight syringe and analyzed every other day for methane and carbon dioxide content via Varian CP-3800 gas chromatograph with helium as carrier gas. Due to the constant pumping of diluted food waste into the system and the long settling time of the low-power heating jacket temperature control, the temperature regularly oscillated around the set point of 35°C +/- 2.5°C. This constant small variation in temperature did not appear to be correlated to the biogas output volume or percent methane.

Table 3.3 Food waste substrate characteristics

Parameter	Average Value
Total Solids (TS)	29%
Volatile Solids (VS)	28%
VS/TS	98%
COD (input) (mg/l)	7,881
Hydraulic Retention Time (days)	6.5
C:N ratio	~23:1

The exact composition for the food waste substrate for this experiment was determined based on the ground-breaking UK study “The Food We Waste” from 2008 in which, for the first time, reliable information was provided about the nature, amount, and origin of food waste

produced by a developed country’s households [67]. The top four categories of food that were discarded in this study were vegetables, fruits, meat & fish, and bakery representing almost 70% of the total. A graph of the total food waste breakdown can be seen in *Figure 3.26*. In order to have a consistent food waste substrate to feed to the digester, the largest components of each major food waste group were chosen as “representative” of that group and those major components were considered to be “100%” of the waste. Weighted percentages of each food group representative could then be determined as seen in *Table 3.4*. The final breakdown of the food waste substrate is shown in *Figure 3.27*.

Table 3.4 Food waste breakdown as determined for the experiment.

Food Waste Group	Representative	Total and Relative %	Weighted %
Vegetables and Salad		30.20%	44%
	<i>Potato</i>	85%	37%
	<i>Lettuce</i>	15%	7%
Fruits		16.40%	24%
	<i>Banana</i>	54%	13%
	<i>Apple</i>	46%	11%
Breads		13.40%	20%
	<i>Sliced Bread</i>	100%	20%
Meat		8.40%	12%
	<i>Chicken</i>	100%	12%
Total		68.40%	100%

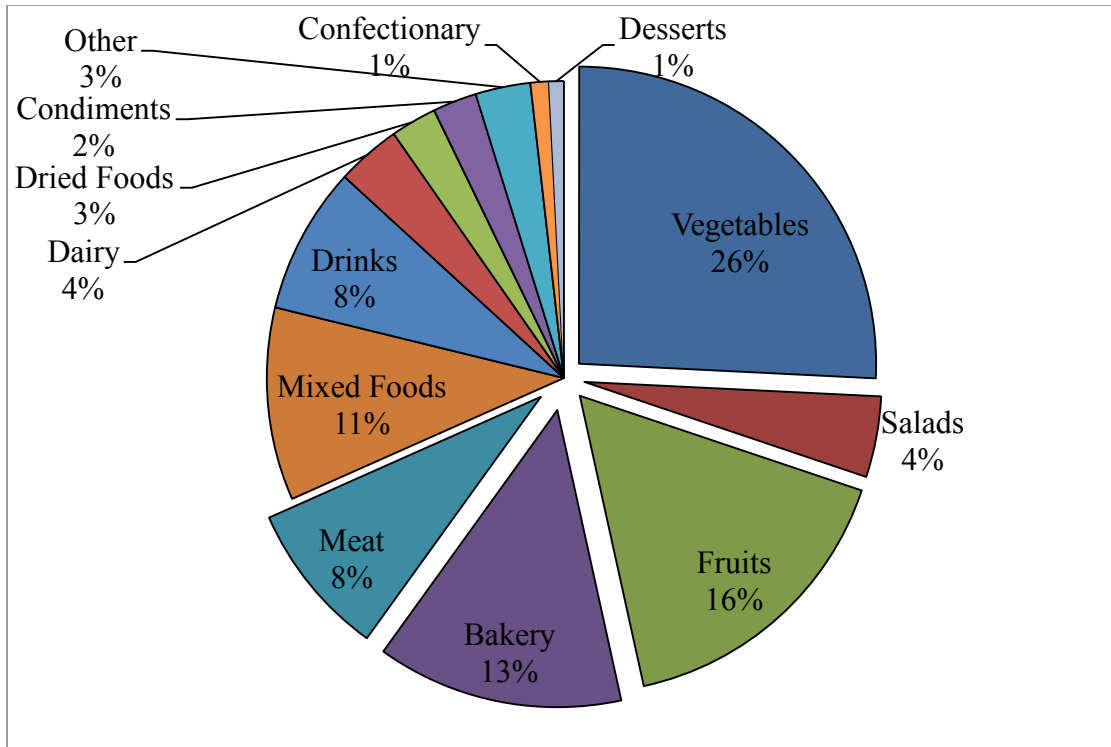


Figure 3.26 Total weight of food waste groups from UK food waste study (2008) with major groups highlighted that were chosen as major representatives

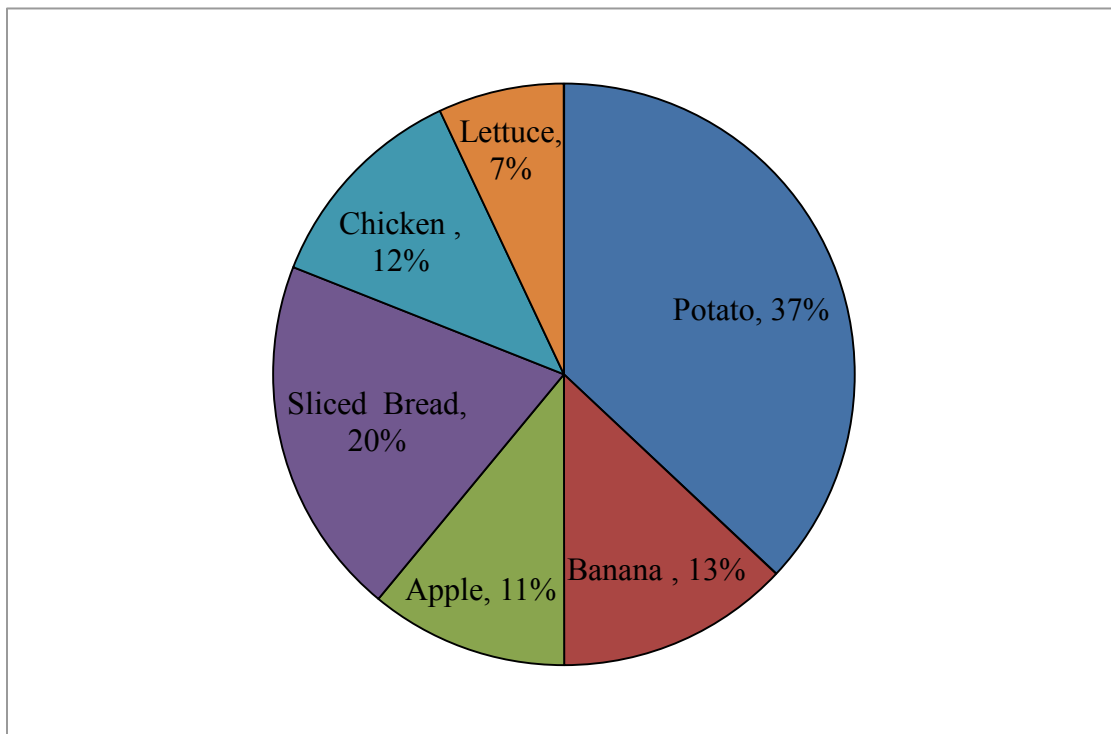


Figure 3.27 Breakdown of food waste representatives used in the experiment.

COD levels of the food waste input and output effluent were tested daily in duplicate during start up and every other day once the system was consistently producing biogas. Samples were tested with Hach Ultra High Range (250-15,000 mg/l) test kits and incubated with Hach DRB 200 for 2 hours at 150°C and analyzed with Hach DR 2800 portable spectrophotometer using Method 10212. The results of COD output/COD input or COD destruction can be seen in *Figure 3.28*. VFA levels of the effluent were tested daily from the water lock sample port located at the water level line near the top of the tank via Hach TNT872 test kits (50-2500 mg/l CH₃COOH). Analysis was done with Hach DR 2800 portable spectrophotometer. The pH of the system was measured using water quality test strips. Total VFA levels and pH of the system are presented in *Figure 3.29*. There were several times when the pH dropped below 7 and ended up at 5.5 due to the buildup of VFAs. The drop in pH caused the gas output to decrease as well as the percent destruction of COD and was corrected through the addition of small amounts of N/10 NaOH solution. The pH of the system is shown separately in *Figure 3.30*.

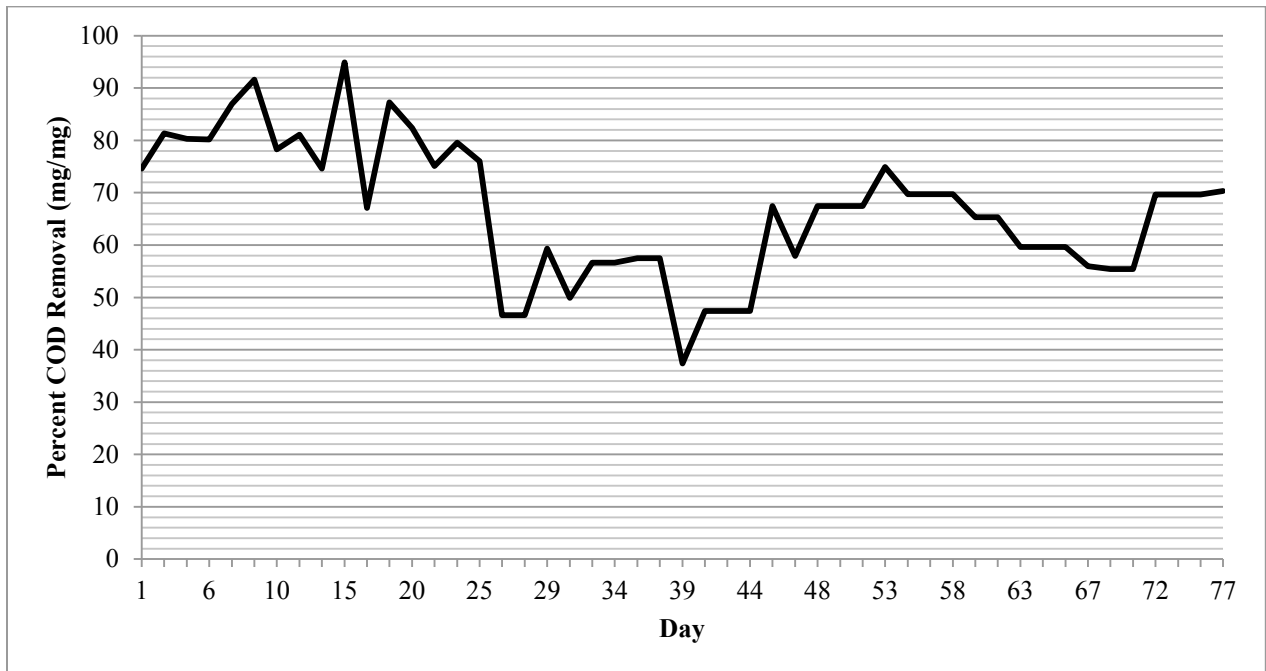


Figure 3.28 Percent COD removed.

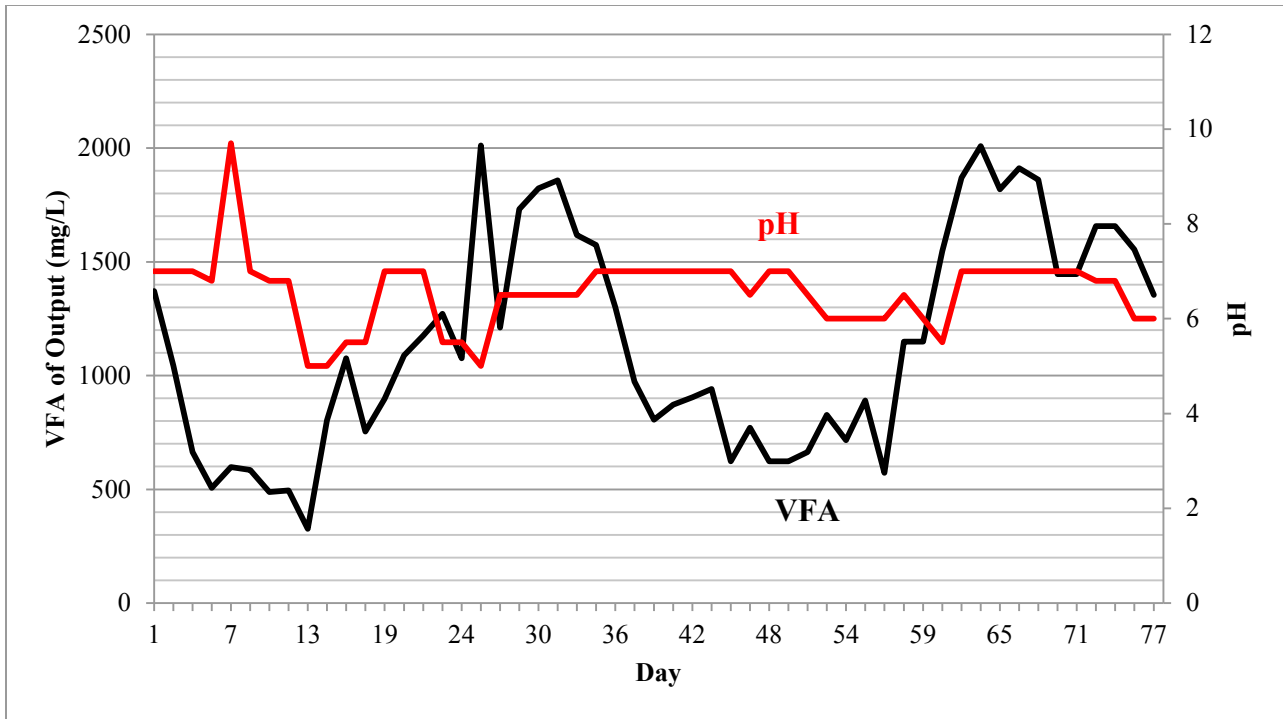


Figure 3.29 Volatile fatty acid levels in digestate in mg/l and pH.

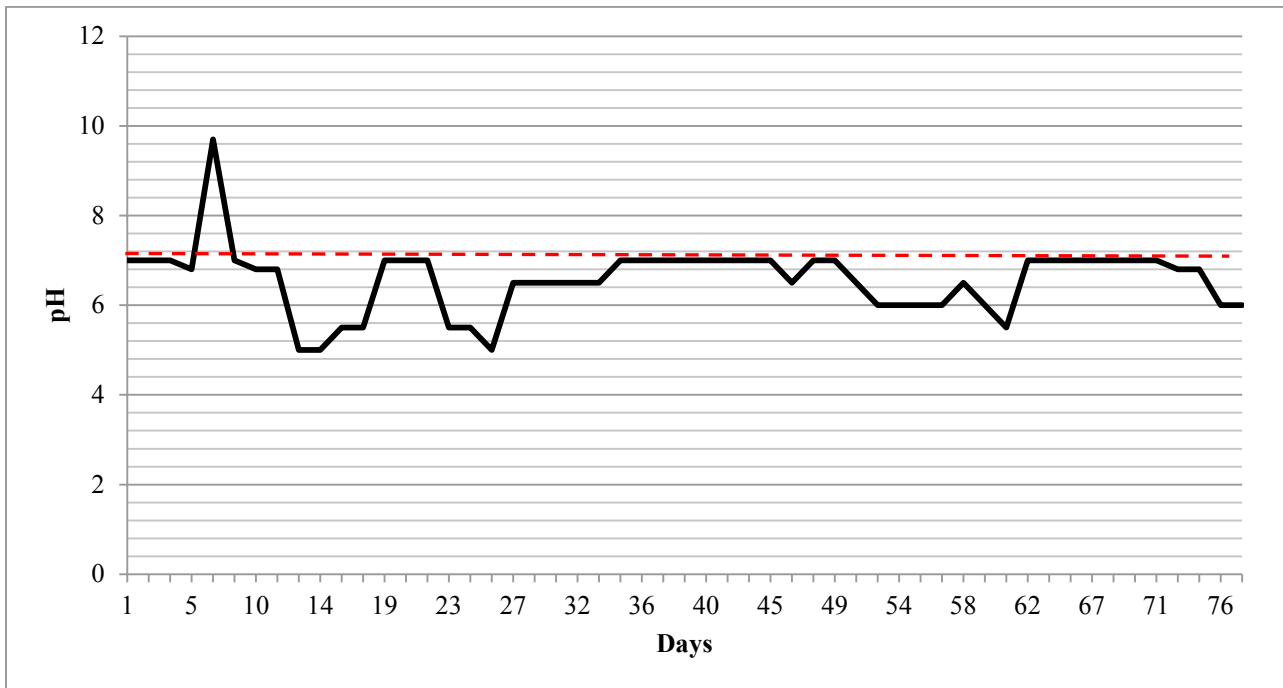


Figure 3.30 pH of slurry in tank

Table 3.5 Literature review of experimental biogas yields of food waste.

Source	Biogas yield m ³ /tVS
Discarded Food	355
Food Waste	367
OFMSW	310-490
OFMSW	300-400
OFMSW	255-494
Food Waste	288
OFMSW	390
Food Waste	472

Gas samples were taken from top of the 5L UASB tank and analyzed every other day for methane and carbon dioxide content via Varian CP-3800 gas chromatograph with helium as carrier gas. Gas volume was determined via calibrated water displacement tank. In *Figure 3.31*, the biogas production level is shown in ml/gVS added. According to the literature review of biogas production from mesophilic digestion of food waste given in *Table 3.5*, the range of biogas production for the second half of the experiment was within the expected range of 288-500 ml/gVS with an average value of 335 ml/gVS [59, 87-93]. In *Figure 3.32* the percent methane in the biogas is presented. Once semi-stable biogas production was achieved, the percent methane increased to an average value of approximately 65% which is also in the expected range for OFMSW substrate.

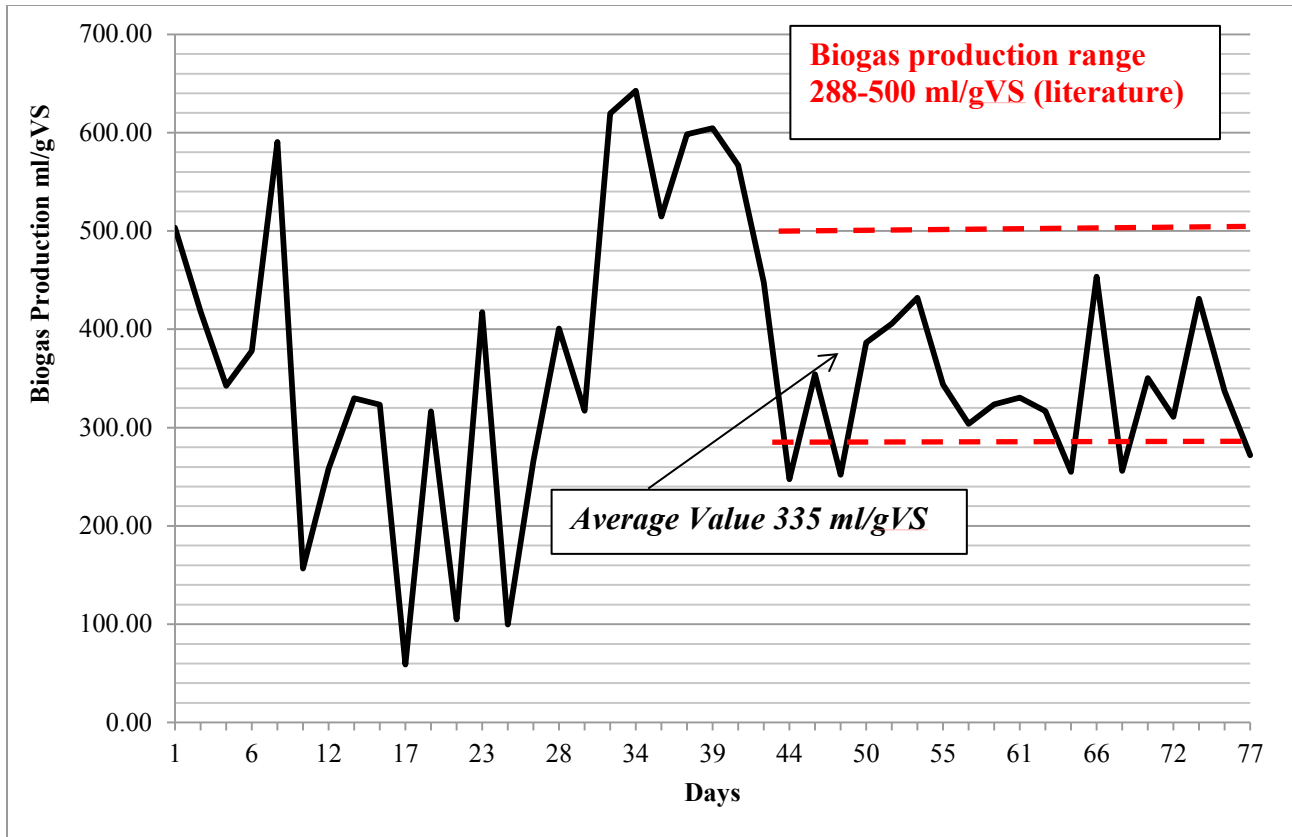


Figure 3.31 Biogas production level in ml/gVS.

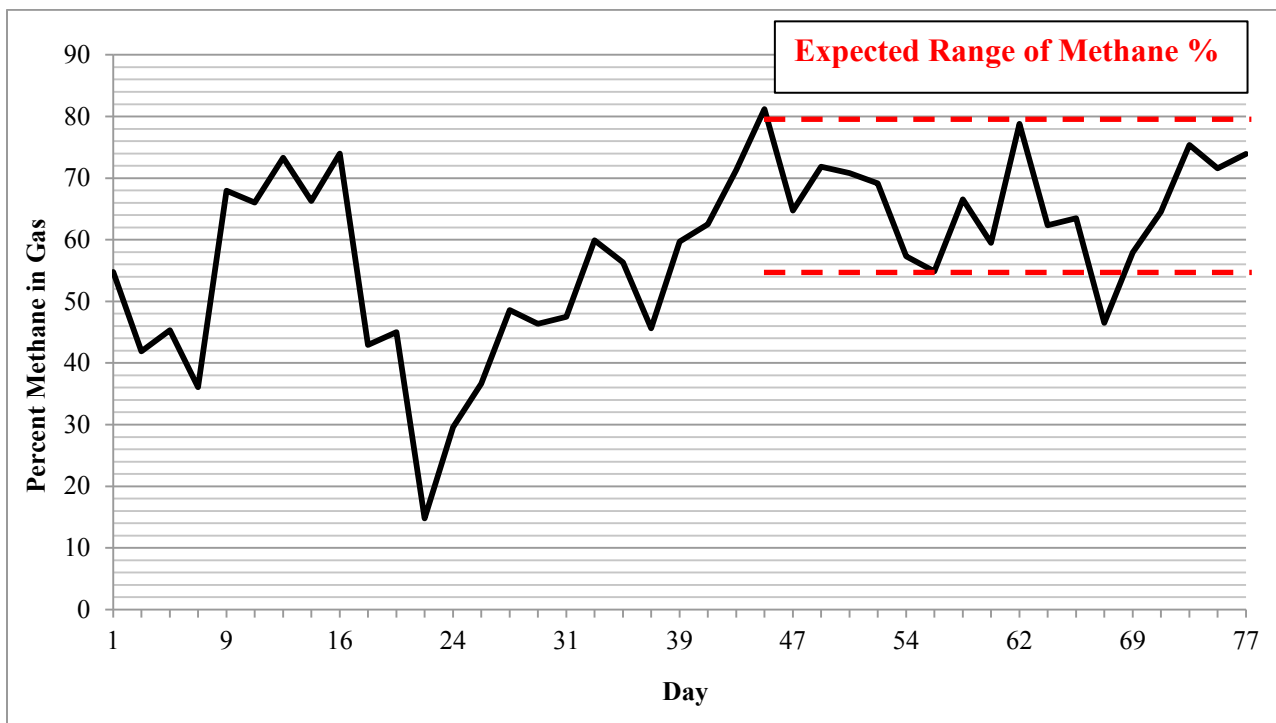


Figure 3.32 Percent methane in biogas over time.

Figure 3.33 presents the COD loading rate of the system in gCOD/l/day. As can be seen in the figure, the COD loading rate was fairly erratic at the beginning of the experiment due to settling of unsuspended solids and the feeding tube becoming clogged. The loading rate stabilized about one third of the way through the experiment once magnetic stirring of the substrate container was added. The loading rate was between 2 and 4 gCOD/l/day for the remainder of the experiment.

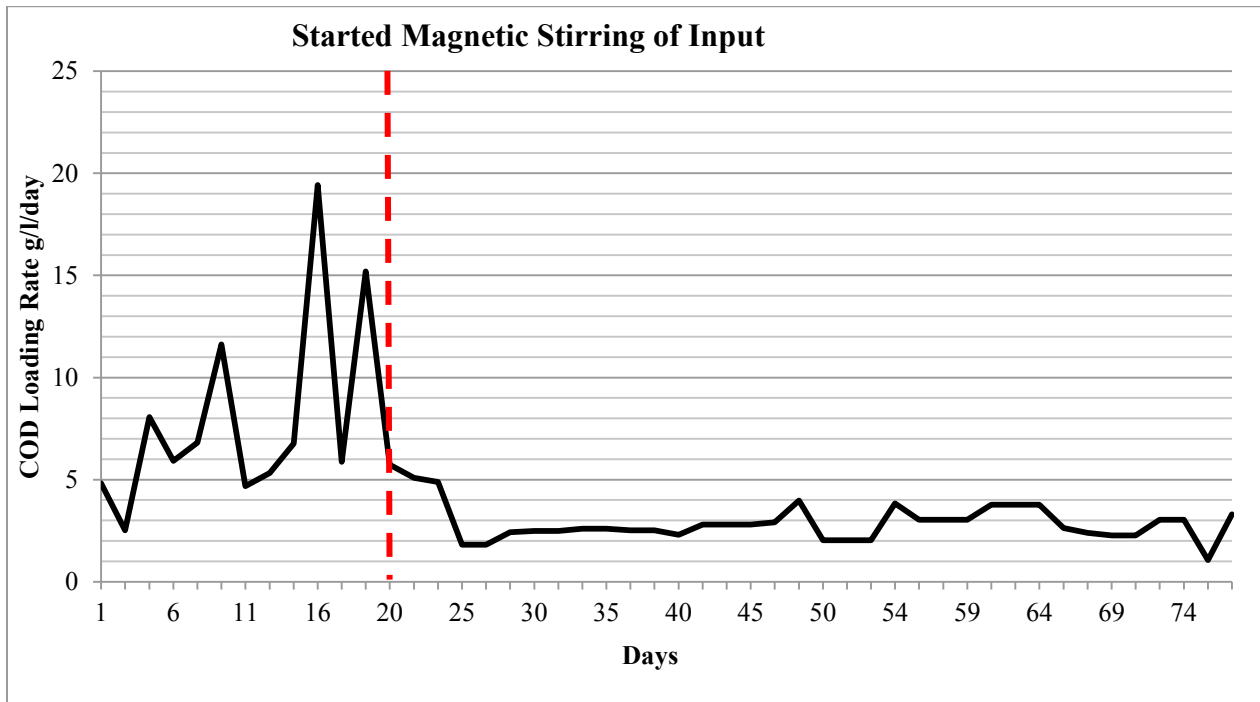


Figure 3.33 COD loading rate in gCOD/l/day.

Theoretically, the temperature of the UASB tank could be controlled manually in 0.1°C degree increments in order to simulate the temperature fluctuation of the solar-heated digest model in *Chapter 3*. This was found not to be possible in practice due to the regular temperature fluctuation of the tank due to the temperature of the input slurry being less than the process temperature (ambient ~21°C) and the fact that the temperature control algorithm of the heating jacket had a large overshoot and settling time even at the tightest settings. These regular

temperature fluctuations could not be shown to have any direct effect on the biogas production or percent methane.

Traditionally, AD systems are run at a constant process temperature. Research has demonstrated the negative effect that large swings in temperature can have on biogas production (10-20°C) but there doesn't seem to be any data available in the literature to predict what happens to the biogas production of an AD system that experiences small (1-5°C) daily temperature fluctuations [73][74][75]. This experiment provides valuable information about the biogas output of an OFMSW AD system operated under these types of conditions. It appears to be the case that small daily temperature fluctuations have no obvious effect on biogas production thereby reinforcing the feasibility of implementation of small-scale, greenhouse-integrated, solar-heated AD systems in the urban environment.

3.10 Conclusions

In conclusion it was shown that it is feasible to provide 8-10kW of heating during daylight hours for a 30 m³ OFMSW anaerobic digestion system with a 2kW_e air source heat pump that utilizes the heat gains of an adjacent greenhouse during the coldest month of the year with temperatures routinely below freezing. It was shown that even if the heat pump system is off for a week due to poor solar radiation or repair, the temperature of the active slurry in the tank would not drop out of the required range for mesophilic digestion. 3-D models of the building with the rooftop greenhouse as well as surrounding buildings were constructed and a solar radiation analysis was performed for the greenhouse during the coldest month of the year. The shading effect of surrounding buildings was investigated in order to ensure that there would be enough energy available to heat the tank as well as keep the greenhouse within required

growing temperatures. The average shadowing effect for the week investigated was a 25% decrease in total solar radiation. Finally, a heat transfer model for an ASHP run only during daylight hours was implemented and a simulation of the temperature fluctuation of the tank was performed for different cases. The results of this simulation show that a small-scale, well insulated AD tank could be feasibly heated using solar heat gains in the middle of winter, freeing up to 15% of the biogas produced for higher-value energy applications instead of using it to heat the digester. Preliminary experimental research suggests that a small regular process temperature fluctuation has no major effect on biogas production or composition.

CHAPTER 4.

WASTE TO ENERGY SYSTEMS FOR EMERGENCY POWER IN URBAN ENVIRONMENTS

4.1 Introduction

Cascading blackouts and localized power outages are becoming more frequent due to an aging and increasingly complex grid infrastructure coupled with extreme weather events related to changing global climate systems. It is necessary to investigate decentralized renewable energy sources for backup power generation and emergency lighting capable of operating without a grid connection. A report published by the US Department of Energy (DOE) states that from 2008 to 2012, the average number of weather-related power outages more than doubled in frequency compared with the previous five years and they have become increasingly more costly in the range of tens of billions of dollars [25][26]. In the urban environment, the integration of black-start capable combined heat and power systems (CHP) supplied by a constant flow of energy-rich biogas from the anaerobic digestion of *in situ* organic waste could provide a reliable way for ensuring backup power in the case of more frequent and extended blackouts.

As mentioned in *Chapter 1*, approximately one third of all food produced for human consumption, or 1.3 billion tonnes per year, is discarded. Most of the food wasted in developed nations occurs at the end of the production and supply chain representing more embedded energy and thus higher costs than food wasted after harvesting. Food waste represents up to 20% of the total MSW stream in the US and is the second largest category of waste. Estimates place the amount of avoidable food waste from 40-60% in the US and UK [67][76][77]. The Federal Ministry of Food and Agriculture in Germany has categorized the food waste distribution across

society and concluded that 61% of food waste happens at the consumer end with only 5% occurring in the grocery retailers stores [78]. The results of this study are shown in *Table 4.1*.

Table 4.1 German food waste distribution by volume.

Sector	Percentage
Retail Stores	5%
Supply Chain	17%
Restaurants	17%
Consumers	61%

From 2005 to 2010, the number of food waste collection programs in the US more than tripled from 20 to 65. From 2010 to 2014, the amount of food waste collection programs more than doubled again and currently stands at more than 150 different programs in 16 states [79][80]. The majority of this food waste is composted and no energy is reclaimed. In almost 90% of the communities where these collection programs exist, the tipping fees for organic waste are cheaper than for MSW. The average tipping fee was \$82 per ton for MSW and \$44 per ton for organic waste (29% cheaper) [76].

There are a few successful anaerobic digestion projects in the US that process food waste but they are mostly research or pilot scale projects. Examples of currently operating AD food waste systems include a joint project between Purdue University and the City of West Lafayette, Indiana. This project sends 1-2 tons of food waste and 3,000 gallons of fats, oil, and grease (FOG) per day to a local wastewater treatment plant to produce biogas and power two 65 kW microturbines. The first dry digestion (up to 30% total solids) system in the US located at the University of Wisconsin Oshkosh that runs on 10,000 tons per year of food waste, yard waste,

and agricultural waste and powers a 370 kW generator that meets 10% of the university's energy demands. The East Bay Municipal Utility District in Oakland, California, that co-digests 100 tons per day of food waste with wastewater and produces a total of 11 MW of electricity from biogas [59][81][82].

In 2013, the first commercial food waste anaerobic digestion system opened in Compton, California, at a food distribution center owned by The Kroger Co. grocery chain. The system digests 150 tons of food waste per day from more than 350 different grocery stores in southern California in a 2 million gallon reactor tank with a 250,000 gallon receiving tank. The biogas produced is sent to several microturbines that provide up to 20% of the energy needs of the distribution center. Having the system located at the distribution center in the urban environment saves over 500,000 miles per year in truck trips to landfill or composting facilities [83].

In the UK, grocery stores are beginning to send their waste to anaerobic digestion facilities in order to reach zero-waste goals. As of 2010, Sainsbury's Grocery was sending food waste from 250 of its 800 stores to anaerobic digestion facilities that produce enough excess electricity to power over 2,500 homes [84]. In 2014, one of Sainsbury's stores became the first UK grocery store to run completely on electricity generated from biogas produced through AD of food waste. A 1.5 km distribution line was run from one of their AD facilities. Another grocer, Waitrose, was sending the waste from half of its 222 stores to anaerobic digestion facilities by 2010 as well. Waitrose performed a waste audit on their stores and found the average amount of food wasted per week was 1.6 tonnes or 83.2 tonnes per year [85]. This represents 57.2 kWh per year of energy and could only power a 2.3 kW genset. The average load size for backup lighting and refrigeration for a standard grocery store runs from 25-35 kW so the waste produced on site from a single grocery store is not enough to run a backup power system.

The National Renewable Energy Lab (NREL) claims there are 7.8 Mt of methane potentially available from biogas produced from the anaerobic digestion of wastewater, landfills, animal manure, and the organic fraction of municipal solid waste (OFMSW) in the United States [86]. A breakdown of biogas methane potential of major US sources can be seen in *Figure 4.1*. Organic waste represents 1.75 million m³ of methane potential or 17.5 GWh of available energy per year. A literature survey of experimentally determined biogas yields from food waste given in meters cubed per tonne of volatile solids (VS) is shown in *Table 4.2* [59, 87-93].

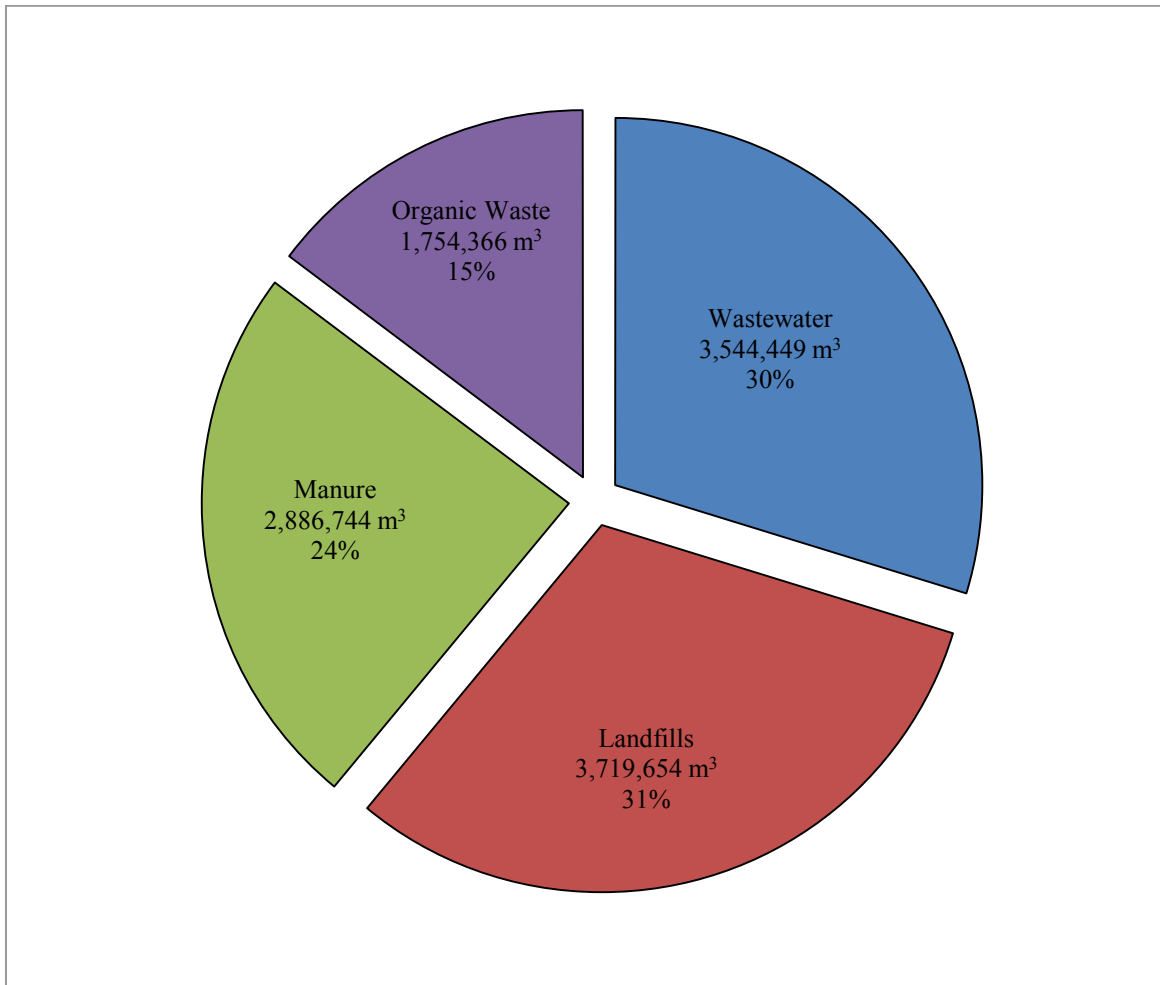


Figure 4.1 Methane potential of major US Sources in m³ (NREL).

Table 4.2 Literature review of experimental biogas yields of food waste.

Source	Biogas yield m ³ /tVS
Discarded Food	355
Food Waste	367
OFMSW	310-490
OFMSW	300-400
OFMSW	255-494
Food Waste	288
OFMSW	390
Food Waste	472

In this chapter, small-scale anaerobic digestion of organic waste will be investigated as a source for emergency power in the urban environment as solution to increased blackouts. Feasibility, sizing, and design of a 20 kW CHP genset to power an emergency lighting system for an urban housing development in New York City is presented as well as several configurations of electric machines for this particular application.

4.2 Energy Available from Small-Scale CHP Systems for Urban Emergency Power Systems

In New York City in the aftermath of Hurricane Sandy in 2012, more than 80,000 people living in over 400 public housing buildings lost essential services including electricity, heat, hot water, and elevators [95]. The number of people without essential services was more than double the amount anticipated by the New York City Housing Authority [96]. Two weeks after the storm, residents in some city housing districts were told that electricity would be unavailable indefinitely. Many backup generators and boilers were located in building basements which were flooded and became unusable. Further, many backup power generators in urban buildings are run on diesel fuel with a short-term supply. During large-scale weather disasters, the transport of

more diesel fuel for back-up generators can be impractical. For many residents, essential services (including plumbing) were unavailable for weeks and months, and in some cases, over a year. More than a year later, many buildings were still running on temporary boilers and generators. If small-scale anaerobic digestion systems are integrated into urban buildings to treat the organic waste generated internally or nearby, a constant stream of methane-rich biogas can be produced providing emergency lighting and hot water via small CHP systems in the 5-150 kW range (depending on the amount of available waste).

Looking at a survey of the public housing developments most affected by Hurricane Sandy with concerning lack of backup power, lighting, and heating as well as a NYC waste survey, a prediction of total energy available from organic waste generated in the buildings can be estimated based on per capita waste production data [97]. The average amount of organic waste produced per resident is 2 kg with approximately 30% of this waste being organics. From the survey of public housing, an estimated amount of organic waste produced per day per development can be determined and ranges from 0.5 tonnes to almost 2 tonnes per day as can be seen in *Table 4.3*.

These numbers do not take into account any food waste from restaurants or cafeterias located in the buildings or nearby. Based on these organic waste calculations, a centralized development-scale anaerobic digestion system that could provide emergency power for all included buildings seems to be the most feasible option when compared with installing multiple systems for each building in each development.

Table 4.3 Overview of affected public housing developments in NYC and daily waste production.

Location	Developments	Buildings	Units	Residents	Residents per building	Units per Building	Buildings Per Development	Building Waste Daily (kg)	Building Organics Daily (kg)	Development Organics Daily (kg)
Lower Eastside	26	139	14440	32401	233	104	5	466	140	700
Coney Island	9	40	4091	9254	231	102	4	462	139	556
Far Rockaway	6	59	3986	10092	171	68	10	342	103	1030
Red Hook	2	30	2878	6351	212	96	15	424	127	1905
Gowanus	3	18	1864	4401	245	104	6	490	147	882
<i>Average</i>					<i>218</i>	<i>95</i>	<i>8</i>	<i>437</i>	<i>131</i>	<i>1015</i>

4.3 CHP Sizing for Small-Scale Anaerobic Digestion CHP Systems

By investigating a range of 1 to 17 tonnes of daily waste production or 0.25 to 5 tonnes of organics generated by 500-8000 individuals and assuming 2 kg per person and 30% organics, a range of potential combined heat and power system sizes can be determined. The amount of biogas produced from a single tonne of organic food waste can range from 350 to 1000 m³ per dry tonne (depending on addition of FOGs) with a 65% methane content and energy content of 6.5 kWh. Assuming maximum efficiency of 38% for the natural gas engine, a range of appropriate generator sizes is shown in *Figure 4.2*. Generator sizes range from 3 to 8 kW_{elec.} for a 0.25 tpd anaerobic digestion system to 54 to 154 kW_{elec.} for a 5 tpd system.

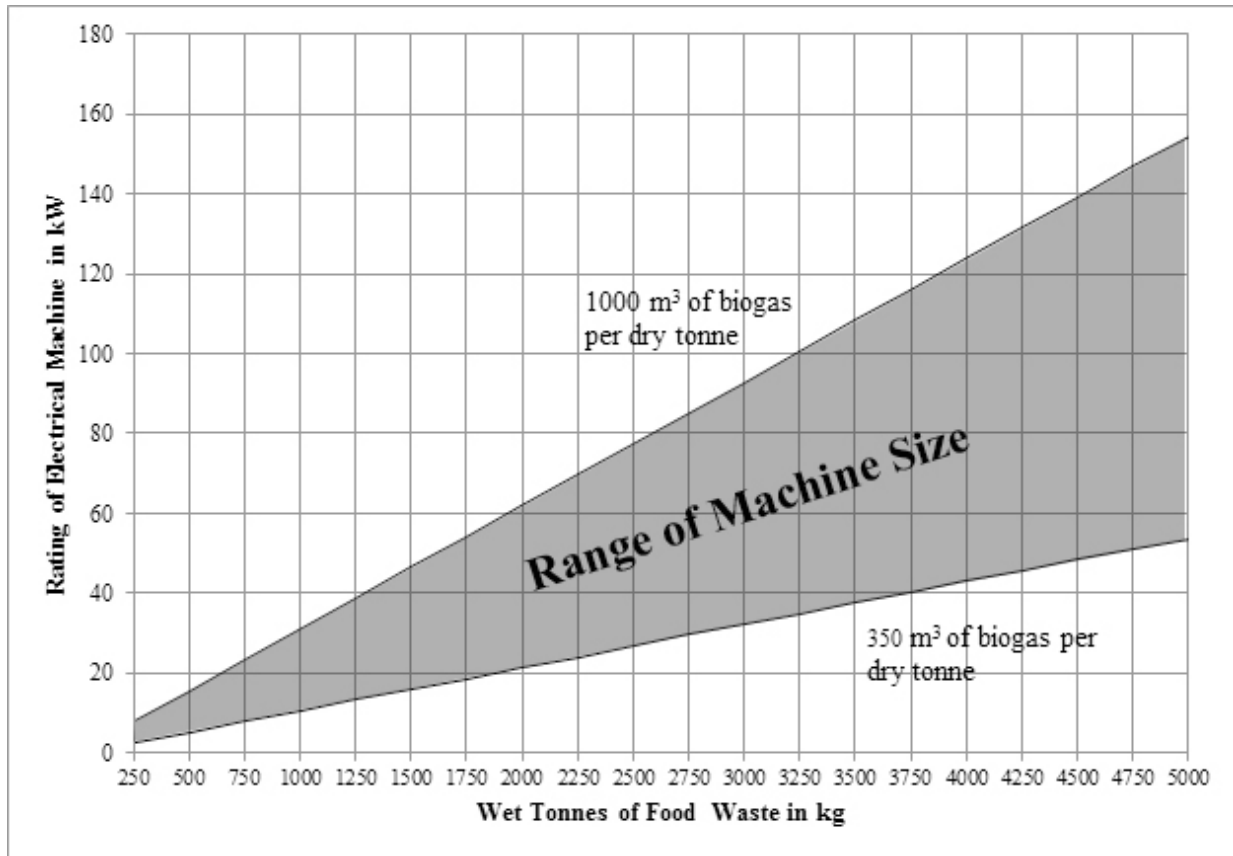


Figure 4.2 Range of electric machine size for 0.25 to 5 tonnes of daily food waste production.

Taking into consideration the ability of CHP systems to recover exhaust heat from the combustion of biogas and provide hot water, the range of energy available from electricity and heat recovery is presented in *Figures 4.3 and 4.4*. It is possible for small-scale CHP systems to reach average efficiency of 85% or greater [98]. Assuming 38% efficiency of the combustion engine, and 85% total efficiency for heat recovery, the installed size of generator and heat recovery systems range from 6 to 17 kW for a 0.25 tpd system and 120 to 345 kW for a 5 tpd anaerobic digestion system with 2.8 to 8 kW of heating energy available for a 0.25 tpd system and 56 to 162 kW available for a 5 tpd system.

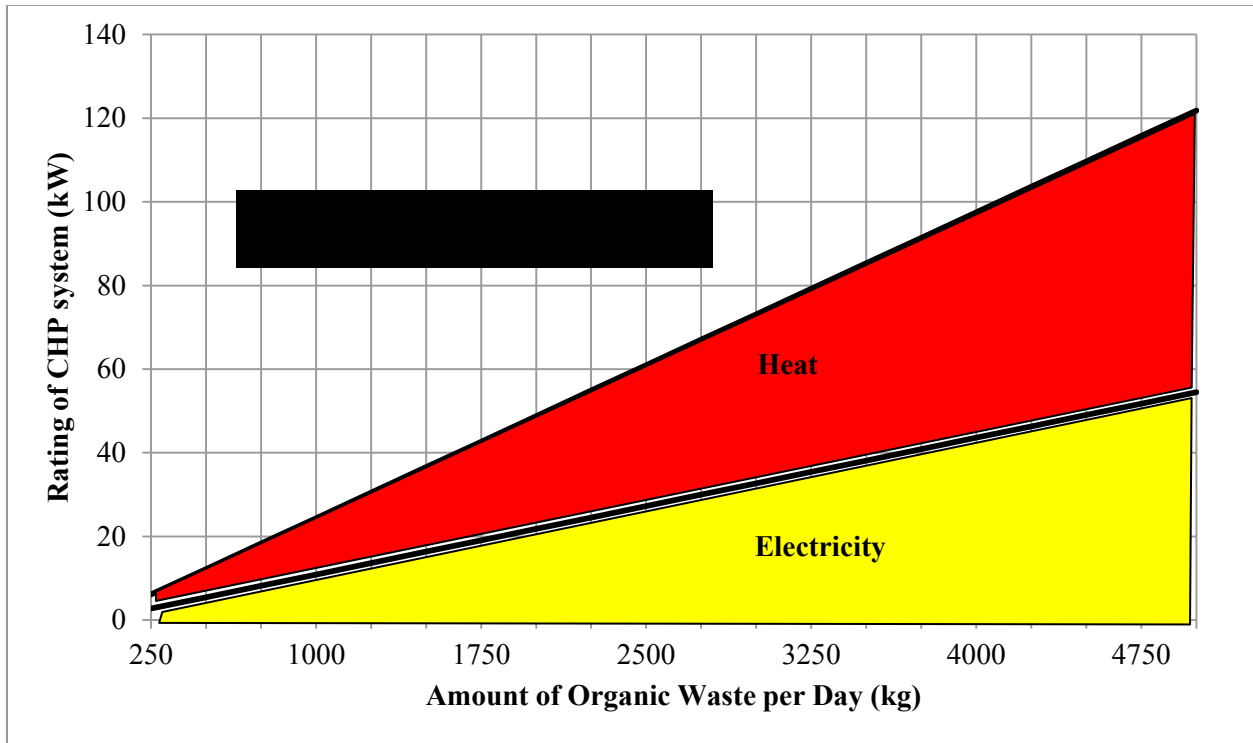


Figure 4.3 Power and heat recovery ratings for 0.25-5 tpd anaerobic digestion systems with 367 m³/tonne_{dry} biogas production at 65% methane.

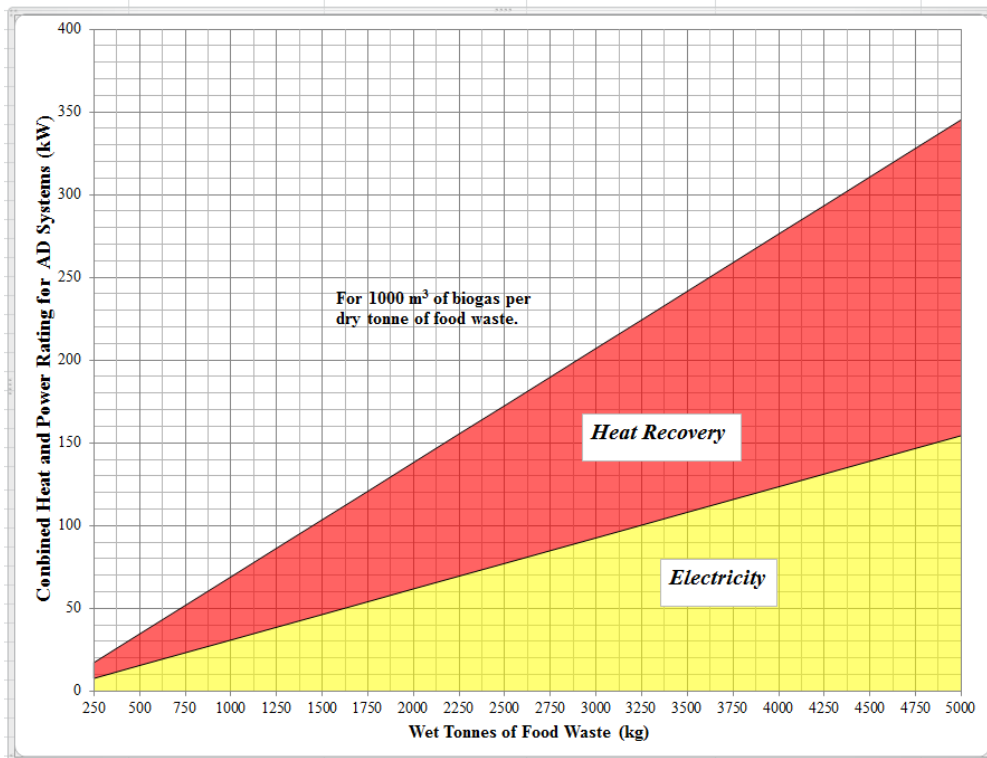


Figure 4.4 Power and heat recovery ratings for 0.25-5 tpd anaerobic digestion systems with 1000 m³/tonne_{dry} biogas production at 65% methane.

4.4 Feasibility and Design of Biomass System To Meet Emergency Power Load Requirements

Usually the design of an anaerobic digestion system and potential energy production is based on the amount of waste available on site. In this case, the reverse of this process will be considered as the power requirement will be the starting point used to assess feasibility. Once the sizing of the system is determined, then system feasibility can be assessed based on available space, weight requirements (if the system is to be located on the roof of the building), and size of available organic waste streams. For this case, a 20 kW emergency lighting system is considered. If a 20 kW CHP system that runs on biogas produced from organic waste is installed in a building development, it could provide constant power to over 1700 energy efficient LED light bulbs (11-12 W) in the case of an extended blackout while also providing 44 kW of heating energy for hot water.

4.4.1 Biogas Production Required

Assuming a 20 kW rated emergency lighting system is to be installed, the necessary biogas flow rate can be determined. There is 6-7 kWh of heating energy or 2-3 kWh of electricity available in each cubic meter of biogas produced depending on methane content. So for a 20kW rated emergency lighting system, a constant flow rate of 6.6 to 10 m³/hour of biogas is required.

4.4.2 Amount of Waste Required

In order to attain 6.6 to 10 m³/hour of steady biogas production, a correct amount of biogas production per dry tonne of food waste substrate is necessary. According to *Table 4.2*, an average of 300 to 400 m³ of biogas per tonne is a reasonable assumption. Based on the hourly flow rate, annually, 57,816 to 87,600 m³ of biogas is required providing an annual waste

requirement in dry tonnes ranging from 144 tonnes to 292 tonnes. Converting this result to wet tonnes requires knowing the dryness level of the food waste substrate. From the references in *Table 4.2*, the food waste dryness ranges from 10-37%. The average value of food waste dryness is close to 30%, yielding 480 to 973 wet tonnes of food waste per year or 1.3 to 2.7 tonnes per day required for a 20kW emergency lighting system.

4.4.3 Digester Tank Sizing

In order to size a tank volume to the amount of waste required, several factors must be considered at once: type of digestion (wet/dry), number of digestion stages (single/multiple), digestion process temperature (mesophilic/thermophilic), hydraulic retention time (HRT), and organic loading rate (OLR). Where hydraulic retention time is defined as the amount of time (in days) that the substrate spends the reactor under ideal conditions and determined by *Equation 4.1*.

$$HRT = \frac{V}{Q} \quad \text{Equation 4.1}$$

Where V: Reactor Volume [m³]

Q: Flow Rate [m³/day]

And, organic loading rate (OLR) is defined as the amount of organic material added to the reactor in a given amount of time; usually measured in a flow rate per day and determined by *Equation 4.2*.

$$OLR = \frac{Q \cdot S}{V} \quad \text{Equation 4.2}$$

Where: OLR: Organic Loading Rate [kg substrate / m³ / day]

Q: Flow rate of input [m³/day]

S: Concentration of VS in the input [kg/m³]

V: Reactor Volume [m³]

In order to determine the upper bound of digester tank size, it can be assumed that the digestion process will occur in a single stage tank at mesophilic temperatures (35-37°C), have a retention time of 30 days, and a total solids content of 5%. This means the food waste will have to be diluted 6x from the present dryness level of 30%. If 973 wet tonnes is considered (2.7 tpd), a maximum tank size of 486 m³ weighing 486 tonnes is required. If the retention time is reduced to 15 days and the total solids level is increased to 10% (still within pumpability range), the tank size is reduced to a volume of 122 m³ and a weight of 122 tonnes. If only 1.3 tonnes of waste per day is used and maximum biogas production is attained, then the tank size is further reduced to 59 m³ with a weight of 59 tonnes.

4.5 Electric Machines for Biomass CHP for Urban Emergency Power Generation

The importance of installing emergency and backup power systems in urban areas will continue to increase as extreme weather events related to changing global climate systems compromise electrical grid systems around the world. In an emergency situation, the need for a constant source of lighting for stairwells, emergency exit pathways, and hallways for the safety and practical benefit of urban residents cannot be overlooked. The standard set by the National Fire Protection Association (NFPA) in the Life Safety Code requires a minimum of 90 minutes of emergency illumination in the case of normal lighting failure [99]. As a result, there are a variety of uninterrupted power supply systems (UPS's) available from the 1.5-80 kW range from different manufacturers that include battery bank, rectifier to provide grid charging, inverter, and isolated AC output that can support incandescent, fluorescent, HID, quartz re-strike, and halogen lamps for up to 90 minutes at full load. Single phase systems are available from the 1.5-15 kW

range and 3-phase systems are available from 5-80 kW [100][101]. For the same power rating, a 3-phase system can be up to 150% more efficient than a single phase system and allow for a reduction in conductor size of 75%.

It is not uncommon for power outages to last longer than 90 minutes and in some cases, like in the case of Hurricane Sandy discussed earlier, weeks and months can pass without having full grid access restored. Reliability and longevity of backup power from diesel powered generator sets can be compromised in the case of flooding or infrastructure damage as not enough diesel is stored on site in most places for backup power to be maintained for more than a day or two. A properly maintained anaerobic digestion (AD) system processing daily organic waste generated on site can produce a steady stream of biogas with 60-70% methane content. It is technically feasible to size a small-scale AD system in order to generate enough biogas to keep an emergency lighting system running continuously for long periods of time by either constantly recharging the battery bank of the installed emergency lighting system, or powering the emergency lighting system directly. A small-scale AD CHP system is able to provide steady AC power and hot water in emergency situations.

In order to provide reliable emergency power in the case of a blackout, biogas or natural gas fired gensets need to be able to operate in island mode. The generator needs to be self-starting and come online usually within 30-60 seconds [102]. Precautions need to be taken to ensure that no power from the emergency power system is capable of being injected back into the grid. This can be ensured via a break-before-make transfer switch and an automatic inverter disconnect switch. In most cases, automatic switching is required in the case of an outage but manual switching can also be acceptable. In any case, the grid-tied connection must be broken before startup of backup or emergency power systems are started.

For emergency power applications there are many possible configurations of generator sets available for small-scale, island-mode, building-integrated biogas CHP systems from a few kW up to the 150 kW range. It is technically possible to use a self-excited induction generator (SEIG), synchronous generator (SG), or permanent magnet synchronous generator (PMSM) as part of a modified natural gas-powered generator set. Each has its advantages and disadvantages depending on application and current regulations. Important design factors to consider are the size of emergency lighting load, whether battery-powered emergency lighting system is already in place, and black-start capability. In order of preference related to cost, reliability, and maintenance, different generator options for black-start emergency lighting power are investigated. It is assumed in all cases that a battery powered emergency lighting system is already in place and the generators will be interfaced with these existing systems.

4.5.1 Self-Excited Induction Generators (SEIG)

For small biogas CHP systems 10 kW and under, it is possible that a single-phase, self-excited induction genset can be used. For 10-150 kW range, a 3-phase SEIG is recommended. Over 10kW, it is difficult to find a single phase SEIG from a manufacturer, but for systems rating 10-100 kW, it is possible that a 3-phase SEIG can be operated as a single-phase generator, producing 20-30% less than its rated output power. Induction generators are typically the cheapest, most robust, and least complicated option for small-scale power generation and also require the least amount of maintenance.

As induction generators typically derive their active power from a grid connection, in order to operate in island mode with black-start capability, a properly sized capacitor bank must be placed across the generator terminals and a suitable amount of residual magnetism must be

present in the rotor. As an AD system produces a near constant flow of biogas, and buffer storage is often present, the generator can be operated at a constant speed, making voltage and frequency control less complicated than in the case of an intermittent prime mover as is the case with wind turbines.

As can be seen in *Figure 4.5*, the capacitor-start SEIG can be connected through a rectifier and charge controller to the battery bank of the emergency lighting system and provide steady backup power for much longer than the 90 minute installed capacity. If the generator is sized properly for the load, it can also be connected directly to the load in case of battery failure or maintenance.

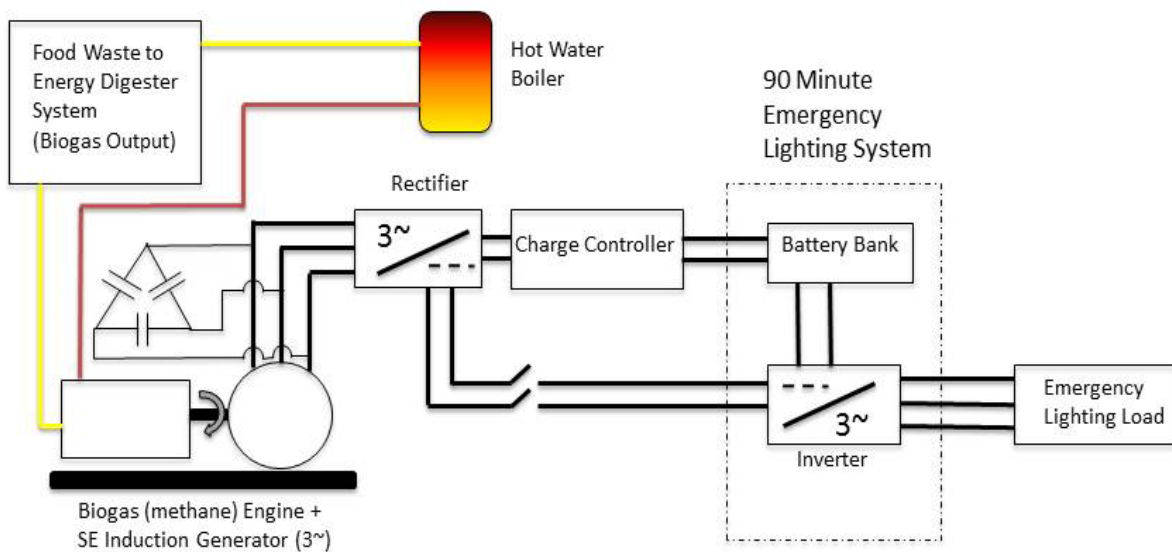


Figure 4.5 Self-Excited Induction Generator charging battery bank for emergency lighting system.

4.5.2 Synchronous Generators (Wound Rotor)

For small biogas CHP systems in the 1-25 kW range, it's possible to install a system that contains a single phase synchronous generator with self-starting capability via a battery

supplying DC power to the rotor field windings. In the range of 6-130 kW, CHP systems containing 3-phase synchronous generators are available that also able to self-start via battery-supplied DC power for the rotor field windings. Most readily available small-scale natural gas generator sets contain a synchronous generator. This may be the most easily obtainable CHP option even though a self-excited induction generator system would be cheaper and require less maintenance. In *Figure 4.6*, the synchronous genset is shown connected to a rectifier and charge controller that would allow it to directly charge the battery bank of the emergency lighting system. If sized correctly to the load, the generator could also supply the load directly.

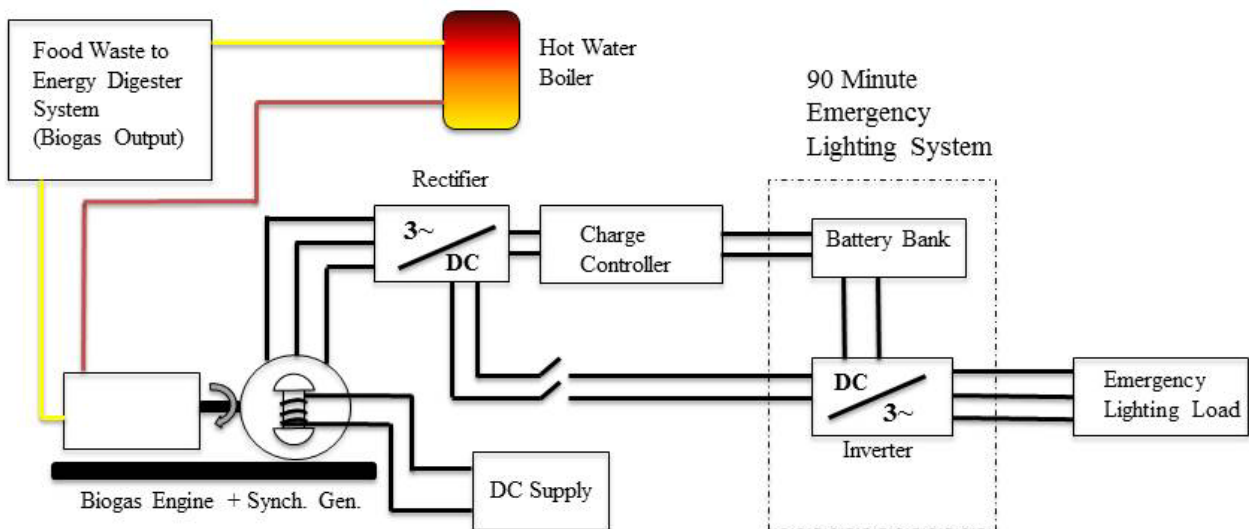


Figure 4.6 Synchronous Generator charging battery bank for emergency lighting system.

4.5.3 Permanent Magnet Synchronous Generator (PMG)

Although currently not readily available on the market, it is technically feasible to have a small-scale biogas CHP system that uses a permanent magnet generator for electrical power generation. There is currently only a 3-phase 100 kW PMSM high-efficiency natural gas CHP system available on the market, but stand-alone PMGs are readily available in the 5-180 kW

range that could be coupled with high-efficiency natural gas combustion engines. Depending on the future of permanent magnet price increases due to their rare-earth status, PMGs may not see increased CHP integration.

Due to the permanent magnets embedded in the rotor, no DC supply is required for rotor field excitation, allowing for the least complicated and most reliable black-start capabilities. As soon as the combustion engine starts spinning the rotor, electrical power can be generated. PMGs have higher efficiency at partial loads than synchronous generators, are simpler in construction, have a smaller footprint, and require less maintenance. As in the previous cases, the PMG would be used to charge the battery bank of the emergency lighting system and connected through a rectifier and charge controller as seen in *Figure 4.7*. If properly sized, the PMG could also supply the emergency lighting load directly.

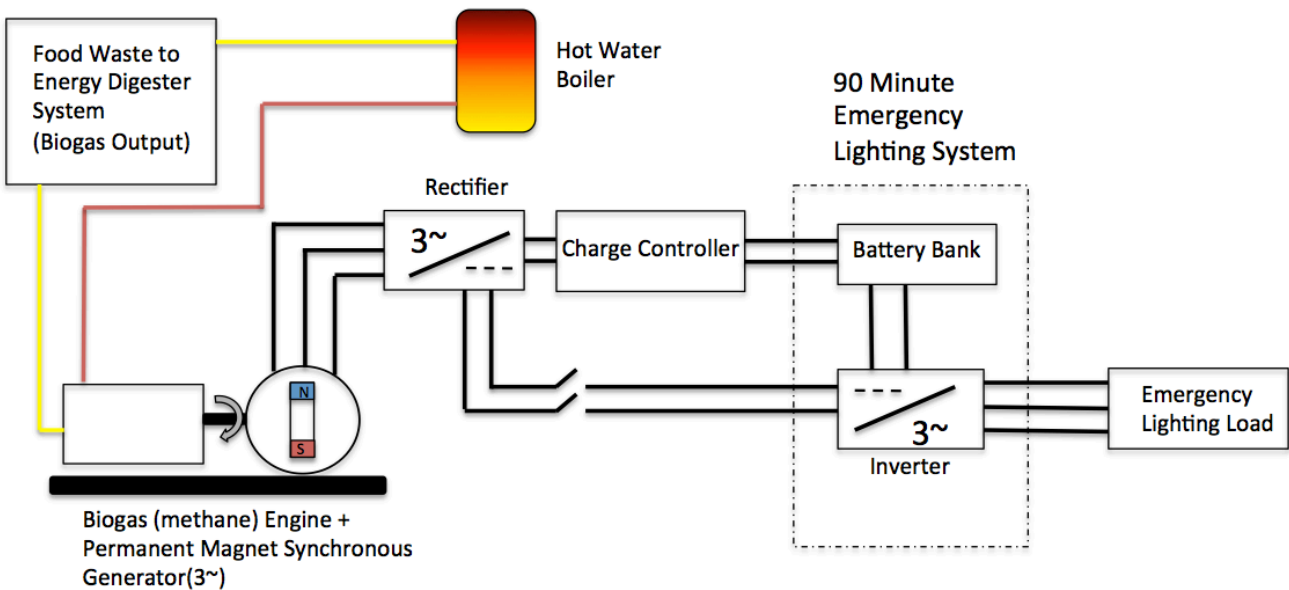


Figure 4.7 Permanent Magnet Synchronous Generator charging battery bank for emergency lighting system.

4.6 Derating for Synchronous Machine with Rectifier/Inverter

4.6.1 Derating and Voltage Unbalance Overview

If a 3-phase generator is used for emergency and backup power, there is the likelihood that under these operating circumstances the generator can experience unbalanced loads causing voltage and current unbalance. The major cause of voltage unbalance in polyphase generator systems is an unequal distribution of single phase loads spread across the phases. Unbalanced operating conditions can occur in rural backup power systems as well as urban power systems whose single-phase demands imposed by the facilities where they are installed are not uniform. Regardless of the cause of the voltage unbalance, extensive damage can occur if an electric machine is not derated appropriately.

When operating under unbalanced voltage conditions, a negative sequence voltage is introduced producing a flux in the airgap of the machine which rotates in the opposite direction of the rotor. This negative sequence voltage can lead to currents in the stator windings that are much higher than in the balanced case. In some cases the currents produced in the stator can be 6 to 10 times higher than the percent voltage unbalance [135][137][140]. These higher currents raise the temperature inside the machine and can weaken and even melt the insulation on the windings causing cumulative and permanent damage to the machine. There are several different classes of insulation used in the windings of electric machines and depending on the insulation used, the effective life of the machine can be decreased dramatically from even small percentage voltage unbalance. For example, an F class insulation rated at 155C can experience a 50% decrease in expected lifetime from operating at a 10C increase in temperature as shown in *Figure 4.8* [142].

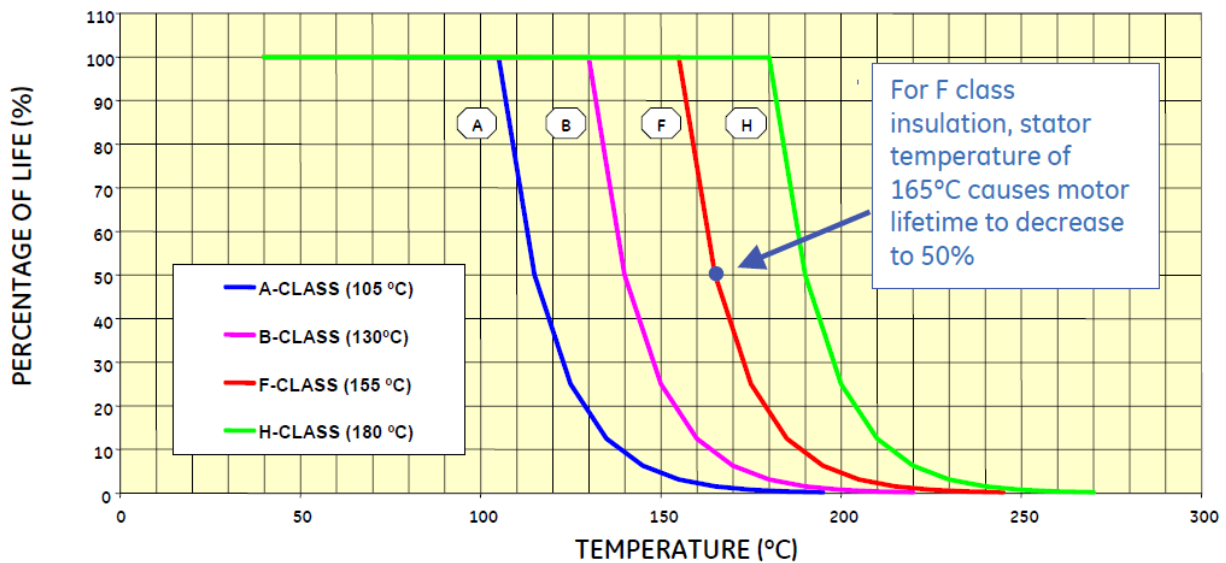


Figure 4.8 Percentage decrease in expected life of electric machine vs. temperature increase

The amount of temperature rise in the machine as it relates to percent unbalance in the voltages across phases rises in an exponential manner and can be approximated to be twice the square of the percent voltage unbalance as shown in *Equation 4.3* and shown graphically in *Figure 4.9* [135][145]. In order to calculate the percent voltage unbalance in line or phase voltages, *Equations 4.4* and *4.5* can be used [136][141][143].

$$\text{Temperature Rise (\% increase)} = 2 * (\% \text{ Voltage Unbalance})^2 \quad (4.3)$$

$$\text{Live Voltage Unbalance Rate (\%LVUR)} = \frac{\text{max voltage deviation from avg. line voltage}}{\text{avg. line voltage}} \quad (4.4)$$

$$\text{Phase Voltage Unbalance Rate (\%PVUR)} = \frac{\text{max voltage deviation from avg. phase voltage}}{\text{avg. phase voltage}} \quad (4.5)$$

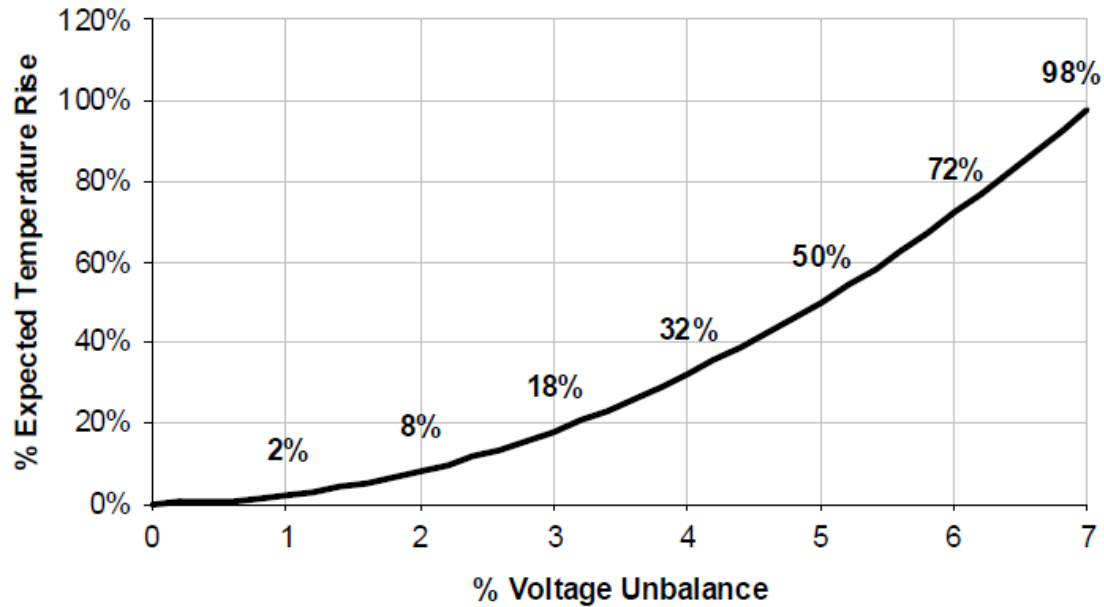


Figure 4.9 Percent temperature rise due to voltage unbalance.

There are several different standards available that recommend different operating limits for voltage unbalance. The American National Standard for Electric Power Systems and Equipment (ANSI C84.1) recommends that the voltage unbalance in an electric power system does not exceed 3 percent¹³⁷. Pacific Gas & Electric utility in the U.S. recommends that the average voltage unbalance between phases does not exceed 2.5 percent [133]. The National Equipment Manufacturers Association (NEMA), representing electric machine and drive manufacturers, is more restrictive and recommends operating at a maximum voltage unbalance of 1% [137]. Some manufacturers of electric machines give a limit of 5% current unbalance (<1% voltage unbalance) in order for the warranty to be honored. This clear difference in recommendations can create issues between utilities, customers, and electric machine manufacturers. Regardless, if the percent voltage unbalance exceeds any of the recommended limits, then the machines should be derated for safe operation.

In order for an electric machine to be run safely under unbalanced voltage percentages that are greater than the recommended 1-3%, it needs to be derated in order to prevent damage from overheating due to higher-than-rated currents. When a machine is derated, it is simply run with a lower power output depending on percent voltage unbalance. Derating is an undesirable method for dealing with voltage unbalance, but it may be necessary in emergency or backup power situations. The derating factor for a machine (*Equations 4.6*) can be determined by calculating the output power required for the percent voltage unbalance divided by the rated output power of the machine. A typical derating curve for an electric machine according to NEMA is shown in in *Figure 4.10* [137].

$$\text{Derating Factor (DF)} = \frac{\text{Derated output power}}{\text{Rated output power}} \quad (4.6)$$

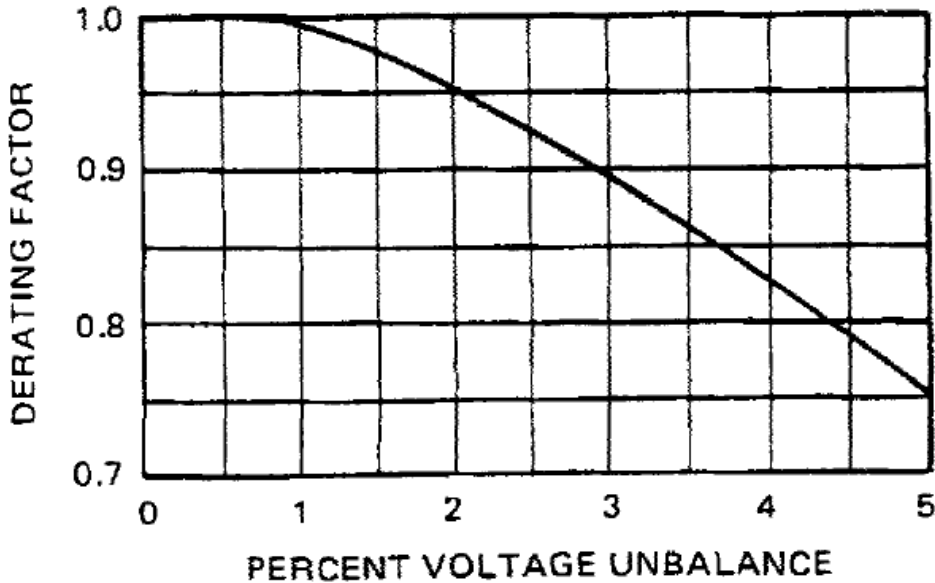


Figure 4.10 Derating factor vs. percent voltage unbalance curve from NEMA MG-1

4.6.2 Overvoltage and Undervoltage Concerns for Emergency and Backup Power

IEEE Standards define undervoltage and undervoltage in the following way: undervoltage conditions occur when rms supply voltages decrease to 0.8-0.9 pu for longer than one minute while overvoltage is defined as an increase in the rms voltage of 1.1-1.2 pu [136][148]. In the case of an emergency or backup power situation in which the loads on the three phases of the generator are not equal and a voltage unbalance occurs, the single phase loads will have to be powered with overvoltage or undervoltage conditions depending on the phase. In the European Union, electrical supply voltages are required to be within the range of 230 V (RMS) +/- 10%. In the United States and Canada, the supply voltages are expected to be within the range of 120 V (RMS) +/- 5%. These are the standards given for typical operating conditions, but individual equipment such as appliances and electronics may be able to operate under more extreme voltage unbalance conditions in the case of an emergency or backup power situation.

In a 2005 report on the effects of temporary overvoltage on residential products, different overvoltage levels were applied for different durations of time in order to determine the effect of extended overvoltage on residential products [144]. In this research, surge protective devices (SPDs), programmable logic controllers (PLCs), personal computers and monitors (PCs and monitors), and incandescent lightbulbs (60 W) were tested. The logic behind testing these devices is that they are the most commonly utilized residential power devices. Many homes employ surge protector plug strips for powering multiple devices, PLCs are found in home security and automation systems, and incandescent lightbulbs are still widely employed despite changing lighting regulations. In order to imitate different overvoltage conditions that residential electric devices may encounter (shown in *Table 4.4*), an overvoltage of 15% (138 V) was applied

to the devices for 6 hours to imitate poor voltage regulation, an overvoltage of 30% (156 V) was applied for 2 seconds to imitate fault conditions, an overvoltage of 50% (180 V) was applied for 4 hours to imitate loss of a secondary neutral line, an overvoltage of 100% (240 V) was applied for 1 minute to imitate ferroresonance, and an extreme overvoltage of 200% (360 V) was applied for 1 second to imitate contact with high-voltage circuits.

Table 4.4 Overvoltage conditions tested in report

Test Number	Imitated Condition	Magnitude	Duration
1	Poor voltage regulation	1.15 PU (138 V)	6 hr
2	During a fault	1.3 PU (156 V)	2 sec
3	Loss of a secondary neutral	1.5 PU (180 V)	4 hr
4	Ferroresonance	2.0 PU (240 V)	1 min
5	Contact to high-voltage circuits	3.0 PU (360 V)	1 sec

The results of this testing are shown in *Table 4.5*. It can be seen in the table that the SPDs, PLCs, PCs and monitors, as well as the lightbulbs were tested to be “OK” for an overvoltage of up to 50% (180 V) for four hours of continuous use. This is much higher than manufacturer recommendations and is promising for emergency and backup power situations that could see an extreme voltage unbalance percentage of greater than 5% but less than 15%.

For undervoltage conditions, a literature survey shows that thermostats have an undervoltage protection threshold of 60% and air conditioner and refrigerator compressors have an undervoltage threshold of 75-85% of rated (and overvoltage threshold of 10-15% above rated)

[146][147]. Many desktop computers have an undervoltage limit of 8% and overvoltage limits of 10% while laptop computers may continue charging for undervoltage conditions of up to 17% [147]. For incandescent lighting, 10% undervoltage requires 30% more lights for the same illumination level as rated and infrared lamps will produce 21% less heat. For an undervoltage of 12%, induction heater output can decrease by 20% and cause damage, shortening the life of the heating elements. For resistive heating, available heating varies as the square of the voltage so a 12% undervoltage will cause a reduction of 22% in the heating output. For charging of battery powered devices, most chargers (universal adapters) will continue to provide reliable charging voltage and current down to a 17% undervoltage level as they are often rated for a range 100 V to 230 V.

Table 4.5 Summary of overvoltage testing of residential equipment

Sample Description		Results Summary				
Type	Technology	Test 1	Test 2	Test 3	Test 4	Test 5
		138V 6 hrs	156V 2 sec	180V 4 hrs	240V 1 min	360V 1 sec
SPD - plug strip	130V MOV	ok	ok	fail	fail	fail
SPD - plug strip	130V MOV	ok	ok	fail	fail	fail
SPD - plug strip	multiple 130V MOVs + filtering	ok	ok	fail	fail	fail
SPD - service entrance	single MOV 40 mm	ok	ok	ok	heat, no fail	fail
SPD - service entrance	single MOV 80 mm	ok	ok	ok	heat, no fail	fail
SPD - service entrance	multiple MOV + multiple gas discharge + sine wave tracking	ok	ok	ok	ok	fail
SPD - service entrance	multiple MOV + multiple gas discharge	ok	ok	ok	ok	fail
PLC		ok	ok			fail
PLC		ok		ok		ok
PLC		ok			ok	ok
PC + monitor		ok				
PC + monitor			ok			
PC + monitor				ok		
PC + monitor					fail	
PC + monitor						fail
Incandescent bulb 60W	tungsten	ok	ok	ok	fail	fail

4.6.2 Simulation of Derating of Synchronous Generator with Unbalanced Load

A 3-phase, 20 kVA, 460V, 60 Hz, wound-rotor synchronous generator with damper windings was modeled in Matlab/Simulink. A 3-phase full bridge rectifier, DC link capacitor, inverter, and resistive load were attached. The load was unbalanced in order to determine inverter sizing and machine derating factor for different percent unbalanced loads. An overview schematic of the system is seen in *Figure 4.11* and the Simulink implementation is shown in *Figure 4.12*.

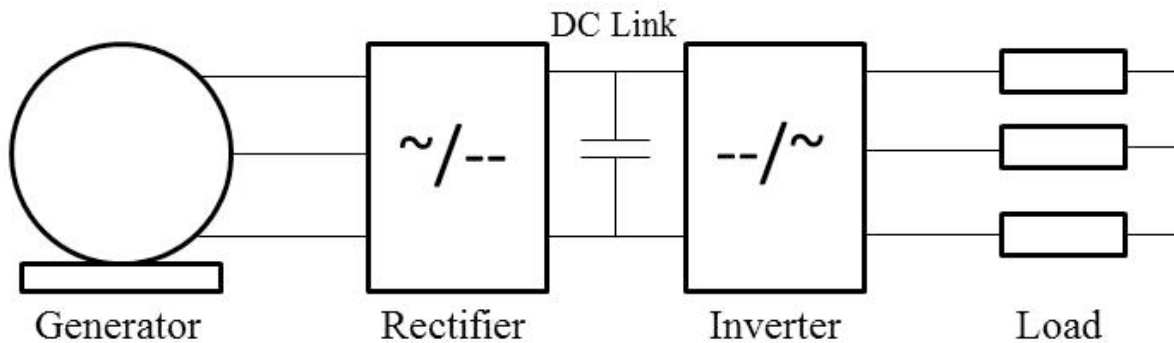


Figure 4.11 Overview of system being modeled including generator, rectifier, DC link, inverter, and load.

The generator was brought up to speed with a step input with a 1 second step. The synchronous speed was 1800 rpm or 188.5 rad/s. A constant voltage of 14.1 V was supplied to the field excitation windings at rated load (10.5 Ω , 10.5 Ω , 10.5 Ω). The output power of the generator with a balanced load was 15.5 kW with a power factor of 0.78. The output power for the inverter was 15.4 kW.

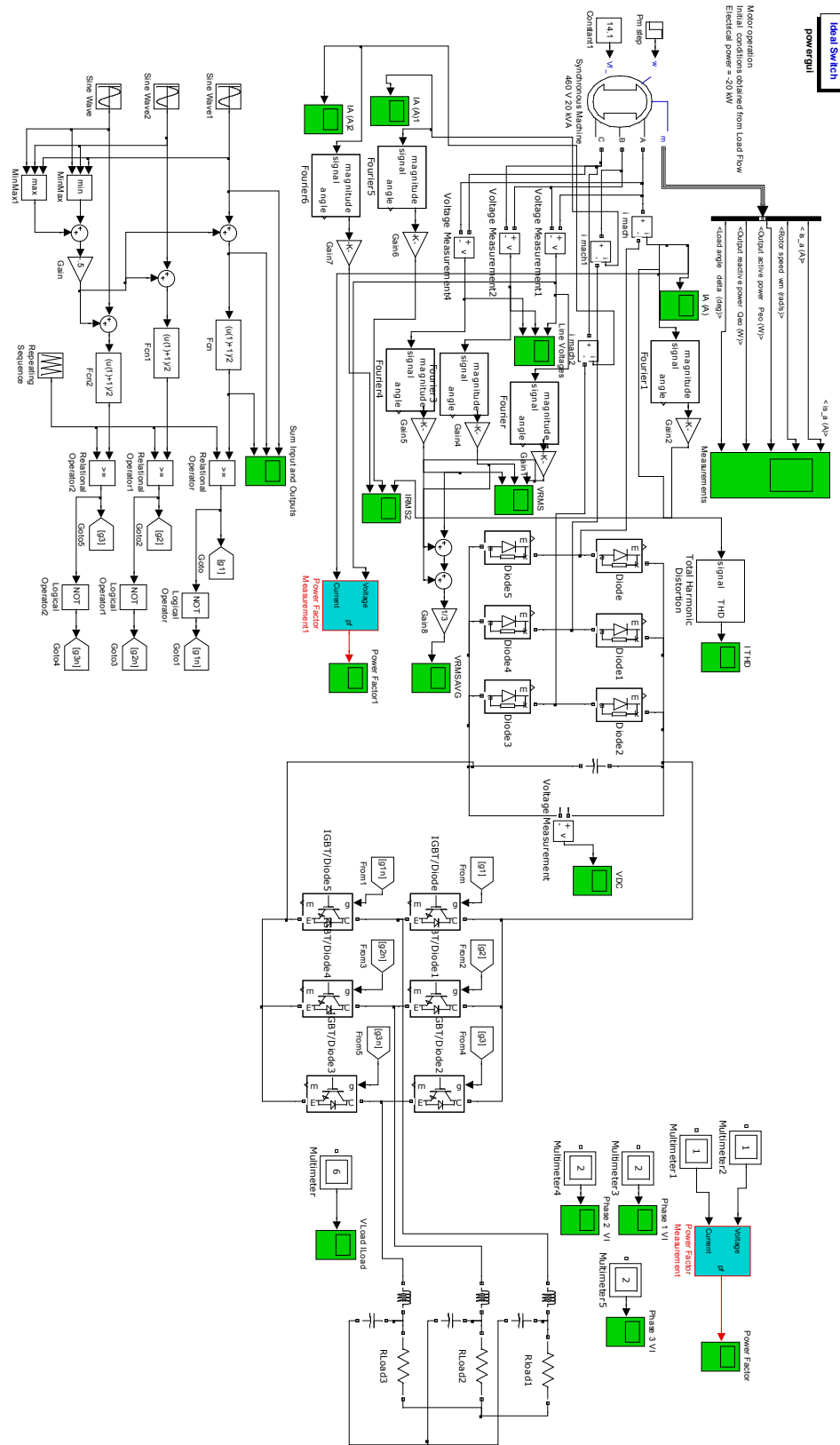


Figure 4.12 Matlab/Simulink schematic of generator, rectifier, DC link, and inverter.

Under balanced conditions and at rated load, the generator output voltages and currents are distorted due to the non-linear aspect of the rectifier operation. The output voltages and currents from the generator can be seen in *Figure 4.13* and *Figure 4.14* respectively. RMS values of generator output voltages and currents were determined through extraction of line-to-line voltage and line current fundamental components via FFT block and scaling the resulting output by the square root of two. The DC output voltage was 600 V (shown in *Figure 4.15*) with a DC link capacitance value chosen to be 300 μF . The inverter output voltages and currents are shown in *Figure 4.16*. The inverter switching was done via space vector equivalent PWM at 2 kHz with a modulation factor of 1. An LC filter (0.01 H and 50 μF , 225 Hz cut-off frequency) was added to the inverter output in order to provide sinusoidal voltages and currents to the load.

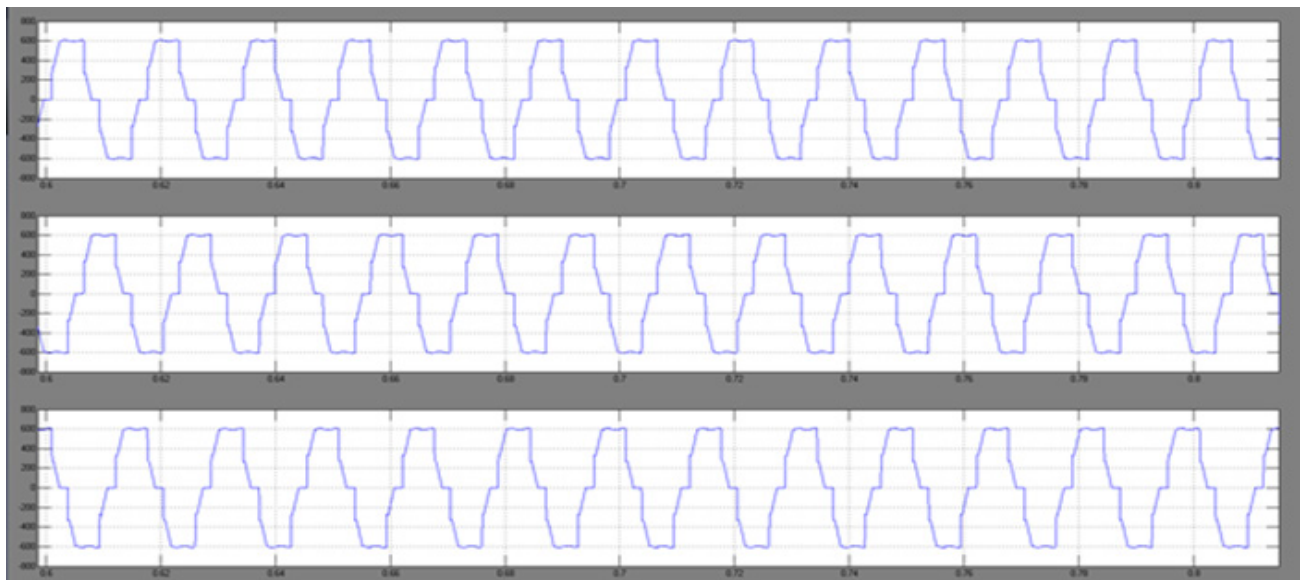


Figure 4.13 Output voltages of generator (460 RMS Value).



Figure 4.14 Output current of generator (phase A) (19.8 A RMS Value).

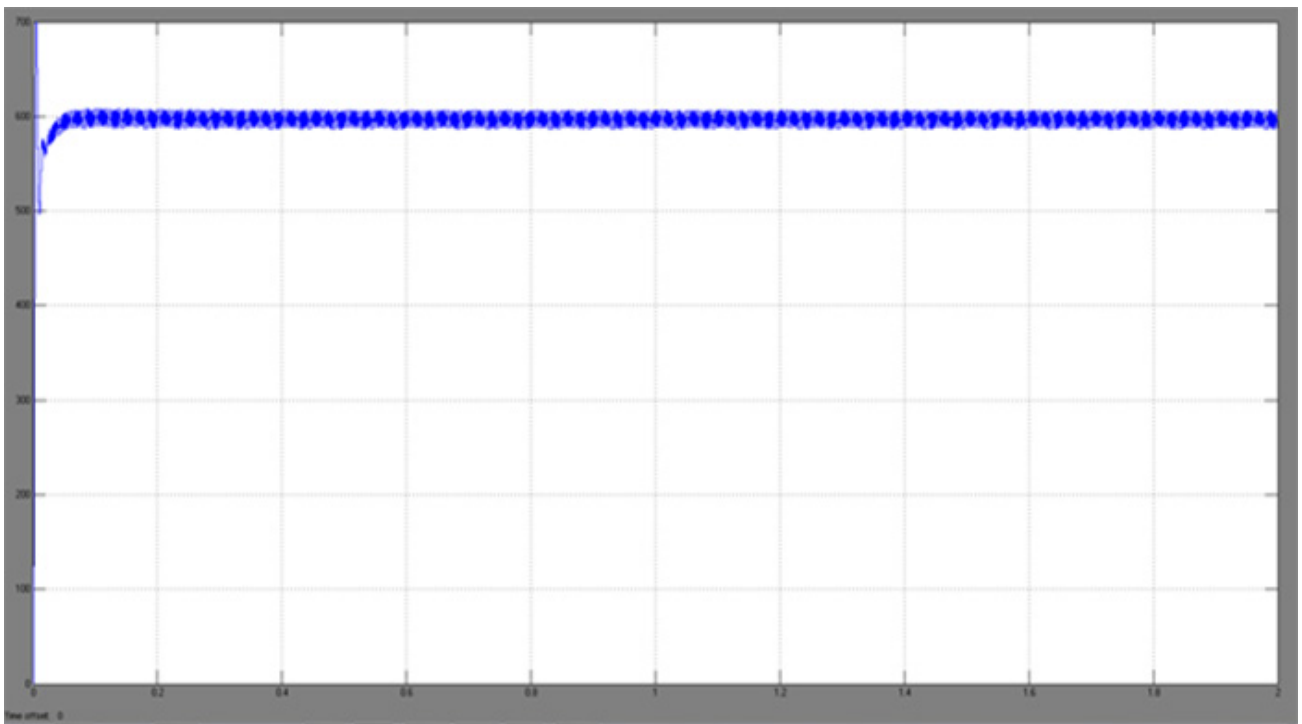


Figure 4.15 DC link output voltage (600 V).

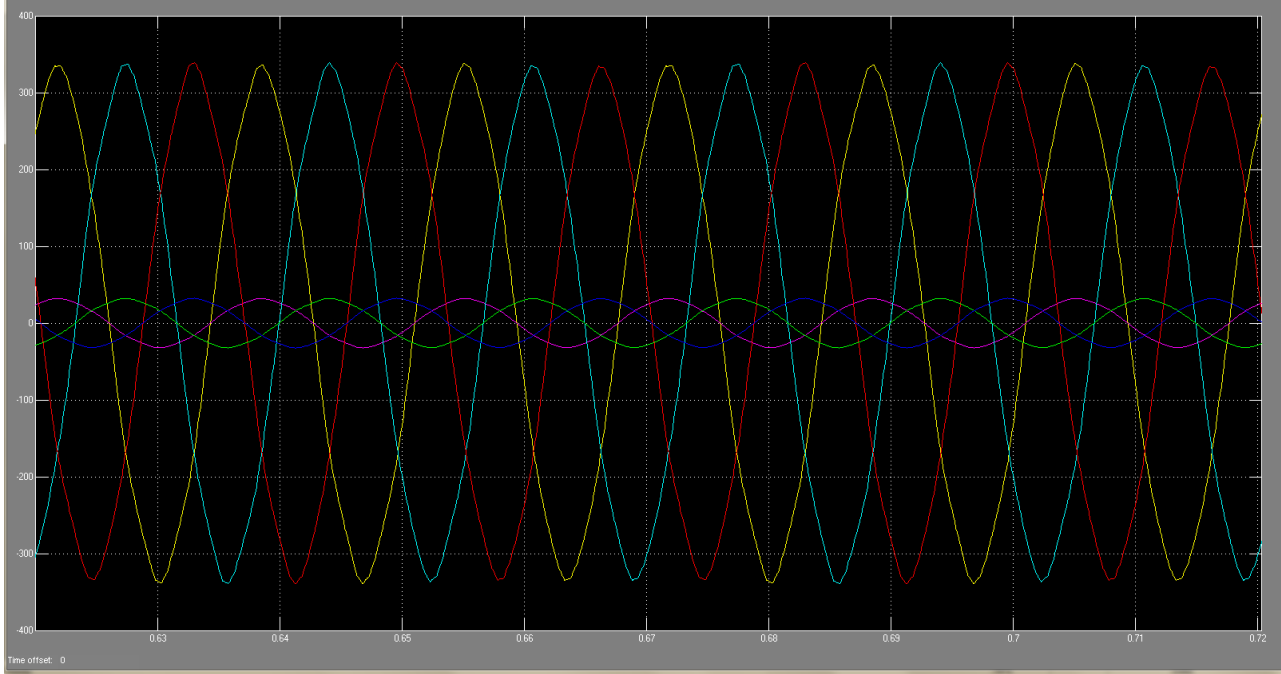


Figure 4.16 Output phase voltages and currents from inverter (340 V_{peak} and 32.2 A_{peak}).

A derating curve was developed for the machine under unbalanced load conditions at rated load (10.5 Ω /phase). This was done by changing the load to different percent unbalance with the same average magnitude as the balanced case. The percent phase voltage unbalance rate (%PVUR) was then calculated by *Equation 4.4* [143]. The I²R losses for the stator and rotor damper windings were then calculated. The unbalanced output currents were then scaled down accordingly until the I²R losses in the unbalanced case were less than or equal to the balanced case I²R losses (1,233 W) and the resulting output power was then calculated. The derating factor (DF) was calculated by *Equation 4.6*. The resulting derating curve up to 15% unbalance can be seen in *Figure 4.17*.

$$\%PVUR = \frac{\text{max voltage deviation from the avg. phase voltage}}{\text{Avg. phase voltage}} \cdot 100 \quad (\text{IEEE Definition}) \quad (4.4)$$

$$\text{Derating Factor (DF)} = \frac{\text{Derated output power}}{\text{Rated output power}} \quad (4.6)$$

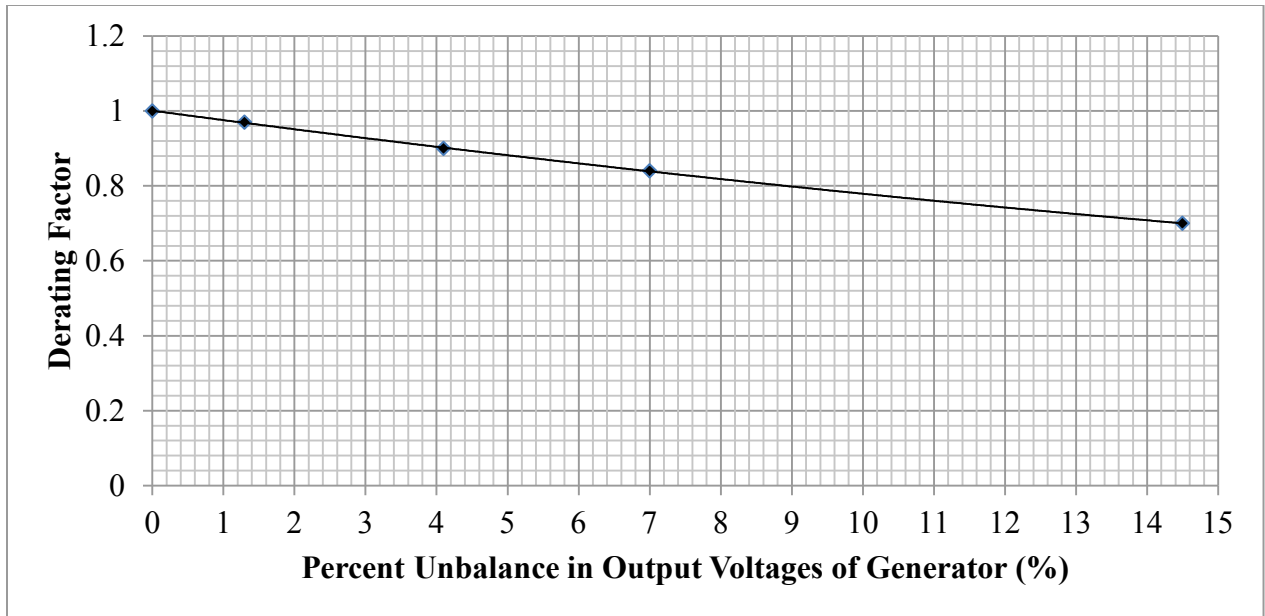


Figure 4.17 Derating factor of generator versus percent voltage unbalance.

Now, the entire system with generator, rectifier, DC link, and inverter was simulated for different percent unbalance loads and a curve was drawn for inverter rating vs percent unbalance. As can be seen in an example in *Table 4.5*, the percent unbalance in the inverter output is much higher than in the generator (27.4% vs 2.4%). The inverter currents were scaled by the corresponding derating factor (from *Figure 4.17*) for the percent unbalance for the generator and the average inverter output voltage remains constant in each case. The rating of the inverter for a certain percent unbalance was determined by taking the highest current in any phase and using that in the power calculation in order to determine the new rating. The resulting inverter rating curve can be seen in *Figure 4.18*.

Table 4.5 Example of voltages, currents, and inverter rating for a specific derating case.

LOAD							
R (Ω)	Vphase (V)	VRMS (V)	Iphase (A)	IRMS (A)	IRMS New (A)		
14.5	404	285.67	28	19.80	18.81		
10.5	352	248.90	33.5	23.69	22.50	Largest	Power at highest current
6.5	248	175.36	38.4	27.15	25.80	26	17450.16 NEW RATING (kW)
	27.4% UB						
GENERATOR				Vf = 14.2 V			
VLL RMS (V)	Iphase RMS (A)						
466.5	18.3						
448.5	21.8		0.95 Derating Factor (From Derating Curve)				
462.5	20.2						
	2.4% UB						

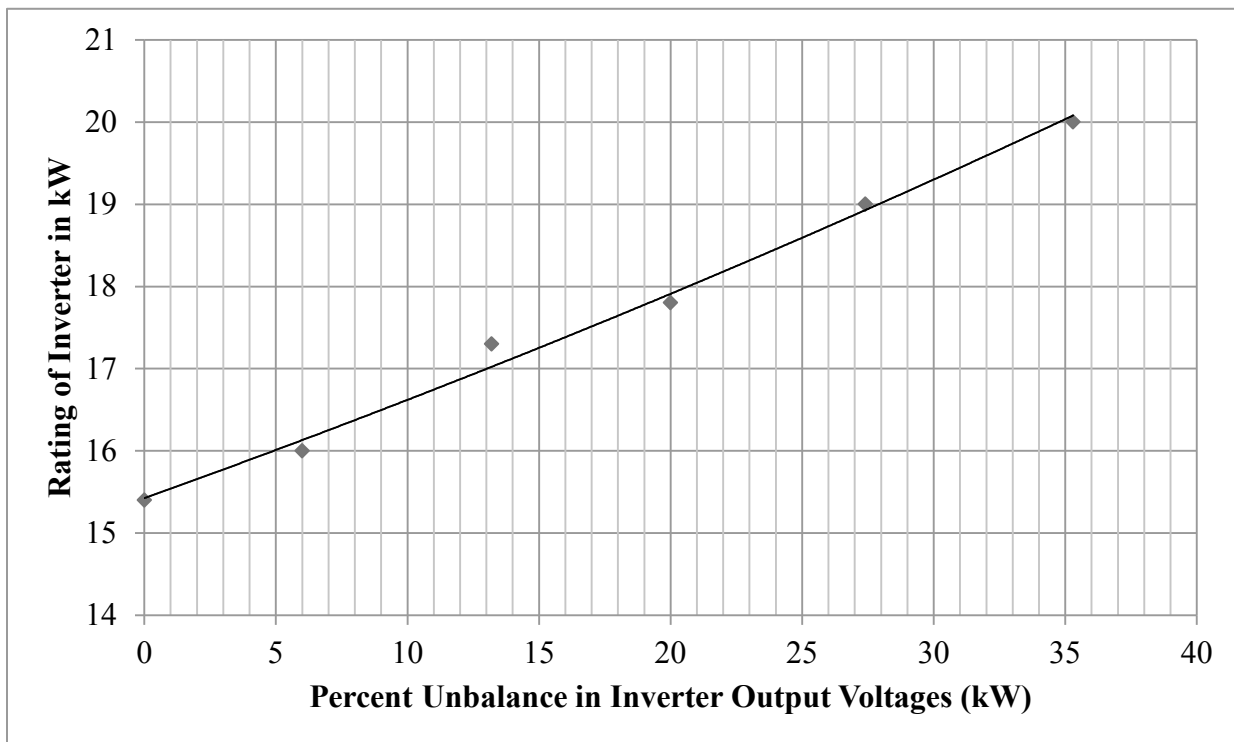


Figure 4.18 Rating of Inverter versus percent unbalance in voltage

4.6 Conclusions

In conclusion, it has been shown that there is definite potential for biogas CHP system implementation in urban buildings for use in emergency power situations. The likelihood of an increase in long term grid outages makes the need for reliable emergency lighting a public health and safety concern. Anaerobic digestion of organic waste is a well-understood technology and a prime candidate for small-scale decentralized power generation as it is the only constant renewable energy source. It has been shown that for a 0.25 to 5 tpd food waste anaerobic digestion system, a 3 to 154 kW electric generator set can be installed to power a similarly rated emergency lighting system while also providing an additional 3 to 160 kW of heating energy via heat recovery. Anaerobic digestion system sizing based on power demand was also presented for a 20 kW emergency lighting system. The most commonly available natural gas fired CHP system contains a 3-phase synchronous generator but it's also possible that self-excited induction generators and permanent magnet generators could be integrated into these systems. A derating curve for a synchronous generator feeding a rectifier and inverter via DC link was developed and an inverter rating curve vs percent voltage unbalance was presented.

CHAPTER 5.

WASTE TO ENERGY SYSTEMS FOR BACKUP POWER IN THE RURAL ENVIRONMENT

5.1 Introduction

In Europe, there are more than 10,000 biogas plants currently in operation with an installed capacity of more than 7,400 MW_e. Germany produces two thirds of the installed capacity or 5,000 MW_e [103]. In contrast, the US has only 2,116 biogas plants with an installed capacity of 60 MW_e (0.8% of installed European capacity) [104]. There is a lot of potential for the US installed biogas electrical capacity to grow. The National Renewable Energy Lab (NREL) claims there is the potential for over 13,000 additional biogas plants producing 7.8 Mt of biogas through the anaerobic digestion of wastewater, landfills, animal manure, and the organic fraction of municipal solid waste (OFMSW) in the United States [104]. This is equivalent to 1.2 billion m³ or 4,000,000 MWh_e of available energy. Further predictions from NREL claim that the methane available from biogas sources could displace up to 46% of natural gas currently consumed by electric power plants as well as the entire natural gas consumption used by the transportation sector (1 billion barrels of gasoline equivalent) [86]. A breakdown of biogas methane potential of major US sources can be seen in *Figure 5.1*.

Looking at the biogas potential of wastewater treatment facilities (WWTF), the US EPA has determined that as of 2011, there were biogas CHP systems in place at 104 WWTFs with installed capacity of 190 MW. It has also been determined that there is potential for CHP facilities at an additional 1,351 facilities with potential installed capacity of over 2,500 MW [105].

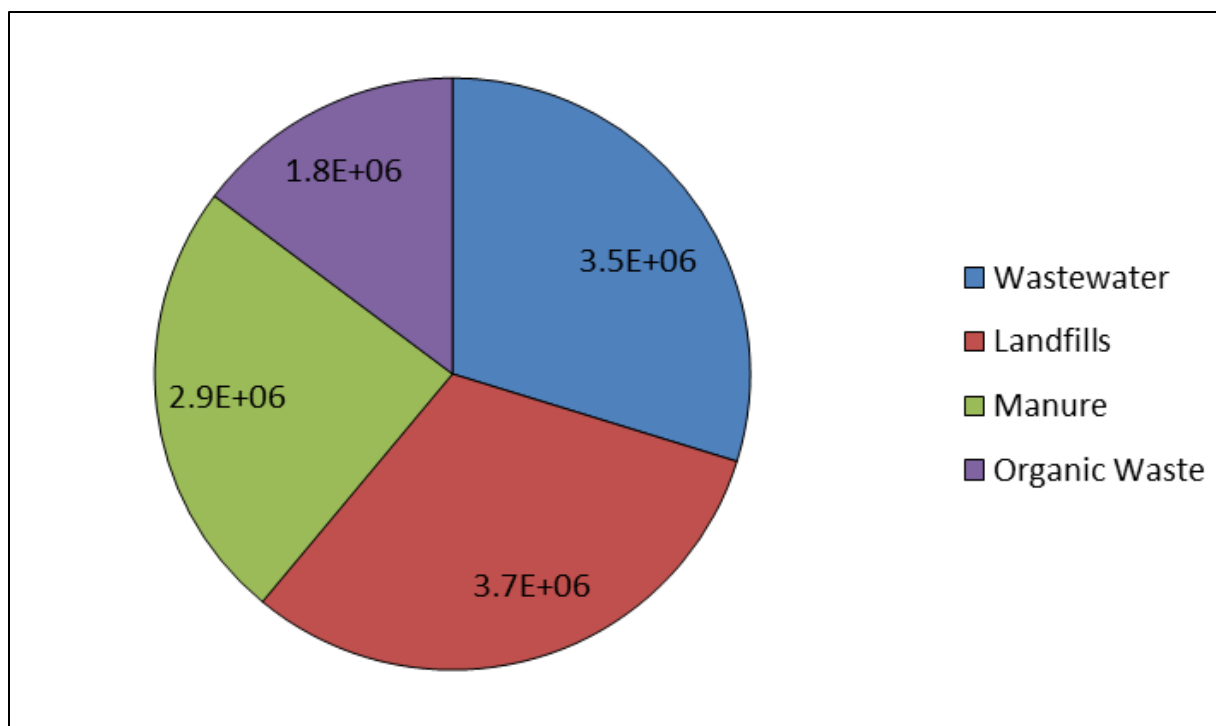


Figure 5.1 Biogas potential (m³) by source in the United States.

According to the “Biogas Opportunities Roadmap” released as part of the US Department of Energy’s “Climate Action Plan” in 2013, there are currently 239 biogas systems installed on farms capable of powering 70,000 average American homes [46]. The report claims that with the proper program incentives and support, there is the potential for up to 11,000 additional agricultural biogas plants to be installed by 2030 that could generate 13 million MWh of electricity per year with an installed capacity of 1,667 MW. This is enough electricity to power over 3 million homes. In addition, if these biogas systems are installed, agricultural sector CO₂ emissions could be reduced by up to 54 million tonnes, equivalent to removing 11.3 million cars from the road each year (4.75 tCO₂/vehicle/year). *Table 5.1* provides an overview of candidate farms for biogas recovery systems.

Table 5.1 Electricity generation potential for agricultural biogas systems.

Animal Sector	Candidate Farms	Energy Generating Potential		
		MW	MWh/year	MMBtu/year
Swine	5,596	804	6,341,527	21,643,632
Dairy	2,645	863	6,802,914	23,218,346
Total	8,241	1,667	13,144,441	44,861,978

In Canada, there also exists great potential for increasing the number of agricultural biogas systems in rural areas. According to a report published in December of 2013 by the Biogas Association of Canada, there are very few agricultural biogas systems installed across Canada, partially due to the lack of feed-in-tariff (FIT) and tipping fee incentives offered. Ontario has 30 agricultural biogas systems installed, Alberta has 5 installed, and only two agricultural AD systems were identified in British Columbia [7]. The agricultural sector (not considering energy crops) in Canada represents the most energy potential from biogas production. According to another Biogas Association report, there is the potential for 550 MW of installed electrical capacity from agricultural biogas systems or the equivalent of 1,650 million m³ per year of renewable natural gas representing 2.1% of Canada's total natural gas demand [106]. The energy potential of different waste sources in Canada is shown in *Table 5.2* and seen represented graphically in *Figure 5.2*.

Table 5.2 Energy potential of different waste sources in Canada.

	Agriculture	Landfills	Organics Residential	Organics Commercial	Wastewater	Total
Electricity Production (MW)	550	95	48	54	60	810
Renewable Natural Gas Production (million m³/year)	1,650	290	140	160	180	2,420
Percent Canadian Electricity Demand	0.9%	0.2%	0.1%	0.1%	0.1%	1.3%
Percent Canadian Natural Gas Demand	2.1%	0.4%	0.2%	0.2%	0.2%	3.0%

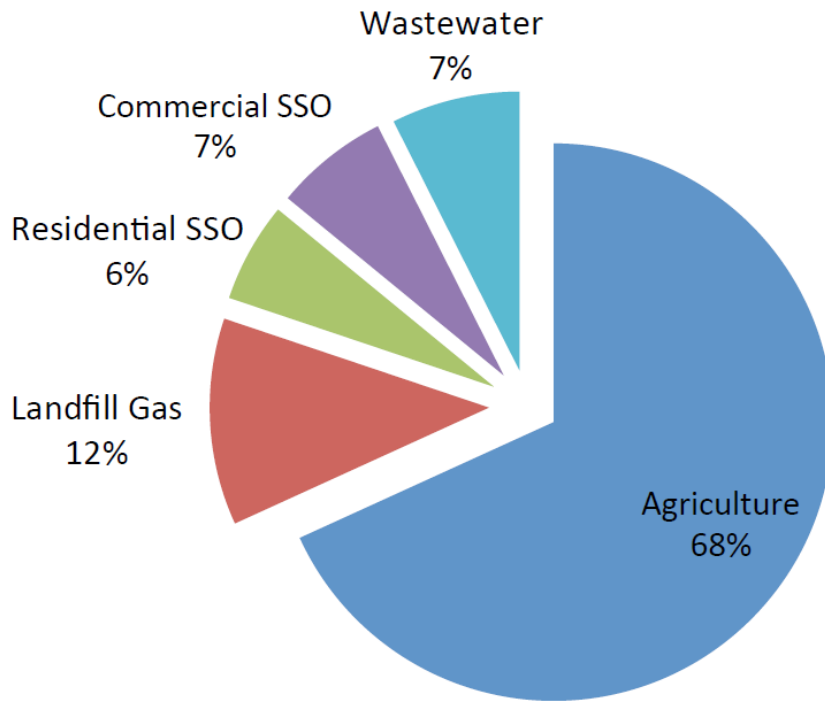


Figure 5.2 Biogas potential in Canada by source.

All of the potential biogas sources taken together could reduce Canada’s greenhouse gas emissions by 37.5 million tonnes of CO₂ equivalent annually. Agricultural biogas production (68%) would represent 25.5 million tonnes of equivalent CO₂ emissions reduction which represents the removal of 5.1 million cars from the road each year. In addition, if the full potential of biogas systems is realized, it would create up to 17,000 short term jobs and almost 3,000 long term system operator and maintenance jobs while adding over \$20 billion dollars to the Canadian economy.

The energy value of the biogas produced from an AD system comes from the methane content of the gas only as carbon dioxide has no energy value. The methane content and total amount of biogas produced can vary greatly depending on which type of substrate is being digested. In order to provide accurate energy estimates for biogas system design and

implementation, the moisture content of the substrate must be known. Further consideration of system type, temperature, organic loading rate, retention time, as well as other factors need to be considered as in order to make accurate energy valuations. The produced gas can be used for combined heat and power (CHP) or fed directly into the natural gas grid as bio-methane once the methane content is upgraded or “sweetened” to natural gas levels. It is also possible to perform a chemical conversion process of the gas into liquid fuels that can be used in the place of traditional hydrocarbon fuels. A basic flow chart of electrical energy production considerations for biogas can be seen in *Figure 5.3*. A summary of electrical energy available from the most commonly digested organic substrates is shown in *Table 5.3* [66][107][108][109].

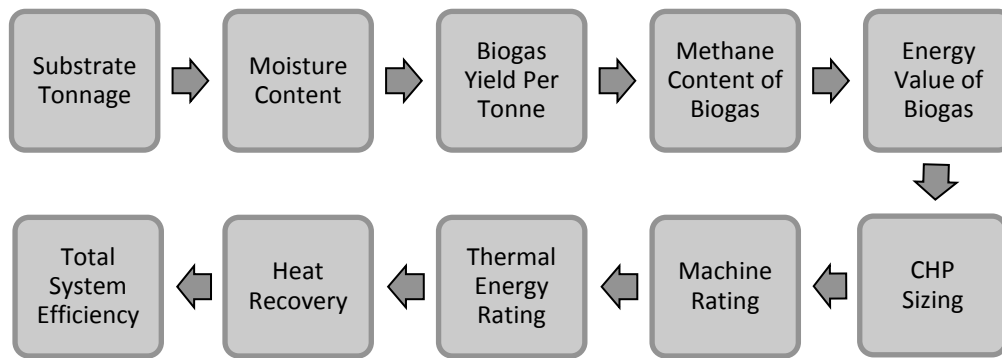


Figure 5.3 Flow chart of energy production from biogas produced through anaerobic digestion.

Table 5.3 Examples of substrates and theoretical biogas yield and electrical power production.

SUBSTRATE	% DRY	BIOGAS (m ³ /t _{DRY})	%CH ₄	POWER (kWh)/m ³
Cattle Manure (liquid)	5-10	100-300	60	6
Cattle Manure (solid)	25-30	600-800	60	6
Pig Manure (liquid)	3-10	300-800	65	6.5
Pig Manure (solid)	20-25	270-450	60	6
Chicken Manure	10-29	300-800	60	6
Grass Cuttings	37	700-800	54	5.4
Corn (ensilaged)	20-40	600-800	52	5.2
Corn (straw)	86	400-1000	68	6.8
Slaughterhouse waste	---	300-700	50	5
Cafeteria Waste	10-37	350-1000	65	6.5

5.2 Waste to Energy CHP System as Backup power for a Dairy Farm

Since the 1980s, the number of power outages in the US affecting more than 50,000 homes or businesses has increased tenfold as can be seen in *Figure 5.4* [26]. Since 2003, the number of power outages caused by extreme weather events has doubled costing between \$20 and \$55 billion dollars [25]. As extreme weather related to changing climate systems lead to more frequent and more severe blackouts in the US, the use of biogas systems that can provide a constant full-load supply of electricity and heat by treating the on-site animal waste and crop residues generated farms should be seriously considered.

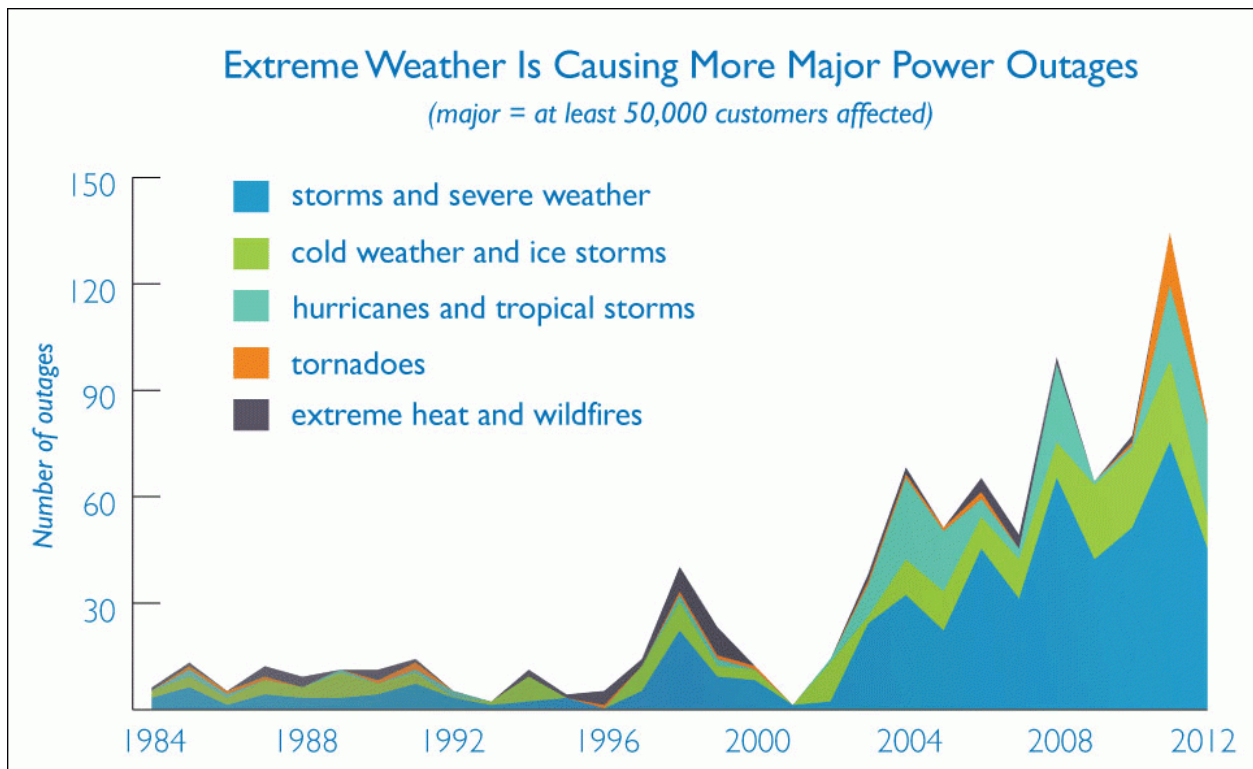


Figure 5.4 Major Power US outages (at least 50,000 customers) from 1984 to 2012.

According to the USDA, there are more than 60,000 dairy farms in operation across the US. The average size of the herd is 135 cows. Approximately 75% of these farms have less than 100 cows but the farms with more than 100 cows produce more than 80% of the milk. The dairy industry is responsible for almost one million jobs in the US and generates close to \$150 billion dollars annually. The largest dairy farms in the US can have more than 15,000 cows but the most prominent herd size with over 22,000 operations in the US is 50-99 cows. The average amount of cows per farm (135) falls in the 100-199 herd size range with nearly 10,000 farms in operation [110].

A New York State Dairy farm energy audit performed in 2003 provides an overview summary of energy use on an average farm and can be seen in *Figure 5.5*. The milk production equipment, including the milk cooling, vacuum pumps to collect the milk, and water heating for washing the milking equipment and bulk storage tank, accounts for 60% of the typical energy usage on a dairy farm [111].

Ventilation and lighting make up 34% of the energy usage. The combination of the energy demand of these five categories represents the essential energy loads of the farm and comprises 94% of total energy usage. This means that in order to keep a dairy farm in operation and functioning properly in the case of an extended power blackout, the emergency load will be essentially the same as the full operating load and a backup generator can be sized with that in mind. It is important to note that the average startup load can be 2-12 times larger than full load conditions of the equipment depending on the state of the equipment at power interruption. It is recommended that backup generators be sized with 20% growth factor included as well [112].

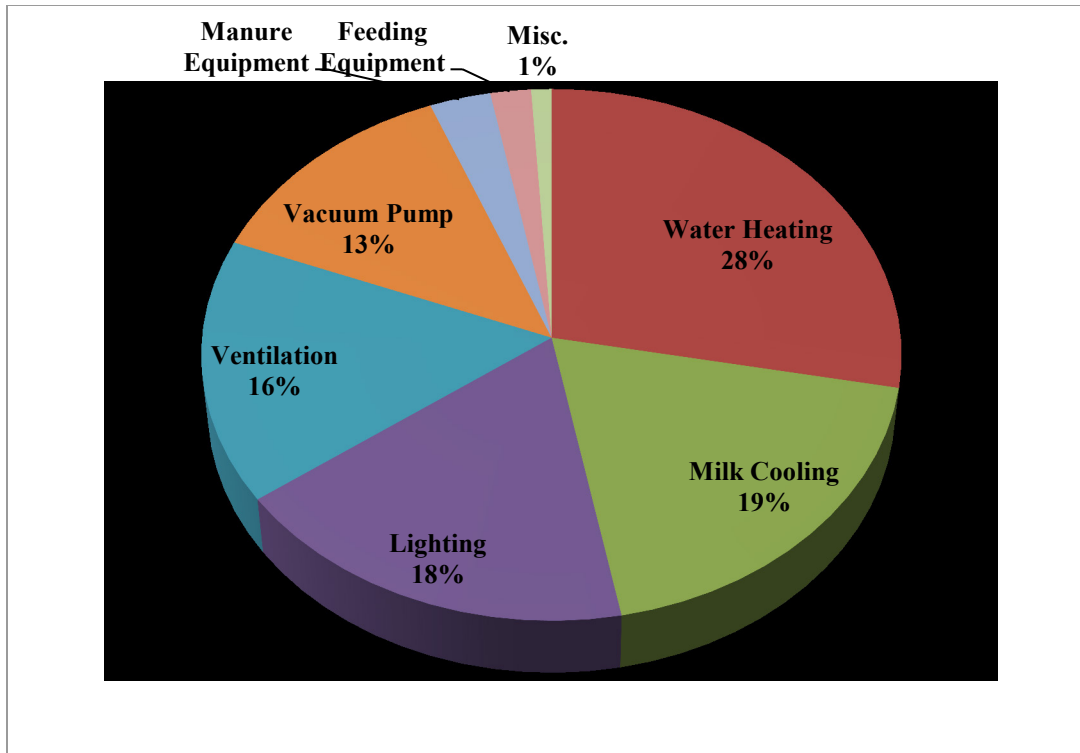


Figure 5.5 Typical energy use by equipment category on a dairy farm.

From a survey of agricultural biogas systems installed in the US, a graph has been developed of the rating of the generator installed at each of these locations to give an idea of the range of system sizing for farms with similar herd sizes [113]. This data is presented in *Figure 5.6* with a line of best fit calculated and the resulting formula given as $y=0.2x+116$. This data can be used to aid in preliminary investigation of biogas generator system sizing.

By taking a closer look at the energy use by equipment category, the proper sizing of a backup generator can be determined. A list of common dairy farm equipment and typical power ratings from a survey of 177 dairy farms (with an average of 70 cows per farm) located in Ontario are provided in *Table 5.4* [114]. The essential equipment load rating ranges from approximately 9 kW up to 40 kW with possible peak loading (all equipment engaged at once) ranging from 15 kW to 75 kW.

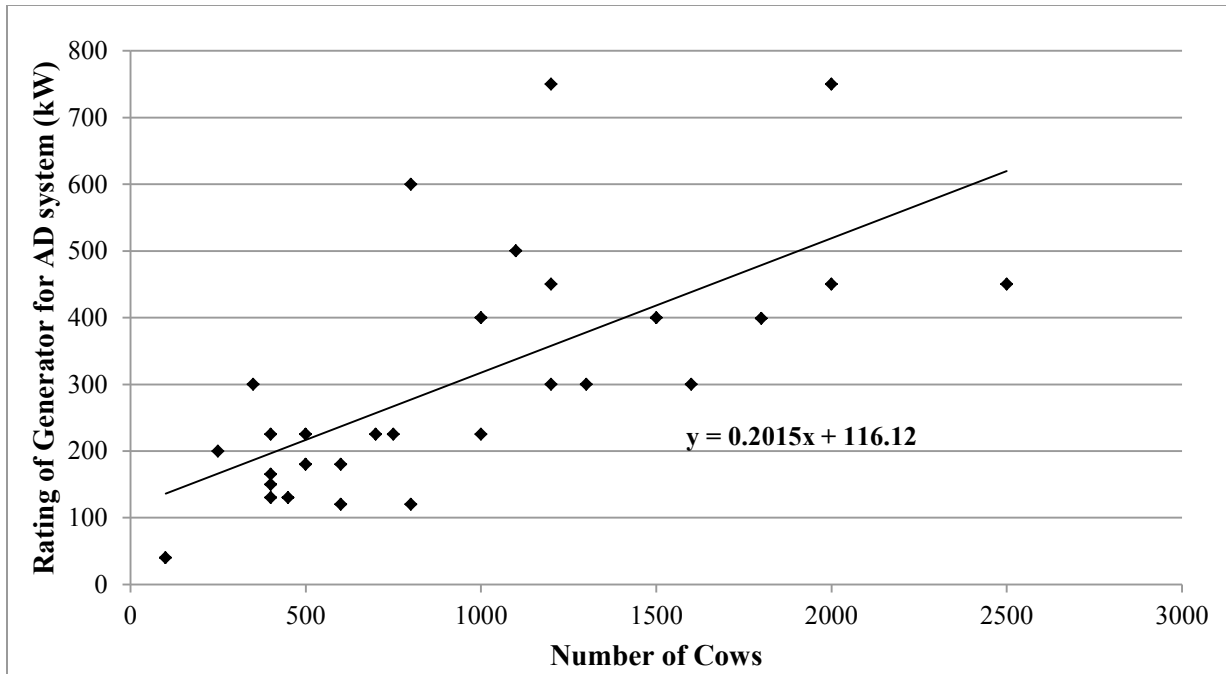


Figure 5.6 Survey of herd size and installed generator capacity of agricultural AD systems.

Table 5.4 Typical wattages of standard dairy farm equipment

Dairy Farm Equipment	Typical Wattage
Bulk Milk Cooler	1500-12,000
Electric Fences	7-10
Feed Conveyor	800-5,000
Feed Grinder	1,000-7,500
Feed Mixing	800-1,500
Gutter Cleaner	3,000-5,000
Infrared Lamp	250
Milking Machine Vacuum Pump	800-5,000
Milking Parlor Heater	2,000-10,000
Shop Tools	300-1,500
Silo Unloader	2,000-7,500
Space Heater	1,000-5,000
Ventilation Fans	300-800
Water Heater	1,000-10,000
Water Pump	500-2,500
Yard Light	100-500

In order to determine the required size of a backup generator for a specific farm, a list of the equipment that needs to be operated simultaneously has to be made. This list of loads can vary from farm to farm depending on several factors including the size of the farm, time of year, time of day, specific workflow of staff, etc. From Statistics Canada, the annual electricity and heating load of an average farmhouse in Ontario is given as approximately 3.4 kW or 30,000 kWh per year [115]. The remainder or majority of the farm load can range from 5-10 kW for a minimum of essential equipment or up to 100 kW of electricity and heating if it is assumed that every piece of equipment needs to be energized at once on a larger farm. The Ontario Ministry of Agriculture, Food, and Rural Affairs (OMAFRA), claims that the total energy demand on a dairy farm ranges from approximately 800 – 1,400 kWh per cow per year with a cost of between \$6,700 and \$10,000 CAD per kilowatt installed or between \$1,000 and \$2800 USD per cow for smaller farms (100-250 cows) [116][117]. A graph of the price range of installing a small biogas project can be seen in *Figure 5.7* and the range of the energy value of the farm waste seen in *Figure 5.8*.

If the average Ontario farm with 70 cows is considered, a CHP system sized from 10 kW to 15 kW is required $((70 \text{ cows} * 800-1400 \text{ kWh/cow/year} + 30,000 \text{ kWh}) / 8760 \text{ hours per year})$ where the 30,000 kWh represents energy needed for the farmhouse. The feasibility of this CHP biogas system sizing can be investigated by comparing these values with information about typical performance of agricultural anaerobic digestion systems in Ontario. According to OMAFRA, a dairy farm with 70 cows (plus replacements) could generate 2800 wet tonnes of manure per year that contains 48 kWh of energy per wet tonne, or 134,400 kWh of energy [117]. This is equivalent to a 16 kW CHP genset running 95% of the time with a 35% electrical efficiency and a 45% heating efficiency. From this example, it can be seen that the theoretical

energy content of the manure generated by a 70 cow dairy farm would be sufficient to meet the entire energy needs of the farm.

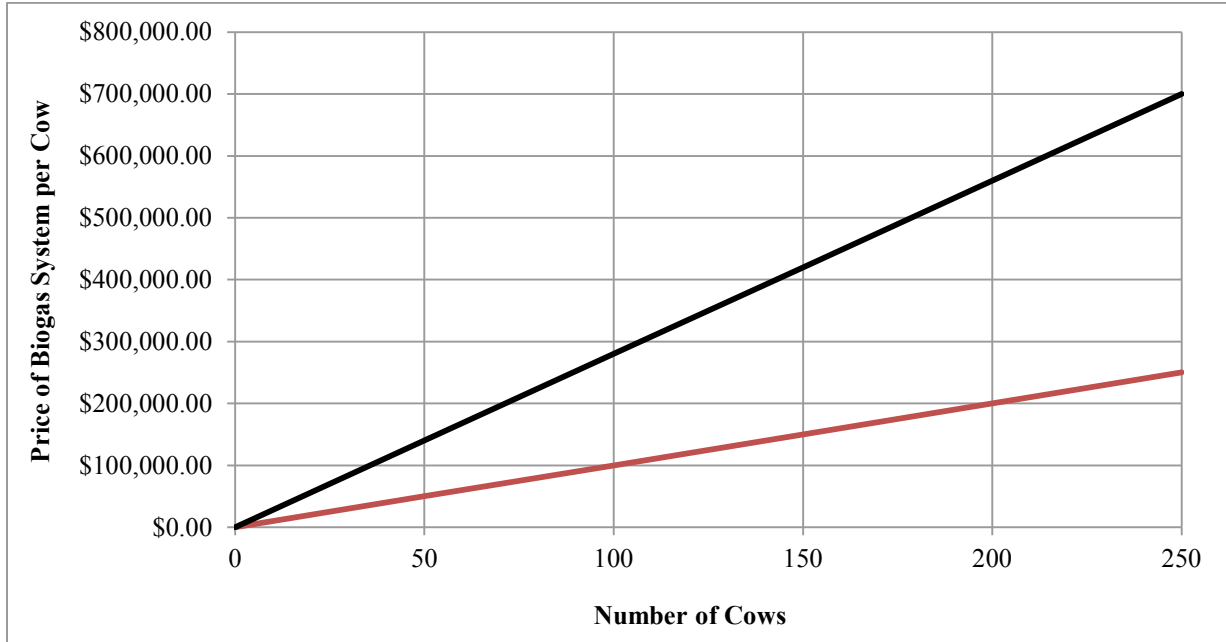


Figure 5.7 Agricultural biogas system cost range per number of cows (100 – 250)

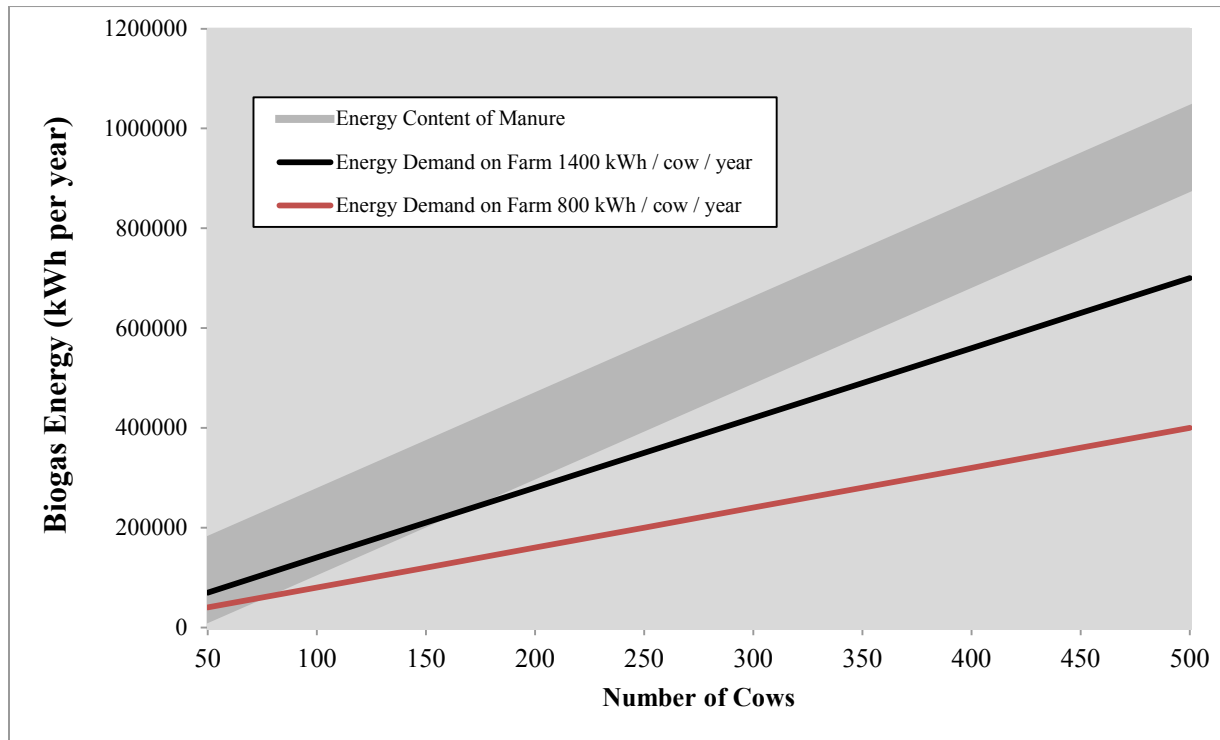


Figure 5.8 Range of energy demand for a dairy farm with energy content of manure.

In order to have a baseline with which to compare an agricultural biogas system, the cost of running a backup diesel generator is investigated for different loading rates from quarter loading up to full loading for generators sized at 20 kW up to 200 kW. The diesel consumption is provided in gallons per hour based on different loading rates in show in *Table 5.5*. Prices are given in US dollars and it is assumed that the price per gallon is \$4 USD. In the next section, a more detailed case study of an agricultural biogas system will be presented that takes into account the effect of climate change related blackouts on the feasibility of installing an agricultural biogas system.

Table 5.5 Diesel generator sizing and fuel consumption and prize per day of operation at full load.

Generator Size (kW)	1/4 Load (gal/hr)	1/2 Load (gal/hr)	3/4 Load (gal/hr)	Full Load (gal/hr) \$4 USD/gal.	Price (\$/hr) <i>full load</i>	Price (\$/day) <i>full load</i>
20	0.6	0.9	1.3	1.6	6.4	153.6
30	1.3	1.8	2.4	2.9	11.6	278.4
40	1.6	2.3	3.2	4	16	384
60	1.8	2.9	3.8	4.8	19.2	460.8
75	2.4	3.4	4.6	6.1	24.4	585.6
100	2.6	4.1	5.8	7.4	29.6	710.4
125	3.1	5	7.1	9.1	36.4	873.6
135	3.3	5.4	7.6	9.8	39.2	940.8
150	3.6	5.9	8.4	10.9	43.6	1046.4
175	4.1	6.8	9.7	12.7	50.8	1219.2
200	4.7	7.7	11	14.4	57.6	1382.4
230	5.3	8.8	12.5	16.6	66.4	1593.6
250	5.7	9.5	13.6	18	72	1728

5.3 Case Study of Anaerobic Digestion System for Backup Power for 140 Cow Dairy Farm

The dairy farm case study being investigated is Cobden Dairy Farm and it is located outside of Peterborough, Ontario. It was selected from the project database in NRCAN's RETScreen Clean Energy Project Analysis Software. The farm is a 200 tie-stall dairy cow farm with 140 milking cows plus replacements (calves). A feasibility study was performed using

reported monthly heat and electricity load profiles for this dairy farm, in order to determine if the farm energy loads could be met by installing an anaerobic digestion system with CHP. In addition, the financial impact that up to 7 days of extreme weather related blackouts per year (without any diesel backup) would have on the farm in question was investigated.

The farm is currently connected to grid electricity (\$0.124 / kWh) (2014) and uses a biomass fired boiler (\$285 / tonne) (2014) for a mini-district heating style system that heats two houses, a machine repair shop, and the milking parlor barn [118][119]. The load profile of the farm can be seen in *Figure 5.9*. In the middle of winter, the heating load peaks at around 68 kW while the electrical load is around 40 kW peak. In the middle of summer, the heating load is only around 2 kW and the peak electrical load is around 58 kW due to the extra ventilation needed for cooling the barns.

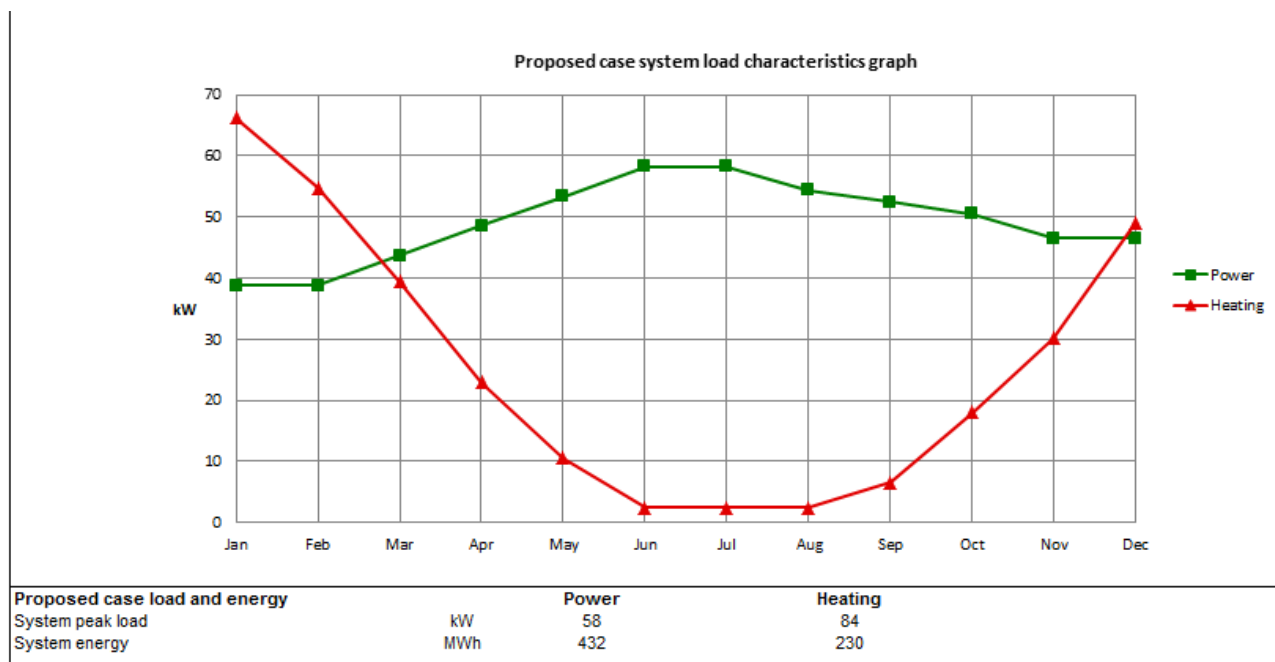


Figure 5.9 Annual heating and electricity load profile for dairy farm.

The following financial and system design information is used for the RETScreen feasibility study of this project. The floor of the farm area that requires heating totals approximately 1,200 m² and the buildings are insulated to a standard of -20°C. The proposed AD system is designed to produce biogas that contains 67% methane. The CHP generator set is a 65 kW biogas engine that runs at 30% efficiency with an attached heat exchanger that runs at 75% efficiency to provide heated water to existing biomass boiler to offset biomass pellet costs. The heating capacity is 127 kW or 152% of the load. The cost of the genset is estimated to be \$110,500 including installation and requires repairs every 50,000 hours at a cost of \$10,000. Including an oil change every 500 hours, an annual operation and management cost is calculated to be \$2,200. A survey of North American biogas generator set prices for 12 kW up to 100 kW (without installation) is shown in *Figure 5.10*.

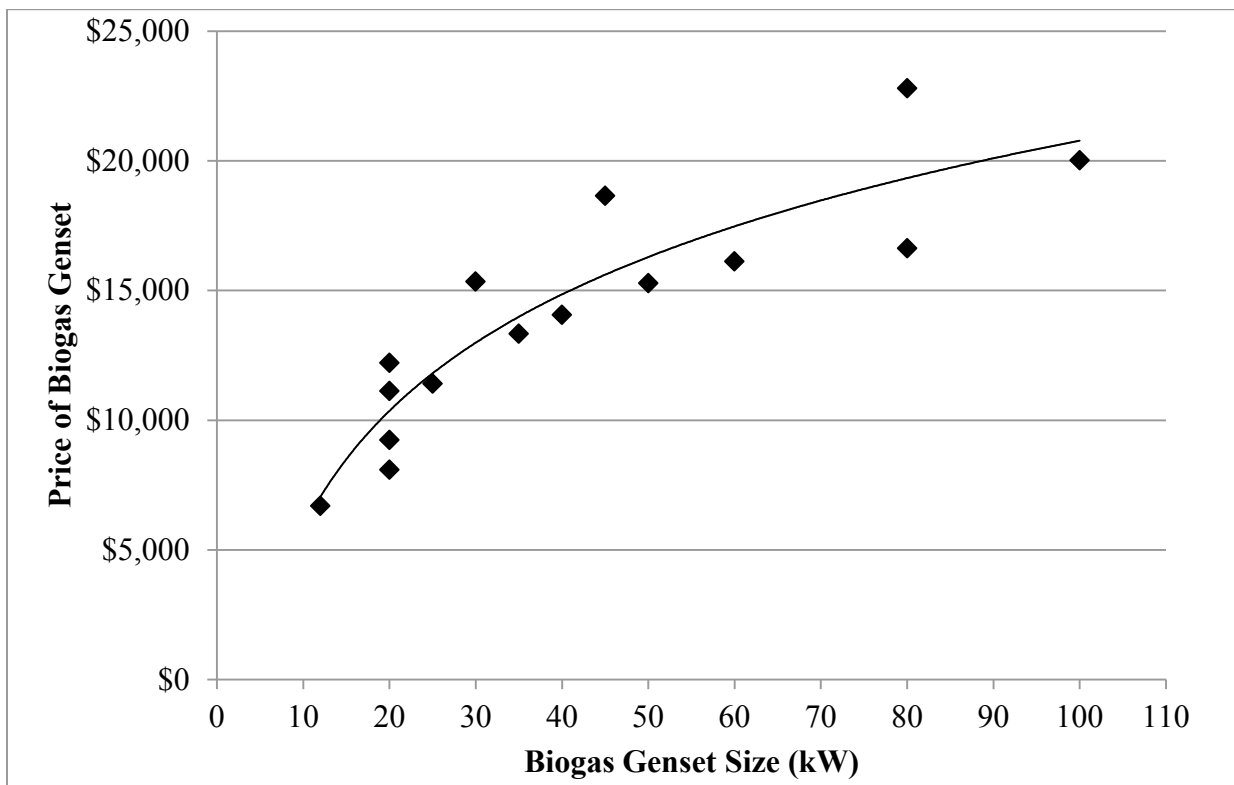


Figure 5.10 Price range of biogas gensets from 12 kW to 100 kW based on market data

The anaerobic digestion tank itself is a gravity-fed holding tank modified with plastic pipes for heating, insulation, a gas cover for biogas storage, and a flare for excess gas at a cost of \$80,000 for the tank modifications and \$25,000 for the flare equipment. Additional costs include a preliminary feasibility study for approximately \$2,400, a net-metering electrical upgrade that include a single-phase changeover switch (for islanding operation) costing \$2,400, and energy efficiency upgrades on the electrical system to reduce the load by 3% for a cost of \$1,000. Additional energy saving upgrades could be made according to a recent study performed by OMAFRA. Based on a survey of energy use on dairy farms, the study concluded that upgrading milking equipment could result in 30-50% energy savings in that area, proper maintenance and control of ventilation systems could save 15-50% of the energy used in that area, and using energy efficient light bulbs (CFL, LED) could save an additional 15-75% of the energy used for lighting. A total of 20-40% of the farm energy use could be reduced through simple, straightforward steps [114].

The project life is set at 20 years and inflation is set at 2%, fuel escalation cost is set at 2%, a discount rate in Net Present Value (NPV) of 10%, and the project will not be financed and paid for upfront. In addition, there is currently a government program in place in Ontario that allows half of the cost of a project that deals with manure management to be funded up to \$50,000 [117]. The system overview schematic can be seen in *Figure 5.11*.

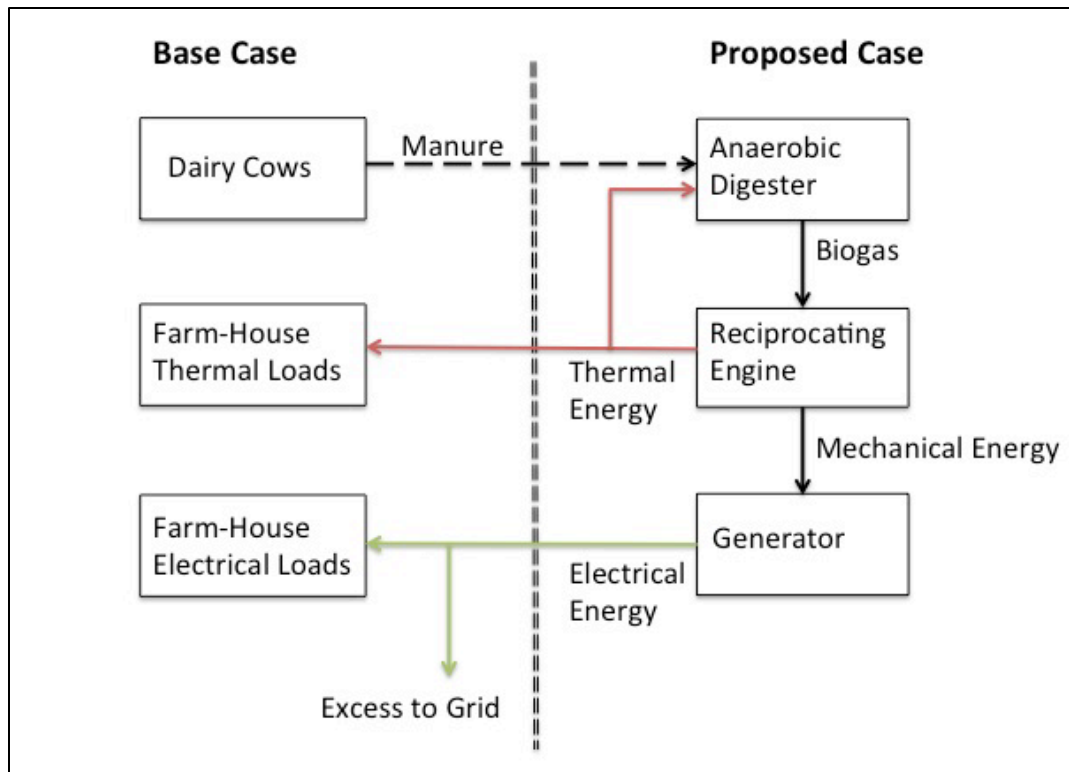


Figure 5.11 Agricultural biogas CHP system schematic

Due to the predicted increase in blackouts related to extreme weather events, it becomes necessary to determine the potential losses that a dairy farm would incur in a case where there is no access to diesel fuel for a back-up generator for a period of one to seven days. This could be due to extreme flooding and erosion cutting off access to roads or destroying grid infrastructure, ice storms wiping out electrical lines and/or preventing travel, high winds destroying lines and grid infrastructure, earthquakes, or a combination of these events.

The milk productivity losses are the largest and most obvious loss that would be incurred from an extended blackout. The measure used for dairy cows is the hundredweight or the centum weight abbreviated as cwt. In the U.S. and Canada a short hundredweight or cwt is given as 100 pounds or 45.36 kg. As of September, 2014, the price that dairy farmers can sell their milk is \$25 USD/cwt. 100 pounds of milk is equivalent to 11.6 gallons or 44 liters. The historical pricing

range can be seen in *Figure 5.12* [120]. A typical dairy cow produces approximately 30 liters of milk per day [25]. This means that a dairy farm would incur losses of \$17 USD per cow per day (eg. 140 milking cows = \$2,380 USD losses per day).



Figure 5.12 US Milk Farm Price Received Chart (2010 to September 2014)

Dairy cows need to be milked twice per day, typically at 5am and again at 5pm. If there is no electricity to power the pumps and robotic milking devices that are typically used on dairy farm, then the cows must be milked manually, requiring extra workers. Most farms in the US and Canada either have less than 250 cows or more than 700 cows. In the US, the majority of dairy farms have 250 cows or less but 86% of milk comes from farms with more than 100 cows [121]. Farms with less than 250 cows average 3.5 workers and 82 cows per employee. Farms larger than 700 cows have an average of 12 workers and 150 cows per employee [122]. On average a worker can manually milk 20 cows per day [123]. Farm hands make on average \$28,000 per year or \$76 per day per worker [124].

Farms in North America also require milk collection from their bulk storage containers every two days referred to as Alternate Day collection. In order to ensure freshness milk in the tank cannot be more than 2 days old. Bulk containers must be kept at 3-4°C. Regulations require milk to be cooled to 5°C within 2 hours of milking as it can spoil in 3-4 hours at ambient temperatures without cooling [125].

In addition, if cows are milked even a few hours late, they can experience discomfort and become restless. If milking is not performed in a timely fashion, the cows can develop mastitis, which is an udder infection, and this infection can be deadly. Also, milk from cows undergoing antibiotic treatment for mastitis cannot be used until the antibiotics have cleared the system. If the cow must be culled, the resulting beef can be sold for approximately \$80/cwt. If cows die due to infection, replacement cows can range from \$1200-1600 per head [126].

A summary of losses per day for dairy farms ranging from 100-200 cows as well as the 140 head farm being investigated are shown in *Figure 5.13*. These losses include milk losses from the cows, the milk storage losses, and additional labor.

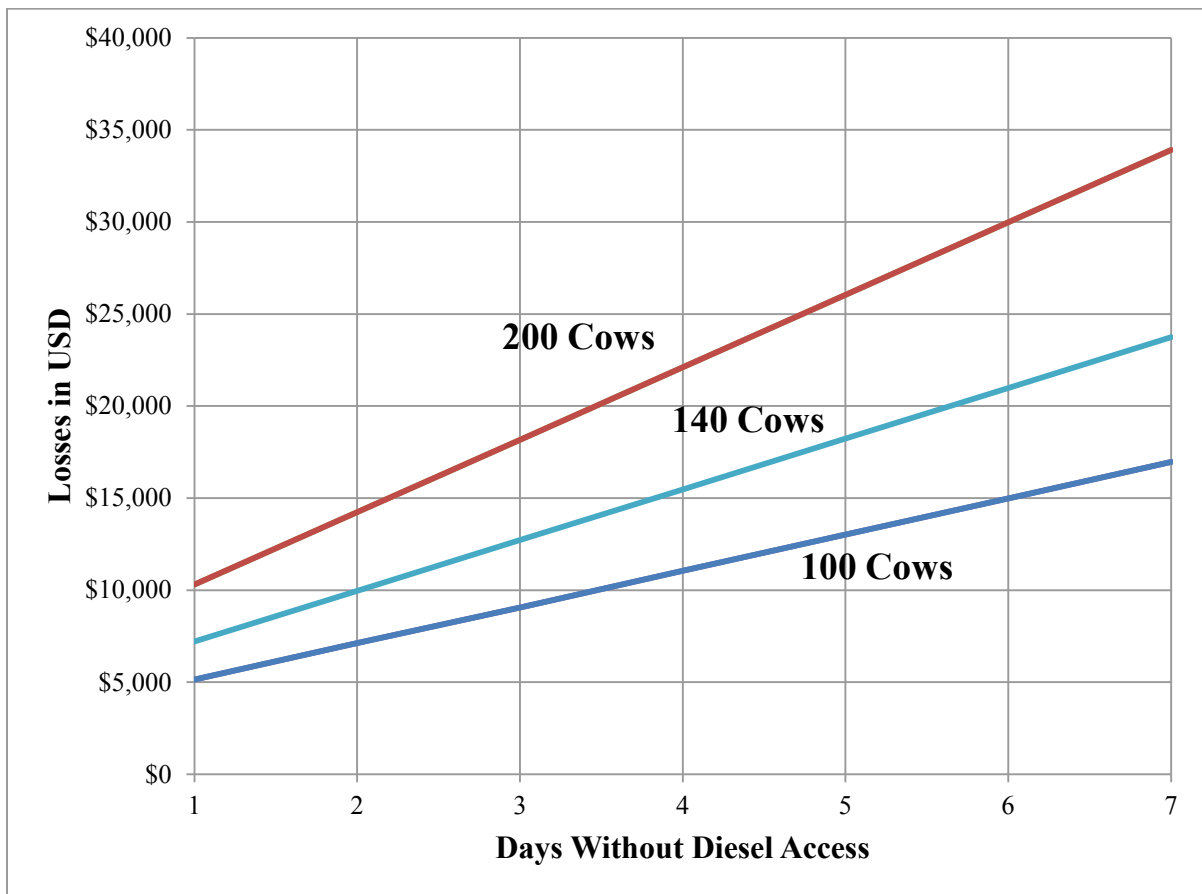


Figure 5.13 Losses for 100-200 cow dairy farm without backup diesel access for up to 1 week.

RETScreen financial analysis was performed for cases where an agricultural biogas system replaces the main grid electrical load as well as the installed heating system performed for the three most common heating systems: biomass wood pellet, natural gas, and propane heating systems. Before the cash flow analysis of the biogas systems are investigated, it is first necessary to look at the current cash flow analysis of farms in Ontario, Canada. The Canadian Dairy Commission released a report in 2014 that provides the financial information for a survey of dairy farms in Ontario from 2004 to 2013. For the year of 2013, the bottom 15 dairy farms had an average of 47.8 cows and average net income of \$1,582, the middle 28 farms have an average of 72.8 cows and an average net income of \$108,376, and the top 15 farms have an average of 146 cows, and an average net income of \$395,046. The average number of cows per dairy farm in the province is 85.3 with an average total net income of \$154,894 [127]. The total revenue, total expenses, and net income for all of the farms surveyed are presented in *Figure 5.14*. In recent years, the total expenses have gone up, and the total revenues are down, making the installation of biogas systems more attractive if the payback period is reasonable and the income generated is substantial.

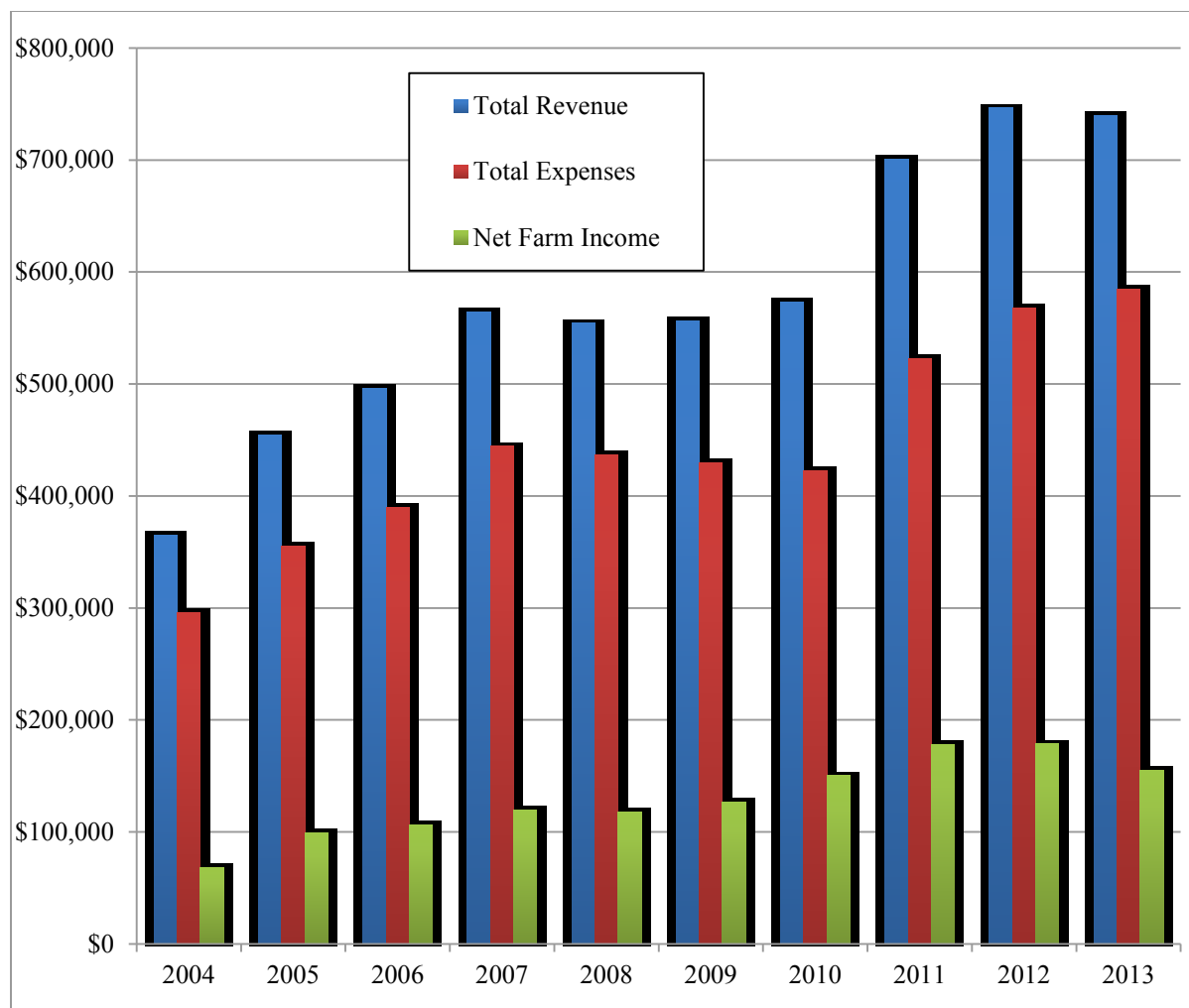


Figure 5.14 Total Revenue, Expenses, and Income for a survey of Ontario Dairy Farms from 2004 to 2013.

A cumulative cash flow analysis was performed using RETScreen for a biogas project with a 20 year lifespan replacing the different heating systems mentioned previously. The case studies include a case where no feed in tariff for electricity is applied, a case where there are no major grid blackouts causing financial losses, and a case where there is a feed in tariff as well as 7 days of blackouts per year. The feed in tariff for Ontario for biogas systems rated below 100 kW currently stands at \$0.26/kWh with a 2% price inflation rate guaranteed for 20 years [128]. Current electricity prices in Ontario average \$0.124/kWh [118]. Biomass heating system wood pellets cost approximately \$285 per tonne of pellets in Ontario (including delivery) [119].

Natural gas prices are currently rated at \$0.20 per meter cubed [129]. Propane prices are currently rated at \$0.71 per liter [130]. A fuel escalation inflation rate was set at 2% for all cases.

In the first case shown in *Figure 5.15*, a biomass wood pellet heating system is replaced and the resulting payback period with no feed in tariff is approximately 2.7 years with a positive cash flow after 20 years of \$1.4 million. With feed in tariff (\$0.26/kWh) and no major outages, the cumulative cash flow after 20 years is approximately 2.4 million dollars and the payback period is 1.5 years. With feed in tariff and 7 days of outages the cumulative cash flow is approximately \$3 million after 20 years with a payback period of only 1.4 years. The \$3 million could be considered a loss when compared with a case with no biogas system installed.

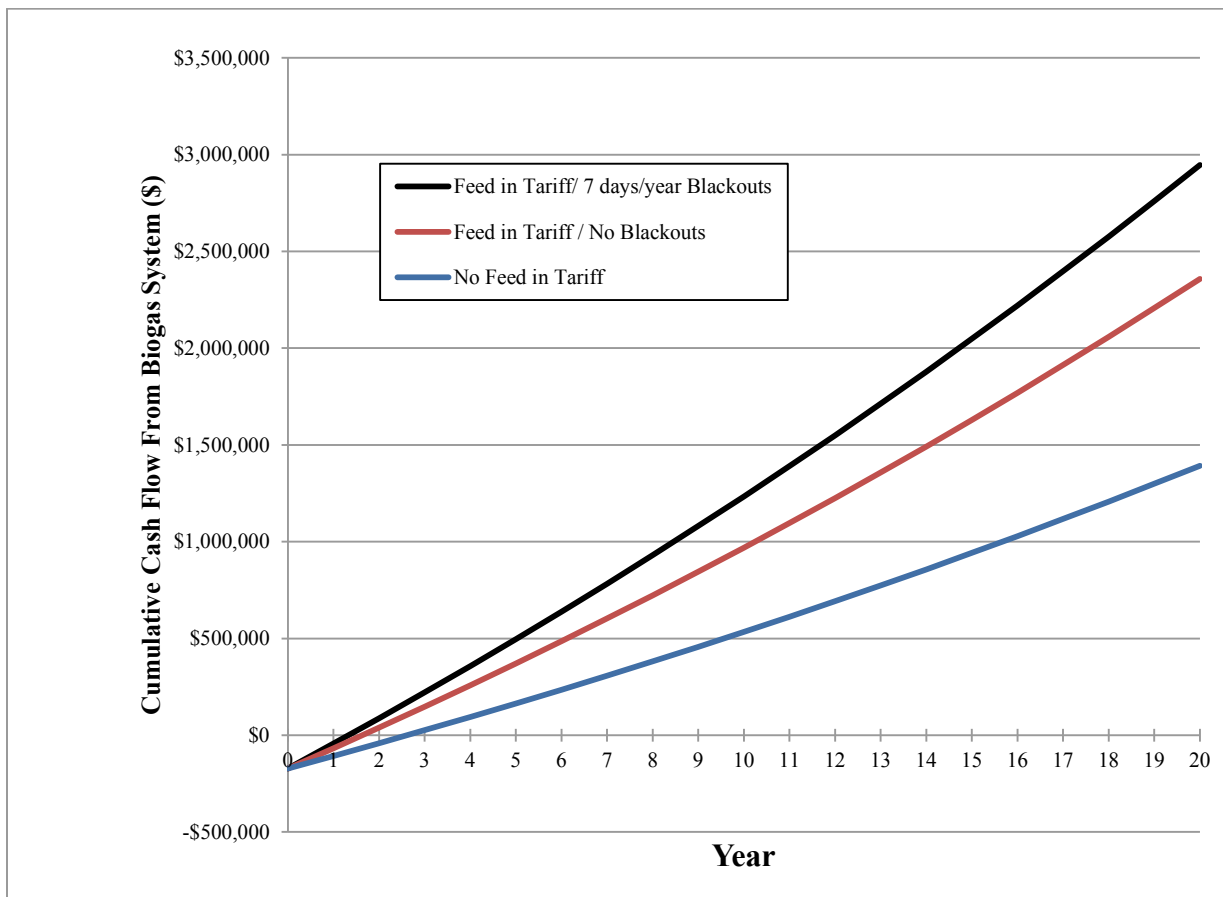


Figure 5.15 Case 1: Cash flow analysis for biogas system replacing biomass heating system including the effect of 7 days per year of blackouts and feed in tariff (\$0.26/kWh)

In the second case shown in *Figure 5.16*, a natural gas heating system is replaced and the resulting payback period with no feed in tariff is approximately 3 years and positive cash flow after 20 years of \$1.1 million. With feed in tariff (\$0.26/kWh) and no major outages, the cumulative cash flow after 20 years is approximately \$2 million and the payback period is 1.8 years. With feed in tariff and 7 days of outages the cumulative cash flow is approximately \$2.6 million after 20 years with a payback period of only 1.5 years. This \$2.6 million could be considered a net loss when compared with the case when no biogas system is installed.

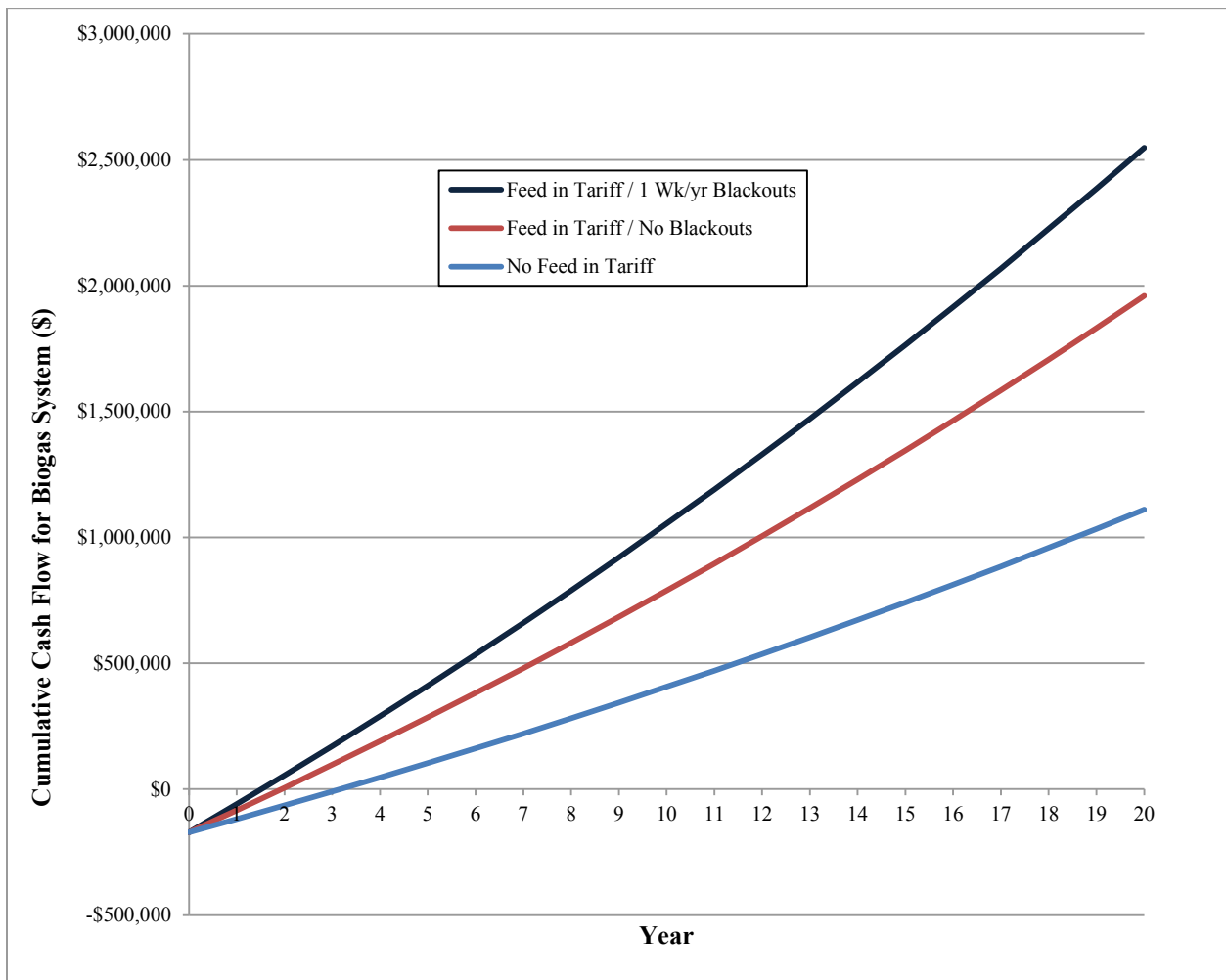


Figure 5.16 Case 2: Cash flow analysis for biogas system replacing natural gas heating system including the effect of 7 days per year of blackouts per year and feed in tariff (\$0.26/kWh)

In the third case shown in *Figure 5.17*, a propane heating system is replaced and the resulting payback period with no feed in tariff is approximately 2 years and positive cash flow after 20 years of \$1.8 million. With feed in tariff (\$0.26/kWh) and no major outages, the cumulative cash flow after 20 years is approximately \$2.7 million and the payback period is 1.4 years. With feed in tariff and 7 days of outages the cumulative cash flow is approximately \$3.3 million after 20 years with a payback period of only 1.1 years. This \$3.3 million could also be considered a net loss when compared with the case when no biogas system is installed.

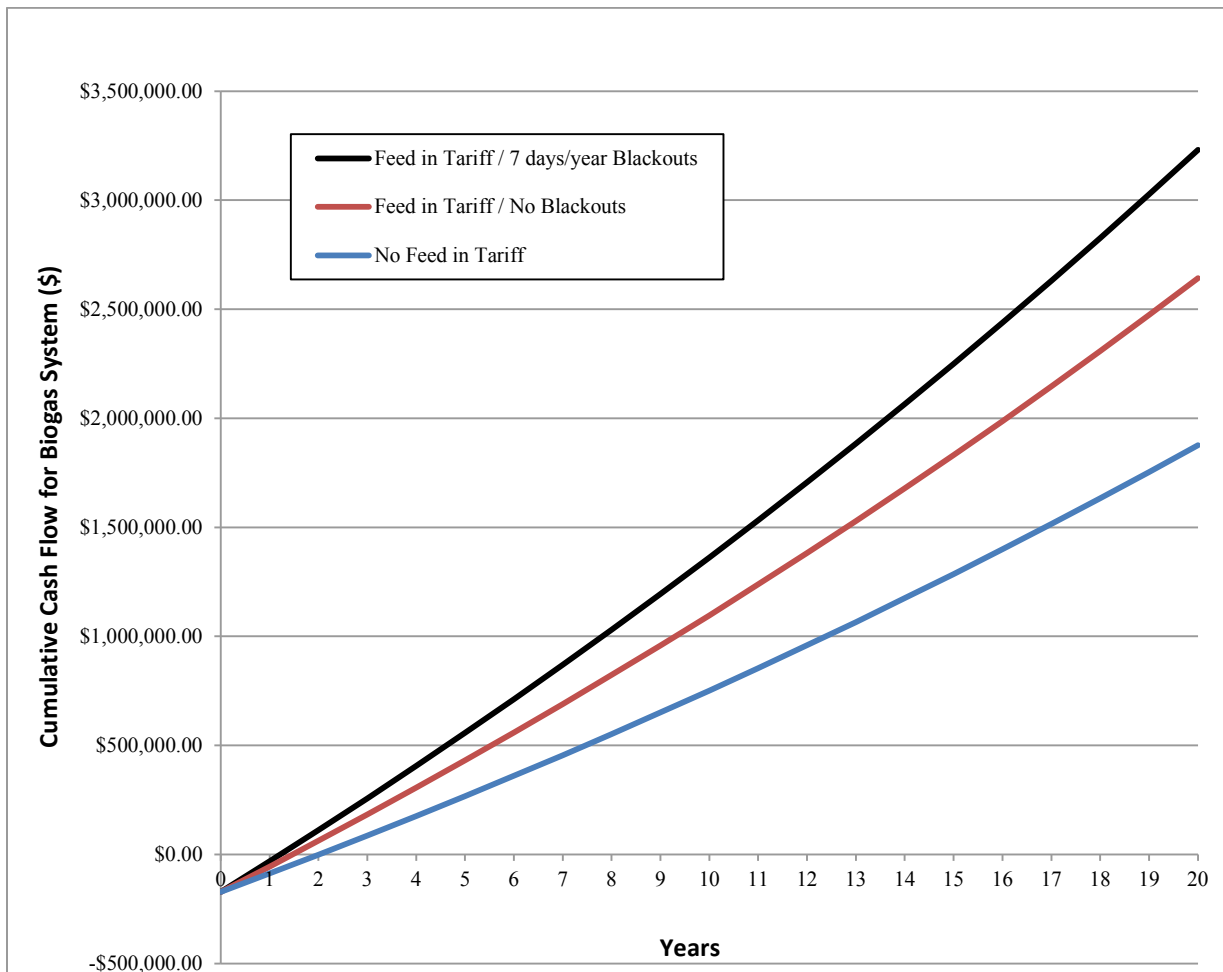


Figure 5.17 Case 3: Cash flow analysis for biogas system replacing propane heating system including the effect of 7 days per year of blackouts per year and feed in tariff (\$0.26/kWh)

Per year, the net average income from this biogas system ranges from \$100,000 to \$200,000 depending on the type of heating system that is being replaced. Considering that the average net income from a farm this size (140 cows) is close to \$400,000, and has decreased over the last few years, the addition of 25% to 50% of net income per year over 20 years while also factoring in the increase in outages and the potential losses incurred for not having a reliable backup power system, makes a biogas system installation attractive at this scale.

5.4 Determining Derating Curve for a Synchronous Generator Operated Under Extreme Unbalanced Load Conditions

A case study for a biogas-fueled genset run under extreme unbalance load conditions was performed. A 30 kVA, 4-pole, 60 Hz, 220V RMS, wound-rotor synchronous generator with damper bars was selected. The machine parameters were provided in the simulation software Wolfram's *System Modeler*. The machine parameters are provided in *Table 5.6* and the system diagram is shown in *Figure 5.18*.

Table 5.6 Synchronous generator parameters from Wolfram's System Modeler.

number of pole pairs p	2	
stator's moment of inertia	0.29	kg.m ²
rotor's moment of inertia	0.29	kg.m ²
nominal frequency fNominal	60	Hz
nominal voltage per phase	220	V RMS
no-load excitation current @ nominal voltage and frequency	10	A DC
warm excitation resistance	2.5	Ohm
nominal current per phase	100	A RMS
nominal apparent power	30000	VA
power factor	1.0	ind./cap.
nominal excitation current	19	A

efficiency w/o excitation	97.1	%
nominal torque	-196.7	Nm
nominal speed	1500	rpm
nominal rotor angle	-57.23	degree
stator resistance	0.03	Ohm per phase at reference temperature
reference temperature TsRef	20	°C
temperature coefficient alpha20s	0	1/K
stator reactance Xd	1.6	Ohm per phase in d-axis
giving Kc	0.625	
stator reactance Xq	1.6	Ohm per phase in q-axis
stator stray reactance Xss	0.1	Ohm per phase
damper resistance in d-axis	0.04	Ohm at reference temperature
damper resistance in q-axis	same as d-axis	
reference temperature TrRef	20	°C
temperature coefficient alpha20r	0	1/K
damper stray reactance in d-axis XDds	0.05	Ohm
damper stray reactance in q-axis XDqs	same as d-axis	
excitation resistance	2.5	Ohm at reference temperature
reference temperature TeRef	20	°C
temperature coefficient alpha20e	0	1/K
excitation stray inductance	2.5	% of total excitation inductance
stator operational temperature TsOperational	20	°C
damper operational temperature TrOperational	20	°C
excitation operational temperature TeOperational	20	°C
These values give the following inductances:		
main field inductance in d-axis	$(X_d - X_{ss}) / (2 * \pi * f_{Nominal})$	
main field inductance in q-axis	$(X_q - X_{ss}) / (2 * \pi * f_{Nominal})$	
stator stray inductance per phase	$X_{ss} / (2 * \pi * f_{Nominal})$	
damper stray inductance in d-axis	$X_{Dds} / (2 * \pi * f_{Nominal})$	
damper stray inductance in q-axis	$X_{Dqs} / (2 * \pi * f_{Nominal})$	

The generator was attached to a 3-phase resistive load as well as line resistance. The transmission line selected was 100 m of 0000 gauge supply line ($R=0.01608$ Ohm/phase) leading to the unbalanced load. In backup or emergency power situations, there is the likelihood for the generator to have to operate under highly unbalanced load conditions. A derating curve was developed in order to determine output power of the generator at different percent unbalance values of the load. The generator was brought up to speed with a step input with a 1 second step. The synchronous speed was 1800 rpm or 188.5 rad/s. A constant current (19 A) was supplied at rated load to the field excitation windings. The rated load was 4.8Ω per phase. The rated current was 45.4 ARMS. The output power with a balanced load was 29.9 kW. The stator copper losses for the balanced case were 748.2 W.

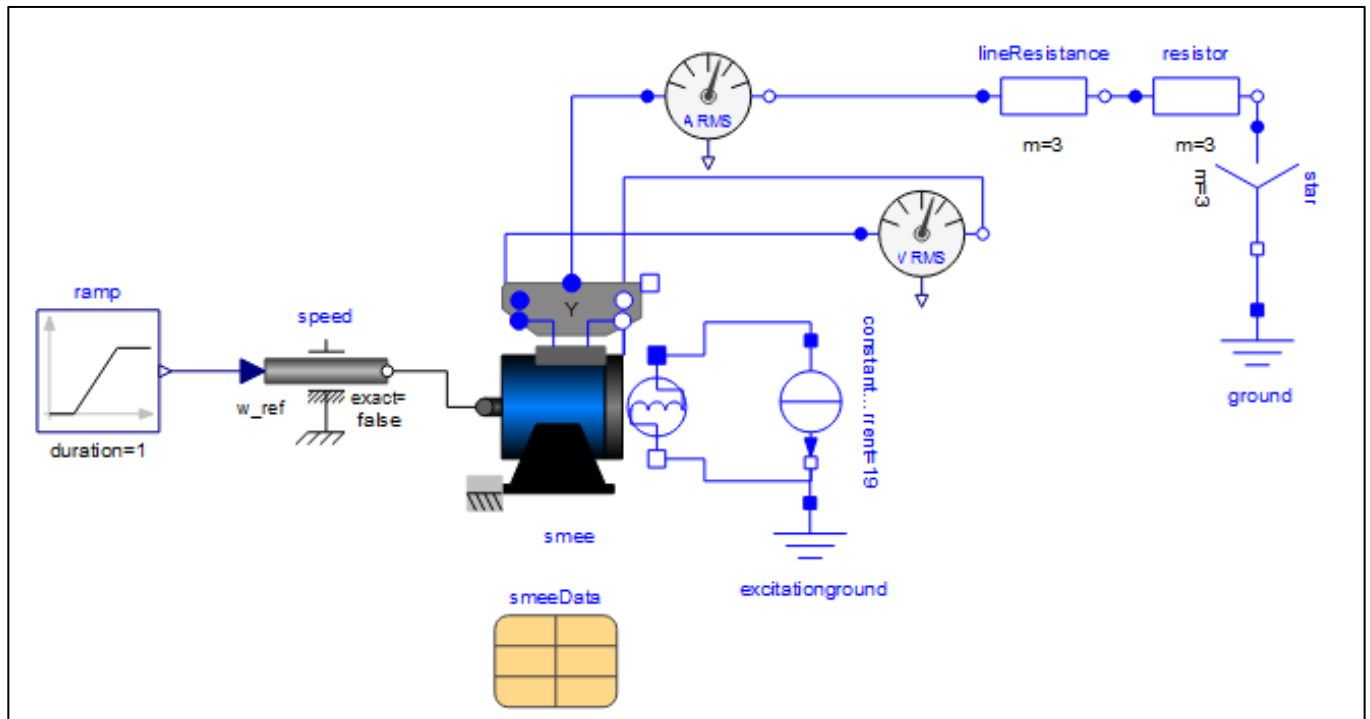


Figure 5.18 Schematic of generator and load in System Modeler.

For the unbalanced case, an unbalanced load was applied and the resulting voltage unbalance percentage was determined. For the case where the load resistances were (5.8, 4.8, 3.8) Ω , the voltage unbalance percentage was calculated to be 3.3%. The stator voltages were unbalanced by 3.3% but their average value also dropped below the rated RMS voltage level of 220 V. The field excitation current was increased to 19.9 A so that the average value of the stator voltages were equal to 220 V RMS. The rotor copper losses (RCL) were 72 W and the stator copper losses (SCL) increased from 748 W to 878 W.

In order to determine the derating factor of the machine, the highest phase current was reduced to the rated value or less (through iteration) so that the sum of RCL and SCL were less than or equal to the rated SCL value. Each of the other phase currents was then reduced by the same percentage reduction as the highest current value phase. In this case, the current value in the third phase increased from 45.4 A RMS to 57 A RMS under this unbalanced load. The load was increased while maintaining the same percent unbalance until this current was equal to its rated value. The resulting stator copper losses were 558 W. Adding the RCL of 72 W gives a total losses of 630 W.

The output power was then calculated to be 25.6 kW. This value was divided by the rated power at balanced load of 29.9 kW, giving a derating factor of 0.86. This process was repeated for different unbalanced loads so that a derating curve could be generated. The derating curve can be seen in *Figure 5.19*. Manufacturer recommendations provide a lower limit of 30% rated output power for running a generator. It has been determined that the highest percentage unbalance allowed for operation of a generator at this scale was approximately 12.5%. This derating curve simulation was repeated for a 6.7 kW synchronous generator as well and the resulting derating curve can be seen in *Figure 5.20*.

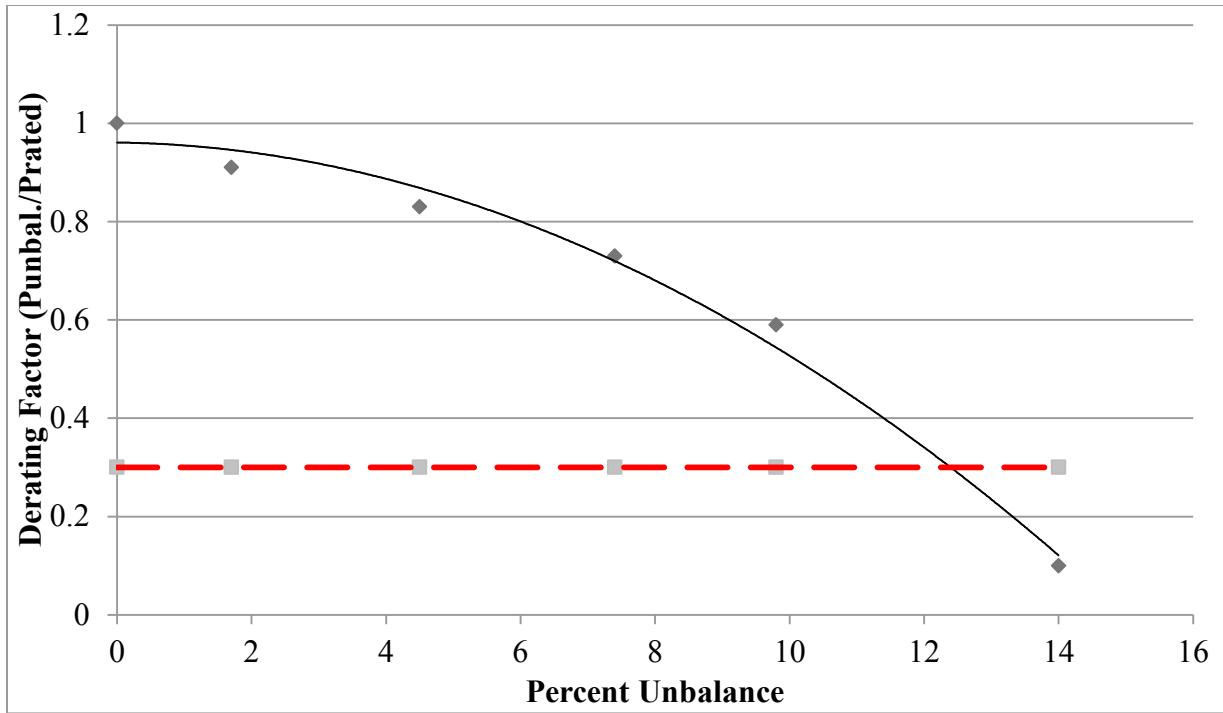


Figure 5.19 Derating curve for different percent unbalance for 30 kW synchronous generator.

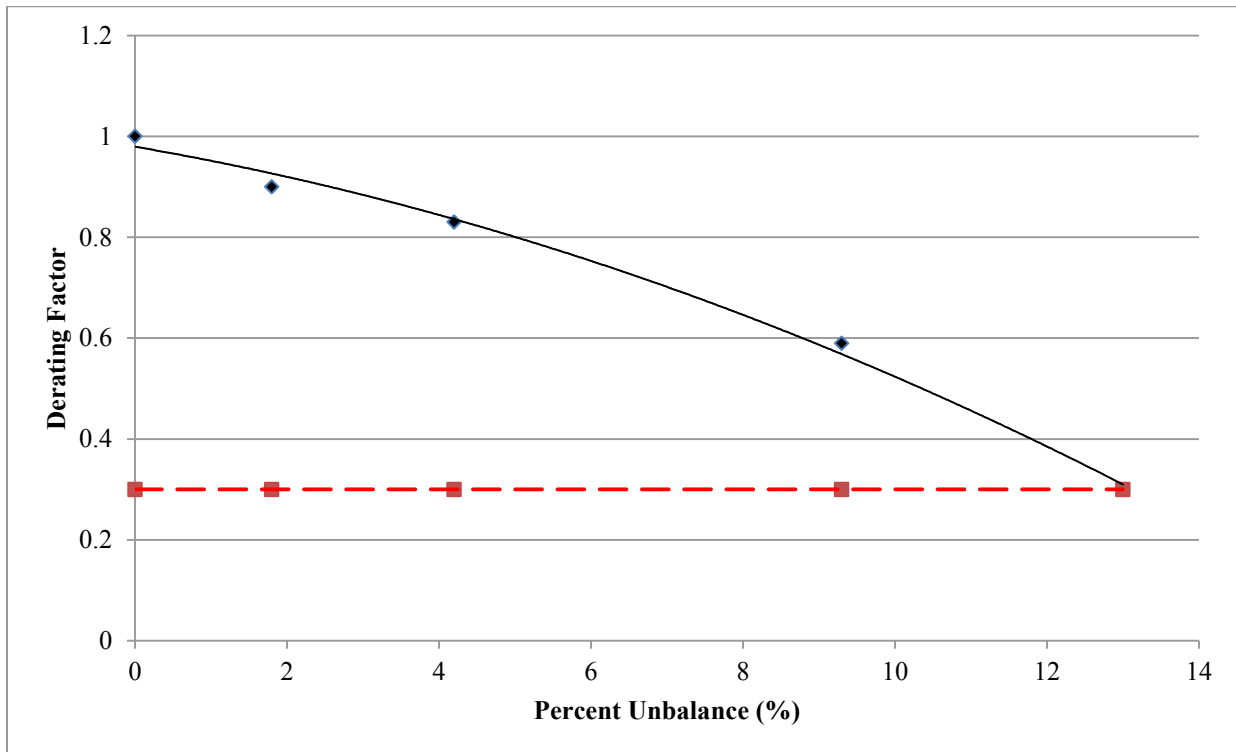


Figure 5.20 Derating curve under different percent unbalance loads for 6.7 kW synchronous generator.

5.5 Experimental Determination of Derating Curve for Generator Operated under Extreme Unbalanced Load Conditions

A derating experiment was performed in the laboratory with a Y-connected, 11 kW, 220V synchronous generator. The prime mover was a series combination of a 5 hp DC motor and a 5 hp induction motor. Total power output of the generator with both motors running at their rated currents and voltages was approximately 6.7 kW or 60% of rated. Stator resistance was measured to be 0.36Ω after running the generator at the “rated” load of 6.7 kW for four hours continuously. The balanced SCL were 350 W. Rated current was measured to be 18 ARMS per phase. The generator set-up with series-connected prime movers can be seen in *Figure 5.21*. A purely resistive Y-connected load (*Figure 5.22*) was added and the unbalance was achieved by changing the values of the resistance of each phase while making sure that the total power consumed remained the same as the balanced case. A neutral line was connected between the generator and the load in order to measure the zero sequence current.

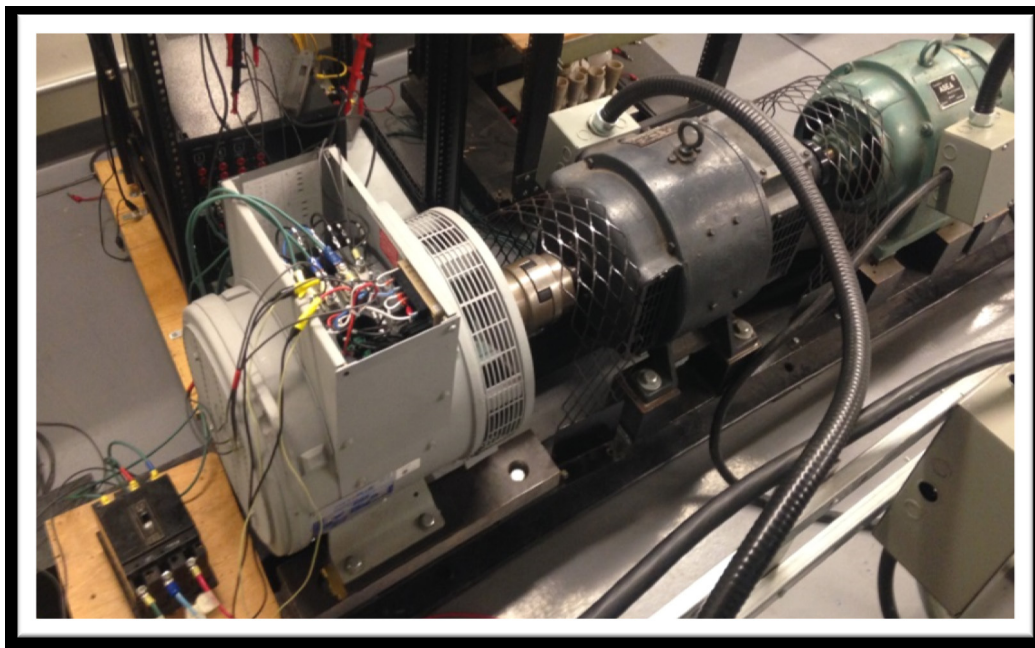


Figure 5.21 11 kW generator and series combination of 5 hp DC and induction motors.

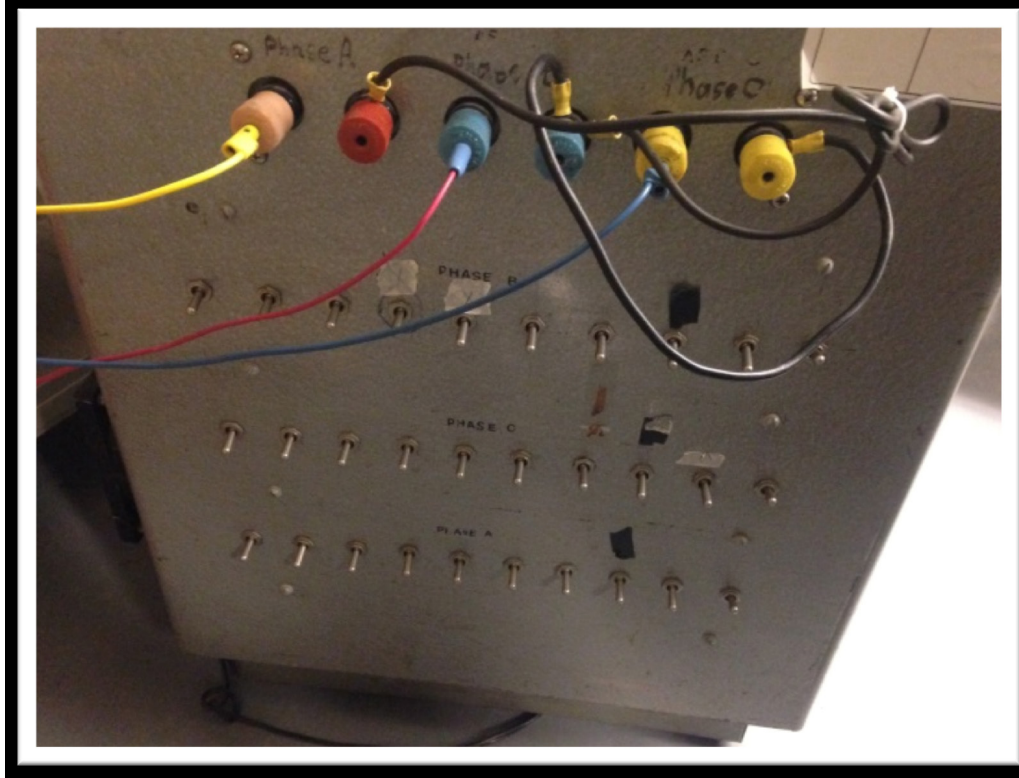


Figure 5.22 Three-phase resistive load bank used in experiment.

The phase voltages and currents were measured for different percent unbalance cases ranging from 0-10% in order to determine the derating curve for the machine under extreme unbalanced conditions. In the most extreme case of a 10% unbalanced load, the current in one of the phases rose to 30 ARMS, approaching the rated current of the generator (32 ARMS). The value of this current was decreased to 18 ARMS and the other two phase currents were decreased by the same relative amount. The resulting power was then calculated with the original measured phase voltages and a derating curve was developed. The experimentally determined derating curve can be seen in *Figure 5.23* and it is compared with the simulated derating curves of the 30 kW and 6.7 kW generators from the previous section. The experimentally determined derating curve tracks very closely with the simulated curves.

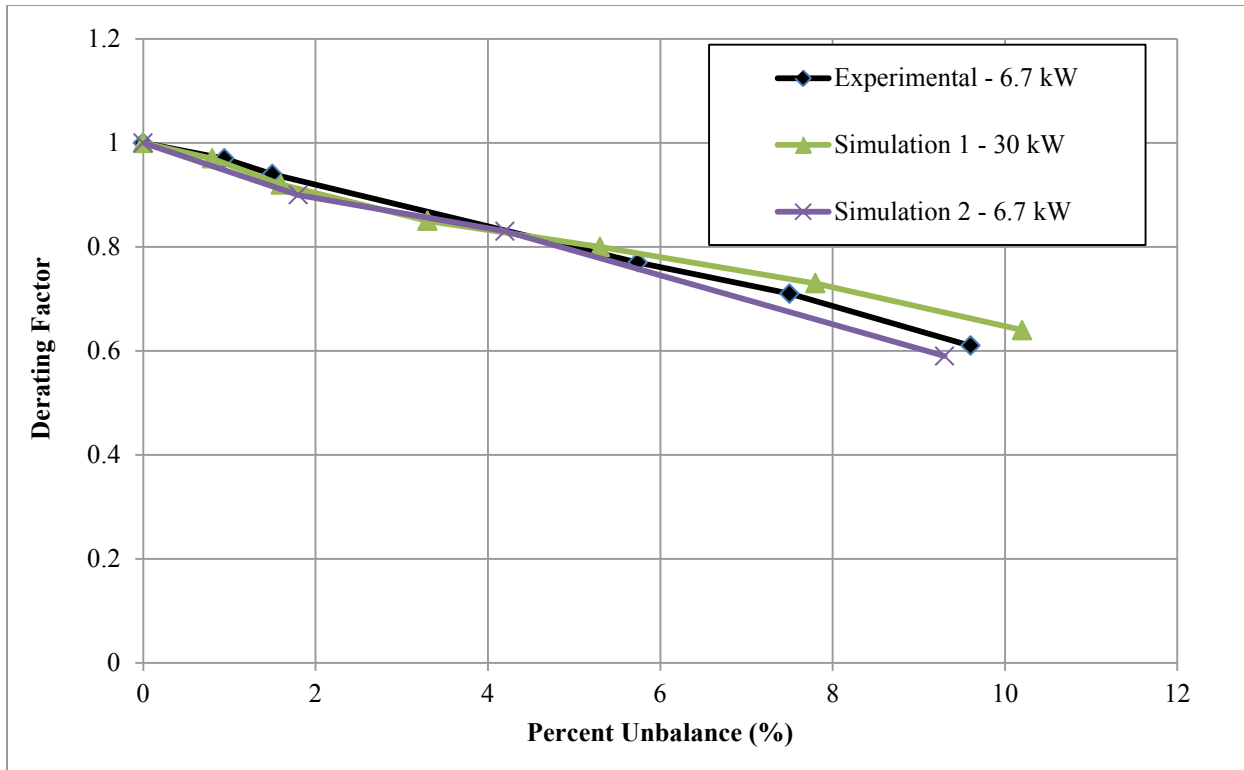


Figure 5.23 Comparison of experimentally determined and simulated derating curves.

5.6 Electric Machines for Rural Anaerobic Biogas Systems

There are many possible configurations of induction and synchronous generator sets available for agricultural biogas systems from a few kW up to several container-based gensets operating together in the MW range depending on requirements and location of owner. The voltage of the potential generator needs to be determined first based on what is available or possible. Operating requirements need to be determined with the most important factor being whether or not the biogas plant will supply a local electric load without any grid connection. To run a biomass CHP system in standalone mode without a grid connection, a synchronous generator will most likely be used. If there is no future consideration given to stand-alone

operation mode, then a grid-tied induction genset can be selected usually up to the 500 kW range.

For grid-tied biogas CHP systems under 50 kW, it is common for a single-phase induction generator to be used. For the 50-100 kW range, it is possible for a 3-phase induction or synchronous generator to be used, depending on the available voltage level, kVA limits, and point of connection. For generators above 100 kW and up to 500 kW, a 3-phase line is required and could be prohibitively expensive to install, depending on proximity to nearest point of interconnection. It can cost up to a million dollars USD for 2-3 km of 3-phase grid extension, and interconnection. [131].

In the US, most farm-scale biogas systems use induction generators below 500 kW because they are cheaper and easier to implement. In Germany, the majority of biogas CHP systems are rated over 100 kW and use synchronous generators with heat recovery and total CHP efficiency of more than 80%.

For off-grid systems less than 50 kW, a single-phase self-excited induction generator or synchronous generator can be used. For off-grid systems rating 50-100 kW, it is possible for a self-excited 3-phase generator to be operated as a single-phase generator, producing less than its rated output power. For off-grid systems rated above 100 kW, it is most likely that a 3 phase synchronous generator will be installed due to black-start capabilities and availability.

For municipal scale facilities like wastewater treatment plants or large scale organic waste anaerobic digestion projects, the system size is likely to be over 500 kW and therefore a biogas CHP system with a synchronous generator is most likely to be used as that is what is most commercially available.

5.7 Implementation Concerns for Biogas CHP Systems

More generally, if CHP biogas plants are to become as common in North America as they are in Europe, there are many implementation concerns that need to be investigated. If synchronous generators are to be used in parallel with the grid, they will have to be accompanied by inverters. This opens up the ability to handle non-linear and unbalanced loads. The compatibility with other renewable technologies in microgrid configurations can also be considered. It's also possible that peak shaving could occur under enhanced efficiency conditions with variable speed drives providing a 25% increase in synchronous generator output for 200-400 hours per year [132]. The black-start capabilities of CHP systems means special care must be taken to install proper safety precautions in order to prevent the accidental interaction of the utility workers with an unexpected electrified portion of the grid in the case of a blackout.

In addition, the automatic voltage regulation of multiple biogas CHP systems on the same bus is also a concern. The complexity of control necessary (synchronizers, reactive power control, dual gain governors, safety features) for synchronous generators operating in parallel with the grid and/or stand-alone mode will be a deciding factor in system design and implementation. Lessons can be taken from successful German implementation of similar systems.

Lastly, policy issues for grid integration of biogas systems will play a large part in the success or failure of these systems. Currently, small synchronous generator CHP systems are impractical to install due to the financial investment required for necessary redundant safety systems in order to comply with substation design and regulation. More specifically, two of the largest utilities in the US, PG&E in California and Con Edison in NY, have placed stringent

interconnection requirements on synchronous generators, effectively barring their use in the sub-MW range [133][134].

5.9 Conclusions

In this chapter, it has been shown that there is definite potential for biogas CHP system growth in the rural environment for use as a backup power system that also functions as a primary power system due the need for full load power on dairy farms in emergency power situations. The likelihood of an increase in long-term grid outages makes it clear that there is a need for a constant, reliable backup power source. The cost of biogas system implementation based on herd sized was presented as well as the generator sizing for 12 kW to 100 kW loads.

It was shown via RETScreen case studies of a 140 cow dairy farm that there is the potential to earn an additional \$2-3 million dollars of net income over 20 years and increase yearly earnings by up to 50% by selling excess electricity back to the grid while saving money on heating costs via the renewable energy source (biogas) generated on site. In addition, based on a commonly used substrates and annual tonnage, recommendations were provided for the type of machines available for electricity generation at different scales up to the MW range. Implementation concerns for CHP generators were also presented with policy issues being the main barrier to further biogas system implementation in North America.

CHAPTER 6

6.1 Conclusions

In conclusion, it has been shown that there is a problem with the growing amount of waste being produced around the world as well as increased risk of food and water shortages from the effects of increased population growth coupled with a changing global climate. The likelihood of increased severe weather events will lead to an increase of power outages and rolling blackouts as well as threaten agricultural yields and water supplies. Using anaerobic digestion as a waste-to-energy solution to not only reduce the amount of waste that goes to landfills by up to 40%, but also the amount of methane emissions produced by humans and the amount of fossil fuel consumption by replacing natural gas with the biogas produced from the AD process. In addition, small-scale anaerobic digestion systems can be used as emergency or backup power generators to in order to provide combined heat and power in the case of extended blackouts.

In addition, it was shown that it is feasible to provide 8-10kW of heating during daylight hours for a 30m³ OFMSW anaerobic digestion system with a 2kW_e air source heat pump that utilizes the heat gains of an adjacent greenhouse during the coldest month of the year with temperatures routinely below freezing. It was shown that even if the heat pump system is off for a week due to poor solar radiation or repair, the temperature of the active slurry in the tank would not drop out of the required range for mesophilic digestion. 3-D models of the building with the rooftop greenhouse as well as surrounding buildings were constructed and a solar radiation analysis was performed for the greenhouse during the coldest month of the year. The shading effect of surrounding buildings was investigated in order to ensure that there would be

enough energy available to heat the tank as well as keep the greenhouse within required growing temperatures. The average shadowing effect for the week investigated was a 25% decrease in total solar radiation. Finally, a heat transfer model for an ASHP run only during daylight hours was implemented and a simulation of the temperature fluctuation of the tank was performed for different cases. The results of this simulation show that a small-scale, well insulated AD tank could be feasibly heated using solar heat gains in the middle of winter, freeing up to 15% of the biogas produced for higher-value energy applications instead of using it to heat the digester. Preliminary research suggests that a small regular process temperature fluctuation has no major effect on biogas production or composition.

It has also been shown that there is a definite potential for biogas CHP system implementation in urban buildings for use in emergency power situations. The likelihood of an increase in long term grid outages makes the need for reliable emergency lighting a public health and safety concern. Anaerobic digestion of organic waste is a well-understood technology and a prime candidate for small-scale decentralized power generation as it is the only constant renewable energy source. It has been shown that for a 0.25 to 5 tpd food waste anaerobic digestion system, a 3 to 154 kW electric generator set can be installed to power a similarly rated emergency lighting system while also providing an additional 3 to 160 kW of heating energy via heat recovery. Anaerobic digestion system sizing based on power demand was also presented for a 20 kW emergency lighting system. The most commonly available natural gas fired CHP system contains a 3-phase synchronous generator but it's also possible that self-excited induction generators and permanent magnet generators could be integrated into these systems. A derating curve for a synchronous generator feeding a rectifier and inverter via DC link was developed and an inverter rating curve vs percent voltage unbalance was presented.

Finally, it was shown that there is definite potential for biogas CHP system growth in the rural environment for use as a backup power system that also functions as a primary power system due the need for full load power on dairy farms in emergency power situations. The likelihood of an increase in long-term grid outages makes it clear that there is a need for a constant, reliable backup power source. The cost of biogas system implementation based on herd sized was presented as well as the generator sizing for 12 kW to 100 kW loads.

It was shown via RETScreen case studies of a 140 cow dairy farm that there is the potential to earn an additional \$2-3 million dollars of net income over 20 years and increase yearly earnings by up to 50% by selling excess electricity back to the grid while saving money on heating costs via the renewable energy source (biogas) generated on site. In addition, based on a commonly used substrates and annual tonnage, recommendations were provided for the type of machines available for electricity generation at different scales up to the MW range. Implementation concerns for CHP generators were also presented with policy issues being the main barrier to further biogas system implementation in North America. Lastly, a derating curve was developed for a synchronous generator operating under extreme unbalance load conditions.

6.2 Future Work

The research presented in this dissertation has made significant contributions to the implementation of small-scale anaerobic digestion systems for emergency and backup power in the urban and rural environments. There is further work that can be done to build on the research presented herein, as highlighted in the following section.

An experimental of demonstration of upgrading greenhouse solar heat gains via air source heat pump should be performed and the integration of a solar ducting fan and compressor

should be investigated so that a completely renewable urban waste-to energy system can be developed in the future. In addition, the investigation of the amount of food that can be grown in urban greenhouses of different sizes should be correlated to the amount of waste that can be processed and the amount of energy that can be produced by small-scale AD systems. The decrease in energy consumption, carbon emissions, water usage, fertilizer, and compost through the integration of these systems should also be investigated.

A sizing and implementation plan should be developed for practical installation of small-scale AD systems for use in emergency power situations in the urban environment. There is a whole level of operational logistics that was not investigated in this research that would be of interest to urban planners, building managers, policy makers, architects, and engineers.

Proper inverter sizing for different unbalanced loads should be confirmed experimentally with resistive and inductive loads. A harmonic analysis of the system should be investigated as well.

REFERENCES

- [1] United Nations Population Division, Department of Economic and Social Affairs. (2014). Population Facts. United Nations. no. 2014/6.
- [2] United Nations Population Funds, Department of Economic and Social Affairs (2007). Urbanization: A Majority in Cities. United Nations. ESA/P/WP/205.
- [3] Themelis N.J., “Introduction to waste-to-energy”, Encyclopedia of Sustainability of Science and Technology 17, Wiley, 2007.
- [4] D. Hoornweg and P Bhada-Tata. (2012). What a Waste : A Global Review of Solid Waste Management. World Bank, Washington, DC, United States.
- [5] European Commission. Directive 2008/98/EC on Waste (Waste Framework Directive). European Parliament. OJ L 312, pp. 3–30, November, 2008.
- [6] UK Department of Energy & Climate Change. (2013, Nov.). UK Renewable Energy Roadmap: 2013 Update. UK Government.
- [7] Direction de l’Environnement et du Developpement Durable. Summary of Waste Management Master Plan for the Agglomeration of Montreal 2010-2014. City of Montreal, August, 2009.
- [8] City of Toronto. (2014). Solid Waste Management Services. [Online]. Available: <http://www1.toronto.ca/wps/portal/contentonly?vgnextoid=e4db433112b02410VgnVCM10000071d60f89RCRD>
- [9] D. Hoornweg and P. Bhada-Tata. “Environment: Waste Production Must Peak This Century,” Nature News, Vol. 502, pp. 615-617, October, 2013.
- [10] A. Robinson, G.C. Sewell, S. Wu, N. Damodaran, N. Kalas-Adams, “Landfill Data From China: Addressing Information Needs for Methane Recovery,” *International Workshop on Investment Opportunities in Coal Mine Methane Projects in China*, Chaoyang District, Beijing, China, September, 2003.

- [11] U.S. Environmental Protection Agency. (2013). Overview of Greenhouse Gases: Methane Emissions. [Online]. Available: <http://epa.gov/climatechange/ghgemissions/gases/ch4.html>
- [12] U.S. Environmental Protection Agency. (2014). Methane and Nitrous Oxide Emissions from Natural Sources. United States Government. Washington, DC, USA.
- [13] U.S. Environmental Protection Agency. (2012). MSW in the United States: Facts and Figures. United States Government. Washington, DC, USA.
- [14] Statistics Canada. (2010). Waste Disposal by source, Province and Territory. [Online]. Available: <http://www.statcan.gc.ca/tables-tableaux/sum-som/101/cst01/envir25a-eng.htm>
- [15] M. McMillan, Statistics Canada. (2013, Aug.). Waste Management Industry Survey: Business and Government Sectors. Government of Canada. Issue 2013001.
- [16] IPCC. (2007). Climate Change 2007: The Physical Science Basis. Contribution of Working Group I to the Fourth Assessment Report of the Intergovernmental Panel on Climate Change. Cambridge University Press, Cambridge, United Kingdom and New York, NY, USA.
- [17] Food and Agriculture Organization of the United Nations. (2013). Global Food Losses and Food Waste. United Nations. *Interpack2011*, Düsseldorf, Germany.
- [18] United Nations Framework Convention on Climate Change. (2011). UNFCCC Greenhouse Gas Inventory Data - Detailed data by Party. [Online]. Available: <http://unfccc.int/di/DetailedByParty.do>
- [19] Food and Agriculture Organization of the United Nations. (2013). *Food Waste Footprint Impacts on Natural Resources*. FAO, 2013. ISBN 978-92-5-107752-8
- [20] U.S. Energy Information Administration. (2014). U.S. Nuclear Generation and Generating Capacity. [Online]. Available: <http://www.eia.gov/nuclear/generation/index.html>
- [21] J. Cook, *et al.* "Quantifying the consensus on anthropogenic global warming in the scientific literature." *Environmental Research Letters*, vol. 8, no. 2, pp. 1-7, 2013.

- [22] IPCC Working Group 2. (2012). Managing the Risks of Extreme Events and Disasters to Advance Climate Change Adaptation. [Online]. Available: http://www.ipcc-wg2.gov/SREX/images/uploads/SREX-SPMbrochure_FINAL.pdf
- [23] M. New, D. Liverman, K. Anderson. “Mind the Gap: Policymakers must aim to avoid a 2°C temperature rise, but plan to adapt to 4°C.” Nature Reports, December, 2009.
- [24] The World Bank. (2012). Turn Down the Heat: climate extremes, regional impacts, and the case for resilience. World Bank, Washington, DC, United States.
- [25] U.S. Department of Energy. (2013). U.S. Energy Sector Vulnerabilities to Climate Change and Extreme Weather. U. S. Government, Washington, DC, United States.
- [26] Climate Central. (2014). Weather-Related Blackouts Doubled Since 2003: Report. [Online]. Available: <http://www.climatecentral.org/news/weather-related-blackouts-doubled-since-2003-report-17281>
- [27] DNV GL. [2014]. ADAPT Framework for Grid Resilience. [Online]. Available: <http://www.dnvkema.com/services/advisory/ope/adapt.aspx>
- [28]. P. Faeth, B. K. Sovacool. (2014). Capturing Synergies Between Water Conservation and Carbon Dioxide Emissions in the Power Sector. CNA Analysis and Solutions, Arlington, VA, United States.
- [29] U.S. Department of the Interior & U.S. Geological Survey. (2009). Estimated Use of Water in the United States in 2005. U.S. Government, Washington, D.C., United States.
- [30] 2030 Water Resources Group. (2009). Charting Our Water Future: Economic frameworks to inform decision-making. McKinsey & Company, 108 Offices Globally.
- [31] IPCC WG 2 Contribution to AR5. (2014). Climate Change 2014: Impacts, Adaptation, and Vulnerability. IPCC.
- [32] United Nations Department of Economic and Social Affairs, UN Water. (2014). Water and Food Security. [Online]. Available: http://www.un.org/waterforlifedecade/food_security.shtml

- [33] UN Division of Sustainable Development. (2012). Food and Agriculture: the future of sustainability. [Online].
<http://sustainabledevelopment.un.org/content/documents/1443sd21brief.pdf>
- [34] IPCC. "Climate Change 2007: Synthesis Report, Summary for Policymakers". IPCC Plenary, Valencia, Spain, November, 2007.
- [35] A. Jagerskog, T.J. Clausen, T. Holmgren, K. Lexen. (2014). Energy and Water: The Vital Link for a Sustainable Future. Report no. 33. SIWI, Stockholm, Sweden.
- [36] P. Faeth, et al. (2014). Water Adequacy and Electric Reliability in China, India, France, and Texas. CNA Analysis and Solutions, Arlington, VA, United States.
- [37] J. Bogner, *et al.* (2007). Waste Management, In Climate Change 2007: Mitigation. Contribution of Working Group III to the Fourth Assessment Report of the Intergovernmental Panel on Climate Change, Cambridge University Press, Cambridge, United Kingdom and New York, NY, USA.
- [38] G. C. Young, "Municipal Solid Waste to Energy Conversion Processes," Wiley & Sons Inc., 2010. ISBN: 978-0-470-53967-5.
- [39] T. Cordero, F. Marquez, J. Rodriquez-Mirasol, J.J. Rodriquez, "Predicting heating values of lignocellulosics and carbonaceous materials from proximate analysis," Fuel, vol. 80, pp.1567-1571, 2001.
- [40] R.P.J.M. Raven, K.H. Gregersen, "Biogas plants in Denmark: Successes and Setbacks," Renewable and Sustainable Energy Reviews, vol. 11, issue 1, pp. 116-132, 2007.
- [41] PEAT International. (2011). "Converting Waste to Energy Through Plasma Thermal Destruction & Recovery," [Online]. Available: www.peat.com/process_overview
- [42] Dovetail Partners, Inc., "Plasma Gasification: An Examination of the Health, Safety, and Environmental Records of Established Facilities," Prepared for the city of Palisade, Minnesota, June 7, 2010, Final Report.
- [43] Juniper Consulting, "The Alter NRG/Westinghouse Plasma Gasification Process," Process Review, November 2008.

- [44] East Bay, California, Municipal Utility District, “Anaerobic Digestion of Food Waste”, March 2008, Final Report.
- [45] Republic of Slovenia Minister of Economy, “Methodology for determining reference costs of electricity generated from renewable resources”, May 2009, Pages 360-381.
- [46] U.S. Department of Energy. (2014). Biogas Opportunities Roadmap. [Online]. Available: <http://www.epa.gov/climatechange/Downloads/Biogas-Roadmap.pdf>
- [47] X. Chen, R. T. Romano, R. Zhang, “Anaerobic digestion of food wastes for biogas production”, International Journal of Agricultural & Biological Engineering, vol. 3, no. 4, 2010.
- [48] A. Davidson, C. Gruvberger, T. Christensen. “Methane yield in source-sorted organic fraction of municipal solid waste,” Waste Management, pp. 406-14, 2007.
- [49] J. Mata-Alvarez, *Biomethanization of the Organic Fraction of Municipal Solid Wastes*, IWA Publishing, 2003, ISBN 1900222140.
- [50] US Environmental Protection Agency. (1978). Use of Solar Energy to Heat Anaerobic Digesters. [Online]. Available: <http://nepis.epa.gov/>
- [51] The University of Southampton and Greenfinch Ltd, “Biodigestion of kitchen waste: A comparative evaluation of mesophilic and thermophilic biodigestion for the stabilisation and sanitisation of kitchen waste”, Final Report.
- [52] Water Environment Federation, “Operation of Municipal Wastewater Treatment Plants (Manual of Practice)”, 1996, ISBN 1572780401
- [53] Heier, Siegfried, “Grid Integration of Wind Energy Conversion Systems”, John Wiley & Sons, 2005, ISBN 0-470-86899-6.
- [54] Zarr, R.R., “Analytical Study of Residential Buildings with Reflective Roofs”, U.S. Department of Commerce, October 1998, NISTIR 6228

- [55] Walton, G.N., *Thermal Analysis Research Program- Reference Manual*, NBSIR 83-2655, U.S. Department of Commerce, March 1983, Update 1985.
- [56] National Resources Canada. (2012). NRCAN Weather Data. [Online]. Available: <http://www.climate.weatheroffice.gc.ca>
- [57] Metcalf & Eddy, Inc., *Wastewater Engineering: Treatment and Reuse*, 4th Edition, McGraw Hill, 2003, ISBN 0070418780
- [58] L. M. Safley Jr., P.W. Westerman, “Psychrophilic Anaerobic Digestion of Animal Manure: Proposed Design Methodology”, *Biological Wastes*, vol. 34, pp. 133-148, 1990.
- [59] East Bay Municipal Utility District. (2008). Anaerobic Digestion of Food Waste – Final Report. [Online]. Available: <http://www.epa.gov/region9/organics/ad/EBMUDFinalReport.pdf>
- [60] Toshiba. (2013). Toshiba 2kW Air-to-water Heat Pump System Specifications. [Online]. Available: http://www.toshiba-aircon.jp/products/estia/data/cat_estia.pdf
- [61] D.R. Vissers, H.N. Maaijen, “Sustainable Building and Systems Modeling”, University of Technology Eindhoven, 2011.
- [62] Rolle, Kurt C., *Thermodynamics and Heat Power*, 6th edition, Prentice Hall, 2005, ISBN 0-13-113928-2
- [63] C. Verhelst, F. Logist, J. V. Impe, L. Helsen, “Study of the optimal control problem formulation for modulating air-to-water heat pumps to a residential floor heating system”, *Energy and Buildings*, vol. 45, pp. 43-53, 2012.
- [64] L. De Baere, B. Mattheeuws, “Anaerobic Digestion of the Organic Fraction of Municipal Solid Waste in Europe – Status, Experience, and Prospects”, *Waste Management*, vol. 3, pp. 517-526, 2012.

- [65] The University of Southampton and Greenfinch Ltd, "Biodigestion of kitchen waste: A comparative evaluation of mesophilic and thermophilic biodigestion for the stabilisation and sanitisation of kitchen waste", Final Report.
- [66] D. House, "The Complete Biogas handbook", House Press, 2006, ISBN 0915238470.
- [67] WRAP UK. (2008). The Food We Waste. [Online]. Available: <http://wrap.s3.amazonaws.com/the-food-we-waste.pdf>
- [68] J. K. Cho, S. C. Park, "Biochemical Methane Potential and Solid State Anaerobic Digestion of Korean Food Waste", *Bioresource Technology*, vol. 52, issue 3, pp. 245-253, 1995.
- [69] Ontario Ministry of Agriculture, "Final Report for the Study of Food-Based Inputs for Biogas Systems in Ontario," Government of Canada, May 2008.
- [70] Asa Davidson, Christopher Gruvberger, Thomas H. Christensen, "Methane Yield in Source-Sorted Organic Fraction of Municipal Solid Waste," *Waste Management* 27, pp. 406-414, 2007.
- [71] R. Zhang, H. M. El-Mashad, K. Hartman, F. Wang, "Characterization of food waste as feedstock for anaerobic digestion," *Bioresource Technology*, vol. 98, issue 4, pp. 929-935, 2007.
- [72] L. De Baere, B. Mattheeuws, "Anaerobic Digestion of the Organic Fraction of Municipal Solid Waste in Europe – Status, Experience, and Prospects", *Waste Management*, vol. 3, pp. 517-526, 2012.
- [73] K.J. Chae, A. Jang, S.K. Yim, I. S. Kim, "The effects of digestion temperature shock on the biogas yields from the mesophilic anaerobic digestion of swine manure," *Bioresource Technology*, vol. 99, issue 1, pp. 1-6, 2008.
- [74] J. Kim, B. Rock, Y. Chun, S. Kim, "Effects of Temperature and hydraulic retention time on anaerobic digestion of food waste," *Journal of Bioscience and Bioengineering*, vol. 102, issue 4, pp. 328-332, 2006.

[75] H. El-Mashad, G. Zeeman, K. P. Wilko, P.A. Gerard. G. Lettinga, “Effect of temperature and temperature fluctuation on thermophilic anaerobic digestion of cattle manure,” *Bioresource Technology*, vol. 95, issue 2, pp. 191-201, 2004.

[76] US Environmental Protection Agency. (2010). Best Management Practices in Food Scraps Programs. [Online]. Available:

http://www.foodscrapsrecovery.com/epa_foodwastereport_ei_region5_v11_final.pdf

[77] US National Resources Defense Council (NRDC). Waste: How America is Losing Up to 40 Percent of Its Food from Farm to Fork to Landfill. [Online]. Available:

<http://www.nrdc.org/food/files/wasted-food-ip.pdf><http://www.nrdc.org/food/files/wasted-food-ip.pdf>

[78] Institute for Sanitary Engineering, Water Quality and Solid Waste Management (ISWA) Stuttgart. (2012). Determination of discarded food and proposals for a minimization of food wastage in Germany. [Online]. Available:

http://www.bmel.de/SharedDocs/Downloads/EN/Food/Studie_Lebensmittelabfaelle_Kurzfassung.pdf?__blob=publicationFile

[79] Biocycle. (2012). Food Waste Collection in the U.S. [Online]. Available:

<http://www.biocycle.net/2012/01/12/residential-food-waste-collection-in-the-u-s/>

[80] Renewable Energy From Waste Conference. (2012). Update on Renewable Energy from Waste Technologies. [Online]. Available: <http://gbbinc.com/gbbwp2013/wp-content/uploads/2013/06/GershmanREW2013.pdf>

[81] US Environmental Protection Agency. (2011). City of West Lafayette Waste to Energy. [Online]. Available: http://www.epa.gov/greenpower/documents/events/17aug11_henderson.pdf

[82] University of Wisconsin OshKosh. (2014). UW Oshkosh Urban Anaerobic Dry Biogas System (BD1). [Online]. Available: <http://www.uwosh.edu/biodigester/About/uw-oshkosh-biodigester>

- [83] BioCycle. (2013). Grocery Chain Unveils On-Site Digester. [Online]. Available: <http://www.biocycle.net/2013/06/19/grocery-chain-unveils-on-site-digester/>
- [84] Jonathan Bloom. *American Wasteland: How America Throws Away Nearly Half Its Food (and What We Can Do About It)*, De Capo Press, 2013, ISBN-10 0738213640.
- [85] WRAP Charity. (2011). Helping consumers reduce food waste – a retail survey 2011. [Online]. Available: <http://www.wrap.org.uk/content/helping-consumers-reduce-food-waste-retail-survey-2011>
- [86] US National Renewable Energy Laboratory. (2013). Biogas Potential in the United States. [Online]. Available: <http://www.nrel.gov/docs/fy14osti/60178.pdf>
- [87] A. Davidson, C. Gruvberger, T. Christensen. “Methane yield in source-sorted organic fraction of municipal solid waste,” *Waste Management*, pp. 406-14, 2007.
- [88] J. Cho, S. Park. “Biochemical methane potential and solid State anaerobic digestion of Korean food waste.” *Bioresource Technology*, vol. 52, issue 3, pp. 245-53, 1995.
- [89] Mohan S, Bindu BK. “Effect of phase separation on anaerobic digestion of kitchen waste.” NRC Research Press, 2008.
- [90] S. Karnchanawong, S. Uparawanna. “Performance of single-phase complete-mix anaerobic digestion of organic fraction of municipal solid waste.” *Joint International Conference on sustainable energy and environment*, Bangkok, Thailand, 2006.
- [91] Peck Cara, US EPA. (2011). Food waste opportunity. [Online]. Available: <http://www.epa.gov/osw/rcc/resources/meetings/rcc-2008/sessions/msw/food/foodwaste/peck.pdf>
- [92] California Integrated Waste Management Board. “Current anaerobic digestion technologies used for treatment of municipal organic solid waste.” Department of Biological and Agricultural Engineering, UC Davis, 2008.
- [93] A. Davidson, J. Jansen, B. Appelqvist, C. Gruvberger, H. Martin. “Anaerobic digestion potential of urban organic waste: a case study in Malmo.” *Waste Management Research*, pp.162-9, 2007.

- [95] Alliance For a Just Rebuilding. (2014). Weathering the Storm: Rebuilding a More Resilient NYC Housing Authority Post-Sandy. [Online]. Available: <http://www.rebuildajustny.org/weathering-the-storm-rebuilding-a-more-resilient-nycha-post-sandy/>
- [96] New Jersey Department of Community Affairs. (2013). Disaster Recovery Action Plan. [Online]. Available: <http://www.nj.gov/dca/announcements/pdf/CDBG-DisasterRecoveryActionPlan.pdf>
- [97] The City of New York. (2014). Waste and Recycling. [Online]. Available: <http://www.nyc.gov/html/planyc/html/sustainability/waste-recycling.shtml>
- [98] COGEN Europe. (2014). Micro-CHP Delivering Energy Savings in the Framework of Energy Efficiency Directive. [Online]. Available: www.cogeneurope.eu
- [99] National Fire Protection Agency. Life Safety Code. [Online]. (2015). Available: <http://www.nfpa.org/codes-and-standards/>
- [100] Staco Energy Products Co. (2014). Three-Phase Central Inverter for Emergency Lighting Applications. [Online]. Available: <http://keyitec.com/FL924-20-30kWBrochure.pdf>
- [101] Controlled Power Company. (2014). UltraLITE Model ELU 1 Phase Emergency Lighting. [Online]. Available: http://www.controlledpwr.com/UltraLITE_Model_ELU_Lighting_Inverter.html
- [102] National Electrical Code (NEC). (2014). NEC Requirements for Generators and Standby Power Systems. [Online]. Available: www.nfpa.org
- [103] University Biogas Association. (2013). Latest Biogas Production Statistics for Europe. [Online]. Available: <http://european-biogas.eu/2013/12/20/eba-presents-latest-biogas-production-statistics-europe-growth-continuous/>
- [104] U.S. Department of Agriculture. (2014). Biogas Opportunities Roadmap. [Online]. Available: <http://www.epa.gov/climatechange/Downloads/Biogas-Roadmap.pdf>

- [105] U.S. Environmental Protection Agency. (2011). Opportunities for Combined Heat and Power at Wastewater Treatment Facilities. [Online]. Available: http://www.epa.gov/chp/documents/wwtf_opportunities.pdf
- [106] Biogas Association of Canada. (2013). Canadian Biogas Study: Benefits to the Economy, Environment and Energy. [Online]. Available: www.biogasassociation.ca
- [107] A. Davidson, C. Gruvberger, T. H. Christensen, “Methane Yield in Source-Sorted Organic Fraction of Municipal Solid Waste,” Waste Management, vol. 27, issue 3, pp. 406-414, 2007.
- [108] Michael Kottner, Jenny Aragundy, “Ontario Biogas Operators Course – Biogas Reference Manual,” IBBK, Weckelweiler, Germany, 2008.
- [109] Lemvi Biogas, “Biogas Handbook”, University of Southern Denmark, 2008, ISBN 978-87-992962-0-0
- [110] U.S. Department of Agriculture. (2008). Changes in the Size and Location of U.S. Dairy Farms. [Online]. Available: http://www.ers.usda.gov/media/430528/err47b_1_.pdf
- [111] NY State Energy Research and Development Authority. (2014). Dairy Farm Energy Audit Summary. [Online]. Available: <http://www.nyserda.ny.gov/Publications/Research-and-Development-Technical-Reports/Other-Technical-Reports/Energy-Audit-Reports.aspx>
- [112] Virginia Tech. (2009). Standby Electric Generators for Emergency Farm Use. [Online]. Available: <http://pubs.ext.vt.edu/442/442-067/442-067.html>
- [113] J. M. Kramer, Resource Strategies, Inc. (2004). Agricultural Biogas Casebook -2004 Update. Energy Center of Wisconsin, Madison, WI, United States.
- [114] Ontario Ministry of Agriculture, Food, and Rural Affairs. (2010). Using Less Energy on Dairy Farms. [Online]. Available: <http://www.omafra.gov.on.ca/english/engineer/facts/10-067.htm>
- [115] Statistics Canada. (2011). Households and the Environment: Energy Use. [Online]. Available: <http://www.statcan.gc.ca/pub/11-526-s/11-526-s2013002-eng.htm>

- [116] T. Shelford, Dairy Environmental Systems (2013). Estimating Farm Size Required to Economically Justify Anaerobic Digestion on Small Dairy Farms. Cornell University College of Agriculture and Life Sciences.
- [117] Ontario Ministry of Agriculture, Food, and Rural Affairs. (2013). Biogas (Anaerobic Digestion) – Basic Numbers. [Online]. Available:
http://www.omafra.gov.on.ca/english/engineer/ge_bib/biogas.htm#4
- [118] Ontario Energy Board. (2014). Electricity Prices. [Online]. Available:
<http://www.ontarioenergyboard.ca/OEB/Consumers/Electricity/Electricity+Prices>
- [119] Gildale Farms. (2014). Wood Pellet Prices. [Online]. Available:
<http://www.gildalefarms.ca/fuel-pellets/>
- [120] YCharts. (2014). US Milk Farm Price As Received. [Online]. Available:
https://ycharts.com/indicators/milk_price
- [121] Dairy Management Inc. (2012). Dairy Farming. [Online]. Available:
<http://www.dairy.org/for-consumers/farming>
- [122] Barbara A. Reed, California Agriculture. (1994). For wages and benefits, bigger dairies may be better. [Online]. Available:
<http://californiaagriculture.ucanr.edu/landingpage.cfm?article=ca.v048n02p9&fulltext=yes>
- [123] Personal communication with farmer at Mapleview Dairy Farm, Madrid, NY. (2014).
- [124] Cornell University Report. (2012). Dairy Farm Business Summary. [Online]. Available:
<http://dyson.cornell.edu/outreach/extensionpdf/2012/Cornell-Dyson-eb1204.pdf>
- [125] U.S. Environmental Protection Agency. (2012). Milking Parlors. [Online]. Available:
<http://www.epa.gov/agriculture/ag101/dairymilking.html>
- [126] U.S. Department of Agriculture Research Service. (2014). LDPM: Livestock, Dairy, and Poultry Outlook Catalog. (Online). Available: <http://www.ers.usda.gov/publications/ldpm-livestock,-dairy,-and-poultry-outlook.aspx>

- [127] Canadian Dairy Commission. (2014). Canadian Dairy Commission Annual Report. [Online]. Available: http://www.cdc-ccl.gc.ca/CDC/userfiles/file/CDC_AR_2012-2013_EN.pdf
- [128] Ontario Ministry of Agriculture, Food, and Rural Affairs. (2013). Ontario Biogas System Update: Feed-In Tariff, Green Energy Act and Regulated Mixed Anaerobic Digestion Facility Rules. [Online]. Available: http://www.omafra.gov.on.ca/english/engineer/facts/fit_prog.htm
- [129] Ontario Energy Board. (2014). Natural Gas Rate Updates. [Online]. Available: <http://www.ontarioenergyboard.ca/OEB/Consumers/Natural+Gas/Natural+Gas+Rates>
- [130] Ontario Ministry of Energy. (2014). Fuel Price Data: Propane. [Online]. Available: <http://www.energy.gov.on.ca/en/fuel-prices/fuel-price-data/?fuel=PRO&yr=2014>
- [131] Alberta Agriculture, Food and Rural Development. (2006). Biogas Energy Electricity Generation and Interconnection to the Power Grid [Online]. Available: <http://www1.agric.gov.ab.ca/>
- [132] Robert Panora, Jean P. Roy, TECOGEN, (2012). Top 10 Reasons to Choose Inverter-Based Engine CHP. [Online]. Available: <http://bpe-ne.com/wp-content/uploads/2012/07/top10-reasons-to-choose-inverter-based-engine-chp.pdf>
- [133] PG&E. (2012). Transmission Interconnection Handbook, Section G3: Operating Requirements for Transmission Generating Entities. [Online]. Available: <http://www.pge.com/includes/docs/pdfs/shared/rates/tariffbook/ferc/tih/g3.pdf>
- [134] ConEdison. (2014). Distributed Generation, Synchronous Generation. [Online]. Available: <http://apps.coned.com/dg/configurations/synchronous.asp>
- [135] Voltage Unbalance and Motors, Pacific Gas and Electric Company, San Francisco, CA, 2009.
- [136] P. Pillay, P. Hofmann. "Derating of Induction Motors Operating with a Combination of Unbalanced Voltages and Over or Undervoltages". IEEE Transactions on Energy Conversaion, vol. 17, no. 4, pp. 485-491, Dec 2002.

- [137] *Standard MG 1-1998 Motors and Generators Rev. 3*, National Electrical Manufacturers Association (NEMA), Rosslyn, VA, 2002.
- [138] R.F. Woll. "Effect of Unbalanced Voltage on the Operation of Polyphase Induction Motors". *IEEE Transactions on Industry Applications*, vol. IA-11, no. 1, pp. 38-42, Jan. 1975.
- [139] O. Rodriguez, A. Medina, "Stability analysis of the synchronous machine under unbalance and loss of excitation conditions," *Power Engineering Society General Meeting, 2003, IEEE* , vol.3, no., pp.,1511 Vol. 3, 13-17 July 2003.
- [140] *Understanding Nonlinear Loads and Generator Set Interaction*, Caterpillar Inc., Peoria, IL, United States.
- [141] C.-Y. Lee, "Effects of unbalanced voltage on the operation performance of a three-phase induction motor," *IEEE Trans. Energy Conv.*, vol. 14, pp. 202–208, June 1999.
- [142] P. B. Cummings, J. R. Dunki-Jacobs, and R. H. Kerr, "Protection of induction motors against unbalanced voltage operation," *IEEE Trans. Ind. Applicat.*, vol. IA-21, May/June 1985.
- [143] P. Pillay, M. Manyage, "Definitions of Voltage Unbalance," *IEEE Power Engineering Review*, pp. 50-51, May 2001.
- [144] R. Schainker, Electronics Power Research Institute. (2005). "Effects of Temporary Overvoltage on Residential Products: Final Report," Electric Power Research Institute, Palo Alto, CA, United States.
- [145] E. L. Brancato, "Estimation of Lifetime Expectancies of Motors", *IEEE Electrical Insulation Magazine*, Vol. 8 No. 3, May/June 1992.
- [146] E. Fuchs, M. A. S. Masoum, *Power Quality in Power Systems and Electrical Machines*, Academic Press, August, 2011.
- [147] R. Bravo, R. Yinger, L. Gaillac, "Air Conditioner Stalling Unit Level Solutions Test Report," TDBU Engineering Advancement Power Systems Technologies, Edison International.
- [148] *IEEE Recommended Practice for Emergency and Standby Power Systems for Industrial and Commercial Applications*, IEEE Std. 446-1995, December 1995.

APPENDIX A – CODE FOR SIMULATIONS

A.1 Air Source Heat Pump Heating of Digester (System Modeler)

model DigesterTankHeatingModelNOVFINAL

Modelica.Thermal.HeatTransfer.Components.HeatCapacitor HeatCapTank(C = 113049000, T.start = 308.15, T.fixed = true) annotation(Placement(visible = true, transformation(origin = {-116.7933, 92.6767}, extent = {{-10.0, -10.0}, {10.0, 10.0}}, rotation = 0)));

Modelica.Thermal.HeatTransfer.Components.ThermalConductor CondTankFloor(G = 0.45 * 10.79 / 0.0254) annotation(Placement(visible = true, transformation(origin = {-75.0, 22.5}, extent = {{-7.5, -7.5}, {7.5, 7.5}}, rotation = 0)));

Modelica.Thermal.HeatTransfer.Components.ThermalConductor CondInsulFloor(G = 0.043 * 10.79 / 0.0762) annotation(Placement(visible = true, transformation(origin = {-35.0, 22.5567}, extent = {{-7.4433, -7.4433}, {7.4433, 7.4433}}, rotation = 0)));

Modelica.Thermal.HeatTransfer.Components.ThermalConductor CondTankWalls(G = 0.45 * 32.37 / 0.0254) annotation(Placement(visible = true, transformation(origin = {-75.0, 45.0}, extent = {{-7.5, -7.5}, {7.5, 7.5}}, rotation = 0)));

Modelica.Thermal.HeatTransfer.Components.ThermalConductor CondInsulWalls(G = 0.0206 * 34.15 / 0.1016) annotation(Placement(visible = true, transformation(origin = {-35.0, 45.0}, extent = {{-7.5, -7.5}, {7.5, 7.5}}, rotation = 0)));

Modelica.Thermal.HeatTransfer.Components.Convection ConvWalls annotation(Placement(visible = true, transformation(origin = {77.8754, 0.0}, extent = {{-7.1246, -7.1246}, {7.1246, 7.1246}}, rotation = 0)));

Modelica.Thermal.HeatTransfer.Components.Convection ConvRoof annotation(Placement(visible = true, transformation(origin = {77.5236, 22.5236}, extent = {{-7.4764, -7.4764}, {7.4764, 7.4764}}, rotation = 0)));

Modelica.Thermal.HeatTransfer.Components.ThermalConductor CondInsulRoof(G = 0.0206 * 10.79 / 0.1016) annotation(Placement(visible = true, transformation(origin = {-35.0, 68.0354}, extent = {{-8.035399999999999, -8.035399999999999}, {8.035399999999999, 8.035399999999999}}, rotation = 0)));

Modelica.Thermal.HeatTransfer.Components.ThermalConductor CondTankRoof(G = 0.45 * 10.79 / 0.0254) annotation(Placement(visible = true, transformation(origin = {-75.0, 67.5}, extent = {{-7.5, -7.5}, {7.5, 7.5}}, rotation = 0)));

```
Modelica.Thermal.HeatTransfer.Celsius.PrescribedTemperature Tambient
annotation(Placement(visible = true, transformation(origin = {130.0752, 62.4248}, extent = {{-
7.5752, -7.5752}, {7.5752, 7.5752}}, rotation = 0)));
```

```
Modelica.Thermal.HeatTransfer.Components.BodyRadiation RadRoof(Gr = 0.4 * 10.89)
annotation(Placement(visible = true, transformation(origin = {77.057, 77.9905}, extent = {{-
10.0, -10.0}, {10.0, 10.0}}, rotation = 0)));
```

```
Modelica.Thermal.HeatTransfer.Components.BodyRadiation RadWalls(Gr = 0.4 * 34.16)
annotation(Placement(visible = true, transformation(origin = {76.8638, 50.0}, extent = {{-10.0, -
10.0}, {10.0, 10.0}}, rotation = 0)));
```

```
Modelica.Thermal.HeatTransfer.Celsius.PrescribedTemperature Tsky
annotation(Placement(visible = true, transformation(origin = {30.0, 87.7638}, extent = {{-
7.2362, -7.2362}, {7.2362, 7.2362}}, rotation = 0)));
```

```
Modelica.Thermal.HeatTransfer.Celsius.FixedTemperature Tbuilding(T = 20)
annotation(Placement(visible = true, transformation(origin = {0.0, 22.6529}, extent = {{7.3471,
7.3471}, {-7.3471, -7.3471}}, rotation = 0)));
```

```
Modelica.Blocks.Sources.CombiTimeTable MTLTempData(fileName =
"mtlweathermonthjan.txt", tableName = "var1", tableOnFile = true)
annotation(Placement(visible = true, transformation(origin = {105.0, 62.1795}, extent = {{-
7.8205, -7.8205}, {7.8205, 7.8205}}, rotation = 0)));
```

```
Modelica.Thermal.HeatTransfer.Celsius.TemperatureSensor TankTempProbe
annotation(Placement(visible = true, transformation(origin = {-128.9869, -6.0131}, extent = {{-
6.0131, -6.0131}, {6.0131, 6.0131}}, rotation = -360)));
```

```
model myExp
```

```
Modelica.Blocks.Interfaces.RealOutput y annotation(Placement(visible = true,
transformation(origin = {145.0, 0.0}, extent = {{-22.8393, -22.8393}, {22.8393, 22.8393}},
rotation = 0), iconTransformation(origin = {110.0, 0.0}, extent = {{-10.0, -10.0}, {10.0, 10.0}},
rotation = 0)));
```

```
Modelica.Blocks.Interfaces.RealInput u annotation(Placement(visible = true,
transformation(origin = {-148.2292, -0.0}, extent = {{-25.0, -25.0}, {25.0, 25.0}}, rotation = 0),
iconTransformation(origin = {-94.2145, -1.1454}, extent = {{-20.0, -20.0}, {20.0, 20.0}},
rotation = 0)));
```

```
equation
```

$y = u^{0.78}$;

```
annotation(Diagram(coordinateSystem(extent = {{-148.5, -105.0}, {148.5, 105.0}},
preserveAspectRatio = true, initialScale = 0.1, grid = {5, 5})));
```

```
end myExp;
```

```
DigesterTankHeatingModelNOVFINAL.TSkyCalculation TSkyCalc
annotation(Placement(visible = true, transformation(origin = {0.7631, 87.43770000000001},
extent = {{-10.7631, -10.7631}, {10.7631, 10.7631}}, rotation = 0)));
```

```
model TSkyCalculation "Calculates TSky from DewPoint Temp and Ambient Temp"
```

```
Modelica.Blocks.Sources.CombiTimeTable DewPointTemp(fileName =
"mtlweathermonthjan.txt", tableName = "var3", tableOnFile = true)
annotation(Placement(visible = true, transformation(origin = {-130.0, 52.3932}, extent = {{-5.0,
-5.0}, {5.0, 5.0}}, rotation = 0)));
```

```
Modelica.Thermal.HeatTransfer.Celsius.FromKelvin fromKelvin1
annotation(Placement(visible = true, transformation(origin = {15.0, 75.0}, extent = {{-6.7423, -
6.7423}, {6.7423, 6.7423}}, rotation = 0)));
```

```
Modelica.Blocks.Math.Add add4 annotation(Placement(visible = true, transformation(origin =
{-5.0, 50.0}, extent = {{-7.5, -7.5}, {7.5, 7.5}}, rotation = 0)));
```

```
Modelica.Blocks.Math.Sqrt sqrt11 annotation(Placement(visible = true, transformation(origin
= {-27.6647, 79.2137}, extent = {{-4.2137, -4.2137}, {4.2137, 4.2137}}, rotation = 0)));
```

```
Modelica.Blocks.Math.Sqrt sqrt1 annotation(Placement(visible = true, transformation(origin =
{-32.5563, 94.4699}, extent = {{-4.4699, -4.4699}, {4.4699, 4.4699}}, rotation = 0)));
```

```
Modelica.Blocks.Sources.Constant Kconv(k = 273) annotation(Placement(visible = true,
transformation(origin = {-135.0, 40.0}, extent = {{-5.0, -5.0}, {5.0, 5.0}}, rotation = 0)));
```

```
Modelica.Blocks.Math.Add add3 annotation(Placement(visible = true, transformation(origin =
{-109.1818, 50.8182}, extent = {{-5.8182, -5.8182}, {5.8182, 5.8182}}, rotation = 0)));
```

```
Modelica.Blocks.Math.Log log1 annotation(Placement(visible = true, transformation(origin =
{-98.9684, 73.9684}, extent = {{-6.0316, -6.0316}, {6.0316, 6.0316}}, rotation = 0)));
```

```
Modelica.Blocks.Math.Product product2 annotation(Placement(visible = true,
transformation(origin = {-75.0, 81.30540000000001}, extent = {{-6.3054, -6.3054}, {6.3054,
6.3054}}, rotation = 0)));
```

Modelica.Blocks.Sources.Constant const2(k = 0.764) annotation(Placement(visible = true, transformation(origin = {-130.0, 77.1606}, extent = {{-4.6001, -4.6001}, {4.6001, 4.6001}}, rotation = 0)));

Modelica.Blocks.Math.Gain gain1(k = 1 / 273) annotation(Placement(visible = true, transformation(origin = {-84.4598, 55.5402}, extent = {{-5.5402, -5.5402}, {5.5402, 5.5402}}, rotation = 0)));

Modelica.Blocks.Sources.Constant const1(k = 0.787) annotation(Placement(visible = true, transformation(origin = {-130.0, 93.29300000000001}, extent = {{-5.0, -5.0}, {5.0, 5.0}}, rotation = 0)));

Modelica.Blocks.Math.Add add2 annotation(Placement(visible = true, transformation(origin = {-51.3189, 85.0}, extent = {{-6.3189, -6.3189}, {6.3189, 6.3189}}, rotation = 0)));

Modelica.Blocks.Math.Product product1 annotation(Placement(visible = true, transformation(origin = {-5.0, 75.0}, extent = {{-7.5, -7.5}, {7.5, 7.5}}, rotation = 0)));

Modelica.Blocks.Interfaces.RealInput u3 annotation(Placement(visible = true, transformation(origin = {106.8418, -95.0}, extent = {{-20.0, -20.0}, {20.0, 20.0}}, rotation = 0), iconTransformation(origin = {-100.0, 0.0}, extent = {{-20.0, -20.0}, {20.0, 20.0}}, rotation = 0)));

Modelica.Blocks.Interfaces.RealOutput Celsius1 annotation(Placement(visible = true, transformation(origin = {29.0804, 82.7638}, extent = {{-10.0, -10.0}, {10.0, 10.0}}, rotation = 0), iconTransformation(origin = {100.0, 0.0}, extent = {{-10.0, -10.0}, {10.0, 10.0}}, rotation = 0)));

equation

connect(fromKelvin1.Celsius, Celsius1) annotation(Line(visible = true, origin = {25.9144, 78.8819}, points = {{-3.4979, -3.8819}, {0.166, -3.8819}, {0.166, 3.8819}, {3.166, 3.8819}}, color = {0, 0, 127}));

connect(u3, add4.u2) annotation(Line(visible = true, origin = {44.9093, -1.5}, points = {{61.9325, -93.5}, {67.2426, -92.28019999999999}, {67.2426, 41.5}, {-69.9093, 41.5}, {-69.9093, 47.0}, {-58.9093, 47.0}}, color = {0, 0, 127}));

connect(const1.y, add2.u1) annotation(Line(visible = true, origin = {-76.80119999999999, 91.04219999999999}, points = {{-47.6988, 2.2508}, {14.8996, 2.2508}, {14.8996, -2.2508}, {17.8996, -2.2509}}, color = {0, 0, 127}));

connect(product2.y, add2.u2) annotation(Line(visible = true, origin = {-62.6922, 81.25709999999999}, points = {{-5.3719, 0.0483}, {0.7906, 0.0484}, {0.7906, -0.0484}, {3.7906, -0.0484}}, color = {0, 0, 127}));

```

connect(const2.y, product2.u1) annotation(Line(visible = true, origin = {-104.0146,
81.882000000000001}, points = {{-20.9253, -4.7214}, {-10.9854, -4.7214}, {-10.9854, 3.118},
{21.4481, 3.118}, {21.4481, 3.2066}}, color = {0, 0, 127}));

connect(log1.y, product2.u2) annotation(Line(visible = true, origin = {-86.508300000000001,
75.7453}, points = {{-5.8253, -1.7769}, {0.9418, -1.7769}, {0.9418, 1.7769}, {3.9418,
1.7769}}, color = {0, 0, 127}));

connect(gain1.y, log1.u) annotation(Line(visible = true, origin = {-92.286,
64.571200000000001}, points = {{13.9204, -9.031000000000001}, {16.9203, -
9.031000000000001}, {16.9203, -0.3662}, {-16.9203, -0.3662}, {-16.9203, 9.3972}, {-13.9203,
9.3972}}, color = {0, 0, 127}));

connect(Kconv.y, add3.u2) annotation(Line(visible = true, origin = {-119.3655, 43.0958},
points = {{-10.1345, -3.0958}, {-0.6345, -6.3888}, {-0.6345, 4.2731}, {3.2018, 4.2731},
{3.2019, 4.2315}}, color = {0, 0, 127}));

connect(add3.y, gain1.u) annotation(Line(visible = true, origin = {-95.5265, 53.1792}, points
= {{-7.2553, -2.361}, {1.4184, -2.361}, {1.4184, 2.361}, {4.4185, 2.361}}, color = {0, 0,
127}));

connect(add2.y, sqrt1.u) annotation(Line(visible = true, origin = {-39.4046,
90.894000000000001}, points = {{-4.9635, -5.894}, {0.9973, -5.894}, {0.9973, 4.106}, {1.4844,
4.106}, {1.4844, 3.5759}}, color = {0, 0, 127}));

connect(sqrt1.y, sqrt11.u) annotation(Line(visible = true, origin = {-29.5504, 87.1979}, points
= {{1.911, 7.272}, {6.0793, 7.272}, {6.0793, 0.7121}, {-5.4496, 0.7121}, {-5.4496, -7.9842},
{-3.1707, -7.9842}}, color = {0, 0, 127}));

connect(sqrt11.y, product1.u1) annotation(Line(visible = true, origin = {-17.7574, 79.3569},
points = {{-5.2722, -0.1432}, {0.7574, -0.1431}, {0.7574, 0.1431}, {3.7574, 0.1431}}, color =
{0, 0, 127}));

connect(Kconv.y, add4.u1) annotation(Line(visible = true, origin = {-73.1173, 46.9265},
points = {{-56.3827, -6.9265}, {-33.5695, -10.2195}, {-33.5695, -3.825}, {0.1435, -3.825},
{0.1435, 10.2577}, {59.1173, 10.2577}, {59.1173, 7.5735}}, color = {0, 0, 127}));

connect(add4.y, product1.u2) annotation(Line(visible = true, origin = {-9.7083, 61.8333},
points = {{12.9583, -11.8333}, {15.9583, -11.8333}, {15.9583, 3.1667}, {-20.2917, 3.1667}, {-
20.2917, 8.666700000000001}, {-4.2917, 8.666700000000001}}, color = {0, 0, 127}));

connect(product1.y, fromKelvin1.Kelvin) annotation(Line(visible = true, origin = {5.0796,
75.0}, points = {{-1.8296, 0.0}, {1.8296, 0.0}}, color = {0, 0, 127}));

```

```
connect(DewPointTemp.y[1], add3.u1) annotation(Line(visible = true, origin = {-119.7477,
53.3512}, points = {{-4.7523, -0.958}, {0.5841, -0.9579}, {0.5841, 0.9579}, {3.5841, 0.9579}},
color = {0, 0, 127}));
```

```
annotation(Icon(coordinateSystem(extent = {{-100.0, -100.0}, {100.0, 100.0}},
preserveAspectRatio = true, initialScale = 0.1, grid = {10, 10}), graphics = {Rectangle(visible =
true, fillColor = {0, 0, 255}, extent = {{-100.0, -100.0}, {100.0, 100.0}}, radius = 25),
Text(visible = true, fillColor = {0, 0, 255}, fillPattern = FillPattern.Solid, extent = {{-100.0, -
100.0}, {100.0, 100.0}}, textString = "%name", fontName = "Arial")})),
Diagram(coordinateSystem(extent = {{-148.5, -105.0}, {148.5, 105.0}}, preserveAspectRatio =
true, initialScale = 0.1, grid = {5, 5})));
```

```
end TSkyCalculation;
```

```
model ConvCoeffCalc
```

```
Modelica.Blocks.Math.Product product3 annotation(Placement(visible = true,
transformation(origin = {-47.2834, 4.8582}, extent = {{-5.0, -5.0}, {5.0, 5.0}}, rotation = 0)));
```

```
Modelica.Blocks.Math.Gain HeightSpeedFactor(k = (43 / 10) ^ 0.34)
annotation(Placement(visible = true, transformation(origin = {-5.9813, -27.0775}, extent = {{-
6.3021, -6.3021}, {6.3021, 6.3021}}, rotation = 0)));
```

```
Modelica.Blocks.Sources.CombiTimeTable MTLWindSpeed(fileName =
"mtlweathermonthjan.txt", tableName = "var2", tableOnFile = true)
annotation(Placement(visible = true, transformation(origin = {-119.0273, -26.9909}, extent = {{-
13.0091, -13.0091}, {13.0091, 13.0091}}, rotation = 0)));
```

```
Modelica.Blocks.Math.Gain SurfaceArea2(k = 34.16) annotation(Placement(visible = true,
transformation(origin = {-13.7973, 20.0}, extent = {{-6.2027, -6.2027}, {6.2027, 6.2027}},
rotation = -360)));
```

```
Modelica.Blocks.Math.Gain SurfaceArea(k = 10.79) annotation(Placement(visible = true,
transformation(origin = {18.8583, 5.0}, extent = {{-6.1417, -6.1417}, {6.1417, 6.1417}},
rotation = -360)));
```

```
Modelica.Blocks.Sources.Constant const(k = 7.8) annotation(Placement(visible = true,
transformation(origin = {-68.958, 7.9225}, extent = {{-5.0, -5.0}, {5.0, 5.0}}, rotation = 0)));
```

```
Modelica.Blocks.Interfaces.RealOutput ConvCoeffRoof annotation(Placement(visible = true,
transformation(origin = {160.0, -60.0}, extent = {{-20.0, -20.0}, {20.0, 20.0}}, rotation = 0),
iconTransformation(origin = {100.0, 0.0}, extent = {{-10.0, -10.0}, {10.0, 10.0}}, rotation =
0)));
```

Modelica.Blocks.Interfaces.RealOutput ConvCoeffWalls annotation(Placement(visible = true, transformation(origin = {157.6556, 81.6245}, extent = {{-20.0, -20.0}, {20.0, 20.0}}, rotation = 0), iconTransformation(origin = {100.0, -50.0}, extent = {{-10.0, -10.0}, {10.0, 10.0}}, rotation = 0)));

DigesterTankHeatingModelNOVFINAL.myExp myExp annotation(Placement(visible = true, transformation(origin = {-20.2809, -47.1242}, extent = {{9.719099999999999, -9.719099999999999}, {9.719099999999999, 9.719099999999999}}, rotation = 0)));

Modelica.Blocks.Math.Gain ConvertKMHtoMS(k = 1000 / 3600)
annotation(Placement(visible = true, transformation(origin = {-77.5, -27.5}, extent = {{-7.5, -7.5}, {7.5, 7.5}}, rotation = 0)));

equation

connect(ConvertKMHtoMS.y, HeightSpeedFactor.u) annotation(Line(visible = true, origin = {-28.9704, -27.2888}, points = {{-40.2796, -0.2112}, {12.4265, -0.2112}, {12.4265, 0.2112}, {15.4265, 0.2112}}, color = {0, 0, 127}));

connect(MTLWindSpeed.y[1], ConvertKMHtoMS.u) annotation(Line(visible = true, origin = {-92.5543, -27.2455}, points = {{-12.163, 0.2545}, {3.0543, 0.2545}, {3.0543, -0.2545}, {6.0543, -0.2545}}, color = {0, 0, 127}));

connect(myExp.y, product3.u2) annotation(Line(visible = true, origin = {-49.2055, -22.633}, points = {{18.2336, -24.4912}, {-7.0779, -24.4912}, {-7.0779, 24.4912}, {-4.0779, 24.4912}}, color = {0, 0, 127}));

connect(HeightSpeedFactor.y, myExp.u) annotation(Line(visible = true, origin = {6.4995, -37.1565}, points = {{-5.5485, 10.079}, {11.586, 10.079}, {11.586, -10.079}, {-17.6235, -10.079}}, color = {0, 0, 127}));

connect(SurfaceArea.y, ConvCoeffRoof) annotation(Line(visible = true, origin = {-84.8556, 79.79389999999999}, points = {{110.4698, -74.79389999999999}, {244.8556, -74.79389999999999}, {244.8556, -139.7939}}, color = {0, 0, 127}));

connect(SurfaceArea2.y, ConvCoeffWalls) annotation(Line(visible = true, origin = {-101.4816, 44.848}, points = {{94.5073, -24.848}, {259.1372, -24.848}, {259.1372, 36.7764}}, color = {0, 0, 127}));

connect(product3.y, SurfaceArea.u) annotation(Line(visible = true, origin = {-3.3297, 4.9291}, points = {{-38.4537, -0.07090000000000001}, {11.8179, -0.07090000000000001}, {11.8179, 0.07090000000000001}, {14.8179, 0.07090000000000001}}, color = {0, 0, 127}));

```
connect(product3.y, SurfaceArea2.u) annotation(Line(visible = true, origin = {-32.2212, -22.2466}, points = {{-9.562200000000001, 27.1047}, {2.3983, 27.1047}, {11.1405, 27.1047}, {11.1405, 27.1047}, {10.9807, 42.2466}}, color = {0, 0, 127}));
```

```
connect(const.y, product3.u1) annotation(Line(visible = true, origin = {-57.327, 7.8903}, points = {{-6.1309, 0.0322}, {1.0436, 0.0322}, {1.0436, -0.0322}, {4.0436, -0.0322}}, color = {0, 0, 127}));
```

```
annotation(Icon(coordinateSystem(extent = {{-100.0, -100.0}, {100.0, 100.0}}, preserveAspectRatio = true, initialScale = 0.1, grid = {10, 10}), graphics = {Rectangle(visible = true, fillColor = {0, 0, 255}, extent = {{-100.0, -100.0}, {100.0, 100.0}}, radius = 25), Text(visible = true, fillColor = {0, 0, 255}, fillPattern = FillPattern.Solid, extent = {{-100.0, -100.0}, {100.0, 100.0}}, textString = "%name", fontName = "Arial")}), Diagram(coordinateSystem(extent = {{-148.5, -105.0}, {148.5, 105.0}}, preserveAspectRatio = true, initialScale = 0.1, grid = {5, 5})));
```

```
end ConvCoeffCalc;
```

```
model HeatPumpUpdate
```

```
Modelica.Blocks.Math.Product COPZeroProduct annotation(Placement(visible = true, transformation(origin = {92.5, 45.0}, extent = {{7.5, -7.5}, {-7.5, 7.5}}, rotation = 180)));
```

```
Modelica.Blocks.Interfaces.RealInput ZeroCOP annotation(Placement(visible = true, transformation(origin = {0.0, 112.6793}, extent = {{-20.0, -20.0}, {20.0, 20.0}}, rotation = -90), iconTransformation(origin = {2.7221, 96.2439}, extent = {{-20.0, -20.0}, {20.0, 20.0}}, rotation = 0)));
```

```
Modelica.Blocks.Interfaces.RealInput EVAPCONSTIN annotation(Placement(visible = true, transformation(origin = {-160.0, 2.6458}, extent = {{-20.0, -20.0}, {20.0, 20.0}}, rotation = 0), iconTransformation(origin = {-102.943, 4.5497}, extent = {{-20.0, -20.0}, {20.0, 20.0}}, rotation = 0)));
```

```
Modelica.Blocks.Interfaces.RealInput CONDCONSTIN annotation(Placement(visible = true, transformation(origin = {-160.0, 90.0}, extent = {{-20.0, -20.0}, {20.0, 20.0}}, rotation = 0), iconTransformation(origin = {-100.7159, 87.14449999999999}, extent = {{-20.0, -20.0}, {20.0, 20.0}}, rotation = 0)));
```

```
Modelica.Blocks.Interfaces.RealInput ElectricalInput annotation(Placement(visible = true, transformation(origin = {-160.0, -85.0}, extent = {{-20.0, -20.0}, {20.0, 20.0}}, rotation = -360), iconTransformation(origin = {-99.9735, -48.6469}, extent = {{-20.0, -20.0}, {20.0, 20.0}}, rotation = 0)));
```

Modelica.Blocks.Interfaces.RealInput TCondIn annotation(Placement(visible = true, transformation(origin = {-160.0, 50.0}, extent = {{-20.0, -20.0}, {20.0, 20.0}}, rotation = 0), iconTransformation(origin = {-100.5874, 46.8882}, extent = {{-20.0, -20.0}, {20.0, 20.0}}, rotation = 0)));

Modelica.Blocks.Interfaces.RealOutput QCondOut annotation(Placement(visible = true, transformation(origin = {158.274, -51.726}, extent = {{-18.274, -18.274}, {18.274, 18.274}}, rotation = 0), iconTransformation(origin = {98.8253, 0.336}, extent = {{-10.0, -10.0}, {10.0, 10.0}}, rotation = 0)));

Modelica.Blocks.Math.Gain COPactual(k = 0.4) annotation(Placement(visible = true, transformation(origin = {70.1764, -10.1764}, extent = {{-4.8236, -4.8236}, {4.8236, 4.8236}}, rotation = 0)));

Modelica.Blocks.Math.Gain C6(k = 1 / 113049000) annotation(Placement(visible = true, transformation(origin = {-69.01900000000001, 35.0}, extent = {{-4.019, -4.019}, {4.019, 4.019}}, rotation = -180)));

Modelica.Blocks.Math.Product Qc annotation(Placement(visible = true, transformation(origin = {25.0, -51.6186}, extent = {{-5.0, -5.0}, {5.0, 5.0}}, rotation = 0)));

Modelica.Blocks.Math.Add PlusQc(k2 = +1) annotation(Placement(visible = true, transformation(origin = {-63.7073, 51.0754}, extent = {{-6.2927, -6.2927}, {6.2927, 6.2927}}, rotation = 0)));

Modelica.Blocks.Math.Product product4 annotation(Placement(visible = true, transformation(origin = {-88.312, 86.0074}, extent = {{-6.688, -6.688}, {6.688, 6.688}}, rotation = 0)));

Modelica.Blocks.Math.Gain C5(k = 1 / 2042227) annotation(Placement(visible = true, transformation(origin = {-80.0, -10.0}, extent = {{-4.019, -4.019}, {4.019, 4.019}}, rotation = 0)));

Modelica.Blocks.Sources.Constant Constant(k = 1) annotation(Placement(visible = true, transformation(origin = {47.2969, -35.0}, extent = {{-5.0, -5.0}, {5.0, 5.0}}, rotation = 0)));

Modelica.Blocks.Math.Add add5(k2 = -1) annotation(Placement(visible = true, transformation(origin = {90.0, -23.0567}, extent = {{-5.0, -5.0}, {5.0, 5.0}}, rotation = 0)));

Modelica.Blocks.Math.Product Qe annotation(Placement(visible = true, transformation(origin = {102.8222, -40.0}, extent = {{-5.0, -5.0}, {5.0, 5.0}}, rotation = 0)));

Modelica.Blocks.Math.Add MinusQe(k2 = -1) annotation(Placement(visible = true, transformation(origin = {-56.7925, 1.7899}, extent = {{-5.0, -5.0}, {5.0, 5.0}}, rotation = 0)));

Modelica.Blocks.Math.Product product1 annotation(Placement(visible = true, transformation(origin = {-110.0, -0.8344}, extent = {{-5.8344, -5.8344}, {5.8344, 5.8344}}, rotation = 0)));

Modelica.Blocks.Math.Gain C4(k = 1 / 2042227) annotation(Placement(visible = true, transformation(origin = {-80.0, 10.0}, extent = {{-4.019, -4.019}, {4.019, 4.019}}, rotation = 0)));

Modelica.Blocks.Math.Gain C(k = 1 / 113049000) annotation(Placement(visible = true, transformation(origin = {-64.0144, 85.98560000000001}, extent = {{-4.0144, -4.0144}, {4.0144, 4.0144}}, rotation = 0)));

Modelica.Blocks.Math.Add TCoutMinusTEout(k1 = -1, k2 = 1) annotation(Placement(visible = true, transformation(origin = {40.778, 29.222}, extent = {{-5.778, -5.778}, {5.778, 5.778}}, rotation = 0)));

Modelica.Blocks.Math.Division COPc annotation(Placement(visible = true, transformation(origin = {52.6055, -10.0}, extent = {{-5.0, -5.0}, {5.0, 5.0}}, rotation = 0)));

Modelica.Blocks.Math.Add add1 annotation(Placement(visible = true, transformation(origin = {25.0, -20.0}, extent = {{-5.0, -5.0}, {5.0, 5.0}}, rotation = 0)));

Modelica.Blocks.Sources.Constant const(k = 273.15) annotation(Placement(visible = true, transformation(origin = {-2.7993, -22.7993}, extent = {{-7.2007, -7.2007}, {7.2007, 7.2007}}, rotation = 0)));

Modelica.Blocks.Sources.Constant TEvapIn(k = 30) annotation(Placement(visible = true, transformation(origin = {-145.0, -45.0}, extent = {{-7.5, -7.5}, {7.5, 7.5}}, rotation = 0)));

DigesterTankHeatingModelNOVFINAL.IntegratorWithReset TEvapOut(initType = 3, y_start = 23) annotation(Placement(visible = true, transformation(origin = {0.0, 33.3254}, extent = {{-10.0, -10.0}, {10.0, 10.0}}, rotation = 0)));

Modelica.Blocks.Interfaces.BooleanInput u annotation(Placement(visible = true, transformation(origin = {75.0, 111.8618}, extent = {{-20.0, -20.0}, {20.0, 20.0}}, rotation = -90), iconTransformation(origin = {49.6171, 98.5609}, extent = {{-20.0, -20.0}, {20.0, 20.0}}, rotation = 0)));

DigesterTankHeatingModelNOVFINAL.IntegratorWithReset TCondOut(initType = 3, y_start = 55) annotation(Placement(visible = true, transformation(origin = {-0.0, 3.3492}, extent = {{-10.0, -10.0}, {10.0, 10.0}}, rotation = 0)));

Modelica.Blocks.Math.Add TEvapInMinusTEvapOut(k2 = -1) annotation(Placement(visible = true, transformation(origin = {-110.0, -48.2634}, extent = {{-6.7366, -6.7366}, {6.7366, 6.7366}}, rotation = 0)));

```
Modelica.Blocks.Math.Add TCondINminusTCondOUT(k2 = -1)
annotation(Placement(visible = true, transformation(origin = {-120.0, 45.0}, extent = {{-7.5, -
7.5}, {7.5, 7.5}}, rotation = 0)));
```

equation

```
connect(TCondOut.y, TCondINminusTCondOUT.u2) annotation(Line(visible = true, origin =
{-53.8571, 36.7426}, points = {{64.8571, -33.3935}, {78.8571, -33.3935}, {78.8571, 38.2574},
{-36.1429, 38.2574}, {-36.1429, -6.7426}, {-75.1429, -6.7426}, {-75.1429, 3.7574}}, color =
{0, 0, 127}));
```

```
connect(TCondINminusTCondOUT.y, product4.u2) annotation(Line(visible = true, origin = {-
100.6322, 68.85639999999999}, points = {{-11.1178, -23.8564}, {5.6322, -23.8564}, {5.6322,
6.1436}, {-4.3678, 6.1436}, {-4.3678, 11.1436}, {4.2946, 11.1436}, {4.2946, 13.1382}}, color
= {0, 0, 127}));
```

```
connect(TCondIn, TCondINminusTCondOUT.u1) annotation(Line(visible = true, origin = {-
138.25, 49.75}, points = {{-21.75, 0.25}, {6.25, 0.25}, {6.25, -0.25}, {9.25, -0.25}}, color = {0,
0, 127}));
```

```
connect(TEvapOut.y, TEvapInMinusTEvapOut.u2) annotation(Line(visible = true, origin = {-
53.8694, -30.4564}, points = {{64.8694, 63.7818}, {68.8694, 63.7818}, {68.8694, -7.3891}, {-
3.0663, -7.3891}, {-3.0663, -34.5436}, {-66.1306, -34.5436}, {-66.1306, -21.849}, {-64.2145, -
21.849}}, color = {0, 0, 127}));
```

```
connect(TEvapInMinusTEvapOut.y, product1.u2) annotation(Line(visible = true, origin = {-
101.3185, -34.1724}, points = {{-1.2713, -14.0911}, {16.3185, -14.0911}, {16.3185, -0.8276},
{-15.6828, -0.8276}, {-15.6828, 29.8373}}, color = {0, 0, 127}));
```

```
connect(TEvapIn.y, TEvapInMinusTEvapOut.u1) annotation(Line(visible = true, origin = {-
124.2504, -44.6108}, points = {{-12.4996, -0.3892}, {3.1665, -0.3892}, {3.1665, 0.3892},
{6.1665, 0.3892}}, color = {0, 0, 127}));
```

```
connect(TCondOut.y, add1.u1) annotation(Line(visible = true, origin = {16.0403, -6.8254},
points = {{-5.0403, 10.1746}, {1.0403, 10.1746}, {1.0403, -10.1746}, {2.9597, -10.1746}},
color = {0, 0, 127}));
```

```
connect(TCondOut.y, TCoutMinusTEout.u2) annotation(Line(visible = true, origin =
{23.7378, 16.4907}, points = {{-12.7378, -13.1415}, {-3.7378, -13.1415}, {-3.7378, 8.5093},
{10.1066, 8.5093}, {10.1066, 9.2645}}, color = {0, 0, 127}));
```

```
connect(PlusQc.y, TCondOut.u) annotation(Line(visible = true, origin = {-28.1571, 23.1},
points = {{-28.6283, 27.9754}, {-1.8429, 27.9754}, {-1.8429, -18.1}, {16.1571, -18.1},
{16.1571, -19.7508}}, color = {0, 0, 127}));
```

connect(u, TCondOut.reset) annotation(Line(visible = true, origin = {17.6, 45.4297}, points = {{57.4, 66.43210000000001}, {57.4, 16.8646}, {-42.6, 16.8646}, {-42.6, -50.0806}, {-29.6, -50.0806}}, color = {255, 0, 255}));

connect(u, TEvapOut.reset) annotation(Line(visible = true, origin = {21.6, 56.828}, points = {{53.4, 55.0339}, {53.4, 8.172000000000001}, {-36.6, 8.172000000000001}, {-36.6, -31.5025}, {-33.6, -31.5025}}, color = {255, 0, 255}));

connect(MinusQe.y, TEvapOut.u) annotation(Line(visible = true, origin = {-25.8231, 17.5577}, points = {{-25.4694, -15.7678}, {5.8231, -15.7678}, {5.8231, 15.7678}, {13.8231, 15.7678}}, color = {0, 0, 127}));

connect(TEvapOut.y, TCoutMinusTEout.u1) annotation(Line(visible = true, origin = {26.6333, 33.0071}, points = {{-15.6333, 0.3183}, {4.2111, 0.3183}, {4.2111, -0.3183}, {7.2111, -0.3183}}, color = {0, 0, 127}));

connect(ElectricalInput, Qc.u2) annotation(Line(visible = true, origin = {-27.25, -69.80929999999999}, points = {{-132.75, -15.1907}, {43.25, -15.1907}, {43.25, 15.1907}, {46.25, 15.1907}}, color = {0, 0, 127}));

connect(ElectricalInput, Qe.u2) annotation(Line(visible = true, origin = {31.1166, -64.0}, points = {{-191.1166, -21.0}, {62.7056, -21.0}, {62.7056, 21.0}, {65.7056, 21.0}}, color = {0, 0, 127}));

connect(Constant.y, add5.u2) annotation(Line(visible = true, origin = {74.69920000000001, -30.5284}, points = {{-21.9023, -4.4716}, {6.3008, -4.4716}, {6.3008, 4.4716}, {9.300800000000001, 4.4717}}, color = {0, 0, 127}));

connect(COPc.y, COPactual.u) annotation(Line(visible = true, origin = {61.3174, -10.0882}, points = {{-3.2119, 0.0882}, {0.0706, 0.0882}, {0.0706, -0.0882}, {3.0707, -0.0882}}, color = {0, 0, 127}));

connect(COPactual.y, add5.u1) annotation(Line(visible = true, origin = {78.3216, -16.7633}, points = {{-2.8392, 6.5869}, {-2.8392, -3.2934}, {5.6784, -3.2934}}, color = {0, 0, 127}));

connect(Qc.y, C6.u) annotation(Line(visible = true, origin = {-32.1655, -15.7008}, points = {{62.6655, -35.9178}, {62.6655, -74.2992}, {-2.8345, -74.2992}, {-2.8345, 35.7008}, {-2.8345, 50.7008}, {-24.7199, 50.7008}, {-32.0307, 50.7008}}, color = {0, 0, 127}));

connect(CONDCONSTIN, product4.u1) annotation(Line(visible = true, origin = {-115.2455, 85.181}, points = {{-44.7545, 4.819}, {5.2455, 5.181}, {16.2455, 5.181}, {18.9079, 4.8392}}, color = {0, 0, 127}));

```
connect(product4.y, C.u) annotation(Line(visible = true, origin = {-73.3625, 85.9965}, points = {{-7.5927, 0.0109}, {1.5309, 0.0109}, {1.5309, -0.0109}, {4.5308, -0.0109}}, color = {0, 0, 127}));
```

```
connect(C.y, PlusQc.u1) annotation(Line(visible = true, origin = {-66.79770000000001, 68.1913}, points = {{7.1991, 17.7943}, {16.7977, 17.7943}, {16.7977, 1.8087}, {-13.2023, 1.8087}, {-13.2023, -13.1913}, {-4.2023, -13.1913}, {-4.4608, -13.3403}}, color = {0, 0, 127}));
```

```
connect(C6.y, PlusQc.u2) annotation(Line(visible = true, origin = {-86.47410000000001, 45.4812}, points = {{13.0342, -10.4812}, {1.4741, -10.4812}, {1.4741, 1.8186}, {11.4741, 1.8186}, {15.2156, 1.8186}}, color = {0, 0, 127}));
```

```
connect(EVAPCONSTIN, product1.u1) annotation(Line(visible = true, origin = {-129.2509, 2.656}, points = {{-30.7491, -0.0102}, {9.249700000000001, -0.0102}, {9.249700000000001, 0.0102}, {12.2496, 0.0102}}, color = {0, 0, 127}));
```

```
connect(C4.y, MinusQe.u1) annotation(Line(visible = true, origin = {-67.48909999999999, 7.3949}, points = {{-8.09, 2.6051}, {1.6967, 2.6051}, {1.6967, -2.605}, {4.6966, -2.605}}, color = {0, 0, 127}));
```

```
connect(C5.y, MinusQe.u2) annotation(Line(visible = true, origin = {-67.48909999999999, -5.6051}, points = {{-8.09, -4.3949}, {1.6967, -4.3949}, {1.6967, 4.395}, {4.6966, 4.395}}, color = {0, 0, 127}));
```

```
connect(product1.y, C4.u) annotation(Line(visible = true, origin = {-94.60120000000001, 4.5828}, points = {{-8.981, -5.4172}, {-0.3988, -5.4172}, {-0.3988, 5.4172}, {9.7784, 5.4172}}, color = {0, 0, 127}));
```

```
connect(COPZeroProduct.y, COPc.u1) annotation(Line(visible = true, origin = {75.1009, 14.1848}, points = {{25.6491, 30.8152}, {33.8991, 30.8152}, {33.8991, -11.245}, {-35.1009, -11.245}, {-35.1009, -21.1848}, {-28.4954, -21.1848}}, color = {0, 0, 127}));
```

```
connect(const.y, add1.u2) annotation(Line(visible = true, origin = {14.0304, -22.8997}, points = {{-8.908899999999999, 0.1004}, {1.9696, 0.1004}, {1.9696, -0.1003}, {4.9696, -0.1003}}, color = {0, 0, 127}));
```

```
connect(COPactual.y, Qc.u1) annotation(Line(visible = true, origin = {33.1859, -33.765}, points = {{42.2965, 23.5886}, {42.2965, 8.765000000000001}, {1.8141, 8.765000000000001}, {1.8141, -6.235}, {-16.4401, -6.235}, {-18.1859, -6.235}, {-18.1859, -14.8536}, {-14.1859, -14.8536}}, color = {0, 0, 127}));
```

```
connect(add1.y, COPZeroProduct.u1) annotation(Line(visible = true, origin = {55.0537, 11.8333}, points = {{-24.5537, -31.8333}, {-21.8926, -31.8333}, {-21.8926, 3.1667}, {19.9463, 3.1667}, {19.9463, 28.6667}, {28.4463, 28.6667}}, color = {0, 0, 127}));
```

```
connect(Qc.y, QCondOut) annotation(Line(visible = true, origin = {110.5857, -26.3175}, points = {{-80.0857, -25.3011}, {22.4115, -25.3011}, {29.4143, -25.4085}, {47.6883, -25.4085}}, color = {0, 0, 127}));
```

```
connect(add5.y, Qe.u1) annotation(Line(visible = true, origin = {95.7649, -31.7746}, points = {{-0.2649, 8.7179}, {9.235099999999999, 8.7179}, {9.235099999999999, 1.7746}, {-5.7649, 1.7746}, {-5.7649, -5.2671}, {-3.8663, -5.2671}, {-3.8663, -5.2254}, {1.0573, -5.2254}}, color = {0, 0, 127}));
```

```
connect(Qe.y, C5.u) annotation(Line(visible = true, origin = {-5.9161, -41.25}, points = {{114.2383, 1.25}, {130.9161, 1.25}, {130.9161, -38.75}, {-59.084, -38.75}, {-59.084, 11.25}, {-94.084, 11.25}, {-94.084, 31.25}, {-78.9067, 31.25}}, color = {0, 0, 127}));
```

```
connect(TCoutMinusTEout.y, COPc.u2) annotation(Line(visible = true, origin = {48.8812, 3.901}, points = {{-1.7474, 25.321}, {10.1188, 25.321}, {10.1188, 3.802}, {-12.0404, 3.802}, {-12.0404, -16.901}, {-2.2757, -16.901}}, color = {0, 0, 127}));
```

```
connect(ZeroCOP, COPZeroProduct.u2) annotation(Line(visible = true, origin = {41.0, 65.2948}, points = {{-41.0, 47.3845}, {-41.0, -15.7948}, {39.5, -15.7948}, {42.5, -15.7948}}, color = {0, 0, 127}));
```

```
annotation(Icon(coordinateSystem(extent = {{-100.0, -100.0}, {100.0, 100.0}}, preserveAspectRatio = true, initialScale = 0.1, grid = {10, 10}), graphics = {Rectangle(visible = true, fillColor = {0, 0, 255}, extent = {{-100.0, -100.0}, {100.0, 100.0}}, radius = 25), Text(visible = true, fillColor = {0, 0, 255}, fillPattern = FillPattern.Solid, extent = {{-100.0, -100.0}, {100.0, 100.0}}, textString = "%name", fontName = "Arial")}, Diagram(coordinateSystem(extent = {{-148.5, -105.0}, {148.5, 105.0}}, preserveAspectRatio = true, initialScale = 0.1, grid = {5, 5})));
```

```
end HeatPumpUpdate;
```

```
model HeatPumpWithController
```

```
DigesterTankHeatingModelNOVFINAL.HeatPumpUpdate heatPumpUpdate1  
annotation(Placement(visible = true, transformation(origin = {115.8254, 19.1746}, extent = {{-15.8254, -15.8254}, {15.8254, 15.8254}}, rotation = 0)));
```

```
Modelica.Blocks.Sources.Constant COPInput1(k = 1) annotation(Placement(visible = true, transformation(origin = {-50.0, 78.154}, extent = {{-5.0, -5.0}, {5.0, 5.0}}, rotation = 0)));
```

Modelica.Blocks.Logical.Switch COPSwitch annotation(Placement(visible = true, transformation(origin = {-26.1172, 73.8828}, extent = {{-6.1172, -6.1172}, {6.1172, 6.1172}}, rotation = 0)));

Modelica.Blocks.Sources.Constant MassFlowTimesCpWater(k = 0.38 * 4187) annotation(Placement(visible = true, transformation(origin = {-20.0, 37.3444}, extent = {{-5.0, -5.0}, {5.0, 5.0}}, rotation = 0)));

Modelica.Blocks.Logical.Switch CondConstIN annotation(Placement(visible = true, transformation(origin = {4.8912, 33.2219}, extent = {{-5.1088, -5.1088}, {5.1088, 5.1088}}, rotation = 0)));

Modelica.Blocks.Sources.Constant MassFlowEvapTimesCpAir(k = 0.7 * 1005) annotation(Placement(visible = true, transformation(origin = {15.0, -25.0}, extent = {{-5.0, -5.0}, {5.0, 5.0}}, rotation = 0)));

Modelica.Blocks.Logical.Switch EvapConstIN annotation(Placement(visible = true, transformation(origin = {64.92480000000001, -32.4855}, extent = {{-7.5145, -7.5145}, {7.5145, 7.5145}}, rotation = 0)));

Modelica.Blocks.Sources.Constant TankSetTemp(k = 35) annotation(Placement(visible = true, transformation(origin = {-120.0, 15.0}, extent = {{-5.0, -5.0}, {5.0, 5.0}}, rotation = 0)));

Modelica.Blocks.Logical.OnOffController onOffController1 (bandwidth = 0.001) annotation(Placement(visible = true, transformation(origin = {-91.72199999999999, 1.722}, extent = {{-8.278000000000001, -8.278000000000001}, {8.278000000000001, 8.278000000000001}}, rotation = 0)));

Modelica.Blocks.Logical.Switch ElecINSwitch annotation(Placement(visible = true, transformation(origin = {75.0145, -90.0145}, extent = {{-10.0145, -10.0145}, {10.0145, 10.0145}}, rotation = 0)));

Modelica.Blocks.Sources.Constant ElecIN(k = 2000) annotation(Placement(visible = true, transformation(origin = {31.6508, -82.057}, extent = {{-5.0, -5.0}, {5.0, 5.0}}, rotation = 0)));

Modelica.Blocks.Logical.And and1 annotation(Placement(visible = true, transformation(origin = {-67.70310000000001, 50.0}, extent = {{-5.0, -5.0}, {5.0, 5.0}}, rotation = 0)));

Modelica.Blocks.Logical.Greater greater1 annotation(Placement(visible = true, transformation(origin = {-90.0, 78.2337}, extent = {{-5.0, -5.0}, {5.0, 5.0}}, rotation = 0)));

Modelica.Blocks.Sources.CombiTimeTable zeros1 (fileName = "daylightzeros.txt", tableName = "var1", tableOnFile = true) annotation(Placement(visible = true, transformation(origin = {-124.2375, 50.0}, extent = {{-5.7625, -5.7625}, {5.7625, 5.7625}}, rotation = 0)));

```
Modelica.Blocks.Sources.CombiTimeTable zeros(fileName = "daylightzeros.txt", tableName = "var3", tableOnFile = true) annotation(Placement(visible = true, transformation(origin = {-50.7625, -97.46080000000001}, extent = {{-5.7625, -5.7625}, {5.7625, 5.7625}}, rotation = 0)));
```

```
Modelica.Blocks.Sources.CombiTimeTable daylighthours(fileName = "daylightzeros.txt", tableName = "var2", tableOnFile = true) annotation(Placement(visible = true, transformation(origin = {-124.2375, 77.532}, extent = {{-5.7625, -5.7625}, {5.7625, 5.7625}}, rotation = 0)));
```

```
Modelica.Blocks.Logical.Switch switch1 annotation(Placement(visible = true, transformation(origin = {96.062, 63.938}, extent = {{-6.062, -6.062}, {6.062, 6.062}}, rotation = 0)));
```

```
Modelica.Blocks.Interfaces.RealInput TankTempIn annotation(Placement(visible = true, transformation(origin = {-156.9858, 25.0}, extent = {{-20.0, -20.0}, {20.0, 20.0}}, rotation = 0), iconTransformation(origin = {-100.0, 0.0}, extent = {{-20.0, -20.0}, {20.0, 20.0}}, rotation = 0)));
```

```
Modelica.Blocks.Interfaces.RealOutput HeatingOutWatts annotation(Placement(visible = true, transformation(origin = {170.0, 65.0}, extent = {{-25.0, -25.0}, {25.0, 25.0}}, rotation = 0), iconTransformation(origin = {100.0, 0.0}, extent = {{-10.0, -10.0}, {10.0, 10.0}}, rotation = 0)));
```

```
DigesterTankHeatingModelNOVFINAL.HeatPumpUpdate heatPumpUpdate1;
```

equation

```
connect(and1.y, heatPumpUpdate1.u) annotation(Line(visible = true, origin = {77.8686, 42.3861}, points = {{-140.0717, 7.6139}, {47.1314, 7.6139}, {47.1314, -7.6139}, {45.8089, -7.6139}}, color = {255, 0, 255}));
```

```
connect(heatPumpUpdate1.QCondOut, switch1.u1) annotation(Line(visible = true, origin = {110.8636, 41.7895}, points = {{20.6013, -22.5617}, {25.1475, -23.2293}, {25.1475, -3.7688}, {-25.076, -3.7688}, {-25.076, 26.9981}, {-22.076, 26.9981}}, color = {0, 0, 127}));
```

```
connect(ElecINSwitch.y, heatPumpUpdate1.ElectricalInput) annotation(Line(visible = true, origin = {94.9984, -39.7671}, points = {{-8.968, -50.2474}, {1.981, -50.2474}, {1.981, 50.2474}, {5.0058, 51.2431}}, color = {0, 0, 127}));
```

```
connect(COPSwitch.y, heatPumpUpdate1.ZeroCOP) annotation(Line(visible = true, origin = {71.0414, 60.7237}, points = {{-90.4297, 13.1591}, {45.2148, 13.1591}, {45.2148, -26.3181}}, color = {0, 0, 127}));
```

```
connect(TankTempIn, heatPumpUpdate1.TCondIn) annotation(Line(visible = true, origin =
{34.1809, 25.6195}, points = {{-191.1667, -0.6195000000000001}, {62.7222, -
0.6195000000000001}, {62.7222, 0.6195000000000001}, {65.7261, 0.9752999999999999}},
color = {0, 0, 127}));
```

```
connect(EvapConstIN.y, heatPumpUpdate1.EVAPCONSTIN) annotation(Line(visible = true,
origin = {85.6027, 6.32}, points = {{-12.4119, -38.8055}, {-12.4119, 12.9352}, {10.9119,
12.9352}, {13.9316, 13.5746}}, color = {0, 0, 127}));
```

```
connect(CondConstIN.y, heatPumpUpdate1.CONDCONSTIN) annotation(Line(visible = true,
origin = {76.03919999999999, 33.0507}, points = {{-65.5283, 0.1712}, {20.8428, 0.1712},
{20.8428, -0.1712}, {23.8475, -0.0851}}, color = {0, 0, 127}));
```

```
connect(and1.y, CondConstIN.u2) annotation(Line(visible = true, origin = {-25.6311,
33.2895}, points = {{-36.5719, 16.7105}, {-24.3689, 16.7105}, {-24.3689, -15.8739}, {18.263, -
15.8739}, {18.263, -0.8027}, {24.3918, -0.8027}, {24.3918, -0.06759999999999999}}, color =
{255, 0, 255}));
```

```
connect(zeros.y[1], CondConstIN.u3) annotation(Line(visible = true, origin = {-15.4193, -
34.163}, points = {{-29.0044, -63.2978}, {7.4122, -63.2978}, {7.4122, 63.2978}, {14.18,
63.2978}}, color = {0, 0, 127}));
```

```
connect(and1.y, EvapConstIN.u2) annotation(Line(visible = true, origin = {19.3143,
8.757199999999999}, points = {{-81.517300000000001, 41.2428}, {22.4621, 41.2428},
{22.4621, -41.2428}, {36.5932, -41.2428}}, color = {255, 0, 255}));
```

```
connect(MassFlowEvapTimesCpAir.y, EvapConstIN.u1) annotation(Line(visible = true,
origin = {45.5556, -25.7369}, points = {{-25.0556, 0.737}, {7.3519, 0.737}, {7.3519, -0.737},
{10.3519, -0.737}}, color = {0, 0, 127}));
```

```
connect(MassFlowTimesCpWater.y, CondConstIN.u1) annotation(Line(visible = true, origin
= {-6.0545, 37.3267}, points = {{-8.445499999999999, 0.0177}, {1.8152, 0.0177}, {1.8152, -
0.0177}, {4.8152, -0.0177}}, color = {0, 0, 127}));
```

```
connect(and1.y, switch1.u2) annotation(Line(visible = true, origin = {46.6461, 56.969}, points
= {{-108.8492, -6.969}, {33.3539, -6.969}, {33.3539, 6.969}, {42.1415, 6.969}}, color = {255,
0, 255}));
```

```
connect(and1.y, ElecINSwitch.u2) annotation(Line(visible = true, origin = {29.37, -34.0029},
points = {{-91.5731, 84.0029}, {12.1595, 84.0029}, {12.1595, -55.9971}, {33.6271, -55.9971},
{33.6271, -56.0116}}, color = {255, 0, 255}));
```

```
connect(ElecIN.y, ElecINSwitch.u1) annotation(Line(visible = true, origin = {55.0355, -82.0299}, points = {{-17.8847, -0.027}, {4.9616, -0.027}, {4.9616, 0.027}, {7.9616, 0.027}}, color = {0, 0, 127}));
```

```
connect(zeros.y[1], EvapConstIN.u3) annotation(Line(visible = true, origin = {29.3246, -67.9789}, points = {{-73.7484, -29.4819}, {23.5828, -29.4819}, {23.5828, 29.4818}, {26.5828, 29.4818}}, color = {0, 0, 127}));
```

```
connect(and1.y, COPSwitch.u2) annotation(Line(visible = true, origin = {-44.1598, 64.8404}, points = {{-18.0432, -14.8404}, {-5.8402, -14.8404}, {-5.8402, 0.1596}, {4.1598, 0.1596}, {4.1598, 10.1596}, {10.702, 10.1596}, {10.702, 9.042400000000001}}, color = {255, 0, 255}));
```

```
connect(greater1.y, and1.u1) annotation(Line(visible = true, origin = {-80.901, 59.4112}, points = {{-3.599, 18.8224}, {-3.599, -9.411199999999999}, {7.198, -9.411199999999999}}, color = {255, 0, 255}));
```

```
connect(onOffController1.y, and1.u2) annotation(Line(visible = true, origin = {-77.43129999999999, 23.861}, points = {{-5.1849, -22.139}, {0.7283, -22.139}, {0.7283, 22.139}, {3.7283, 22.139}}, color = {255, 0, 255}));
```

```
connect(daylighthours.y[1], greater1.u1) annotation(Line(visible = true, origin = {-102.9747, 77.8828}, points = {{-14.9241, -0.3508}, {3.9747, -0.3508}, {3.9747, 0.3508}, {6.9747, 0.3508}}, color = {0, 0, 127}));
```

```
connect(zeros1.y[1], greater1.u2) annotation(Line(visible = true, origin = {-102.9747, 62.1168}, points = {{-14.9241, -12.1168}, {3.9747, -12.1168}, {3.9747, 12.1168}, {6.9747, 12.1168}}, color = {0, 0, 127}));
```

```
connect(COPInput1.y, COPSwitch.u1) annotation(Line(visible = true, origin = {-37.7184, 78.4653}, points = {{-6.7816, -0.3113}, {1.2605, -0.3113}, {1.2605, 0.3113}, {4.2605, 0.3113}}, color = {0, 0, 127}));
```

```
connect(onOffController1.u, TankTempIn) annotation(Line(visible = true, origin = {-131.4282, 10.8776}, points = {{29.7726, -14.1224}, {-2.1075, -14.1224}, {-2.1075, 14.1224}, {-25.5575, 14.1224}}, color = {0, 0, 127}));
```

```
connect(TankSetTemp.y, onOffController1.reference) annotation(Line(visible = true, origin = {-106.3667, 10.8444}, points = {{-8.1333, 4.1556}, {1.7111, 4.1556}, {1.7111, -4.1556}, {4.7111, -4.1556}}, color = {0, 0, 127}));
```

```
connect(zeros.y[1], switch1.u3) annotation(Line(visible = true, origin = {53.9848, -19.1862}, points = {{-98.40860000000001, -78.27460000000001}, {-98.98480000000001, 78.27460000000001}, {31.8028, 78.27460000000001}, {34.8028, 78.27460000000001}}, color = {0, 0, 127}));
```

```
connect(switch1.y, HeatingOutWatts) annotation(Line(visible = true, origin = {138.9013,
64.46899999999999}, points = {{-36.1711, -0.531}, {2.5362, -0.531}, {2.5362, 0.531},
{31.0987, 0.531}}, color = {0, 0, 127}));
```

```
connect(zeros.y[1], ElecINSwitch.u3) annotation(Line(visible = true, origin = {34.6419, -
97.7435}, points = {{-79.0656, 0.2826}, {25.3552, 0.2826}, {25.3552, -0.2826}, {28.3552, -
0.2826}}, color = {0, 0, 127}));
```

```
connect(zeros.y[1], COPSwitch.u3) annotation(Line(visible = true, origin = {-37.6993, -
14.2359}, points = {{-6.7244, -83.22490000000001}, {1.2415, -83.22490000000001}, {1.2415,
83.22490000000001}, {4.2415, 83.22490000000001}}, color = {0, 0, 127}));
```

```
annotation(Icon(coordinateSystem(extent = {{-100.0, -100.0}, {100.0, 100.0}},
preserveAspectRatio = true, initialScale = 0.1, grid = {10, 10}), graphics = {Rectangle(visible =
true, fillColor = {0, 0, 255}, extent = {{-100.0, -100.0}, {100.0, 100.0}}, radius = 25),
Text(visible = true, fillColor = {0, 0, 255}, fillPattern = FillPattern.Solid, extent = {{-100.0, -
100.0}, {100.0, 100.0}}, textString = "%name", fontName = "Arial")}),
Diagram(coordinateSystem(extent = {{-148.5, -105.0}, {148.5, 105.0}}, preserveAspectRatio =
true, initialScale = 0.1, grid = {5, 5})));
```

```
end HeatPumpWithController;
```

```
DigesterTankHeatingModelNOVFINAL.ConvCoeffCalc convCoeffCalc
annotation(Placement(visible = true, transformation(origin = {129.9204, -23.4204}, extent =
{{13.4204, -13.4204}, {-13.4204, 13.4204}}, rotation = 0)));
```

```
model IntegratorWithReset
```

```
extends Modelica.Blocks.Continuous.Integrator;
```

```
Modelica.Blocks.Interfaces.BooleanInput reset annotation(Placement(visible = true,
transformation(origin = {-120, -60}, extent = {{-20, -20}, {20, 20}}, rotation = 0),
iconTransformation(origin = {-120, -80}, extent = {{-20, -20}, {20, 20}}, rotation = -360)));
```

```
equation
```

```
when reset then
```

```
  reinit(y, y_start);
```

```
end when;
```

end IntegratorWithReset;

model GasProduction

Modelica.Blocks.Interfaces.RealInput u annotation(Placement(visible = true, transformation(origin = {-157.0754, 0.0}, extent = {{-20.0, -20.0}, {20.0, 20.0}}, rotation = 0), iconTransformation(origin = {-99.6853, 0.319}, extent = {{-20.0, -20.0}, {20.0, 20.0}}, rotation = 0)));

Modelica.Blocks.Interfaces.RealOutput y annotation(Placement(visible = true, transformation(origin = {148.3676, 0.0}, extent = {{-10.0, -10.0}, {10.0, 10.0}}, rotation = 0), iconTransformation(origin = {99.9109, 0.0}, extent = {{-10.0, -10.0}, {10.0, 10.0}}, rotation = 0)));

Modelica.Blocks.Math.Gain gain1(k = 367) annotation(Placement(visible = true, transformation(origin = {55.0, 0.0}, extent = {{-10.0, -10.0}, {10.0, 10.0}}, rotation = 0)));

model Arrhenius

Modelica.Blocks.Interfaces.RealInput u annotation(Placement(visible = true, transformation(origin = {-155.0, 0.0}, extent = {{-20.0, -20.0}, {20.0, 20.0}}, rotation = 0), iconTransformation(origin = {-98.78319999999999, 0.0}, extent = {{-20.0, -20.0}, {20.0, 20.0}}, rotation = 0)));

Modelica.Blocks.Interfaces.RealOutput y annotation(Placement(visible = true, transformation(origin = {150.0, 0.0}, extent = {{-10.0, -10.0}, {10.0, 10.0}}, rotation = 0), iconTransformation(origin = {100.5874, 0.319}, extent = {{-10.0, -10.0}, {10.0, 10.0}}, rotation = 0)));

equation

$y = \exp(63492 * (u + 273 - 308) / (8.314399999999999 * (u + 273) * 308));$

annotation(Diagram(coordinateSystem(extent = {{-148.5, -105.0}, {148.5, 105.0}}, preserveAspectRatio = true, initialScale = 0.1, grid = {5, 5})));

end Arrhenius;

DigesterTankHeatingModelNOVFINAL.GasProduction.Arrhenius arrhenius1

annotation(Placement(visible = true, transformation(origin = {5.0, 0.0}, extent = {{-20.0, -20.0}, {20.0, 20.0}}, rotation = 0)));

equation

```
connect(u, arrhenius1.u) annotation(Line(visible = true, origin = {-85.916, 0.0}, points = {{-71.15940000000001, 0.0}, {71.15940000000001, 0.0}}, color = {0, 0, 127}));
```

```
connect(arrhenius1.y, gain1.u) annotation(Line(visible = true, origin = {37.0294, 0.0319}, points = {{-11.9119, 0.0319}, {2.9706, 0.0319}, {2.9706, -0.0319}, {5.9706, -0.0319}}, color = {0, 0, 127}));
```

```
connect(gain1.y, y) annotation(Line(visible = true, origin = {107.1838, 0.0}, points = {{-41.1838, 0.0}, {41.1838, -0.0}}, color = {0, 0, 127}));
```

```
annotation(Diagram(coordinateSystem(extent = {{-148.5, -105.0}, {148.5, 105.0}}, preserveAspectRatio = true, initialScale = 0.1, grid = {5, 5}));
```

end GasProduction;

```
Modelica.Thermal.HeatTransfer.Sources.PrescribedHeatFlow prescribedHeatFlow1(T_ref = 308.15, alpha = 0) annotation(Placement(visible = true, transformation(origin = {-22.8792, -40.0}, extent = {{-10.0, -10.0}, {10.0, 10.0}}, rotation = 0));
```

```
DigesterTankHeatingModelNOVFINAL.HeatPumpWithController heatPumpWithController annotation(Placement(visible = true, transformation(origin = {-74.22360000000001, -25.7764}, extent = {{-14.2236, -14.2236}, {14.2236, 14.2236}}, rotation = 0));
```

equation

```
connect(TankTempProbe.T, heatPumpWithController.TankTempIn) annotation(Line(visible = true, origin = {-98.5877, -15.8947}, points = {{-24.3861, 9.881600000000001}, {7.1228, 9.881600000000001}, {7.1228, -9.8817}, {10.1405, -9.8817}}, color = {0, 0, 127}));
```

```
connect(prescribedHeatFlow1.Q_flow, heatPumpWithController.HeatingOutWatts) annotation(Line(visible = true, origin = {-51.7109, -32.8882}, points = {{18.8317, -7.1118}, {-5.2713, -7.1118}, {-5.2713, 7.1118}, {-8.2891, 7.1118}}, color = {0, 0, 127}));
```

```
connect(prescribedHeatFlow1.port, HeatCapTank.port) annotation(Line(visible = true, origin = {-74.6365, 15.6717}, points = {{61.7573, -55.6717}, {69.6365, -55.6717}, {69.6365, -27.7287}, {29.6365, -27.7287}, {29.6365, -12.3226}, {-35.3635, -12.3226}, {-35.3635, -2.2751}, {-52.6314, -2.2751}, {-52.6314, 64.3283}, {-42.1568, 64.3283}, {-42.1568, 67.005}}, color = {191, 0, 0}));
```

```
connect(ConvWalls.Gc, convCoeffCalc.ConvCoeffWalls) annotation(Line(visible = true, origin = {99.8434, -6.5775}, points = {{-21.968, 13.7021}, {-21.968, 16.7021}, {13.6398, 16.7021}, {13.6398, -23.5531}, {16.6566, -23.5531}}, color = {0, 0, 127}));
```

```

connect(ConvRoof.Gc, convCoeffCalc.ConvCoeffRoof) annotation(Line(visible = true, origin
= {94.3094, 9.831899999999999}, points = {{-16.7858, 20.1681}, {-16.7858, 23.1681},
{5.6906, 23.1681}, {5.6906, -33.2522}, {22.1906, -33.2523}}, color = {0, 0, 127}));

connect(HeatCapTank.port, CondTankFloor.port_a) annotation(Line(visible = true, origin = {-
105.3622, 42.5589}, points = {{-11.4311, 40.1178}, {-11.4311, -20.0589}, {22.8622, -
20.0589}}, color = {191, 0, 0}));

connect(HeatCapTank.port, CondTankWalls.port_a) annotation(Line(visible = true, origin = {-
105.3622, 57.5589}, points = {{-11.4311, 25.1178}, {-11.4311, -12.5589}, {22.8622, -
12.5589}}, color = {191, 0, 0}));

connect(HeatCapTank.port, CondTankRoof.port_a) annotation(Line(visible = true, origin = {-
105.3622, 72.55899999999999}, points = {{-11.4311, 10.1178}, {-11.4311, -5.0589}, {22.8622, -
5.0589}}, color = {191, 0, 0}));

connect(HeatCapTank.port, TankTempProbe.port) annotation(Line(visible = true, origin = {-
128.9173, 46.0008}, points = {{12.124, 36.6759}, {12.124, 33.6759}, {-9.082700000000001,
33.6759}, {-9.082700000000001, -52.0139}, {-6.0827, -52.0139}}, color = {191, 0, 0}));

connect(CondInsulWalls.port_b, ConvWalls.solid) annotation(Line(visible = true, origin =
{25.8127, 22.5}, points = {{-53.3127, 22.5}, {4.1873, 22.5}, {4.1873, -22.5}, {44.9381, -
22.5}}, color = {191, 0, 0}));

connect(CondInsulRoof.port_b, ConvRoof.solid) annotation(Line(visible = true, origin =
{34.626, 41.7189}, points = {{-61.5906, 26.3165}, {3.2195, 26.3165}, {3.2195, -16.7189},
{35.4212, -16.7189}, {35.4212, -19.1953}}, color = {191, 0, 0}));

connect(CondInsulWalls.port_b, RadWalls.port_a) annotation(Line(visible = true, origin =
{44.5134, 31.1892}, points = {{-72.0134, 13.8108}, {-4.5134, 13.8108}, {15.4866, 13.8108},
{15.4866, 18.8108}, {22.3504, 18.8108}}, color = {191, 0, 0}));

connect(RadWalls.port_b, Tsky.port) annotation(Line(visible = true, origin = {54.5929,
81.8843}, points = {{32.2708, -31.8843}, {35.4071, -31.8843}, {35.4071, 11.2222}, {-14.5929,
11.2222}, {-14.5929, 6.1985}, {-19.5929, 6.1985}, {-19.5929, 8.1157}, {-17.3567, 8.1157}, {-
17.3567, 5.8795}}, color = {191, 0, 0}));

connect(MTLTempData.y[1], Tambient.T) annotation(Line(visible = true, origin = {117.6394,
62.3022}, points = {{-4.0368, -0.1227}, {0.3456, -0.1227}, {0.3456, 0.1227}, {3.3456,
0.1227}}, color = {0, 0, 127}));

connect(Tambient.port, ConvWalls.fluid) annotation(Line(visible = true, origin = {125.9925,
31.2124}, points = {{11.6578, 31.2124}, {14.6673, 31.2124}, {14.6673, -31.2124}, {-40.9925, -
31.2124}}, color = {191, 0, 0}));

```

```
connect(Tambient.port, ConvRoof.fluid) annotation(Line(visible = true, origin = {125.9925, 42.4742}, points = {{11.6578, 19.9506}, {14.6673, 19.9506}, {14.6673, -19.9506}, {-40.9925, -19.9506}}, color = {191, 0, 0}));
```

```
connect(MTLTempData.y[1], TSkyCalc.u3) annotation(Line(visible = true, origin = {50.4389, 9.2097}, points = {{63.1636, 52.9698}, {63.1636, 90.7903}, {49.5611, 90.7903}, {-65.4389, 90.7903}, {-65.4389, 78.1083}, {-60.4389, 78.22799999999999}}, color = {0, 0, 127}));
```

```
connect(Tsky.port, RadRoof.port_b) annotation(Line(visible = true, origin = {64.14960000000001, 86.3986}, points = {{-26.9134, 1.3652}, {-23.9044, 1.3652}, {-23.9044, 7.0429}, {25.9074, 7.0429}, {25.9074, -8.408099999999999}, {22.9074, -8.408099999999999}}, color = {191, 0, 0}));
```

```
connect(CondInsulRoof.port_b, RadRoof.port_a) annotation(Line(visible = true, origin = {42.0516, 73.01300000000001}, points = {{-69.0162, -4.9776}, {22.0054, -4.9776}, {22.0054, 4.9776}, {25.0054, 4.9776}}, color = {191, 0, 0}));
```

```
connect(Tsky.T, TSkyCalc.Celsius1) annotation(Line(visible = true, origin = {15.4805, 87.6007}, points = {{5.836, 0.1631}, {-0.9409, 0.1631}, {-0.9409, -0.1631}, {-3.9543, -0.1631}}, color = {0, 0, 127}));
```

```
connect(Tbuilding.port, CondInsulFloor.port_b) annotation(Line(visible = true, origin = {-21.0043, 22.6048}, points = {{13.6572, 0.0481}, {-3.5524, 0.0481}, {-3.5524, -0.0481}, {-6.5524, -0.0481}}, color = {191, 0, 0}));
```

```
connect(CondTankFloor.port_b, CondInsulFloor.port_a) annotation(Line(visible = true, origin = {-50.2075, 22.5284}, points = {{-17.2925, -0.0284}, {4.7642, -0.0284}, {4.7642, 0.0283}, {7.7642, 0.0283}}, color = {191, 0, 0}));
```

```
connect(CondTankWalls.port_b, CondInsulWalls.port_a) annotation(Line(visible = true, origin = {-55.0, 45.0}, points = {{-12.5, 0.0}, {12.5, 0.0}}, color = {191, 0, 0}));
```

```
connect(CondTankRoof.port_b, CondInsulRoof.port_a) annotation(Line(visible = true, origin = {-50.6516, 67.76770000000001}, points = {{-16.8484, -0.2677}, {4.6162, -0.2677}, {4.6162, 0.2677}, {7.6162, 0.2677}}, color = {191, 0, 0}));
```

```
end DigesterTankHeatingModelNOVFINAL;
```

A.2 Synchronous Generator Derating Test (System Modeler)

model synchgenworkingLINERESISTANCE

```
Modelica.Electrical.Analog.Basic.Ground excitationground annotation(Placement(visible = true, transformation(origin = {6.68, -56.601}, extent = {{-10, -10}, {10, 10}}, rotation = 0)));
```

```
import Modelica.Constants.pi;
```

```
constant Integer m = 3 "Number of phases";
```

```
parameter Modelica.SIunits.AngularVelocity wNominal = 2 * Modelica.Constants.pi * smeeData.fsNominal / 2 "Nominal speed";
```

```
parameter Real powerFactor(min = 0, max = 1) = 1 "Load power factor";
```

```
parameter Modelica.SIunits.Resistance RLoad = 3 * smeeData.VsNominal ^ 2 / smeeData.SNominal * powerFactor "Load resistance";
```

```
Modelica.Electrical.MultiPhase.Basic.Star star annotation(Placement(visible = true, transformation(origin = {80, 5}, extent = {{-10, -10}, {10, 10}}, rotation = -90)));
```

```
Modelica.Electrical.Analog.Basic.Ground ground annotation(Placement(visible = true, transformation(origin = {80, -25}, extent = {{-10, -10}, {10, 10}}, rotation = 0)));
```

```
Modelica.Electrical.Machines.Utilities.TerminalBox terminalBox(terminalConnection = "Y") annotation(Placement(visible = true, transformation(origin = {-32.378, 0.79}, extent = {{14.21, -14.21}, {-14.21, 14.21}}, rotation = 0)));
```

```
Modelica.Electrical.MultiPhase.Basic.Resistor resistor(R = fill(RLoad, m)) annotation(Placement(visible = true, transformation(origin = {70, 20}, extent = {{-10, -10}, {10, 10}}, rotation = 0)));
```

```
Modelica.Electrical.MultiPhase.Basic.Resistor lineResistance(useHeatPort = false, R = fill(0.01608, m)) "100 m of 13 gauge wire" annotation(Placement(visible = true, transformation(origin = {45, 20}, extent = {{-10, -10}, {10, 10}}, rotation = 0)));
```

```
parameter Modelica.Electrical.Machines.Utilities.SynchronousMachineData smeeData(IeOpenCircuit = 10, SNominal = 30000, Ta = 0.014171268, Td0Subtransient = 0.006963029, Td0Transient = 0.261177343, TeRef = 293.15, TeSpecification = 293.15, Tq0Subtransient = 0.123345081, TrRef = 293.15, TrSpecification = 293.15, TsRef = 293.15, TsSpecification = 293.15, VsNominal = 100, alpha20e = Modelica.Electrical.Machines.Thermal.Constants.alpha20Copper, alpha20r = Modelica.Electrical.Machines.Thermal.Constants.alpha20Copper, alpha20s =
```

```
Modelica.Electrical.Machines.Thermal.Constants.alpha20Copper, fsNominal = 60, x0 = 0.1, xd
= 1.6, xdSubtransient = 0.121428571, xdTransient = 0.1375, xq = 1.6, xqSubtransient =
0.148387097) annotation(Placement(visible = true, transformation(origin = {-35, -67.56}, extent
= {{-10, -10}, {10, 10}}, rotation = 0)));
```

```
Modelica.Blocks.Sources.Ramp ramp(duration = 1, height = 188.49)
annotation(Placement(visible = true, transformation(origin = {-132.06, -30}, extent = {{-10, -
10}, {10, 10}}, rotation = 0)));
```

```
Modelica.Mechanics.Rotational.Sources.Speed speed(f_crit = 60) annotation(Placement(visible
= true, transformation(origin = {-93.28, -30}, extent = {{-10, -10}, {10, 10}}, rotation = 0)));
```

```
Modelica.Electrical.Machines.BasicMachines.SynchronousInductionMachines.SM_ElectricalEx
cited smee(Jr = 0.29, Js = 0.29, p = 2, fsNominal = 60, TsOperational = 293.15, TrOperational =
293.15, TeOperational = 293.15, Rs = smeeData.Rs, TsRef = smeeData.TsRef, alpha20s =
smeeData.alpha20s, Lssigma = smeeData.Lssigma, Lmd = smeeData.Lmd, Lmq =
smeeData.Lmq, VsNominal = smeeData.VsNominal, IeOpenCircuit = smeeData.IeOpenCircuit,
Re = smeeData.Re, TeRef = smeeData.TeRef, alpha20e = smeeData.alpha20e, sigmae =
smeeData.sigmae, useDamperCage = true, Lrsigma = smeeData.Lrsigma, Lrsigmaq =
smeeData.LrsigmaqLrsigma, Rrd = smeeData.Rrd, Rrq = smeeData.Rrq, TrRef =
smeeData.TrRef, alpha20r = smeeData.alpha20r) annotation(Placement(visible = true,
transformation(origin = {-32.56, -30.88}, extent = {{14.12, -14.12}, {-14.12, 14.12}}, rotation =
0)));
```

```
Modelica.Electrical.Machines.Sensors.VoltageQuasiRMSSensor voltageQuasiRMSSensor
annotation(Placement(visible = true, transformation(origin = {25, -2.52}, extent = {{-10, -10},
{10, 10}}, rotation = 0)));
```

```
Modelica.Electrical.Analog.Sources.ConstantCurrent constantCurrent(I = 19)
annotation(Placement(visible = true, transformation(origin = {7.381, -30}, extent = {{-10, -10},
{10, 10}}, rotation = -90)));
```

equation

```
connect(constantCurrent.n, excitationground.p) annotation(Line(visible = true, origin = {7.031,
-43.451}, points = {{0.351, 3.451}, {0.351, -0.15}, {-0.351, -0.15}, {-0.351, -3.15}}, color = {0,
0, 255}));
```

```
connect(constantCurrent.n, smee.pin_en) annotation(Line(visible = true, origin = {-4.984, -
40.941}, points = {{12.365, 0.941}, {12.365, -2.059}, {-5.637, -2.059}, {-5.637, 1.589}, {-
13.456, 1.589}}, color = {0, 0, 255}));
```

```

connect(constantCurrent.p, smee.pin_ep) annotation(Line(visible = true, origin = {-4.984, -
19.763}, points = {{12.365, -0.237}, {12.365, 2.763}, {-5.637, 2.763}, {-5.637, -2.645}, {-
13.456, -2.645}}, color = {0, 0, 255}));

connect(currentQuasiRMSSensor.plug_n, lineResistance.plug_p) annotation(Line(visible =
true, origin = {17.5, 20}, points = {{-17.5, 0}, {17.5, 0}}, color = {0, 0, 255}));

connect(voltageQuasiRMSSensor.plug_n, terminalBox.plug_sn) annotation(Line(visible = true,
origin = {-0.311, -4.985}, points = {{35.311, 2.465}, {35.311, 11.704}, {-23.541, 11.704}, {-
23.541, -17.439}, {-23.541, -8.435000000000001}}, color = {0, 0, 255}));

connect(voltageQuasiRMSSensor.plug_p, terminalBox.plug_sp) annotation(Line(visible = true,
origin = {-28.105, -7.97}, points = {{43.105, 5.45}, {-15.153, 5.45}, {-15.153, -5.45}, {-12.799,
-5.45}}, color = {0, 0, 255}));

connect(speed.flange, smee.flange) annotation(Line(visible = true, origin = {-58.901, -30.44},
points = {{-24.38, 0.44}, {6.079, 0.44}, {6.079, -0.44}, {12.221, -0.44}}));

connect(smee.plug_sn, terminalBox.plug_sn) annotation(Line(visible = true, origin = {-24.009,
-14.533}, points = {{-0.078, -2.226}, {-0.078, 1.113}, {0.157, 1.113}}, color = {0, 0, 255}));

connect(smee.plug_sp, terminalBox.plug_sp) annotation(Line(visible = true, origin = {-40.989,
-14.533}, points = {{-0.043, -2.226}, {-0.043, 1.113}, {0.08500000000000001, 1.113}}, color =
{0, 0, 255}));

connect(ramp.y, speed.w_ref) annotation(Line(visible = true, origin = {-113.17, -30}, points =
{{-7.89, 0}, {7.89, 0}}, color = {0, 0, 127}));

connect(currentQuasiRMSSensor.plug_p, terminalBox.plugSupply) annotation(Line(visible =
true, origin = {-23.252, 17.024}, points = {{3.252, 2.976}, {-9.125999999999999, 2.976}, {-
9.125999999999999, -27.602}}, color = {0, 0, 255}));

connect(lineResistance.plug_n, resistor.plug_p) annotation(Line(visible = true, origin = {57.5,
20}, points = {{-2.5, 0}, {2.5, 0}}, color = {0, 0, 255}));

connect(resistor.plug_n, star.plug_p) annotation(Line(visible = true, origin = {80, 16.667},
points = {{0, 3.333}, {0, -1.667}, {0, -1.667}}, color = {0, 0, 255}));

connect(star.pin_n, ground.p) annotation(Line(visible = true, origin = {80, -10}, points = {{0,
5}, {0, -5}}, color = {0, 0, 255}));

annotation(experiment(StopTime = 5, NumberOfIntervals = 10000),
Diagram(coordinateSystem(extent = {{-148.5, -105}, {148.5, 105}}, preserveAspectRatio =
true, initialScale = 0.1, grid = {5, 5}));
end synchgenworkingLINERESISTANCE;

```